1971

Finite element analyses of elastic-plastic plates and eccentrically stiffened plates, Ph.D. dissertation, 1971.

Anton W. Wegmüller

FINITE ELEMENT ANALYSES OF ELASTIC-PLASTIC PLATES AND ECCENTRICALLY STIFFENED PLATES

by

Anton W. Wegmuller

A Dissertation
Presented to the Graduate Committee
of Lehigh University
in Candidacy for the Degree of
Doctor of Philosophy

in

Civil Engineering

Lehigh University
Bethlehem, Pennsylvania

1971

Approved and recommended for acceptance as a dissertation in partial fulfillment of the requirements for the Degree of Doctor of Philosophy.

December 20, 1971
Acceptance Date

Special Committee directing the
doctoral work of Mr. Anton W. Wegmuller

Celal N. Kostem David A. VanHorn

Dissertation Supervisors

Other Members

Professor John W. Fisher

Professor Ti Huang

Professor Dean Updike

TABLE OF CONTENTS

ACKNOWLEDGMENTS

The research reported herein was carried out during the author's graduate study for the Ph.D. degree in Civil Engineering at Lehigh University, in Bethlehem, Pennsylvania. The author wishes to express his gratitude to Professors C. N. Kostem and D. A. VanHorn, under whose supervision this work was conducted; and to Professors J. W. Fisher, T. Huang and D. Updike, members of his dissertation committee for their helpful guidance and assistance. The work was sponsored in part by the National Science Foundation through Grant No. GK-23589. The Lehigh University Computing Center provided its facilities for the extensive computer work.

Special acknowledgement is due Mr. Suresh Desai for his continuing interest and encouragement to the author. Thanks are also due to Mrs. Ruth Grimes, who typed the final manuscript and to Mr. John Gera and Mrs. Sharon Balogh for the preparation of the drawings included in this work.

ABSTRACT

This report deals with the analysis of plates and stiffened plates in the elastic and elastic-plastic range using the finite element stiffness approach. The analysis is based on the classical theory of thin plates exhibiting small deformations.

A short description of the finite element techniques in use to date, and a review of some existing plate bending elements are presented. A refined rectangular plate bending element based on a higher order polynomial expression is then derived and a systematic procedure for the derivation of its stiffness matrix is outlined. The accuracy and convergence of solutions obtained with this new element are demonstrated on a few example structures showing that the new element compares favorably with presently known plate elements.

Chapter 3 deals with the analysis of stiffened plate structures in the linear elastic range. The derivation of the component stiffness matrices is carried out first, and the assemblage of the system stiffness matrix is described. The outlined general approach is then applied extensively to highway girder bridges, and the versatility and accuracy of the method are demonstrated.

In Chapter 4, a general procedure for the analysis of elastic-plastic plates is presented. A description of the mathematical model, consisting of a plate element subdivided into a

finite member of layers is given, and the associated incremental elastic-plastic solution technique is outlined. A few example solutions show the accuracy and versatility of the proposed tangent stiffness approach.

Finally, in Chapter 5, a general procedure for the elastic-plastic analysis of stiffened plate structures is presented. The layered plate model used in the elastic-plastic analysis of plates is supplemented by a similar layered beam element for this analysis, and the associated step-by-step iteration technique used to solve the linearized governing equations is described.

All presented types of analyses have been implemented with the essential aid of a high speed digital computer (CDC 6400) and examples of application prove their validity and versatility.

1. INTRODUCTION

1.1 Objective and Scope

Plates of various shapes are commonly used as structural systems or structural components. Most frequently, plates form part of floor systems in buildings or bridges, and are often used in connection with beams and columns. Generally, there is ample room for a variation in geometry, thickness and loading, as illustrated in Fig. 1 and hence, the analysis of such complex structures often presents considerable difficulties.

Stiffened plates of arbitrary shape are complex and highly redundant structures, the analysis of which is beyond the scope of currently used methods of analysis. Plates are often used in combination with beams and columns in floor systems of buildings and bridges, and in these cases, are predominantly loaded by forces acting perpendicular to the plate surface. In buildings, many different floor layouts are possible; consequently, there is virtually no restriction placed as far as geometry of the stiffened plate structure is concerned. The in-plane loading (if any) applied to such structures can often be neglected, thus simplifying the analysis considerably. This investigation is limited to the problem of analyzing transversely loaded stiffened plates; i.e. no in-plane loading is considered. However, due to the fact that the beams are eccentrically attached to the plate, in-plane deformation must be considered. To date, the analysis of beam-slab type

structures still constitutes a challenge to the structural engineer because no fully satisfactory method of analysis is available.

It is widely accepted that a structure should be properly analyzed for working loads, as well as at its failure stage. By means of an elastic analysis, one is able to determine the stresses and deformations, occurring under working loads, at selected points of a structure. If the determined stresses are kept below allowable stresses, then experience shows that a structure is not likely to fail. An accurate elastic analysis is also needed for considerations of fatigue and control of cracking in reinforced and prestressed concrete structures; i.e. stresses must be kept below certain levels in order to avoid fatigue or excessive cracking. Although the fatigue strength of reinforced or prestressed concrete structures is difficult to establish, and reliable criteria for crack control have not been established, an accurate elastic analysis is the prerequisite for establishing such guidelines.

On the other hand, an elastic analysis cannot predict the response of a structure stressed beyond the elastic limit load, and up to its failure load. An analysis of the post-elastic range is needed to predict eventual damages, and to determine the deformations occurring during the application of overloads. No damage is desired to occur under working loads, but at the same time it is required that a structure should be able to withstand a certain overload. The strength of a structure of the type considered in this investigation is needed to ascertain that failure should not

occur under working load, and hence, to design a structure with an adequate factor of safety. An attempt to analyze complex shaped plate structures in the post-elastic range, as well as to predict the failure load, is developed in Chapter 4.

Most engineering materials, such as steel, aluminum, and properly designed reinforced concrete are ductile, and can withstand strains much greater than the strain associated with the elastic limit state. As the structure is loaded beyond this state, plastic straining occurs, causing a redistribution of stress in a redundant structure. The ductility in redundant structures permits a redistribution of stresses beyond the elastic limit, allowing a structure to carry considerable additional loads. Thus, it is felt today that a design should also consider the post-elastic behavior of a structure, as well as its ultimate strength. The post-elastic response of a structure is of interest because it enables the designer to judge the effects of possible overloads. The knowledge of the load carrying capacity, or ultimate strength, of a structure is twofold: (1) it allows the determination of the factor of safety of a structure against failure, and (2) the stress resultants resisted by the structural components at ultimate load are required to properly dimension each structural part.

The goal of the reported study is the development of an approach which will allow the tracing of the entire load-deformation behavior of complex shaped stiffened plate structures, as well as

to find the ultimate load-carrying capacity of such structures. The application to the inelastic analysis of beam-slab type bridges will allow the study of the behavior of such bridges in the post-elastic range as well as at failure. It is obvious that due to the current trend of increasing vehicular weight limits, the behavior of bridges above the elastic limit stage must be known in order to judge the effects of overloading. Current permit regulations are not based on a rational structural analysis of the bridge superstructure under the load level in question. Also, there is no existing rational method to judge the effects of overloading of bridge superstructures. The continuous load-deformation behavior of a stiffened plate structure stressed beyond its elastic limit is needed to judge the effects of overloading. At this point it would be appropriate to note that the concept of Ultimate Strength Design, as outlined in the ACI Building Code (Ref. 1), does not account for a redistribution of stresses due to redundancy of the structure. Recognizing that this redistribution actually plays an important role in highly redundant structures, it is felt that modern bridge design philosophy should reflect the inelastic behavior.

Within the framework of this report, only the numerical technique by which the elastic-plastic response of complex shaped stiffened plates can be obtained, is described. The application of the developed technique to beam-slab type highway bridge superstructures of arbitrary material behavior is the subject of future research.

1.2 Previous Work

For each of the problems considered in this report, a review of the previous work done in the area considered is given in the chapter devoted to each problem. Due to the practical importance of plate structures, engineers have long been faced with the task of analyzing plates of various geometry and loading. Unfortunately, the governing differential equations are solvable only for simple geometry and boundary conditions, and as a consequence, many types of approximate analyses have been proposed to date. Extensive surveys of the state-of-the-art of current plate analysis are given by Timoshenko (Ref. 3) and Girkman (Ref. 4).

Probably the most commonly used approximate method of analysis for solving plate problems of complex geometry is the method of finite differences. In this method, the governing differential equation of equilibrium is satisfied only at selected points of the plate structure. The satisfaction of boundary conditions at boundary points of the plate leads to additional equations which, together with the original set of equations, must be solved simultaneously. These additional equations, however, depend on the type of boundary and make it difficult to develop general purpose programs.

During the last two decades much progress has been made in the development of structural methods of analysis based on matrix algebra and a discretization of the structure into an assembly of discrete structural elements. In these methods, a displacement or

a stress distribution is assumed within the element, and a complete solution is then obtained by combining these approximate displacement or stress distributions in a manner which satisfies the force-equilibrium and displacement-compatibility requirements at all interfaces of the elements. Methods based on such approaches have been proven to be suitable for the analysis of complex structures. This led to the development of the finite element methods (Ref. 6), which are essentially generalizations of standard structural procedures as described in Reference 5, for example. To date, these methods have been successfully applied to many complex plate problems. Within the framework of the reported study a refined finite element for plate bending is developed. This new plate bending element is presented in Chapter 2 of this report.

To date, the elastic analysis of stiffened plate structures, as shown in Fig. 16, is performed in a more or less approximate manner. Though various types of methods are available, their application to complex shaped beam-plate type structures is doubtful for other than simple geometry of the structure to be analyzed. Particular attention has been given in the past to the analysis of floor systems of highway girder bridges. Consequently, most methods were originally developed for bridge structures.

In summary, it can be stated that as yet, no fully adequate analysis exists which is capable of determining stresses and deformations in complex shaped beam-slab type structures. Current

design methods are not completely rational, and are not based on a rigorous analysis, elastic or plastic (Ref. 2). Despite the fact that designs performed to date have resulted in structures which perform successfully, it cannot be said with assurance that the designs resulting from such procedures are the best possible, or that different parts of the same structure have consistent factors of safety against the failure load, until better analytical methods are available. A survey of available methods of analysis, some of which will be described, led to the conclusion that the finite element method, due to its great versatility, is best suited for the analysis of arbitrarily shaped stiffened plates, as shown in Fig. 16. This analysis is presented in Chapter 3.

The analysis of the complete load-deformation behavior of complex shaped plates is mathematically difficult to accomplish. The inclusion of the non-linear material behavior in plate analysis results in partial differential equations which are amenable to analytic solution only for some very simple structures. As a consequence, simplified methods designed to compute the ultimate strength of structures have been developed by a number of investigators (Refs 55, 56, 57). These methods are based on the theorems of limit analysis, and allow the establishment of bounds on the collapse load. However, the prediction of the elastic-plastic behavior of complex shaped plates cannot be accomplished using these methods. Using a numerical approach, a general method for the analysis of elastic-plastic plates of complex shape is presented in Chapter 4.

Virtually no work has been done in the elastic-plastic analysis of stiffened plate structures. A general method which enables the analysis of such inelastic structures is presented in Chapter 5.

2. ANALYSIS OF ELASTIC PLATES

2.1 Introduction

The structural engineer is often faced with the analysis of complex shaped and loaded plates, as shown in Fig. 1. During the last decade, the versatility of the finite element approach has been well demonstrated and a number of plate bending elements have been developed. While most of these elements lead to accurate predictions for the displacement field, the internal moments computed are, in general, far less accurate.

In this chapter, the development of a rectangular refined plate bending element is discussed. For the purpose of establishing the notation used in this text and the connection with conventional plate analyses, a review of the basic equations governing the behavior of plates is first presented. A short description of the finite element techniques in use to date is then given, followed by a review of some existing plate bending elements. The refined element, which is based on a higher order polynomial displacement field, is then described, and the derivation of the element stiffness matrices is outlined. Kinematically consistent load vectors are derived, and the enforcement of boundary conditions is described. A highly efficient technique for the solution of the often large system of stiffness equations is next described. Finally, the accuracy obtained with the new element is demonstrated on a few example solutions, and a comparison is made

with some presently known plate elements.

2.2 Small Deflection Theory of Thin Plates

2.2.1 Assumptions and Basic Equations

A transversely loaded plate structure should be treated as a three-dimensional problem of elasticity. Strain and stress components acting on an infinitesimal plate element of thickness h is shown in Fig. 2. The sign convention used in this study is shown in Fig. 3. By definition, stresses and forces are considered positive when acting in the directions shown. Introducing the assumptions of the classical theory of thin plates, a plate problem can be simplified into a two-dimensional elasticity problem. These assumptions can be stated as follows:

1. Plane sections normal to the middle surface before deformation remain plane and normal during deformation; also known as Kirchoff's assumption (Ref. 3).
2. The transverse displacement (w) is small in comparison to the thickness of the plate; i.e. $w \ll h$.
3. Stresses normal to the plane of the plate are negligible.

The first two assumptions imply that (1) shearing stresses in the transverse direction are neglected, and (2) the deflection (w) at any point of the plate is approximately equal to the deflection of the corresponding point located on the middle plane of the plate. The state of deformation can therefore be described in terms of

the transverse displacement (w) alone. Since the middle plane of the plate is assumed to be free of in-plane deformation, in-plane behavior is not considered in this chapter. Making use of the simplifying assumptions introduced above, the following relationships between in-plane displacements and the transverse displacement w exist:

$$U = u - z \frac{\partial w}{\partial x} \tag{2.1 a}$$

$$V = v - z \frac{\partial w}{\partial y} \tag{2.1 b}$$

where: u,v = Displacement in x-direction, or y-direction respectively, of a point lying in the middle plane of the plate.

U,V = Displacement in x-direction, or y-direction respectively, of a point lying at a distance z from the reference plane.

Both displacements u and v are assumed to be negligible in the classical theory of thin plates. The strain-displacement relations can be found by differentiating Eqs. 2.1:

$$\epsilon_x = \frac{\partial U}{\partial x} = \frac{\partial u}{\partial x} - z \frac{\partial^2 w}{\partial x^2} \tag{2.2 a}$$

$$\epsilon_y = \frac{\partial V}{\partial y} = \frac{\partial v}{\partial y} - z \frac{\partial^2 w}{\partial y^2} \tag{2.2 b}$$

$$\gamma_{xy} = \frac{\partial U}{\partial y} + \frac{\partial V}{\partial x} = \frac{\partial u}{\partial y} + \frac{\partial v}{\partial x} - 2 z \frac{\partial^2 w}{\partial x \partial y} \tag{2.2 c}$$

The stresses must satisfy the following two equations of equilibrium:

$$\frac{\partial \sigma_x}{\partial x} + \frac{\partial \tau_{yx}}{\partial y} = 0 \qquad (2.3\ a)$$

$$\frac{\partial \tau_{xy}}{\partial x} + \frac{\partial \sigma_y}{\partial y} = 0 \qquad (2.3\ b)$$

Using the strain-displacement relations (Eqs. 2.2), and assuming isotropic material, Hooke's Law can be written in terms of derivatives of displacement w:

$$\sigma_x = -\frac{E\,z}{1-\nu^2}\left[\frac{\partial^2 w}{\partial x^2} + \nu \frac{\partial^2 w}{\partial y^2}\right] \qquad (2.4\ a)$$

$$\sigma_y = -\frac{E\,z}{1-\nu^2}\left[\frac{\partial^2 w}{\partial y^2} + \nu \frac{\partial^2 w}{\partial x^2}\right] \qquad (2.4\ b)$$

$$\tau_{xy} = -2Gz\,\frac{\partial^2 w}{\partial x \partial y} \qquad (2.4\ c)$$

where: E = Modulus of Elasticity

G = Shear Modulus

ν = Poisson's Ratio

and G is related to E by

$$G = \frac{E}{2(1+\nu)} \qquad (2.5)$$

Stress resultants acting per unit width of the plate, as shown in Fig. 3, can be found by integrating appropriate stress components over the plate thickness:

$$M_x = \int_{-h/2}^{h/2} \sigma_x \, z \, dz \qquad (2.6\,a)$$

$$M_y = \int_{-h/2}^{h/2} \sigma_y \, z \, dz \qquad (2.6\,b)$$

$$M_{xy} = -\int_{-h/2}^{h/2} \tau_{xy} \, z \, dz \qquad (2.6\,c)$$

$$Q_x = \int_{-h/2}^{h/2} \tau_{xz} \, dz \qquad (2.6\,d)$$

$$Q_y = \int_{-h/2}^{h/2} \tau_{yz} \, dz \qquad (2.6\,e)$$

These equations can be easily integrated and lead to the well-known moment curvature relations:

$$\begin{bmatrix} M_x \\ M_y \\ M_{xy} \end{bmatrix} = \begin{bmatrix} D_{11} & D_{12} & 0 \\ D_{21} & D_{22} & 0 \\ 0 & 0 & D_{33} \end{bmatrix} \begin{bmatrix} \phi_x \\ \phi_y \\ \phi_{xy} \end{bmatrix} \qquad (2.7)$$

where: $D_{11} = D_{22} = Eh^3/12\,(1-\nu^2)$

$D_{12} = D_{21} = \nu\, D_{11}$

$D_{33} = (1 - \nu)\, D_{11}/2$

Defining the two vectors:

$$\{M\}^T = < M_x \quad M_y \quad M_{xy} > \tag{2.8 a}$$

$$\{\emptyset\}^T = < -\frac{\partial^2 w}{\partial x^2} \quad -\frac{\partial^2 w}{\partial y^2} \quad 2\frac{\partial^2 w}{\partial x \partial y} > \tag{2.8 b}$$

Eq. 2.7 can be written in compact form as

$$\{M\} = [D]\{\emptyset\} \tag{2.9}$$

2.2.2 The Differential Equation of Equilibrium

The fundamental equation of equilibrium is best derived by considering equilibrium of forces acting on an infinitesimal element of the continuum (Fig. 3). Summing up forces in z-direction yields:

$$\frac{\partial Q_x}{\partial x} + \frac{\partial Q_y}{\partial y} + q = 0 \tag{2.10}$$

Similarly, summation of forces about x-axis and y-axis, leads to

$$-\frac{\partial M_y}{\partial y} + \frac{\partial M_{xy}}{\partial x} + Q_y = 0 \tag{2.11}$$

$$\frac{\partial M_x}{\partial x} + \frac{\partial M_{yx}}{\partial y} - Q_x = 0 \tag{2.12}$$

Differentiating Eq. 2.11 and Eq. 2.12 and substituting the terms into Eq. 2.10 leads to the fundamental plate equilibrium equation in terms of moments:

$$\frac{\partial^2 M_x}{\partial x^2} + 2\frac{\partial^2 M_{xy}}{\partial x \partial y} + \frac{\partial^2 M_y}{\partial y^2} + q = 0 \qquad (2.13)$$

Finally, substitution of Eq. 2.9 into Eq. 2.13 yields

$$\frac{\partial^4 w}{\partial x^4} + 2\frac{\partial^4 w}{\partial x^2 \partial y^2} + \frac{\partial^4 w}{\partial y^4} - \frac{q}{D} = 0 \qquad (2.14\,a)$$

or

$$\nabla^4 w = \frac{q}{D} \qquad (2.14\,b)$$

2.3 Analysis of Plates Using the Finite Element Method

2.3.1 The Displacement Approach

The finite element technique is a relatively new, but very powerful, approach for the solution of engineering problems. The dominant reason for the extensive use of the finite element technique in solving structural problems is its great versatility and complete generality. In fact, the same basic procedure can be applied to structures of arbitrary shape, loading and boundary conditions. As a result, a single computer program can be used to solve a variety of problems.

The finite element concept, of which a comprehensive presentation is given in Reference 6, was developed by extending known matrix structural theories to two and three-dimensional solids. Argyris (Ref. 7) introduced the two fundamental methods of matrix structural analysis, the force and the displacement method of

analyses, in which a systematic approach to automatic computation of displacements and forces was first attempted. The work by Turner et al. (Ref. 8), which may be interpreted as the first major step in the development of the finite element method, describes the direct stiffness approach. In this approach, insight into the behavior of elements in representation of structures is achieved, and consideration is given directly to the condition of equilibrium and compatibility. However, in the treatment of refined elements the physical behavior is obscured due to the more complex behavior of such elements.

The first step in the displacement approach is to discretize a structure into a suitable number of finite elements. The behavior of the actual structure is assumed to be approximated by the behavior of the discretized structure; i.e. by an assemblage of finite elements having simple elastic properties and being connected so as to represent the actual continuum. For practical reasons, the geometry of the elements must be simple, but generally could be of any shape. The elements are assumed to be interconnected at their nodal points, and the displacements of these nodal points constitute the basic unknown parameters of a problem.

Displacement functions, often called shape functions, are then chosen for each element to uniquely define the state of deformation in terms of nodal values, which are referred to a global coordinate system. Elemental displacement fields should be continuous (single-valued), and should satisfy deformation

continuity within the element and along element interfaces. Consequently, the entire displacement field of the discretized structure is continuous, piecewise differentiable, and in addition, is restrained to satisfy displacement boundary constraints. The displacement field assumed for an element is called compatible if full continuity of deformation is achieved within the element, as well as along its boundaries. In this case, the chosen displacement function uniquely defines the state of strain within an element in terms of its nodal displacements. Hence, together with possible initial strains, these strains will define the state of stress throughout the element, and on its boundaries.

The loading acting upon the system is approximated by a set of equivalent concentrated nodal forces, again referred to a global coordinate system. These external forces should equilibrate the internal boundary stresses, distributed loads and forces due to initial strains. This requirement leads to the relationship between generalized displacements and associated generalized forces. The matrix relating these two vectors is called the element stiffness matrix. Its elements are a function of the geometric and elastic properties of the element.

At this stage, a finite element solution follows standard structural procedures as described in detail in a number of references (e.g. Ref. 9). By appropriate superposition of the individual element stiffness relations, the corresponding relationship for the entire structure can be established. In this process, the

requirements of compatibility and equilibrium must be satisfied. Any system of displacements listed for the entire structure automatically satisfies all compatibility requirements. Establishing equilibrium conditions at all nodes leads to the force-displacement relationship of the entire structure. For this purpose, the element stiffness matrices, connecting nodal displacements to nodal forces must be transformed to a common coordinate system or reference frame. The formulation of the overall structural stiffness matrix proceeds then by adding appropriate element stiffness contributions framing into a common node. This procedure leads to a system of linear algebraic equations.

Finally, all kinematic restraints have to be imposed, and the resulting system of equations must be solved simultaneously for the unknown nodal displacements. Clearly, the satisfaction of a minimum number of prescribed displacements to prevent rigid body displacements is mandatory; otherwise the displacements could not be determined uniquely. The structure stiffness matrix is usually well-conditioned, sparsely populated, and narrowly banded if adequate nodal numbering of nodal points is provided. These properties permit an efficient, automatic assembly and solution of large systems of simultaneous equations. Once the solution of the unknown displacements has been obtained, the determination of internal stresses, or stress resultants, is straightforward. The selection of displacement functions and the evaluation of the element stiffness matrix are the most important steps in the finite

element displacement approach and will be discussed in subsequent sections.

Early derivations of finite element force-displacement relationships made no reference to variational considerations. Only recent developments have shown that these methods also have a solid theoretical foundation. The basic principles of linear structural mechanics are the principle of minimum total potential energy and the principle of minimum complementary energy. These variational methods form the basis for the derivation of element stiffness equations. The principle of minimum total potential energy is stated as (Ref. 19):

> Of all compatible displacement fields satisfying given boundary conditions, those which satisfy also the equilibrium conditions make the total potential energy π assume a stationary value.
>
> $$\delta \pi = \delta (U + V) = 0 \qquad (2.15)$$
>
> where: U = Strain energy of deformation.
>
> V = Potential of external forces.

The stationary value of π is always a minimum, and therefore, a structure under a system of external loads represents a stable system. It can be shown (Ref. 10) that if the system of displacements is defined throughout the structure by the element displacement functions, with nodal parameters acting as undetermined parameters, then the procedure of minimizing the potential energy of

the system will result in precisely the same formulation as described above. This alternate approach of establishing stiffness equations shows that the finite element procedure is, in fact, identical with the Rayleigh-Ritz Approach.

In the finite element method the assumed displacement functions are associated with individual elements only. The displacements in the elements are uniquely defined in terms of the nodal point values, and the entire displacement field is assumed to consist of a number of piecewise continuous displacement fields each extending over the region of an element. Clearly, the finite element method, as well as the Ritz method, are approximate methods of analysis. However, if conforming elements are used, it can be shown that if the mesh size is gradually decreased, the solution tends toward the true solution; i.e. convergence is assured for a valid minimum potential energy approach. One can also show for this case that the strain energy is a lower bound, and the discretized structure is stiffer than the actual one if external loads are applied only.

2.3.2 Displacement Functions and Convergence Criteria

One of the most important steps in the finite element displacement approach is the selection of displacement functions which discretize the displacement field within an element. These assumed shape functions limit the infinite degrees of freedom of the system by expressing the deformation within a plate element in terms of displacement parameters at the nodal points. The accuracy obtained depends on the extent to which the assumed deformation

pattern can approximate the true displacement pattern. Generally, finer meshes lead to a closer approximation, although convergence is not necessarily assured if the displacement functions are not properly chosen.

So far, only limited attention has been given to the establishment of general rules for the selection of functional representations of element behavior. Recent research (Ref. 11) led to requirements for the assumed displacement functions in order to arrive at a convergent finite element solution.

As mentioned earlier, an approach based on a valid minimum potential energy solution assures monotonic convergence with decreasing mesh size. Melosh (Ref. 12) and Fraeijs de Veubeke (Ref. 13) set out specific conditions under which a valid minimum potential energy approach is preserved in a finite element formulation. One of the basic requirements for generating deformation consistent stiffness matrices is complete compatibility of displacement within the element and along its boundaries. Elements derived from such displacement fields are called compatible.

Melosh (Ref. 12) has shown that the selection of appropriate displacement fields can be accomplished by use of Langrangian or Hermitian interpolation techniques. The functions are chosen such that they become dependent only on the displacements of the end points, and additional points along a side of the element in consideration. Bogner et al. (Ref.14) used this approach to derive the stiffness matrix for a compatible rectangular plate element.

Another general method for the selection of functions directly in terms of degrees of freedom is the spline interpolation concept. This approach was developed by Birkhoff (Ref. 15) as a general mathematical procedure and employed by Pian (Ref. 16).

A third approach used successfully in the functional representation of a displacement field is the concept of isoparametric element formulation. The shape functions chosen to describe the element boundaries are identical to those used to prescribe the variation of the displacement function. Ergatoudis (Ref. 17) has pioneered this approach, and Zienkiewicz (Ref. 18) has applied it to generate stiffness matrices for different two- and three-dimensional elements.

Often these interpolation concepts are difficult to apply; then a function is chosen, as outlined in Section 2.3.1, in terms of unknown nodal displacement parameters. These are normally chosen equal in number to the number of degrees of freedom for the element in consideration, and can be evaluated from the enforcement of compatibility conditions at the element nodes. The choice of this function proved to be a major source of difficulty since an arbitrary choice may result in an unsatisfactory element displacement behavior, and as a consequence, may not lead to convergence. Thus, the question arises as to which requirements the assumed displacement function should satisfy in order that the associated finite element solution will converge toward the true solution as the mesh size is reduced. At present, the

view is held that the sufficient conditions for the derivation of deformation consistent stiffness matrices are as follows:

1. Internal and interface compatibility must be satisfied.
2. Displacement function must depend linearly on nodal parameters.
3. Proper representation of all rigid body displacement states is required.
4. All uniform states of strain must be included.
5. The displacement field must be spatially isotropic.

Requirement (1), as already discussed, leads to a valid minimum potential energy approach, and this, in turn, bounds the strain energy of the discretized structure. As a result, monotonic behavior is obtained if the mesh is subdivided into elements of the same type so that all previous displacement states are contained in the new ones. This condition, as postulated by Melosh (Ref. 12), is in fact a sufficient criteria for monotonic convergence. On the other hand, if all of the above given conditions are met, with the exception of requirement (1), then numerical evidence has shown that satisfactory convergence can still be achieved; though it cannot be proved anymore via the principle of minimum total potential energy.

Requirement (2) leads to the desired linear system of equations since linearly elastic material is assumed.

Requirement (3) is needed to include the conditions of global equilibrium. Self-straining would occur when the nodal displacements were caused by rigid body displacements. Hence, the presence of all rigid body motion terms in the selected displacement function is essential.

Requirement (4) is necessary for the convergence to the actual strain field. In fact, the exclusion of constant strain states could result in convergence toward an incorrect result. As the mesh size is decreased, nearly constant strain conditions will prevail in the element. If the condition is not met, such strain states could not be attained as the mesh size is reduced. Hence, it must be possible to represent constant curvatures in the case of pure plate bending. Conditions (3) and (4) are often referred to as completeness criterion. Furthermore, rigid body displacements are actually a particular case of the constant strain conditions, having zero values for strain.

Requirement (5) insures that the resulting generalized force-displacement relations are independent of the position of the global coordinate system. Hence, the chosen displacement functions must be independent of the particular shape of the element and the orientation of the element with respect to the coordinate system to which the functions are referred. Thus, attention should be given to requirement (5) when truncated polynomials are used as displacement functions.

Polynomial expressions have been used nearly exclusively

for the generation of different element stiffness matrices. First, this choice simplifies algebraic as well as automatic manipulations. Furthermore, polynomials satisfy the constant strain criteria and simplify the investigation of compatibility requirements. Complete polynomials also satisfy the invariance criterion.

A lower bound to the strain energy and monotonic convergence to the correct solution is obtained if conforming shape functions are used and the completeness criterion is satisfied. Oliveira (Ref. 11) proved that completeness and conformity are necessary but not sufficient criteria for convergence. According to Oliveira, completeness is the only requirement which the displacement function must meet to arrive at a convergent finite element solution. However, completeness does not necessarily lead to monotonic convergence.

Considerable difficulty is experienced, in some cases, to find fully compatible displacement functions. Non-conforming displacement functions will cause, in general, infinite strains at the element interfaces. Hence, only an approximation to the true strain energy is found since,in calculating the energy as in the usual finite element approach, no consideration is given to the contributions to energy at the lines of discontinuity. However, if for finer mesh sizes the extent of the discontinuity tends to vanish, then an incompatible formulation will lead to the correct result. Indeed, some finite element stiffness matrices derived from discontinuous displacement functions yield excellent results.

2.3.3 Alternate Approaches

Most of the finite element approaches developed to date are based on the principle of minimum total potential energy, as described in Section 2.3.1. However, an alternate procedure is possible if the functional to be minimized is the complementary energy of a system. The basis for such an approach is the principle of minimum complementary energy, which can be stated as follows (Ref. 19):

> Of all statically admissible stress states, i.e. satisfying equations of equilibrium and all boundary conditions on stresses, those which also satisfy the compatibility equations make the total complementary energy π^* assume a stationary value. It can be shown again that this value is a minimum.

$$\delta \pi^* = \delta (U^* + V) = 0 \qquad (2.16)$$

where: U^* = Complementary strain energy.

V = Potential of applied loads.

Therefore, it is possible to arrive at an alternate finite element formulation if, in place of a compatible displacement field, an admissible stress field is taken to define strains, and hence the complementary energy. In this context, a stress field is called conforming if it is in equilibrium within the element and balances all prescribed surface stresses. The stresses within the element are assumed in terms of stress functions which in turn are

expressed in terms of nodal parameters. The principle of minimum complementary energy is then applied to derive flexibility equations. Hence, the emphasis in this approach lies in the search for conforming stress fields.

Pioneered by DeVeubeke (Ref. 20), this approach is in general much more difficult since the search for equilibrium stress fields is more demanding than that of compatible displacement fields. It can be shown that this approach will give an upper bound of the strain energy and thus overestimates the displacements. If both the compatible displacement approach and the approach based on the principle of minimum complementary energy are taken, valuable bounds to the true displacements are obtained. The principle of minimum complementary energy has so far been applied to derive element stiffness matrices for simple elements in the elastic range. An extension of this formulation to arrive at flexibility equations for more complex elements is difficult since conforming stress fields are difficult to establish. An extension of this approach to elastic-plastic problems is not feasible since for a non-linear material behavior, the complementary energy does not provide for a reliable basis for the derivation of flexibility equations.

Besides these two basic formulations, a number of alternate avenues can be taken to establish stiffness or flexibility equations. A comprehensive study of such approaches is given in the survey by Pian and Tong (Ref. 21). For example, other functionals

could be selected, permitting the simultaneous variation of stresses and displacements together with assumptions made on both these quantities. Such approaches are called mixed formulations. In these methods, generally neither equilibrium nor compatibility is fully satisfied, and for this reason, convergence must be proven for each particular case.

2.3.4 Existing Rectangular Plate Bending Elements

During the last decade, much research effort has been devoted to determine reliable element stiffness matrices for various shapes of plate bending finite elements. Attention has been given to triangular, rectangular, and quadrilateral elements. Recent surveys of presently available triangular elements are given by Bell (Ref. 22) and Gallagher (Ref. 23). These surveys show that a variety of fine performing triangular elements are available.

Comparative studies have shown that rectangular elements show greater accuracy than triangular elements for the same number of degrees of freedom. In view of the refined rectangular plate element developed in this report, a short review of some published rectangular and quadrilateral plate elements is given in this section. It should be stated that in the case of plate bending, continuity of displacement throughout the plate element implies continuity of deflection and slopes, i.e. first derivatives of the lateral displacement w. Thus, both the deflection and the

slopes must be continuous within the element and across its boundaries in order to fully satisfy the conditions of displacement compatibility.

A survey of rectangular finite elements for plate bending is given by Clough and Tocher (Ref. 24). Various displacement functions have been used to develop the stiffness matrix for a rectangular plate element. Within the framework of Kirchhoff's plate bending theory, the deformations in a plate element are completely defined by the lateral deflection w. With this deflection and two rotations unknown at each nodal point, a rectangular element, as shown in Fig. 4, possesses twelve degrees of freedom.

One of the earliest functional representations for the deflection was suggested by Pappenfuss (Ref. 25):

$$w = (a_1 + a_2x + a_3x^2 + a_4x^3)\quad(b_1 + b_2y + b_3y^2 + b_4y^3) \quad (2.17)$$

It can be verified that this function satisfies interelement continuity of w, and the rigid body displacement modes are included. However, due to the absence of the term representing constant twist, the constant strain condition is not satisfied, and hence, convergence does not occur towards the correct solution.

In another early paper, Melosh (Ref. 26) derived a different plate bending stiffness matrix, on the basis of physical reasoning.

The simplest expression which has been used in deriving

DeVeubeke (Ref. 27) derived a compatible finite element by subdividing an arbitrary quadrilateral into four triangles and assuming a complete cubic polynomial displacement field within each triangle. Besides the four corner nodes, four midside nodes, with one degree of freedom at each of those nodes, were defined.

Clough and Felippa (Ref. 28) derived a compatible quadrilateral element having four corner nodes, only with three degrees of freedom each. It was built up from four triangles, and each of these triangles in turn consists of three subtriangles represented by a complete third order polynomial in w, the transverse displacement.

Of all the elements discussed so far, the last three approaches show the best results. In most of the available literature, the convergence of an element is judged by plotting the accuracy of the solution against the number of subdivisions for a problem in consideration. A more appropriate comparison would be to plot the accuracy versus the total number of degrees of freedom involved.

Little work has been done to date in the derivation of stiffness matrices based on the alternate approach of minimizing the total complementary energy. Efforts to accomplish formulations based on this functional or on Reissner's energy principle have been mainly concerned with the triangle. A number of mixed approaches however, have been advanced during recent times. In a paper by Pian (Ref. 29), a hybrid approach was developed in

the element stiffness matrix for a rectangular plate element, known as ACM element (Ref. 34), is the twelve term polynomial

$$w = a_1 + a_2x + a_3y + a_4xy + a_5x^2 + a_6y^2 + a_7xy^2 + a_8x^2y + a_9x^3 + a_{10}y^3 + a_{11}x^3y + a_{12}xy^3 \qquad (2.18)$$

It is noted first that the chosen function does not represent a complete polynomial. Geometric isotropy is maintained, due to the choice of the two fourth order terms. It is observed that the rigid body mode is included and constant strain states are allowed for in this expression. A test reveals that transverse displacements are interelement compatible, but the element lacks compatibility of normal slope. However, lack of satisfaction of interelement compatibility does not necessarily result in lack of convergence, due to this reason this functional representation yields relatively good accuracy in displacement but at the same time less accuracy in internal moments is obtained.

As an example of achieving interelement compatibility by means of the Hermitian interpolation concept, Bogner et al. (Ref. 14) developed a compatible rectangular plate element having four degrees of freedom at each nodal point. In addition to the usual displacement components w, $\partial w/\partial x$ and $\partial w/\partial y$, the twist $\partial^2 w/\partial x\partial y$ was introduced as an unknown displacement component. Numerical results indicate that in addition to exhibiting monotonic convergence, a good approximation of the displacement behavior was achieved; however, no results for internal moments are reported.

which stresses were selected within the element, and a displacement function was prescribed on the boundaries. A similar approach was undertaken by Severn and Taylor (Ref. 81) and generalized to the arbitrary quadrilateral by Allwood and Cornes (Ref. 30).

In summary, a number of rectangular or quadrilateral finite elements for plate bending analysis are presently in use. Most elements show good convergence for displacements towards the true solution. However, the rate of convergence does differ substantially for different elements. Moreover, despite acceptable accuracy for displacements, some elements show poor accuracy for internal moments.

2.4 A Refined Rectangular Plate Bending Element

2.4.1 Choice of Displacement Field

Investigations on triangular elements, using higher order polynomial approximations for the assumed shape functions, showed that the use of such expressions leads to improved accuracy on displacement and stresses. Similar investigations have not yet been made for rectangular elements. Hence, in this chapter the stiffness matrix for a refined rectangular plate bending element is derived and comparisons are made with some presently available rectangular and quadrilateral elements.

Refinements in a finite element approach can be achieved, for example, by a better approximation of the displacement field. In order to arrive at a valid variational formulation based on

minimum potential energy, certain continuities of the unknown function must be maintained. This allows the determination of the functional to be minimized, which will be unique. Thus, as was noted earlier, the deflection w and two slopes must be continuous for a plate bending problem. One can prove that, in this case, the solution will converge monotonically towards the correct solution. On the other hand, formulations based on deflection functions not satisfying compatibility of normal slopes along interelement boundaries will not necessarily show monotonic convergence as the mesh size is decreased. It is the basic thought of the present investigation that a refinement in element behavior can be achieved through the use of a higher order polynomial approximation of the displacement field.

Consider the rectangular finite element, shown in Fig. 4, along with the introduced local coordinate system with its origin located at the centroid of the element. The displacement components are assumed positive as shown. The basic unknowns in a plate bending problem are the lateral deflection w, the two slopes θ_x and θ_y, and the internal moments per unit length, defined in Eq. 2.6. For the present approach, at each node (i) of a finite element, the following generalized displacement components are introduced.

$$\{\delta_i\}^T = < w \quad \theta_x \quad \theta_y \quad \emptyset_x \quad \emptyset_y \quad \emptyset_{xy} > \tag{2.19}$$

where: w = $w(x,y)$ = lateral deflection in z-direction

θ_x = slope about x-axis

θ_y = slope about y-axis

ϕ_x = curvature of plate surface in x-direction

ϕ_y = curvature of plate surface in y-direction

ϕ_{xy} = twist of plate surface

Under the assumptions of the theory of thin plates, the slopes and curvatures can be expressed in terms of derivatives of the lateral deflection w, as follows:

$$\theta_x = \partial w/\partial y \qquad (2.20\ a)$$

$$\theta_y = -\partial w/\partial x \qquad (2.20\ b)$$

$$\phi_x = -\partial^2 w/\partial x^2 \qquad (2.20\ c)$$

$$\phi_y = -\partial^2 w/\partial y^2 \qquad (2.20\ d)$$

$$\phi_{xy} = \partial^2 w/\partial x \partial y \qquad (2.20\ e)$$

Element displacements can now be given as the listing of nodal displacements:

$$\{\delta^e\}^T = < \delta_i^T \quad \delta_j^T \quad \delta_k^T \quad \delta_l^T > \qquad (2.21)$$

Similarly, the element force vector is defined as:

$$\{F^e\}^T = < F_i^T \quad F_j^T \quad F_k^T \quad F_l^T > \qquad (2.22)$$

The six degrees of freedom introduced at each nodal point lead to a 24-degree-of-freedom element, and permit the choice of a higher order polynomial for the approximation of the displacement field. Using this improved field, it should be possible to approximate the actual displacement field more closely, resulting in an improvement in the accuracy and convergence. The presence of curvature terms in the vector of unknown nodal parameters should also allow certain types of boundary conditions to be satisfied more properly than can be done in the usual displacement approach, having w and its slopes as unknowns. The continuity requirements imposed on the curvature terms should especially improve the moment field since moments at all mesh points can be made continuous in this approach. Finally, since the internal moments are obtained directly by summing the appropriate curvature terms, they need not be computed separately. The chosen polynomial can be conveniently represented by Pascal's triangle, as shown in Fig. 5. Twenty-eight free constants are associated with this polynomial, i.e. one constant for each term. A completely conforming solution could be constructed by introducing additional nodes at each of the midsides of the rectangle and requiring that the normal slope be continuous at these points. Possessing the same number of known conditions as there are unknowns in this case, the interpolation problem could be solved uniquely. However, this approach is not taken here, since it would result in different degrees of freedom for different nodal points, and hence, complicate the assembly of the system stiffness

matrix. In addition, it would increase the band width of the resulting system of linear equations. It would however, result in a valid potential energy approach.

For the present approach, only twenty-four terms of the complete sixth-order polynomial are retained (the terms underlined in Pascal's triangle are omitted), since the deflection function for w can be defined in terms of these twenty-four parameters only. With geometric symmetry of the element, no preferential direction should exist. The terms with the highest even powers in x and y must be omitted in order to satisfy compatibility of w. Despite omitting these terms, geometric isotropy is retained. It will be seen later that the retention of inappropriate terms would result in a singular transformation matrix. Inspecting the chosen function, it is recognized that along any line of constant x or y coordinate, the displacement w varies as a fifth-order function. The element boundaries, for example, are composed of such lines. A fifth-order polynomial is uniquely defined by six constants. The two end values of deflection, slopes, and curvatures at the end points will therefore uniquely define the displacement along these boundaries. As such values are common to adjacent elements, continuity of w will result along all interfaces.

Furthermore, it can be seen that the gradient of w normal to any boundary varies as a fourth-order function. With only one slope and curvature term imposed at each of the two end points of a boundary line, this function is not uniquely specified, and hence,

discontinuity of the normal slope generally occurs. Clearly, the chosen displacement function is of the non-conforming type. However, it is evident that the completeness criterion is satisfied, since all rigid body displacement modes, as well as all constant curvatures, are included in the chosen functional representation.

For the sake of a simpler derivation, it is best to introduce at this point non-dimensionalized coordinates defined as:

$$\xi = \frac{x}{a} \quad \text{and} \quad \eta = \frac{y}{b} \tag{2.23}$$

The displacement field can then be written as:

$$\begin{aligned} w = w\ (x,y) = {} & \alpha_1 + \alpha_2\xi + \alpha_3\eta + \alpha_4\xi^2 + \alpha_5\xi\eta + \alpha_6\eta^2 + \alpha_7\xi^3 \\ & + \alpha_8\xi^2\eta + \alpha_9\xi\eta^2 + \alpha_{10}\eta^3 + \alpha_{11}\xi^4 + \alpha_{12}\xi^3\eta \\ & + \alpha_{13}\xi^2\eta^2 + \alpha_{14}\xi\eta^3 + \alpha_{15}\eta^4 + \alpha_{16}\xi^5 + \alpha_{17}\xi^4\eta \\ & + \alpha_{18}\xi^3\eta^2 + \alpha_{19}\xi^2\eta^3 + \alpha_{20}\xi\eta^4 + \alpha_{21}\eta^5 \\ & + \alpha_{22}\xi^5\eta + \alpha_{23}\xi^3\eta^3 + \alpha_{24}\xi\eta^5 \end{aligned} \tag{2.24}$$

Listing all polynomial terms in the row-vector

$$\langle P \rangle = \langle\ 1 \quad \xi \quad \eta \quad \xi^2 \quad \xi\eta \quad \eta^2 \quad \cdots\cdots \quad \xi\eta^5\ \rangle \tag{2.25}$$

Eq. 2.24 can be written as

$$w = w\ (x,y) = < 1 \quad \xi \quad \eta \quad \cdots \quad \xi\eta^5 > \begin{bmatrix} \alpha_1 \\ \alpha_2 \\ \vdots \\ \alpha_{24} \end{bmatrix} \tag{2.26 a}$$

or simply as

$$w = w\ (x,y) = < P > \ \{\alpha\} \tag{2.26 b}$$

The constants α_i, with i = 1, 2, ... 24 can be evaluated by establishing compatibility of deformation in displacement w, its slopes and curvatures at each of the four nodal points. The determination of these twenty-four generalized coordinates solves this interpolation problem in two dimensions.

First define a modified nodal displacement vector as:

$$\{\bar{\delta}_i\}^T = < w \quad b\theta_x \quad a\theta_y \quad a^2\emptyset_x \quad b^2\emptyset_y \quad ab\emptyset_{xy} > \tag{2.27 a}$$

or

$$\{\bar{\delta}_i\}^T = < w \quad b\frac{\partial w}{\partial y} \quad -a\frac{\partial w}{\partial x} \quad -a^2\frac{\partial^2 w}{\partial x^2} \quad -b^2\frac{\partial^2 w}{\partial y^2} \quad ab\frac{\partial^2 w}{\partial x \partial y} > \tag{2.27 b}$$

and similarly the corresponding modified element displacement vector

$$\{\bar{\delta}^e\}^T = < \bar{\delta}_i^T \quad \bar{\delta}_j^T \quad \bar{\delta}_k^T \quad \bar{\delta}_l^T > \tag{2.28}$$

After the enforcement of compatibility of deformation, the twenty-four equations in matrix form will be listed as:

$$\{\bar{\delta}^e\} = [\bar{C}]\ \{\alpha\} \tag{2.29}$$

where $[\bar{C}]$ is a square matrix of size 24 x 24, consisting of numbers only. This non-symmetric and fully populated transformation matrix can conveniently be inverted in a digital computer, and the unknown vector of generalized coordinates can be found from

$$\{\alpha\} = [\bar{C}]^{-1}\ \{\bar{\delta}^e\} \tag{2.30}$$

The inverse of matrix $[\bar{C}]$ remains the same for all elements involved in the analysis and must be evaluated only once. The value of the determinant of this matrix is a measure of how well this matrix is conditioned. No complications in the inversion process occur if the absolute value of the determinant is large. In fact, this was found to be so, underlining the importance of the choice of appropriate terms in a truncated polynomial expression. A bad choice could, in fact, lead to a singular matrix $[\bar{C}]$ and would thus complicate the inversion.

The unknowns in the final solution are listed in the originally defined nodal displacement vector; this vector being related to the modified nodal displacement vector by

$$\{\bar{\delta}^e\} = [T_1]\ \{\delta^e\}$$

where the transformation matrix $[T_1]$ is a diagonal matrix composed of four diagonal submatrices of the form

$$[T_1] = \begin{bmatrix} 1 & 0 & 0 & 0 & 0 & 0 \\ 0 & b & 0 & 0 & 0 & 0 \\ 0 & 0 & a & 0 & 0 & 0 \\ 0 & 0 & 0 & -a^2 & 0 & 0 \\ 0 & 0 & 0 & 0 & -b^2 & 0 \\ 0 & 0 & 0 & 0 & 0 & ab \end{bmatrix} \qquad (2.32)$$

The vector of generalized coordinates can therefore be found by the relationship

$$\{\alpha\} = [\bar{C}]^{-1} \; [T_1] \; \{\delta^e\} \qquad (2.33\,a)$$

or

$$\{\alpha\} = [C]^{-1} \; \{\delta^e\} \qquad (2.33\,b)$$

The transformation matrix $[T_1]$ being sparsely populated, the matrix product in Eq. 2.33 a can be evaluated in an efficient way. It is now possible to write the function describing the displacement within an element in terms of the nodal displacement components

$$w = w\,(x,y) = \langle P \rangle \; \{\alpha\} = \langle P \rangle \; [C]^{-1} \; \{\delta^e\} \qquad (2.34)$$

2.4.2 Derivation of Element Stiffness Matrices

In this section, the element stiffness matrix for the proposed refined element is generated. The derivation is valid for small strains and rotations; i.e. the linearized form of the strain-displacement equations is assumed to be valid.

For the purpose of a plate analysis, it is simplest to define the curvatures as generalized strains. In order to

properly evaluate the internal work in the determination of the strain energy, a factor of two must be added to the twisting curvature. This in turn allows the retention of the twisting moment M_{xy} only in the analysis, since M_{yx} is numerically identical. The curvatures are related to the lateral displacement by Eq. 2.20. As introduced in Section 2.2.1, and defined in Eq. 2.8 b, the vector of generalized strains can be written as:

$$\{\emptyset\}^T = < -\frac{\partial^2 w}{\partial x^2} \quad -\frac{\partial^2 w}{\partial y^2} \quad 2\frac{\partial^2 w}{\partial x \partial y} >$$

and the corresponding vector of generalized stresses (Eq. 2.8 a) as

$$\{M\}^T = < M_x \quad M_y \quad M_{xy} >$$

The vector of generalized strains must be related to the joint displacements. This vector can be written in terms of generalized coordinates by simply evaluating all needed derivatives:

$$\{\emptyset\} = [Q] \quad \{\alpha\} \tag{2.35}$$

Using Eq. 2.34, it follows immediately that

$$\{\emptyset\} = [Q] \quad [C]^{-1} \quad \{\delta^e\} = [B] \quad \{\delta^e\} \tag{2.36}$$

One of the essential features in a finite element displacement approach is the definition of the displacement field for the purpose of establishing this fundamental relationship.

Examining matrix [Q], it is of interest to note that the chosen displacement function permits a state of constant curvatures to exist, and hence, satisfies the criterion of constant strain, stated in Section 2.3.2.

The constitutive law for a linearly elastic material, already introduced in Section 2.2.1, is generally written in the form

$$\{M\} = [D] \quad \{\emptyset\} \tag{2.37}$$

where [D] is a symmetric elasticity matrix, relating generalized stresses (in this case, internal moments) to generalized strains (in this case, curvatures). For a general anisotropic material, matrix [D] is fully populated, and of the form

$$[D] = \begin{bmatrix} D_{11} & D_{12} & D_{13} \\ D_{21} & D_{22} & D_{23} \\ D_{31} & D_{32} & D_{33} \end{bmatrix} \tag{2.38 a}$$

Six constants at most are needed, since matrix [D] is always symmetric, i.e.

$$D_{ij} = D_{ji} \quad \text{for } i \neq j$$

Isotropic materials are characterized by only two constants, E and ν,

where E = Modulus of elasticity of plate material

ν = Poisson's ratio

Thus, for an isotropic material, matrix [D] will reduce to

$$[D] = \frac{Eh^3}{12(1-\nu^2)} \begin{bmatrix} 1 & \nu & 0 \\ \nu & 1 & 0 \\ 0 & 0 & \frac{1-\nu}{2} \end{bmatrix} \qquad (2.38\,b)$$

In this expression, h denotes the plate thickness. For an orthotropic plate material, with principal axis of orthotropy coinciding with the x and y axis of the local coordinate system, four constants are needed to define the behavior of the plate, i.e.

$$[D] = \begin{bmatrix} D_x & D_1 & 0 \\ D_1 & D_y & 0 \\ 0 & 0 & D_{xy} \end{bmatrix} \qquad (2.38\,c)$$

As shown in greater detail in Appendix I, the application of the principle of minimum total potential energy leads to the derivation of the element stiffness matrix:

$$[K^e] = \iint_A [B]^T [D] [B] \, dxdy \qquad (2.39)$$

Substituting Eq. 2.36 into the above equation yields

$$[K^e] = [C^{-1}]^T \left(\iint_A [Q]^T [D] [Q] \, dxdy \right) [C^{-1}] \qquad (2.40)$$

In the above formula, the integration is to be carried out over area A of the finite element. The introduction of non-dimensionalized

coordinates leads to a particularly simple integration. This integration could in fact be carried out automatically due to the simplicity of the terms to be integrated. The integration was performed algebraically, considering one term of the elasticity matrix [D] at a time. The matrices within the integration can easily be multiplied out and integrated without difficulty. This operation leads to the final expression for the stiffness matrix of the refined rectangular plate element. Assuming orthotropic material it can be written as:

$$[K^e] = [C^{-1}]^T \left[D_x [K_1] + D_1 [K_2] + D_y [K_3] + D_{xy} [K_4] \right] [C^{-1}] \quad (2.41)$$

This derivation is described in more detail in Appendix I, where the component matrices $[K_i]$, $i = 1, 2, 3, 4$, are listed.

The final evaluation of the element stiffness matrix, which is of size 24 x 24, is performed in the digital computer. It should be noted that the component matrices $[K_i]$, $i = 1, 2, 3, 4$, are sparsely populated, and if made use of in the actual computations, this property would reduce the time required for the generation of the element stiffness matrix. Furthermore, use can be made of the fact that all component matrices are symmetric.

The resulting element stiffness matrix generated is a symmetric, square and singular matrix. Its singularity stems from the fact that rigid body displacements are included in the assumed displacement function, as given by Eq. 2.24. Enforcing known

boundary conditions, these rigid body modes will be eliminated after the formulation of the overall stiffness matrix.

The system stiffness matrix can be assembled as described in Section 2.3.1. The element stiffness matrix, as derived above, is referred to the local coordinate system. The first step in the assembly procedure would be to transfer this relation to a global or reference coordinate system. However, in the present investigation the local coordinate system is always parallel to the global coordinate system, therefore the stiffness relations established need not be transformed. The formation of the complete stiffness matrix for the discretized plate structure is finally accomplished by the direct addition of appropriate element stiffnesses at nodal points.

2.4.3 Kinematically Consistent Force Vectors

Applied loads are usually distributed on structural elements. Equivalent concentrated forces, at the location and in the direction of the global or reference coordinate system, are required for the analysis. In addition, concentrated forces may be applied at points other than nodal points of an element, and forces caused by initial strain conditions need to be considered. The latter may be caused by temperature, shrinkage, or lack of fit. Considering all of these contributions, the basic stiffness equation for an element can be cast into the form

$$\{R\}^e = [K^e]\ \{\delta^e\} + \{F\}^e_p + \{F\}^e_c + \{F\}^e_i \qquad (2.42)$$

where: $\{R\}^e$ = Vector of external forces applied at the nodes

$\{F\}_p^e$ = Nodal forces required to balance distributed loads

$\{F\}_c^e$ = Nodal forces required to balance concentrated forces acting within an element

$\{F\}_i^e$ = Nodal forces required to balance initial strains caused by temperature, lack of fit, etc.

The final system of simultaneous equations is obtained by establishing equilibrium at all nodal points. Each external force component must be equated to the sum of the component forces contributed by the elements meeting at the node in consideration. All forces can be collected and the final equilibrium equation can be written in the form:

$$\{F\} = [K] \{\delta\} \tag{2.43}$$

where: $\{\delta\}$ = Overall systems displacement vector

$\{F\}$ = Resultant systems force vector consistent with the overall displacement vector

$[K]$ = Overall structural stiffness matrix

For all common loading conditions, the equivalent concentrated nodal forces can be determined from an energy approach which is consistent with the evaluation of the element stiffness matrix. For example, for distributed loads $p(x,y)$, defined as acting on

a unit area of the element, this derivation leads to the following equivalent nodal force vector

$$\{F\}_p^e = -[C^{-1}]^T \iint_A \langle P \rangle^T \, p(x,y) \, dxdy \qquad (2.44)$$

This vector is listed in Appendix II along with a more detailed description of the derivation.

2.4.4 Enforcement of Boundary Conditions

The system of linear simultaneous equations represented by Eq. 2.43 can only be solved after sufficient boundary conditions are prescribed. The equation includes the rigid body displacements of the structure. Therefore, a minimum number of prescribed displacements must be substituted in the equation. The number of kinematic restraints prescribed is usually far greater than the number required to prevent rigid body motions. These constraints can be imposed by deleting appropriate rows and columns of the system stiffness matrix. This constitutes a relatively cumbersome and time consuming procedure for an automatic computation, though it results in a reduction of the total number of equations.

This investigation uses a more convenient approach, proceeding with a direct solution of the original number of equations to avoid rearranging of rows and columns. In this approach, the diagonal element of the system stiffness matrix, at the point concerned, is multiplied by a very large number. At the same time the term on the left-hand side of the equation, i.e. the element

of the global force vector at the point concerned, is replaced by the same large number multiplied by the prescribed displacement value. The effect of these manipulations is to replace the original equation by one which states that the displacement in question is equal to the specified displacement. This procedure of enforcing boundary conditions is easily implemented in a general computer program, and all programs described in this report operate successfully, using this approach.

The deformed shape of a plate structure must be found in such a way that all boundary conditions adhering to a problem under consideration are satisfied. In a finite element displacement approach, such restraints can be at the selected nodal points only, since only the deformation components at the nodes are entered as field quantities. Boundary conditions in plate bending problems usually include both the force (or static) and displacement (or kinematic) types. Only displacement type boundary conditions, i.e. restraints which can be expressed in terms of displacement components, can usually be satisfied in a pure finite element displacement approach. However due to the fact that in the present approach the three curvature terms are included in the final displacement vector, certain types of plate boundary conditions can be approximated more closely if the plate is made of isotropic or orthotropic material.

Some common boundary conditions to be satisfied in a plate problem, along with the associated constraint equations, are listed in Fig. 6. The top half of the figure lists the boundary

conditions as introduced in conventional plate theory. As derived in Section 2.2.1, the internal moments are linear combinations of the curvatures of w. The introduction of the curvatures as nodal parameters also makes it possible to exactly satisfy some static boundary conditions. If the boundary conditions of a simply supported plate are considered (Fig. 6) the classical theory of thin plates requires the following boundary conditions to be satisfied, at x = a

$$w = 0 \tag{2.44 a}$$

$$\theta_x = \frac{\partial w}{\partial y} = 0 \tag{2.44 b}$$

$$M_x = - D \left(\frac{\partial^2 w}{\partial x^2} + \nu \frac{\partial^2 w}{\partial y^2}\right) = 0 \tag{2.44 c}$$

A conventionally formulated displacement approach will not satisfy Eq. 2.44 c, called the static boundary condition. However, from the geometry of the deformed plate surface, it is known that

$$\frac{\partial^2 w}{\partial y^2} = 0 \tag{2.45 a}$$

along the straight and simply supported edge at x = a. From a consideration of the static boundary condition (Eq. 2.44 c) it can be concluded that the following equation will also hold

$$\frac{\partial^2 w}{\partial x^2} = 0 \tag{2.45 b}$$

Therefore, the proposed approach allows all boundary conditions

associated with a simply supported edge to be satisfied exactly. This conclusion is only valid if no externally applied moments are acting along the boundary under consideration.

Similarly, the boundary conditions associated with a clamped edge can also be satisfied exactly, as this can be done in the conventional displacement approach where only displacement-type boundary conditions are to be met.

The boundary conditions for a free edge are due to Kirchhoff (Ref. 3), and are listed in the classical theory as follows:

$$V_x = Q_x - \frac{\partial M_{xy}}{\partial y} = 0 \qquad (2.46\ a)$$

$$\frac{\partial^3 w}{\partial x^3} + (2 - \nu) \frac{\partial^3 w}{\partial y^2} = 0 \qquad (2.46\ b)$$

and

$$M_x = 0 \qquad (2.47\ a)$$

or

$$\frac{\partial^2 w}{\partial x^2} + \nu \frac{\partial^2 w}{\partial y^2} = 0 \qquad (2.47\ b)$$

The condition for zero vertical reaction at the free edge cannot be satisfied since in the present approach it is not possible to express this quantity in terms of nodal parameters. This is due to the fact that no third order derivatives are listed in the vector of unknown nodal displacement components. The requirement of zero normal moment could be satisfied exactly if, instead of the curvature

terms, their linear combinations, i.e. internal moments, would be introduced in the displacement vector. However, since the case of a free edge is relatively rare, no effort was made in this investigation to arrive at a more refined approach for satisfying this particular boundary condition.

2.4.5 Solution of the Stiffness Equations

The displacement approach as described in Section 2.3.1, and in more detail in Ref. 31, leads very often to a large system of linear simultaneous equations. In this set, the structure stiffness matrix connects the known vector of generalized forces to the unknown vector of generalized displacements. This matrix is always positive definite and symmetric for a linear elastic analysis. In addition, the stiffness matrix is usually well-conditioned and sparsely populated, and with adequate arrangement of the equations narrowly banded. These properties permit a very efficient, automatic assembly and solution of large systems.

The time required for the solution of the set of simultaneous equations is the single most important expense in solving large scale problems. Hence, the availability of an efficient solution technique is of upmost importance in solving elastic, and especially elastic-plastic, problems.

There are two fundamental groups of methods for solving linear algebraic equations, the methods of iteration or relaxation, and methods based on elimination. The main advantages of iterative

solution techniques are the relatively easy coding of such methods and the small amount of computer storage required. Solutions can be obtained with reasonable computer time if the governing system of equations is well-conditioned. The latter requirement is not always met and considerable difficulties may be experienced in solving large ill-conditioned systems. Though these methods can be efficiently applied in the solution of linear elastic problems, their application in solving elastic-plastic problems is doubtful due to the fact that the initially elastic and diagonally dominant system can become ill-conditioned at latter stages following extensive plastic flow. At such a stage, the diagonal elements of the stiffness matrix become small compared to the off-diagonal elements. For this reason, iterative or relaxation methods can become inefficient in solving elastic-plastic problems. In addition, elastic-plastic procedures require the solution of the stiffness equations in incremental form if the complete load-deflection behavior of a structure is sought. Each step, in turn, requires an iterative solution technique itself, and hence, the entire analysis would become too time-consuming. Furthermore, iterative methods do not allow multiple load vectors to be processed simultaneously. This is a serious drawback in the elastic analysis of structures subjected to many different loading conditions.

On the other hand, elimination methods do not require a well-conditioned system; only the number of equations to be solved and the bandwidth of the system are important. These methods do,

however, require larger amounts of computer storage. The Choleski decomposition method is among the most efficient and accurate elimination methods. This method was chosen as basis for the solution of the resulting set of stiffness equations, for all the analyses presented in this report. The key to this method is the fact that any symmetric square matrix can be expressed as the product of an upper and a lower triangular square matrix. Hence, it is possible to decompose the symmetric and banded structure stiffness matrix [K] into the product of a triangular matrix [L] and its transpose $[L]^T$, as shown in Fig. 7. This can be written as:

$$[K] = [L] \quad [L]^T \tag{2.48}$$

in which the terms $L_{ij} = 0$ for $i < j$, and $L_{ij}^T = 0$ for $i > j$. Hence, the first step in this approach is to decompose matrix [K] into these two component matrices. It is observed that both of these matrices are also of banded nature with a bandwidth which is equal to half the bandwidth of the system stiffness matrix. Considering the special coordinate system introduced, the elements of [L] can be obtained by simple recursive relations. It is further noted that in order to calculate column j of [L], only the elements in the shaded triangular area, as shown in Fig. 7, and the elements of column number j of the original matrix [K] are required. The fundamental stiffness equation, Eq. 2.43, can now be written in the form:

$$[L] \quad [L]^T \quad \{\delta\} = \{F\} \tag{2.49}$$

Introducing an auxiliary vector, defined as:

$$\{Y\} = [L]^T \{\delta\} \tag{2.50}$$

the stiffness equation can be written as

$$[L] \{Y\} = \{F\} \tag{2.51}$$

The solution of the original stiffness equation is accomplished in two steps: first vector $\{Y\}$ is found by a forward sweep, and the unknown vector $\{\delta\}$ is finally determined by backward substitution of $\{Y\}$ into Eq. 2.50.

The fact that only a small part of the overall matrix is used at any time during processing is of considerable importance in the development of finite element programs capable of handling structures involving many thousands of degrees of freedom. In order to save on core storage, the stiffness matrix is generated in blocks in the present approach, and the information is transferred to magnetic disc storage. The efficient use of the OVERLAY feature and of magnetic discs allows large scale problems to be treated using relatively little computer storage. A subroutine, capable of handling large banded systems of simultaneous equations was developed, based on the above described decomposition technique. The amount of information needed for processing at any time can be adjusted, and is called from discs accordingly.

The analyzed examples show that the described direct elimination technique is very efficient and accurate. The fact

that multiple load vectors can be processed at the same time, allows complex structures to be analyzed for different loading conditions in a very efficient way. Provided the bandwidth is not excessive, this method also proved to be very powerful for the elastic-plastic analysis of plates, as described in a subsequent section.

It should be noted in this context that for a large bandwidth, the described method, which operates on all elements within the band, may require considerable computer time. Improved solution routines, processing non-zero elements or submatrices only, have been developed in recent years. Whetstone (Ref. 32) presented recently a method which virtually eliminates both trivial arithmetic and wasted data storage space. Melosh (Ref. 33) describes a solution algorithm based on the wavefront concept and a modified Gauss algorithm.

According to these authors, such approaches can treat larger problems than bandwidth programs, involve negligible penalities, and at the same time, yield more accurate solutions than approaches using the Choleski algorith. However, such approaches clearly involve years of intensive research, and hence, were not possible to accomplish within the framework of this investigation.

2.5 Examples of Solution

2.5.1 Selected Examples

The following examples have been selected to illustrate

the application of the derived refined finite element, and to discuss its rate of convergence and accuracy. To simplify the comparison with analytic solutions, isotropic material is assumed and only simple examples are chosen. It should be noted here that the general computer program developed is capable of handling plates of arbitrary geometry, as defined in Section 2.1, and orthotropic material can be treated.

Four example problems, schematically represented in Fig. 8, have been selected in this investigation. For all problems, four different meshes, as shown in Fig. 9, were processed with the mentioned digital computer program, using the derived refined element as the basic element. Making use of symmetry, only one quadrant of each problem was analyzed. All structures were subjected either to a uniformly distributed load, or a single concentrated load acting at the center of the plate. The equilibrium equations were solved using the very efficient solution technique described in Section 2.4.5. All runs were processed in the CDC 6400 computer of the Lehigh University Computing Center.

In a first example (Problem P1), a square isotropic plate with four fully fixed boundaries was discretized using the four meshes shown in Fig. 9. The boundary conditions, as described in Section 2.4.4, can be satisfied exactly for this example. Poisson's ratio was assumed to be $\nu = 0.30$.

Problem P2 represents the analysis of a simply supported square isotropic plate. Again all boundary conditions can be

satisfied exactly, and the same value for ν was assumed as in Problem P1.

In a third example (Problem P3), a panel of a plate supported by rows of equidistant columns (flat plate) was analyzed. In order to be able to compare with available solutions, a value of $\nu = 0.20$ was chosen for this example. All boundary conditions can be deduced from the geometry of the deflected surface and can be satisfied exactly. To simplify this problem, it was assumed that the cross-sectional dimensions of the columns were small in comparison to the span of the plate panel, and could be neglected in so far as deflection and moments at the center of the plate are concerned. Timoshenko (Ref. 3) has discussed in length the implication of this assumption. However, the dimensions of the columns could be easily included in the analysis.

The fourth example (Problem P4) is a square isotropic plate supported by columns at the corners only. As discussed in Section 2.4.4, the boundary conditions for free edges cannot be satisfied exactly by the presented finite element approach. This example was chosen to study the effect of this deficiency. No exact solution to this problem is available, though various experimental and approximate solutions are known.

2.5.2 Accuracy and Convergence of Solutions

The plate geometry and the finite element idealization of the selected examples are shown in Fig. 8 and Fig. 9,

respectively. For the four problems, Tables 1, 2, and 3 list in sequence, the computed center deflection for both loading cases, along with some results found from existing plate elements and the exact values, where available (Ref. 3). Excellent accuracy and convergence is observed for both loading cases. The complete deflection profiles along a center-line of the plate together with exact values, are given in Table 4 for uniformly distributed loading and in Table 5 for the case of a single concentrated load. Exact values were found by evaluating the series solutions derived in Ref. 1 at all points of interest. Good agreement of displacements is apparent, as the convergence is fast and monotonic.

Tables 6 through 9 list the computed internal moments M_x and M_y along a center-line of the plate, together with exact values, where available. It can be seen that even for relatively rough meshes, the computed values for internal moments show good accuracy. Finally, Table 10 shows the internal twisting moment along a diagonal of the plate for the case of uniformly distributed load. From the results found, it is evident that excellent accuracy for displacements and internal moments is obtained with the refined plate element.

In order to study the effect of the enforcement of boundary conditions, as discussed in Section 2.4.4, a number of comparisons have been made. For the purpose of these comparisons the following types of boundary conditions can be defined:

Type I: Only displacement type boundary conditions associated with w, $\partial w/\partial x$ and $\partial w/\partial y$ are enforced.

Type II: In addition to the constraints of Type I, curvature terms derived from a knowledge of the geometry of the deflected surface are enforced.

Type III: In addition to the constraints of Type II, curvature terms derived from static considerations are enforced.

Tables 11 and 12 list, in part, the results of this investigation. In the conventional finite element displacement formulation, which is based on three degrees of freedom per node, i.e. on deflection w and its first derivatives, only boundary conditions of Type I can be satisfied. The present formulation also allows the enforcement of boundary conditions of the Types II and III. Comparing the computed values for the center deflection of problems P1 and P2 for the different types of boundary conditions enforced, it can be stated that if boundary conditions of Types II and III are enforced, then the structures tend to become stiffer. However, for finer meshes no difference can be recognized, thus leading to the conclusion that the imposition of additional curvature constraints does not improve the computed center deflection. As can be seen from Tables 13 and 14, in which results from this investigation for internal moments are compiled, the imposition of additional curvature terms does, however, improve the moment field, especially in the vicinity of the boundaries.

2.5.3 Comparison with Existing Plate Elements

Results found in the literature for the different elements discussed in Section 2.3.4, are compiled in Tables 1, 2, and 3. Internal moments are mostly reported in the form of graphs, thus lacking the numerical accuracy needed for an exact comparison. Hence, in order to be able to compare the results obtained with the refined plate element, missing internal moments were found for the ACM (Ref. 34) element in particular, using an auxiliary finite element plate program.

A direct comparison of the different finite elements used in the examples, in terms of mesh size, is not appropriate, since the computational effort is different for different elements and meshes. Most results available in the literature are listed separately for each mesh, and hence Tables 1, 2, and 3 were set up for reference only.

In a finite element approach involving fine meshes, the major part of the computer time required is used for the solution of the typically large system of simultaneous equations. Hence, a more reasonable way of comparing the results is to plot the percentage error in deflection or internal moment against the number of degrees of freedom; the solution time being directly proportional to this number in the proposed decomposition technique. The total number of degrees of freedom is defined here as the number of nodal points involved in the analysis, times the number of degrees of freedom per nodal point.

In Figs. 10, 11, 12, and 13 the percentage error in central deflection is plotted against the number of degrees of freedom of a problem for different finite elements for plate bending. Clearly, the new element shows improved results over most other elements at a given number of degrees of freedom. Similarly, in Figs. 14 and 15, the percentage error in internal moments is plotted against the total number of degrees of freedom.

As already pointed out in Section 2.3.4, existing plate elements are deficient because they are not capable of predicting internal moments with sufficient accuracy, unless very fine mesh idealizations are used. It may be added that the evaluation of internal moments using some of these elements represents a significant computational effort. As shown in the above-cited figures, the refined element is capable of determining reliable internal moment values even for relatively rough meshes, thus confirming one of the basic ideas for the derivation of this element.

An even better index for comparison would be the time of the computational effort needed for the entire solution of larger sized problems. In fact, the computer time needed to generate the element stiffness matrices, to assemble the system stiffness matrix, to generate force vectors, to solve the resulting large system of simultaneous equations, and finally, to find all internal moments would be a better measure for the discussion of the relative merits of different proposed elements.

2.6 Summary

A refined rectangular plate element for use in a finite element analysis of arbitrarily shaped plates is presented. Along with the three usual nodal displacements, three curvature terms are entered as unknowns in the vector of generalized displacements. Results found for four example solutions indicate that the refined element gives very good accuracy for displacements as well as for internal moments. The new approach, though of a non-conforming type, leads to a better accuracy at any given number of degrees of freedom than obtained with most presently known rectangular or quadrilateral finite elements.

3. ELASTIC ANALYSIS OF STIFFENED PLATES

3.1 Introduction

In this chapter, an analysis of complex shaped stiffened plates, as shown in Fig. 16, using the finite element stiffness approach is presented. Some of the currently used approximate analysis techniques applicable to beam-slab type structures are discussed. This survey of available methods of analysis shows that there is as yet no fully adequate method of analysis capable of determining stresses and deformations in complex shaped beam-slab type structures.

It is shown that a stiffened plate structure can adequately be discretized using plate and stiffener elements. Stiffness matrices for bending and in-plane behavior are derived for the beam and plate elements. A new approach for the evaluation of the St. Venant torsional constant is presented, and the stiffness relations associated with torsion in the stiffener elements are derived. Also discussed are the assembly of the stiffness matrix and the solution of the final set of equilibrium equations.

The outlined approach is applied to the analysis of a beam-slab highway bridge which was field tested. An extensive study of the effects of the variables governing the lateral load distribution is made, demonstrating the applicability and versatility of the proposed approach. The inclusion of curb and parapet sections, as well as diaphragms, in the analysis is discussed. Finally,

convergence and accuracy of the method are studied.

3.2 Methods of Analysis for Stiffened Plate Structures

A structural analysis is performed in order to determine stresses and deformations at selected points of a structure which is subjected to external forces, or constraint to deform, in a prescribed pattern. In this section, a short survey of some available methods of analysis of plate-beam type structures is given. A complete survey of the state of the art of current grillage design was made by Kerfoot and Ostapenko (Ref. 36).

For a beam-slab type structure, an elastic analysis can be formulated by combining the classical beam and plate theories. As is usually done in continuum mechanics, the equations of equilibrium and compatibility, together with the stress-strain relations, could be used to develop a set of partial differential equations for deformations or stresses at every point of the structure. However, the exact solution of these equations is virtually impossible for complex shaped structures, because of the task of determining suitable solution functions which satisfy both the governing differential equations and the specified boundary conditions. The assumptions introduced in the theory of plates and the conventional beam theory allow for a reduction in the number of independent variables and make certain boundary conditions more tractable. These assumptions of the conventional plate theory which are applicable to thin plates are listed in Section 2.2.

In classical beam theory it is assumed that all deformations can be described in terms of the displacements of the longitudinal axis and the rotation of the beam cross-section. The latter assumption precludes a deformation of the cross-section, and hence, strains normal to the longitudinal axis are neglected. Formulating equilibrium of a beam element leads to a set of three differential equations.

Conceptually at least, plate and beam theories can be directly applied to the analysis of stiffened plate type structures. For this purpose, different physical models are used to represent the beam-slab type structure. These models are highly redundant. The compatibility and the load-deformation behavior of the elements of the models must be taken into account to develop the additional requirements beyond those obtained from static equilibrium in order to determine the response of the assumed model. A force or deformation method of analysis is usually applied to solve for the unknown quantities. However, by inspecting the resulting partial differential equations it can be recognized that these equations are not readily solvable for other than simple structures.

Often the effective width concept is utilized to reduce the analysis of stiffened plates to the analysis of the stiffeners. This approach assumes that the stiffeners behave as beams, the flanges of which are made up of some portion of the slab. The portion of the plate assumed to act effectively as a flange of the

beam is called the effective width of that cross section, and is often assumed to be constant along the length of the beam. This concept is used in most methods of analysis in which the structure is treated as an open grid or as an orthotropic plate. The effective width concept can be used to advantage in an analysis performed to determine stresses in the beams of a beam-slab type structure, but it has little merit when plate stresses are of interest. Furthermore, the effective width is not constant along the length of the stiffeners and depends on the specified boundary conditions and the distribution of applied loads.

A common method of analysis is to replace the beam-plate structure by an equivalent gridwork. The resulting structure is a framework of intersecting bars, and the stiffnesses are adjusted to approximate those of the slab and girders. The works of Lightfoot and Sawko (Ref. 37), Hendry and Jaeger (Ref. 38) are examples of this approach. Frequently, the torsional resistance of the stiffeners is neglected and the effective width is always assumed to be constant along the stiffeners. A force or deformation method of analysis is usually applied to determine the unknown stresses or deformations in the resultant highly indeterminate structure. Clarkson (Ref. 39) has presented an example of the application of the force method to the analysis of grillages under transverse loads, neglecting the effects of torsion and shear. The same author (Ref. 39) also used the deformation method of analysis to analyze transversely loaded grillages, taking into account the

effects of shear and St. Venant torsion. In a similar approach, Lightfoot and Sawko (Ref. 37) analyzed transversely loaded grillages, neglecting the shearing deformations. In addition, a number of approximate methods have been proposed, each necessitating a number of additional assumptions and thus reducing the scope of applicability of such methods. Although these methods are apparently adequate for determining the bending moments in the beams under transverse loading, their range of applicability is restricted to simple geometry. Furthermore, these methods cannot be used directly to accurately predict the stresses in the plate of such a structure.

Since the structural behavior of some grillages is similar to that of a plate, approaches have been proposed using orthotropic plate theory in the analysis of grillages. Here, the stiffness of the plate and beams are lumped into an orthotropic plate of equivalent stiffness. Strictly speaking, orthotropic plate theory could only be used if the beams are symmetric with respect to the plate and if transverse stiffeners are perpendicular to longitudinal stiffeners. In the case of a large deformation analysis, the behavior of the analogous orthotropic plate is governed by two coupled non-linear partial differential equations and again, these equations are difficult to solve. In a stress analysis of grillages subjected to transverse loads alone, the set of differential equations can be reduced further. Vitols, Clifton, and Au (Ref. 40) have applied this form of analysis to highway girder bridges

consisting of a concrete slab acting compositely with steel beams. Bares and Massonnet (Ref. 41) have published a book devoted to the analysis and design of grillages under transverse loads by means of the orthotropic plate theory. This approach cannot be used to adequately predict the state of stress in the plate and the governing differential equations are again difficult to solve for other than simply bounded structures.

Another group of approaches are the discrete element methods. These methods replace the actual structure by a system of discrete elements which leads to a set of simultaneous algebraic equations. These equations are developed directly by replacing the differential equation by the corresponding finite difference equations. Hennikoff (Ref. 42) presented a number of gridwork models for the solution of plate bending and elasticity problems, along with guidelines for establishing the equivalence between the model and the continuum. Newmark (Ref. 43) has proposed a model made up of rigid bars and springs for plate bending. Recently, Lopez and Ang (Ref. 44) developed a lumped parameter model by means of which the effects of large deformation and inelastic behavior can be included in the analysis of plates. In order to simplify the problem, the analysis herein has been restricted to sandwich plates. Although the formulation would become more difficult, this method could probably be used to analyze stiffened plates.

To analyze complex shaped stiffened plate structures, the finite element method is found to be best suited. For reasons

explained in Chapter 1, the finite element displacement approach is preferable. Gustafson (Ref. 45) has employed the finite element approach in the analysis of skewed grillage structures subjected to transverse loads. The results of this analysis were found to compare well with the results of tests performed on such structures. Little work has been done to take into account second order effects and inelastic action of the material in the analysis of plates and virtually no work has been done as far as stiffened plate structures are concerned.

3.3 A Finite Element Analysis of Stiffened Plates

3.3.1 Application of the Method to the Plate and Stiffener System

In this section, the application of the finite element displacement approach in the analysis of beam-slab type structures is described. The beam-slab type structure, shown in Fig. 16, can be bounded by arbitrarily shaped boundaries as long as they fit into a rectilinear mesh. The plate is stiffened by a set of beams running in longitudinal direction, which is assumed to be parallel to the global x-axis for all further discussions. In addition, a set of transverse stiffeners (called diaphragms) can be present although their inclusion in the analysis will be discussed in a later section. Neither the plate nor the stiffeners need to be of uniform thickness.

The first step is to discretize the structure into a

suitable number of finite plate and stiffener elements. In order to arrive at a simple formulation for this analysis, it is necessary that the stiffeners are attached along the mesh lines of the plate elements. However, they need not be continuously attached along the entire plate. Two types of finite elements, plate and stiffener elements, are needed to discretize the structure. In order to be able to study the convergence behavior of the method with respect to the criterion postulated by Melosh (Ref. 12) the broader mesh must always be contained in the next finer mesh. As shown in Fig. 16, a rectangular element involves the four nodal points I, J, K and L, and the beam element, being a straight line element, involves the two nodal points I and K. The mesh lines, or surfaces of separation, are again to be considered imaginary. The structure can be arbitrarily loaded by concentrated loads or uniformly distributed loads.

Due to the fact that the stiffeners are eccentrically attached to the plate, coupling between bending and stretching exists in the middle plane of the plate, and hence, in-plane deformations must be considered. The approach is described assuming small deformation theory and linearly elastic material. It should be noted that elements of different shapes can easily be used in combination in a finite element displacement approach, if they possess the same number of degrees of freedom at all common nodes. Here, all nodal points are best defined in a common plane. This plane will be called plane of reference for all further discussions, and

is assumed to coincide with the middle plane of the plate. The response of the beams must first be found with respect to this plane, and one of the objectives of this report is to illustrate how the eccentricity of the stiffeners can be taken into account.

Five displacement components are introduced as unknowns at each nodal point in the present approach. These are the displacement u in x-direction and the displacement v in y-direction. In addition, the deflection w and the two slopes θ_x and θ_y are considered. These five deformation components enable the description of the state of deformation in a plate and stiffener element. An analysis based on small deformation theory is greatly simplified since the in-plane and the out-of-plane stiffness matrices of the involved finite elements can be derived separately. However, deformation compatibility between beam and plate elements must be enforced and overall equilibrium must be established at each nodal point.

3.3.2 Derivation of Bending and In-Plane Plate Stiffness Matrices

The classical theory of plates assumes that the state of deformation in the plate can be described entirely in terms of the deformations of the middle plane of the plate. Basically, the refined plate element, as described in Chapter 2, could be used in representing the plate behavior of the stiffened plate structure. However, due to the presence of the torsional resistance of

the beam elements, discontinuities in some curvature terms occur along the lines of intersection of the stiffeners with the plate. Since these terms were entered as unknowns in the nodal displacement vector and made continuous at the nodal points, the refined element is best not used in the present approach. Basically, any known finite element could be used to represent the out-of-plane plate behavior.

For the present analysis, the ACM element, as originally proposed by Adini, Clough and Melosh (Ref. 34) and described in detail by Zienkiewicz (Ref. 6), is taken to represent the out-of-plane plate behavior. An incomplete third-order polynomial, as indicated in Fig. 5, is assumed for the representation of the displacement behavior within the element:

$$w = w\ (x,y) = \alpha_1 + \alpha_2 x + \alpha_3 y + \alpha_4 xy + \ldots + \alpha_{12} xy^3 \qquad (3.1)$$

Although this element is of the non-conforming type, it yields reasonably accurate results. The vertical displacement w and the two slopes θ_x and θ_y are entered as unknowns in the nodal displacement vector. Since this element will also be used for the elastic-plastic analysis of plates and stiffened plates, which will be presented in later chapters, the stiffness matrix is presented in Appendix III.

In order to determine the stiffness characteristics of the entire structure, which are required in the analysis, the stiffness properties of the plate elements for in-plane behavior

must also be established. As shown in Fig. 4, the displacement components governing the in-plane behavior are denoted by u and v, respectively. The selection of appropriate displacement functions is again subject to the requirements listed in Section 2.3.2. If the stiffness for a rectangle in plane stress is sought, eight force-displacement equations are to be formulated. Clough (Ref. 31) suggested the following functions:

$$u = \alpha_1' + \alpha_2' x + \alpha_3' y + \alpha_4' xy \tag{3.2}$$

$$v = \alpha_5' + \alpha_6' x + \alpha_7' y + \alpha_8' xy \tag{3.3}$$

A prime is attached to the unknown generalized coordinates to underline that they are not the same set as originally used. From Pascal's triangle, as shown in Fig. 5, it is noted that all of the constant and linear terms are chosen, along with one of the quadratic terms. The chosen functions are not complete polynomials. But, with the choice of the symmetric terms $\alpha_4' xy$ and $\alpha_8' xy$, and because of the geometric symmetry of the element itself, no preferential direction exists. Inclusion of all pertinent constant strains is assured, as well as proper representation of the rigid body motion states. From the equations it can be concluded that all edges displace as straight lines. Hence, the chosen displacement functions automatically guarantee continuity of displacement with adjacent elements. The assumed shape functions are of the conforming type

and since all the criteria listed in Section 2.3.2 are met, convergence to the true solution should occur. Enforcing compatibility of deformation at all nodal points, the unknown vector of generalized coordinates can be determined. The evaluation of the stiffness matrix governing the in-plane behavior of the plate element follows standard procedures. This derivation is performed in more detail in Appendix IV.

3.3.3 Derivation of Bending and In-Plane Beam Stiffness Matrix

The final stiffness relations for the stiffened plate structure express equilibrium at nodal points lying in the plane of reference. The response of the beams with respect to this plane of reference is needed. It is first assumed that a stiffener, as shown in Fig. 17, is attached to the plate along a boundary of the rectangular plate element. Next, it is assumed that external loads are applied only at plate elements or directly at the nodal points. Furthermore, it is assumed that the stiffener is symmetric with respect to its local z-axis, and weak in bending about this axis. In addition, shearing deformations are neglected. It should be noted that some of these restrictions could be lifted in a more refined analysis.

Owing to the above assumptions, only four of the five displacement components introduced at each nodal point of the reference surface are used to describe the behavior of the stiffener

element. The assumed displacement function for the in-plane behavior of the plate element predicts straight lines for the edges of the deformed plate elements. Consequently, no bending moments about the local z-axis are taken by the stiffener elements. Hence, the displacement component v in the direction of the y-axis does not need to be considered in describing the behavior of the beam elements. Since the stiffener element is assumed to be integrally attached to the plate, compatibility of deformation must be enforced along the juncture line between beam and plate. The same displacement functions chosen for the in-plane and the out-of-plane behavior of the plate element must be taken for the stiffener element in order to be able to satisfy this requirement:

$$u = \alpha_1'' + \alpha_2'' x \tag{3.4 a}$$

$$w = \alpha_3'' + \alpha_4'' x + \alpha_5'' x^2 + \alpha_6'' x^3 \tag{3.4 b}$$

Introducing the nodal displacement vector for node I of the beam element associated with its bending and in-plane behavior:

$$\{\delta_i^s\}_B^T = < u \quad w \quad \theta_y > \tag{3.5}$$

the element displacement vector needed for the generation of the stiffness matrix governing bending and in-plane behavior can be written as:

$$\{\delta^s\}_B^T = < u_i \; w_i \; \theta_{yi} \quad u_k \; w_k \; \theta_{yk} > \tag{3.6}$$

Enforcing compatibility at the two nodal points I and K leads to six algebraic equations which can be written as:

$$\{\delta^s\}_B = [C_s''] \quad \{\alpha''\} \tag{3.7}$$

where the vector of generalized coordinates is defined as:

$$\{\alpha''\}^T = < \alpha_1'' \quad \alpha_2'' \quad \alpha_3'' \quad \alpha_4'' \quad \alpha_5'' \quad \alpha_6'' > \tag{3.8}$$

These six generalized coordinates are uniquely defined by the nodal displacements introduced at the ends of the stiffener element. Inversion of Eq. 3.7 leads to

$$\{\alpha''\} = [C_s'']^{-1} \quad \{\delta^s\}_B \tag{3.9 a}$$

which can be written explicitely as:

$$\begin{bmatrix} \alpha_1'' \\ \alpha_2'' \\ \alpha_3'' \\ \alpha_4'' \\ \alpha_5'' \\ \alpha_6'' \end{bmatrix} = \begin{bmatrix} 1 & 0 & 0 & 0 & 0 & 0 \\ -1/L & 0 & 0 & 1/L & 0 & 0 \\ 0 & 1 & 0 & 0 & 0 & 0 \\ 0 & 0 & -1 & 0 & 0 & 0 \\ 0 & -3/L^2 & 2/L & 0 & 3/L^2 & 1/L \\ 0 & 2/L^3 & -1/L^2 & 0 & -2/L^3 & -1/L^2 \end{bmatrix} \begin{bmatrix} u_i \\ w_i \\ \theta_{yi} \\ u_k \\ w_k \\ \theta_{yk} \end{bmatrix} \tag{3.9 b}$$

Using the displacement relations, which, for the case of a uniaxially stressed stiffener, reduce to

$$U(z) = u - z \frac{\partial w}{\partial x} \tag{3.10}$$

in which u is the displacement in x-direction of a point lying in the reference surface, and U is the displacement in x-direction of a point lying outside this plane, the strain-displacement relation can be written as:

$$\epsilon_x = \frac{\partial U}{\partial x} = \frac{\partial u}{\partial x} - z \frac{\partial^2 w}{\partial x^2} \tag{3.11}$$

Introducing Hooke's law, which for the present case reduces to its simplest form, leads to the stress-displacement relation:

$$\sigma_s = E_s \left[\frac{\partial u}{\partial x} - z \frac{\partial^2 w}{\partial x^2} \right] \tag{3.12}$$

The joint forces shown in Fig. 17 associated with the joint displacements must be defined at the location and in the direction of these deformation components. Forces defined at the centroid of the beam element could be found using an appropriate transformation matrix which would have to be derived from a consideration of equilibrium of forces applied to the stiffener element. Integrating the stresses with respect to the plane of reference, and using Eq. 3.12 leads to

$$N_s = \iint_{A_s} \sigma_s \, dA_s = E_s \left[\frac{\partial u}{\partial x} A_s - \frac{\partial^2 w}{\partial x^2} S_s \right] \qquad (3.13\,a)$$

$$M_s = \iint_{A_s} \sigma_s \, z \, dA_s = E_s \left[\frac{\partial u}{\partial x} S_s - \frac{\partial^2 w}{\partial x^2} I_s \right] \qquad (3.13\,b)$$

where: E_s = Modulus of elasticity of stiffener

A_s = Cross-sectional area of stiffener

S_s = First moment of the stiffener area with respect to the plane of reference

I_s = Moment of inertia of the stiffener area with respect to the plane of reference

Eqs. 3.13 a and 3.13 b, constituting the force-displacement relations for the eccentrically stiffened beam element, can be written in the form:

$$\begin{bmatrix} N_s \\ M_s \end{bmatrix} = E_s \begin{bmatrix} A_s & S_s \\ S_s & I_s \end{bmatrix} \begin{bmatrix} \frac{\partial u}{\partial x} \\ -\frac{\partial^2 w}{\partial x^2} \end{bmatrix} \qquad (3.14\,a)$$

or simply as:

$$\{M_s\} = [D_s] \{\epsilon_s\} \qquad (3.14\,b)$$

This equation relates the internal stress resultants acting on a stiffener element, and defined at nodal points lying in the plane of reference, to the vector of generalized strains. The vector of

generalized strains can be found in terms of the vector of generalized coordinates making use of the assumed displacement fields:

$$\begin{bmatrix} \frac{\partial u}{\partial x} \\ -\frac{\partial^2 w}{\partial x^2} \end{bmatrix} = \begin{bmatrix} 0 & 1 & 0 & 0 & 0 & 0 \\ 0 & 0 & 0 & 0 & -2 & -6x \end{bmatrix} \begin{bmatrix} \alpha_1'' \\ \alpha_2'' \\ \alpha_3'' \\ \alpha_4'' \\ \alpha_5'' \\ \alpha_6'' \end{bmatrix} \qquad (3.15\ a)$$

which can be simply written as:

$$\{\epsilon_s\} = [Q_s] \quad \{\alpha''\} \qquad (3.15\ b)$$

in which the matrix $[Q_s]$ is found by differentiating Eqs. 3.4. Making use of Eq. 3.9 a, the above expression can be written as:

$$\{\epsilon_s\} = [Q_s] \quad [C_s'']^{-1} \quad \{\delta^s\}_B = [B_s] \quad \{\delta^s\}_B \qquad (3.15\ c)$$

Hence, Eq. 3.14 b can be written as

$$\{M_s\} = [D_s] \quad [B_s] \quad \{\delta^s\}_B \qquad (3.16)$$

Having established all basic relationships, the stiffness matrix relating beam bending moment, shear, and axial force to corresponding displacement components can be derived using the virtual work

principle. In this approach a set of virtual nodal displacements is imposed on the beam element, and the external and internal works done by the various forces are equated. Application of this procedure leads to:

$$\{\tilde{\delta}^s\}_B^T \{F_s\}_B = \int_0^L \{\epsilon_s\}^T \{M_s\} \, dx \tag{3.17}$$

Using Eqs. 3.15 c and 3.16 gives:

$$\{\tilde{\delta}^s\}_B^T \{F_s\}_B = \{\tilde{\delta}^s\}_B^T \left\{ \int_0^L [B_s]^T [D_s] [B_s] \, dx \right\} \{\delta^s\}_B$$

Since this relationship must hold for any arbitrary set of virtual displacements, one can conclude that the stiffness relation is given by:

$$\{F_s\}_B = \left\{ \int_0^L [B_s]^T [D_s] [B_s] \, dx \right\} \{\delta^s\}_B \tag{3.18}$$

The stiffness matrix is found to be:

$$[K_s]_B = \int_0^L [B_s]^T [D_s] [B_s] \, dx \tag{3.19}$$

where the integration is to be taken over the length of the prismatic stiffener element. Performing this integration leads to:

$$\begin{bmatrix} N_i \\ Z_i \\ M_i \\ N_k \\ Z_k \\ M_k \end{bmatrix} = E_s \begin{bmatrix} A_s/L & 0 & S_s/L & -A_s/L & 0 & -S_s/L \\ & 12I_s/L^3 & -6I_s/L^2 & 0 & -12I_s/L^3 & -6I_s/L^2 \\ & & 4I_s/L & -S_s/L & 6I_s/L^2 & 2I_s/L \\ & & & A_s/L & 0 & S_s/L \\ & \text{Symmetric} & & & 12I_s/L^3 & 6I_s/L^2 \\ & & & & & 4I_s/L \end{bmatrix} \begin{bmatrix} u_i \\ w_i \\ \theta_{yi} \\ u_k \\ w_k \\ \theta_{yk} \end{bmatrix} \tag{3.20}$$

3.3.4 Inclusion of Torsional Stiffness of Beam Elements

The torsional resistance of the beams is often of importance in the behavior of stiffened plates. In beam theory (Ref. 46), it is shown that the total twisting moment applied to a beam is resisted by two different kinds of torsion, St. Venant or pure torsion, and warping torsion:

$$T = T_{St.V.} + T_w \tag{3.21}$$

The St. Venant torsional moment is resisted by shearing stresses, whereas the warping torsional moment is carried by axial stresses introduced due to flange bending. For rectangular or stocky solid beam cross sections, most of the applied twisting moment is carried by St. Venant torsion, whereas thin-walled I-sections carry most of the applied torsional moment by warping action. Both twisting moments are related to the angle of twist $\emptyset$ as follows:

$$T_{St.V.} = GK_T \, \phi' \tag{3.22}$$

$$T_w = -EI_w \, \phi''' \tag{3.23}$$

where: $\phi' = \frac{\partial}{\partial x} \left(\frac{\partial w}{\partial y}\right)$ = Rate of change of angle of twist

G = Shear modulus

K_T = St. Venant torsional constant

I_w = Warping constant

Warping is not considered in the presently proposed finite element approach for the analysis of stiffened plates. To account for warping, the higher order derivatives of the angle of twist should be included in the choice of the unknown displacement components introduced at the nodal points. It can be seen that owing to the assumed displacement pattern for the vertical displacement w, the rate of twist ϕ', i.e. the change of θ_x along a line of constant y-coordinate, varies as a cubic function. Since only two boundary conditions are available at the ends of the stiffener elements, the last two terms in the cubic function are disregarded. A linear variation of the angle of twist is assumed:

$$\theta_x = \frac{\partial w}{\partial y} = \alpha_1''' + \alpha_2''' \, x \tag{3.24}$$

Introducing the displacement vector associated with the torsional modes of the beam element:

$$\{\delta^s\}_T^T = < \theta_{xi} \quad \theta_{xk} > \tag{3.25}$$

one can write:

$$\{\delta^s\}_T = [C_s^{III}] \quad \{\alpha^{III}\} \tag{3.26}$$

where the vector of generalized coordinates is defined as:

$$\{\alpha\}^T = < \alpha_1^{III} \quad \alpha_2^{III} > \tag{3.27}$$

Enforcing compatibility of deformation for the angle of twist at the ends of the stiffener element, the two generalized coordinates are uniquely determined. Solution of Eq. 3.26 leads to

$$\{\alpha^{III}\} = [C_s^{III}]^{-1} \quad \{\delta^s\}_T \tag{3.28 a}$$

or written explicitly:

$$\begin{bmatrix} \alpha_1^{III} \\ \alpha_2^{III} \end{bmatrix} = \begin{bmatrix} 1 & 0 \\ -1/L & 1/L \end{bmatrix} \quad \begin{bmatrix} \theta_{xi} \\ \theta_{xk} \end{bmatrix} \tag{3.28 b}$$

Using the differential equation for St. Venant torsion, Eq. 3.22, which is derived, for example, in Ref. 47, the force-displacement relationship becomes:

$$\{T_s\} = [D_s] \quad \{\phi'\} \tag{3.29}$$

where

$$[D_s] = GK_T \tag{3.30}$$

The vector of generalized strains $\{\emptyset'\}$ can be found in terms of the vector of generalized coordinates by making use of the assumed displacement function Eq. 3.24:

$$\{\emptyset'\} = \begin{bmatrix} 0 & 1 \end{bmatrix} \begin{bmatrix} \alpha_1''' \\ \alpha_2''' \end{bmatrix} = [Q_s] \{\alpha'''\} \tag{3.31}$$

Using Eq. 3.28 a, this relationship in turn can be written as:

$$\{\emptyset'\} = [Q_s] [C_s''']^{-1} \{\delta^s\}_T = [B_s] \{\delta^s\}_T \tag{3.32}$$

Again applying the principle of virtual work, the stiffness matrix for a beam element subjected to torsion is found to be:

$$[K_s]_T = \int_0^L [B_s]^T [D_s] [B_s] \, dx \tag{3.33}$$

The integration can be carried out in a straight forward manner leading to:

$$\begin{bmatrix} T_i \\ T_k \end{bmatrix} = \frac{GK_T}{L} \begin{bmatrix} 1 & -1 \\ -1 & 1 \end{bmatrix} \begin{bmatrix} \theta_{xi} \\ \theta_{xk} \end{bmatrix} \tag{3.34}$$

This stiffness relation, together with the previously derived Eq. 3.20, describes the behavior of an eccentrically stiffened beam element with respect to the plane of reference. These

relationships, together with the previously derived stiffness relations for the in-plane and out-of-plane behavior of the plate elements, are the basic components of the presented analysis of stiffened plate structures.

3.3.5 Evaluation of the St. Venant Torsional Constant K_T

The torsional stiffness matrix derived in the previous section can be evaluated once the St. Venant torsional constant K_T of the stiffener section is known. The estimation of K_T may present difficulties depending on the cross section of the stiffener. As shown in Ref. 48, for example, St. Venant torsion is governed by the partial differential equation:

$$\nabla^2 \psi = \frac{\partial^2 \psi}{\partial y^2} + \frac{\partial^2 \psi}{\partial z^2} = -2G\,\phi' \qquad (3.35)$$

where: $\psi = \psi\,(y,z)$ = Stress function

ϕ' = Rate of twist

This is Poisson's equation, which is encountered frequently in mathematical physics. Its solution can be obtained by different techniques,and for simple shapes no problems arise. A solution to the elastic torsion problem can also be obtained experimentally by means of the membrane analogy suggested by Prandtl, which is described in Ref. 49. As given in Ref. 50, a number of approximate formulae have been proposed for irregular shapes. Using membrane

analogy, the St. Venant torsional constant K_T for a thin-walled open section, which is composed of n rectangularly shaped elements, can be evaluated as:

$$K_T = \sum_{i=1}^{n} b_i \, t_i^3 \tag{3.36}$$

where: b_i = Length of element i

t_i = Width of element i

However, this formula is accurate only if the elements are small. Solid cross-sections with reentrant corners are best broken down into parts, and the St. Venant torsional constant K_T for such a section can be approximately evaluated as follows:

$$K_T = \sum_{i=1}^{n} \frac{A_i^4}{40 I_{pi}} \tag{3.37}$$

where: A_i = Area of element i

I_{pi} = Polar moment of inertia of element i

These formulae can be used to obtain an estimate on the torsional constant K_T; however, in some cases, significant errors might be introduced when using these approximations, thus necessitating a more accurate analysis. A means of solving the governing partial differential equation is to use the finite-difference method since its application is relatively simple.

An alternate way of solving this differential equation was found in the process of this investigation. The method is based

on the fact that the differential equation of torsion and that of the corresponding transversely loaded plate problem are formally identical, and thus, a solution can be accomplished by solving the corresponding plate problem using the finite element method. This technique is described in detail in Appendix V. Due to the versatility of the finite element approach, the St. Venant torsional constant K_T for complex shaped solid cross sections can be computed easily using the general plate program described in Chapter 2.

3.3.6 Assembly of the System Stiffness Matrix and Solution of the Field Equations

The assembly of the component stiffness matrices, as derived in the previous sections, to the system stiffness matrix is described in this section. The stiffness matrices of the individual elements can be assembled to form a single stiffness matrix, called system stiffness matrix of the entire structure. This procedure is explained in detail in Section 2.3.1.

For the present analysis, the in-plane displacements u in x-direction and v in y-direction, the deflection w, and the two slopes of the deflected surface are entered as unknowns at each nodal point. The vector of nodal displacements at node i is introduced as follows:

$$\{\delta_i\}^T = < u \quad v \quad w \quad \theta_x \quad \theta_y > \tag{3.38}$$

In a first step, the torsional stiffness matrix of the stiffener element, as given by Eq. 3.34, is combined with the stiffness for

bending, shear and axial force, given by Eq. 3.20, to form one single stiffness relation for the stiffener element:

$$\{F_s\} = [K_s]\ \{\delta^s\} \tag{3.39 a}$$

Explicitely, Eq. 3.39 a can be written as:

$$\begin{Bmatrix} N_i \\ V_i \\ Z_i \\ T_i \\ M_i \\ N_k \\ V_k \\ Z_k \\ T_k \\ M_k \end{Bmatrix} = \frac{E_s}{L^3} \begin{bmatrix} A_s L^2 & 0 & 0 & 0 & S_s L^2 & -A_s L^2 & 0 & 0 & 0 & -S_s L^2 \\ & 0 & 0 & 0 & 0 & 0 & 0 & 0 & 0 & 0 \\ & & 12I_s & 0 & -6I_s L & 0 & 0 & -12I_s & 0 & -6I_s L \\ & & & \gamma L^2 & 0 & 0 & 0 & 0 & -\gamma L^2 & 0 \\ & & & & 4I_s L^2 & -S_s L^2 & 0 & 6I_s L & 0 & 2I_s L^2 \\ & & & & & A_s L^2 & 0 & 0 & 0 & S_s L^2 \\ & & & & & & 0 & 0 & 0 & 0 \\ & & & & & & & 12I_s & 0 & 6I_s L \\ & & & & \text{Symmetric} & & & & \gamma L^2 & 0 \\ & & & & & & & & & 4I_s L^2 \end{bmatrix} \begin{Bmatrix} u_i \\ v_i \\ w_i \\ \theta_{xi} \\ \theta_{yi} \\ u_k \\ v_k \\ w_k \\ \theta_{xk} \\ \theta_{yk} \end{Bmatrix} \tag{3.39 b}$$

where, in order to have a compatible listing of deformation components for the entire structure, the nodal force and nodal displacement vectors are defined as:

$$\{\delta^s\}^T = < u_i \quad v_i \quad w_i \quad \theta_{xi} \quad \theta_{yi} \quad u_k \quad v_k \quad w_k \quad \theta_{xk} \quad \theta_{yk} > \tag{3.40}$$

$$\{F_s\}^T = < N_i \quad V_i \quad Z_i \quad T_i \quad M_i \quad N_k \quad V_k \quad Z_k \quad T_k \quad M_k > \tag{3.41}$$

where γ is defined as:

$$\gamma = \frac{GK_T}{E_s} \tag{3.42}$$

In a similar way, the stiffness relations governing the in-plane and out-of-plane behavior of the plate elements, as derived in the Appendices III and IV, can be cast into one single relationship:

$$\{F_p\} = [K_p] \quad \{\delta^p\} \tag{3.43}$$

where the element displacement vector is defined as:

$$\{\delta^p\}^T = < \{\delta_i\}^T \quad \{\delta_j\}^T \quad \{\delta_k\}^T \quad \{\delta_l\}^T > \tag{3.44}$$

and $\{F_p\}$, the element force vector, is defined consistent with the element displacement vector. The stiffness matrix $[K_p]$ governing the in-plane and out-of-plane behavior of a plate element is of size 20 x 20, and is best assembled in a digital computer.

The stiffness coefficients for each adjoining element can simply be added for the different elements framing into a common node. In fact, this operation establishes equilibrium of forces at a node in the direction of each of the five introduced nodal displacement components. Each row of the assembled stiffness matrix represents an equilibrium equation found by enforcing equilibrium of nodal forces and the generalized loads at a given node, for one of the five degrees of freedom. Once this system stiffness matrix is assembled, the final stiffness relations for

the entire stiffened plate structure can again be cast into one single matrix equation of the form:

$$\{F\} = [K] \quad \{\delta\} \tag{3.45}$$

where: $\{F\}$ = Systems vector of generalized loads

$[K]$ = Overall or systems stiffness matrix

$\{\delta\}$ = Systems displacement vector

From this point on, one can proceed as in the usual finite element displacement approach, described in Section 2.3.1. It should be noted that only displacement type boundary conditions can be satisfied exactly because only displacement components are entered as unknowns in the nodal displacement vector. Upon enforcement of the known displacements as described in Section 2.4.3, the system of simultaneous equations, represented by Eq. 3.45, can be solved. Large systems of simultaneous equations require special solution techniques in order to minimize computer costs. The Choleski decomposition technique, as described in Section 2.4.5, was used, and proved to be very efficient.

Once the unknown systems displacement vector is determined, all unknown field quantities can be found by substituting appropriate displacement components back into the relations derived either in the appendices or the main text. In addition, at each nodal point, the forces acting on beam elements and the stress resultants associated with the in-plane and out-of-plane behavior of

the plate elements are determined. The fact that the forces acting on beam and plate elements can be separated in the proposed method of analysis is of significant importance in the design of a stiffened plate structure.

In order to implement the above described approach, a general computer program was developed for the analysis of arbitrarily shaped stiffened plates. Any shape, as long as it fits into a rectilinear mesh, can be treated and transverse stiffeners can be included. Orthotropy of the plate can be considered and multiple load vectors can be processed simultaneously.

3.4 Application of the Method to the Analysis of Highway Bridges

3.4.1 Description of the Test Structure

The need for a more rational analysis of beam-slap type bridges is great, especially in regard to a more reliable analysis of the stresses occurring in the bridge deck, the effect of diaphragms on lateral distribution of load and on slab stresses, and the effect of the orthotropic behavior of the bridge deck.

It was decided to verify the proposed finite element approach with the aid of field test results of an I-beam girder bridge field tested in 1969 by a research team at Fritz Engineering Laboratory, Lehigh University. Chen and VanHorn (Ref. 51) describe in detail the field testing of this existing beam-slab type highway bridge, which is constructed with five prestressed concrete I-beams supporting a cast-in-place concrete slab. A

description of the behavior of the slab of the same bridge structure is given in Ref. 52. The testing of this bridge was part of an overall investigation, initiated in 1968, to develop information on several aspects of the structural behavior of I-beam bridges. Prior to this investigation, the problem of load distribution in spread box beam bridges was studied extensively by the field testing of several bridges of the box-beam type (Ref. 35) and by means of a theoretical analysis (Ref. 53). From all of these investigations it was concluded that the present AASHO Standard Specifications for Highway Bridges (Ref. 54) do not give an accurate prediction for the lateral distribution of load in box-beam and I-beam bridges. Furthermore, the specifications do not account for many variables which have significant effects on load distribution.

The structure analyzed in this investigation is a simply supported, right I-beam bridge with a span length of 68 feet 6 inches center-to-center of bearings. The cross section of the test bridge, as shown in Fig. 18, consists of five identical prestressed I-beams, of AASHO Type III cross section, covered with a cast-in-place reinforced concrete deck. The deck provides a roadway width of 32 feet and the specified minimum thickness of the slab is 7-1/2 inches. However, measurements indicated that the actual slab thickness ranges from 6.1 to 7.3 inches at the section of maximum moment, which is located 3.55 feet off midspan. Diaphragms between the beams are located at the ends of the span above the end supports

and at midspan. The dimensions of the midspan diaphragm, as well as those of the beam cross section, are shown in Fig. 19. The test vehicle used for testing was a tractor and semi-trailer unit, approximating the AASHO HS 20-44 design loading (Ref. 54). A photo of the test vehicle, along with the wheel spacings and the actual axle loading, is shown in Fig. 20. Four loading lanes were located on the roadway, as shown in Fig. 21, such that the center-line of the truck would coincide with the center-line of the girders or with a line located midway between girders.

3.4.2 Study of Variables Governing Load Distribution

Although the actual cross section of the bridge could be approximated more closely in the present analysis, it was, for the sake of a simpler input, approximated as shown in Fig. 21. The slab thickness was assumed to be 7.5 inches throughout the width of the deck. First, the curb and parapet sections, as well as the midspan diaphragm, were neglected. Their inclusion will be discussed in subsequent sections. The entire bridge was considered to be made of an isotropic material. Poisson's ratio was taken as 0.15, and a modulus of elasticity of $E = 5000$ ksi was assumed. A ratio of torsional-to-bending stiffness of the beam elements $\gamma^* = GK_T/E_sI_s = 0.035$ was taken, as found from an analysis as discussed in Section 3.3.5. The actual truck loading was simulated by appropriate concentrated forces instead of the distributed wheel loads. The structure was analyzed for a truck centered, in turn, in each of the lanes as shown in Fig. 21.

The general finite element program yields the entire displacement field at all specified nodal points, as well as all internal stress resultants acting on the beam and plate elements. The forces associated with in-plane and out-of-plane behavior are printed separately for all plate elements. Due to space limitations, only the results associated with the lateral distribution of load will be presented. All following results are for a discretization of the structure shown in Fig. 22. A mesh with N subdivisions in the transverse direction and M subdivisions in the longitudinal direction is referred to as Mesh N * M in the remainder. During the actual testing of this structure, a section near midspan, shown as Section M in Fig. 22, was gaged. This section corresponds to the section of maximum moment for the structure idealized as a simple beam, and subjected to the given group of loads.

The results obtained from tests, as reported in detail in Ref. 51, were derived based upon an experimentally measured strain distribution in the beams. This distribution of strain is due to the combined action of all stress resultants acting on a beam element. It is not possible to separate these forces in an experimental investigation. For the sake of simplicity, it was assumed that only beam bending occurs. The proposed finite element analysis determines all stress resultants acting on the beam and plate elements separately. In order to compare the results obtained from the analysis with the test results, equivalent beam bending moments causing the same distribution of strain as would

result under the combined action of axial force and beam bending moment must be obtained from the analysis. This procedure is based on the concept of equating the first moments of area of the compressive and tensile areas of each composite beam (Ref. 51). Finally, distribution coefficients (or moment percentages) were computed. These are defined as the moment carried by a particular beam divided by the sum of moments carried by all beams.

Fig. 23 shows distribution coefficients obtained from the analysis and the field test results for a truck moving in lane 1. Similarly, Figs. 24 and 25 show distribution coefficients for a truck moving in lanes 3 and 4, respectively. Influence lines for beam bending moments could be constructed as shown in Figs. 26 and 27. Such plots could be used to advantage by the designer to determine the maximum bending moment occurring at the section of maximum moment under the action of multiple trucks crossing the bridge simultaneously. It should be noted that theoretical values are obtained for a bridge without diaphragms at midspan, whereas the actual field test results include their effect. The inclusion of the diaphragms brings theoretical results closer to field results. In addition, analytical results are obtained for a bridge with a theoretical slab thickness of 7.5 inches, and subject to the assumptions listed at the beginning of this section.

3.4.2.1 Effect of Span Length

Fig. 28 shows the effect of the span length on the lateral

distribution of load for the I-beam bridge investigated. Figs. 29 and 30 show influence lines for the outermost and center beam bending moment, respectively, pointing out the influence of the span length on the beam bending moment. A study of these figures reveals a significant influence of the span length on the lateral distribution of load. Plotting the distribution coefficient for the center beam bending moment against the span length, as done in Fig. 31, reveals clearly this dependency. An almost linear relationship is obtained if the moment percentages of the center beam are plotted against the reciprocal of the span length, as done in Fig. 32. Hence, it can be concluded that the load distribution is likely to be inversely proportional to the span length, a factor not accounted for in the present AASHO Standard Specifications for highway bridges. A similar conclusion was reached in the investigation on bridges of the box-beam type (Ref. 53).

3.4.2.2 Effect of Deck Thickness

The effect of the thickness of the slab is shown in Fig. 33. It is seen from this graph that the thickness of the deck significantly affects the lateral load distribution for an I-beam bridge. This is in contrast to results found from the analysis of a box-beam bridge (Ref. 53), where it was concluded that the load distribution is not very sensitive to a variation in slab thickness. The present investigation shows that a thicker slab distributes the load more uniformly to the girders. Again, this effect is not accounted for in the present specifications.

3.4.2.3 Effect of Beam Spacing

Another important factor influencing the lateral distribution of load is the spacing of the girders, as shown in Fig. 34. As can be seen from this figure, a closer spacing distributes the load more evenly. This effect is partly accounted for in the present AASHO Standard Specifications for Highway Bridges (Ref. 54) in which the load distribution factors are given in the form of spacing, divided by a constant number. Actually, the optimum spacing should be determined for a given roadway width of the bridge. Such an investigation could be easily made using the present finite element program.

3.4.2.4 Effect of Beam Size

The effect of the size of the beam cross section on lateral distribution of load is illustrated in Fig. 35. Four standard precast beams of a size suggested by AASHO (Ref. 54) have been included in this investigation. This effect is significant and smaller beams are seen to distribute the load more evenly to the girders.

3.4.2.5 Effect of Torsional Stiffness of Beams

The effect of the torsional resistance of the beams on the lateral distribution of load is shown in Fig. 36. The moment percentages are plotted in this figure for torsionally weak beams with $GK_T/E_sI_s = 0$ as well as for a ratio of 0.120. As expected, it is recognized that this ratio has some effect on the

lateral distribution of loads, and it underlines the need for an accurate analysis of K_T, as shown in Section 3.3.5 as well as for a consideration of the torsional resistance of the beams in future specifications.

3.4.2.6 Effect of Eccentricity of Beams

This eccentricity is defined here as distance from the centroid of the beam element to the plane of reference, as indicated in Fig 37. For a theoretical slab thickness of 7.5 inches, this distance becomes 27.98 inches using AASHO Type III beams. The figure depicts the structural behavior of an I-beam bridge for a variation of this distance of $\pm$ 0.5 inches, caused, for example, by a misfit during the construction of the bridge. It is seen that the load distribution is not significantly affected by such a deviation.

3.4.2.7 Effect of Poisson's Ratio

Poisson's ratio varies widely, depending upon the age of concrete, type of aggregate, and other factors. To observe the effect of this ratio, a high and low limiting values of $\nu = 0.25$ and $\nu = 0.05$ were chosen for this comparison, and the effect of these two values of ν on the lateral distribution of load is shown in Fig. 38. It can be concluded that the distribution of load is nearly unaffected by this ratio. However, the slab bending moments and the in-plane forces are considerably dependent on ν.

3.4.2.8 Effect of Moduli of Elasticity of Beams and Slab

An accurate determination of the moduli of elasticity of the beam and slab material used in an actual bridge is not possible. Hence, some degree of engineering judgment must be used in the assumption of appropriate values for these material properties. For the lateral distribution of load, only the ratio of the moduli of elasticity of the beam and slab materials is of importance, and hence, the effect of this ratio was studied in this investigation. Usually, the modulus of elasticity of the precast prestressed concrete beams is higher than that of the cast-in-place reinforced concrete slab. The response of the structure was analyzed for different ratios of moduli of elasticity and the result of this investigation is plotted in Fig. 39. It is seen from this figure that the effect of this paratmeter on the lateral distribution of load is not very significant. However, the shifting of load to the center beam for larger values of the modulus of elasticity of the beam should be noted.

3.4.2.9 Effect of Orthotropy of Bridge Deck

Orthotropy is caused by unequal amounts of reinforcing steel for the transverse and longitudinal reinforcement of the bridge slab, or by cracking of the slab, for example. The effect that such cracking might have on the lateral distribution of load is of interest. For the sake of simplicity, it was assumed in this investigation that the entire slab width was cracked uniformly, parallel to the girders, along the total length of the

bridge. The associated decrease in stiffness is accounted for in the ratio D_y/D_x, of transverse to longitudinal stiffness of the slab. Figure 40 illustrates that a cracked slab causing a loss in transverse stiffness shifts slightly more load to the center girder, and at the same time, decreases the load in both exterior girders. Further results of this investigation are compiled in Table 15. It should be noted that the crack pattern described above leads to an orthotropic behavior of the slab as described by Timoshenko (Ref. 3). The stress matrix for this particular case becomes:

$$[D] = \begin{bmatrix} D_{11} & D_{12} & 0 \\ D_{21} & D_{22} & 0 \\ 0 & 0 & D_{33} \end{bmatrix}$$

where the terms in the matrix should be evaluated according to Huber (Ref. 3) as follows:

$$D_{11} = \frac{E_c I_{cx}}{1-\nu^2}$$

$$D_{22} = \frac{E_c I_{cy}}{1-\nu^2}$$

$$D_{12} = D_{21} = \nu\sqrt{D_{11} D_{22}}$$

$$D_{33} = \frac{1-\nu}{2} \sqrt{D_{11} D_{22}}$$

in which: E_c = Modulus of elasticity of concrete deck

I_c = Transformed moment of inertia, taking reinforcement into account

ν = Poisson's ratio

A generally anisotropic material behavior would result if the cracks were not to open parallel to the global x-axis. However, such cracking could also be investigated by first finding the stiffness of a cracked panel with respect to a local coordinate system with x-axis in the direction of the cracks, and then transforming this stiffness to the global coordinate system.

3.4.2.10 Effect of Type of Loading

The effect of different types of loading encountered in bridge design on the lateral distribution of load is shown in Fig. 41. Two loading cases must be considered according to the AASHO specifications: (1) uniformly distributed lane load, and (2) the truck load. The analysis of the structure yields almost identical distribution percentages for these two loading cases. However, a significantly different distribution of load is obtained for a single concentrated load.

3.4.2.11 Two-Span Continuous Bridge

This example is chosen to demonstrate the versatility of the proposed finite element approach and the effect of different boundary conditions on the lateral distribution of loads. In

Fig. 42, a comparison of load distribution for a single span and a two-span continuous bridge is made. Two trucks are located in such a way on the bridge as to obtain symmetry of loading with respect to the center support. It is interesting to observe that the load distribution at the center support and at Section M, the section of maximum moment for the corresponding single span bridge, is not very different. However, the pronounced difference in load distribution between a single span and a two-span continuous bridge should be observed in the design of such bridges.

3.4.3 Inclusion of Diaphragms

One of the features of the method is the inclusion of stiffeners running in transverse direction, often called diaphragms. The general computer program developed for this investigation is capable of including any pattern of transverse stiffeners, as long as they are attached along plate element interfaces. As mentioned above, the test structure investigated so far has one midspan diaphragm only, the cross section of which is shown in Fig. 19. The results of the analysis performed for a structure including this diaphragm are shown in Figs. 23, 24 and 25. It is seen that for I-beam bridges the effect of such a midspan diaphragm on the lateral distribution of load is significant, and hence, due consideration should be given in the design.

3.4.4 Inclusion of Curb and Parapet

The results presented so far are for an idealized bridge

cross section, as shown in Fig. 21, neglecting curb and parapet. Basically, curbs and parapets are not intended as load-carrying members in a bridge. However, field tests (Ref. 35) showed a partial effectiveness of the curb and parapet section acting compositely with the exterior beam. In a field test, the effect of the diaphragm can not be separated from the behavior of the exterior beam. The results of the analysis on the effectiveness of curb and parapet are shown in Figs. 23, 24, and 25. For this analysis, curb and parapet were approximately accounted for by considering the curb and parapet together with the exterior beam as one unit and treating this unit as a modified exterior beam. A more refined analysis could be performed by taking the curb and parapet as separate beam elements and proceeding as discussed in Section 3.3.6. From Figs. 23 through 27 it can be concluded that the effect of curbs and parapets on the lateral distribution of load in the I-beam type superstructure may not be very significant, thus the designer is on the conservative side, at least for the interior beams, if he chooses to disregard their effects.

3.5 Convergence and Accuracy of Solutions

The above study of variables governing the lateral distribution of load in I-beam bridges makes it clear that the developed finite element analysis is well suited for the analysis of beam-slab type bridge structures. For this analysis, a minimum of simplifying assumptions in the idealization of the structure are required. A comparison of the values for displacements and stress

resultants predicted by the finite element method with those of the field tests proves the validity of the developed approach. Although only results associated with the lateral distribution of load are shown in this report, it should be pointed out that the method allows for the determination of the entire stress and displacement field at all predefined nodal points. A study of the behavior of the slab of the Bartonsville Bridge (Ref. 52), revealed that there is no satisfactory method of slab analysis presently available. In fact, currently used methods of slab analysis do not account for many variables involved in the structural behavior of the slab, and none is thoroughly verified by test results. On the other hand, since the present analysis allows for a separation of forces acting on beam and plate elements, it would be ideally suited for a more extensive study of the behavior of the slab. The response of a slab panel acted upon by a distributed wheel load could be determined accurately by reanalyzing this panel as a plate, enforcing the boundary conditions as found form an analysis of the entire structure.

The accuracy to be expected from the developed finite element approach depends on the discretization of the structure. In a finite element displacement approach making use of fully compatible elements, the displacement field converges toward the true displacement field if the mesh size is reduced. However, no bounds can be given for the associated stress field. For the present formulation, a non-conforming displacement function was chosen

for the representation of the out-of-plane behavior of the plate. A compatible formulation was chosen for the representation of the in-plane behavior of the plate and the behavior of the beam elements. The convergence of the combined model cannot be proven via the principle of minimum total potential energy. A numerical evaluation of the structural response of the I-beam bridge was investigated for different mesh sizes in order to study the convergence behavior of the proposed approach. All dimensions and material properties were chosen as listed in Section 3.4.1, and the effects of diaphragm, curb and parapet were not considered. The structure was again loaded by a truck load, and three different mesh sizes were processed. Some results of these investigations are shown in Tables 16 through 19 for the section of maximum moment and the truck occupying lanes 1 through 4. The tables also contain the deflection values measured during the actual field testing of this bridge. In comparing the theoretical results with the experimental values, it should be kept in mind that the theoretical and the actual bridge have different dimensions. A comparison of different mesh sizes indicates convergence for a decreasing mesh size. Furthermore, the validity of the solutions is supported by the actual field test results listed in the same tables.

3.6 Summary

A method of analysis based on the finite element displacement approach capable of analyzing complex shaped stiffened

plates has been presented. Stiffeners in longitudinal as well as in transverse direction can be taken into account, and the stiffness of the slab can be arbitrarily varied to account for thickness changes in the slab. The orthotropic nature of the plate can be accounted for, as well as a varying cross section of the beams. A minimum of simplifying assumptions associated with the discretization of a structure is required in the analysis.

On the basis of the application of this method to the analysis of an I-beam bridge, described in detail, a few conclusions can be drawn: (1) The model approximates the true physical behavior of a structure more closely than methods which use either the effective width concept to find an equivalent grid structure, or orthotropic plate theory, which is not able to predict the slab stresses accurately. (2) The presented approach allows a separation of forces acting on beam and plate elements, thus giving the designer more detailed information about the behavior of a structure. (3) The study of variables governing the lateral distribution of load demonstrates the versatility of the proposed approach.

4. ANALYSIS OF ELASTIC-PLASTIC PLATES

4.1 Introduction

It is generally accepted that a structure is capable of redistributing high local stresses and, if properly dimensioned, is able to withstand loads significantly higher than the elastic limit load.

A general method of analysis based on the finite element displacement concept and capable of predicting the entire load-deformation behavior of complex shaped transversely loaded plates is presented. A description of the layered model used in the present analysis is given which significantly simplifies the mathematical description of the elastic-plastic behavior of a plate element. Elastic and plastic stress-strain relations are derived, and yield conditions and a flow rule are discussed.

The applied incremental elastic-plastic solution procedure is based on the tangent stiffness concept. The assembly of the system tangent stiffness matrix and the iterative solution technique are described. Loading and unloading of a layer are discussed, as well as the yield surface correction used in the analysis.

Finally, a number of example solutions are presented demonstrating the power and versatility of the proposed approach. Convergence and accuracy of the presented approach are shown.

4.2 Existing Methods of Analysis

4.2.1 Upper and Lower Bound Approaches

The theory of plastic analysis has developed from two directions: (1) the classical approach known as limit analysis and, (2) the yield line theory. Tresca, Von Mises, Prager and Hodge (Ref. 56) have pioneered the classical point of view, whereas Bach (Ref. 58) and Johansen (Ref. 59) developed the yield line theory. These methods allow the structural analyst to establish bounds on the collapse load. However, none can be applied to study the entire load-deflection behavior of complex shaped plate structures. Many investigators have dealt with the plastic analysis of structures composed of beam, plate or shell components. Most of the investigations have been concerned with the determination of the collapse load using the two fundamental theorems of limit analysis. These theorems were proved for elastic perfectly-plastic material by Drucker, Prager and Greenberg (Ref. 60).

Most of the approximate solutions for the collapse load are based on the upper bound approach. The limit load is computed on the basis of an assumed plastic velocity field, and the rate of internal plastic work is equated to the rate of external work. Upper bound solutions for a variety of plate problems are known and compiled in Refs. 61 and 62. Since the assumed collapse mechanism is chosen on a trial basis in such a way as to seek a minimum for the upper bound values obtained, this method is tedious. In addition, without the availability of at least one lower bound

solution, a designer cannot predict the accuracy of the best upper bound value. The application of this approach to structures combined of beams and plates is cumbersome since the true collapse pattern is difficult to establish. Furthermore, in this approach the material is assumed to be elastic-perfectly plastic, and the strain hardening effect is neglected. The yield line theory is based on the work of Bach (Ref. 58) and Johansen (Ref. 59). This theory is extensively used in the design of reinforced concrete slabs. Sawzuk and Jaeger (Ref. 62) summarize this theory and give a comprehensive bibliography of literature in this area. This method is subject to the same restrictions as discussed above.

Lower bound solutions are based on the lower bound theorems of limit analysis. In this approach the load is computed on the basis of an assumed equilibrium state of stress distribution which nowhere violates the yield condition. Very little work has been done in finding lower bound solutions needed to test the accuracy of upper bounds. Hodge (Ref. 56) gives a summary of the limit analysis theory pertaining to rectangular and circular plates. Shull and Hu (Ref. 63) utilized Tresca's yield criterion to arrive at lower bounds for uniformly loaded, simply supported rectangular plates. No exact solution is yet available for this relatively simple plate problem. Koopman and Lance (Ref. 64) introduced the concept of linear programming to arrive at lower bounds of the collapse load of plates made of perfectly-plastic material. A similar approach was pioneered by Wolfensberger

(Ref. 65) for reinforced concrete plates by linearizing the yield condition and using finite difference approximations.

In summary, although limit analysis techniques provide valuable information concerning the collapse mechanism and the collapse load, they cannot be used to predict the response of complex shaped plates in the post-elastic range.

4.2.2 Finite Difference Methods

Approximate solutions using the finite difference approach were obtained by Bhaumik and Hanley (Ref. 66) for the case of uniformly loaded rectangular plates. However, for this investigation it was assumed that at any mesh point of the plate the entire thickness is either fully elastic or fully plastic. This assumption facilitates the solution of a plate bending problem; however, for some structural materials the approximation of the moment-curvature relationship by two straight lines is unrealistic. In addition, finite difference approaches are not well-suited for automatic computation, and are greatly complicated if in-plane behavior is to be considered.

4.2.3 Discrete and Finite Element Methods

Among the methods that have been used successfully in the determination of approximate solutions to continuum problems are approaches in which the continuum is represented by a lumped parameter model. A model capable of treating flexural problems in plates was developed by Ang and Lopez (Ref. 44). This discrete

flexural model, in which the stiffness of the actual plate is lumped into a system of bars and springs, has been applied to small and large deformation plate problems. The field equations are derived in incremental form, leading to a linearization of the problem in the case of the small deflection analysis, and are shown to be the finite difference equivalent of the corresponding equations of the continuous plate. The inelastic analysis is greatly simplified in this approach by assuming that the plate can be represented by a sandwich plate consisting of two layers of an elastic perfectly-plastic material, and of a shear core between these two layers. Due to the tedious way of satisfying the boundary conditions, this method is not ideally suited for the development of a fully automated approach.

To date, finite element methods for the inelastic analysis of structures have been primarily developed for the analysis and design of aircraft structures. A review of the current state of the art of finite element analysis applied to inelastic problems is given by Armen, et al. (Ref. 67). It appears that most of the work has been done for plane stress or plane strain problems associated with either the Von Mises or the Tresca yield condition. Little work has been done in the inelastic analysis of plates and shells. To date, two different approaches have emerged. In the first approach, the accumulated plastic strains are treated as initial strains, and applied as forces to the structure. A solution is then obtained by using an appropriate convergent iterative

technique. This approach is referred to as the initial strain or initial stiffness approach, and was the earliest approach to plasticity analysis in the context of the finite element methods. The alternative approach requires the modification of the system stiffness matrix for each step, taking into account plastification when and wherever occurring, and resolving the final system of equilibrium equations at each step of an iteration. This approach is referred to as the tangent stiffness approach. Pope (Ref. 68) describes the application of the tangent stiffness approach for the analysis of plane elastic-plastic problems. In another recent paper, Anand, et al. (Ref. 69) describe a finite element stiffness approach to elastic-plastic plane stress problems based on Tresca's yield criterion.

Armen and Pifko (Ref. 70) used the initial stiffness approach in the analysis of beams, plates and shells. These authors point out the difficulties encountered in depicting the progressive yielding through the thickness of plates and shells subjected to bending, and base their analysis on an assumed variation in plastic strain from the surfaces of the element to an elastic-plastic boundary within the element. Popov, et al. (Ref. 71) divide the thickness of the plate into layers in their solution of elastic-plastic circular plate problems. Whang (Ref. 72) describes both the initial and the tangent stiffness approach in the solution of orthotropic plane stress, plate and shell problems, and presents elastic-plastic solutions for plates, using the initial stiffness

approach. Surveys and summaries of recent progress in the application of finite element techniques applied to materially and geometrically nonlinear problems have been given by Armen, et al. (Ref. 70) and Oden (Ref. 73).

4.3 A Finite Element Stiffness Approach Using a Layered Model

4.3.1 Description of the Layered Model

In this section a finite element displacement approach is described which allows the establishment of the entire load-formation behavior of arbitrarily shaped and loaded plates. Since the process and the extend of plastification are difficult to describe, a solution is accomplished by dividing each finite plate element into a number of layers in order to study its elastic-plastic behavior. The procedure is based on linear geometry; hence, it is applicable to problems where the structure experiences significant plasticity before the deformations become excessive. First, the in-plane deformations are neglected, but the model will allow in-plane behavior to be included, as will be shown in Chapter 5.

The method is based on the tangent stiffness concept. The load is applied in incremental form, and the method requires a modification of the element stiffness matrices at each incremental load step. The incremental approach allows the study of the entire load-deformation behavior of a plate structure. The method is outlined here for isotropic elastic linearly strain hardening material. However, it can easily be extended to arbitrary stress-strain

relationships, or orthotropic material, if the associated constitutive relations are known.

The process and the extent of plastification is difficult to describe in an arbitrarily shaped and supported plate. At loads higher than the elastic limit load, plastification begins and spreads in the plane of the plate, as well as through its thickness. In the present approach, a finite plate element is subdivided into a number of layers, as shown in Fig. 43. It is assumed here that the elastic-plastic behavior of a finite plate element can adequately be described by this layered model. Since the thickness of the plate can be subdivided into any desired number of layers, the approach should in the limit be able to represent the behavior of the actual plate. Each layer is assumed to be in a state of plane stress, and the state of stress at the centroid of a layer is taken as representative for the entire layer. The effect of this assumption can be studied by observing the convergence of solutions for different mesh sizes. Any even number of layers can be chosen in the present approach. Increasing the number of layers reduces the error introduced in the approximation of the real problem. Any layer is considered to be either elastic or elastic-plastic according to a criterion to be specified. In the case of transversely loaded plates, neglecting in-plane behavior, the strain distribution is symmetric with respect to the neutral axis of the plate, and only the layers lying on one-half of the finite plate element need be considered. It should be emphasized

that with this model the method is not restricted to a particular stress-strain relation. However, for demonstration purposes, the problems solved in this chapter are confined to materials exhibiting isotropic elastic perfectly-plastic behavior.

It is assumed that Kirchhoff's assumptions are satisfied by the model. In addition, compatibility of strain between any two layers is assumed. For the present investigation, all layers are assumed to be of the same thickness; however, differently thick layers could easily be incorporated. It is again assumed that the transverse shear stresses need not be considered. The four nodal points of a finite plate element are defined again at the middle plane of the plate, and internal stress resultants are defined at the centroid of a plate element. As seen from Fig. 43, the strains at any distance z_k from the middle plane of the plate to the centroid of layer k are given by:

$$\begin{bmatrix} \epsilon_x^k \\ \epsilon_y^k \\ \gamma_{xy}^k \end{bmatrix} = z_k \begin{bmatrix} 1 & 0 & 0 \\ 0 & 1 & 0 \\ 0 & 0 & 1 \end{bmatrix} \begin{bmatrix} \phi_x \\ \phi_y \\ \phi_{xy} \end{bmatrix} \qquad (4.1\,a)$$

or

$$\{\epsilon^k\} = [H^k] \{\phi\} \qquad (4.1\,b)$$

Having found the displacement field by the finite element displacement approach, which will be described in more detail in Section 4.4, the curvatures which are defined at the centroid of a finite

plate element, and the strains and stresses for each layer can be determined. The stress resultants per unit width of plate, defined at the centroid of a plate element, are then found by summing up the contributions of each of the layers:

$$M_x = \sum_{k=1}^{\ell} \sigma_x^k \; z_k \; t_k \qquad (4.2\text{ a})$$

$$M_y = \sum_{k=1}^{\ell} \sigma_y^k \; z_k \; t_k \qquad (4.2\text{ b})$$

$$M_{xy} = \sum_{k=1}^{\ell} \tau_{xy}^k \; z_k \; t_k \qquad (4.2\text{ c})$$

where ℓ is the number of layers and t_k the thickness of layer k, as shown in Fig. 43. Eqs. 4.1 and 4.2 can immediately be cast into an incremental form, and are used in this form in the proposed incremental approach. It should be mentioned that the number of degrees of freedom in the described approach will not be increased by increasing the number of layers, and is dependent only on the mesh size used and the number of degrees of freedom involved per nodal point of the selected finite plate element.

4.3.2 Loading and Elastic Stress-Strain Relations of a Layer

Each layer is assumed to be in a state of plane stress. The stresses acting in a layer are shown in Fig. 44. Each layer is loaded according to a loading program which can vary widely

for practical examples. The loading path, indicated by an arrow in Fig. 44, is described by successive values of the elements of the stress vector $\{\sigma\}$, which is defined as:

$$\{\sigma\}^T = < \sigma_x \quad \sigma_y \quad \tau_{xy} > \tag{4.3}$$

Since the proposed approach is formulated in incremental form, and makes use of plastic stress-strain relations derived from the flow theory, which are themselves incremental, no restrictions must be placed on the loading path. Unloading may or may not occur, and can be accounted for as will be described in Section 4.4.3. An approach based on the deformation theory would not be valid for other than monotonically increasing stresses, and would not allow unloading to occur.

In any elastic-plastic layer the total strains are composed of an elastic, recoverable part of strains and a plastic, irretrievable part of strains. Therefore, in incremental form one can write:

$$\{\dot{\epsilon}\} = \{\dot{\epsilon}^e\} + \{\dot{\epsilon}^p\} \tag{4.4}$$

where the individual strain rate vectors are defined as:

$$\{\dot{\epsilon}\}^T = < \dot{\epsilon}_x \quad \dot{\epsilon}_y \quad \dot{\gamma}_{xy} > \tag{4.5 a}$$

$$\{\dot{\epsilon}^e\}^T = < \dot{\epsilon}^e_x \quad \dot{\epsilon}^e_y \quad \dot{\gamma}^e_{xy} > \tag{4.5 b}$$

$$\{\dot{\epsilon}^p\}^T = < \dot{\epsilon}^p_x \quad \dot{\epsilon}^p_y \quad \dot{\gamma}^p_{xy} > \tag{4.5 c}$$

Elastic strain increments are related to the stress increments by Hooke's law, which in incremental form can be written as:

$$\{\dot{\sigma}\} = [D] \quad \{\dot{\varepsilon}^e\} \tag{4.6}$$

where [D] is the stress matrix as defined earlier, and for an isotropic material, is given by:

$$[D] = \frac{E}{1-\nu^2} \begin{bmatrix} 1 & \nu & 0 \\ \nu & 1 & 0 \\ 0 & 0 & \frac{1-\nu}{2} \end{bmatrix} \tag{4.7}$$

4.3.3 Yield Condition and Flow Rule for a Layer

No universal laws governing the plastic behavior of materials have yet been developed. Thus, a choice must be made, among the several existing plasticity theories, of one that successfully combines mathematical simplicity with good representation of the experimentally observed material behavior. A review of currently available plasticity theories is given in Ref. 74. One of the advantages of the finite element approach is that this method is capable of treating complex stress-strain relationships, including strain hardening of the material. The method is able to treat most engineering materials as long as the fundamental laws governing the plastic behavior of a material are known. The present approach is based on isotropic elastic-linearly strain hardening material. In addition, isotropic strain hardening is assumed, hence

simplifying the problem considerably. This theory assumes that during plastic flow the yield surface expands uniformly about the origin of the stress space. Since it is not the purpose of this investigation to develop new concepts in plasticity, no discussion pertaining to the validity of the basic equations is given. As postulated by Ziegler (Ref. 75), the plastic behavior of a material can be described by specifying the following relationships:

1. An initial yield condition defining the elastic limit of a material.
2. A flow rule relating the plastic strain increments to the stresses and stress increments.
3. A hardening rule, used to establish conditions for subsequent yielding from a plastic state of stress.

It can be shown that the points where initial yielding occurs form a space surface which is closed, convex and of the form

$$f^* (\sigma_{ij}) = f^* (\sigma_x, \sigma_y, \tau_{xy}) = 0 \qquad (4.8)$$

where σ_{ij} is the stress tensor describing the state of stress at the centroid of a layer. As shown in Fig. 44, all stress points lying inside the initial yield surface and producing no permanent strains in the virgin material are characterized by

$$f^* (\sigma_{ij}) < 0 \qquad (4.9)$$

and constitute the initial elastic range. A number of yield criteria are currently being used in the elastic-plastic analysis of structures. The most common ones are shown in Fig. 45 and are discussed for the case of plane stress.

Tresca's yield condition is depicted in Fig. 45 a and can be represented by

$$\max \left(|\sigma_1| ; |\sigma_2| ; |\sigma_1 - \sigma_2| \right) = \bar{\sigma} \qquad (4.10)$$

where σ_1 and σ_2 are the principal stresses in the layer and $\bar{\sigma}$ is the current yield stress in simple tension.

Von Mises' yield condition, as shown in Fig. 45 b, is often used since it describes the initial yield surface as a smooth surface in the stress space, and is representable in simple mathematical form. This yield condition is given by

$$J_2 - \frac{1}{3}\bar{\sigma}^2 = \frac{1}{2} S_{ij} S_{ij} - \frac{1}{3}\bar{\sigma}^2 = 0 \qquad (4.11)$$

where: J_2 = Second invariant of the stress deviator tensor

and S_{ij} = Stress deviator tensor defined as

$$S_{ij} = \sigma_{ij} - \frac{1}{3}\sigma_{kk} \qquad (4.12)$$

in which σ_{kk} is the sum of the principal normal stress components.

Johansen's yield condition is a special case of the maximum stress theory introduced by Rankine. This yield condition is

depicted in Fig. 45 c and is the basis of Johansen's approach to the yield line theory.

Although the presently discribed approach could be easily extended to any one of the shown yield conditions, and to other yield conditions as well, Von Mises yield condition is chosen for all investigations described in this report. In Cartesian coordinates, this condition is given by:

$$\sigma_x^2 + \sigma_y^2 - \sigma_x\sigma_y + 3\tau_{xy}^2 - \bar{\sigma}^2 = 0 \qquad (4.13)$$

For an isotropic strain hardening material, the subsequent yield surface can be represented by:

$$f\ (\sigma_{ij},\ m) = 0 \qquad (4.14)$$

where m is a measure of the degree of strain hardening of the material. It is assumed that the concept of effective stress can be used to describe the beginning of yielding in a strain hardening material which is subjected to a biaxial state of stress. The basis of this concept is the equivalent stress versus total strain curve (as shown in Fig. 46), which is assumed to be identical with the stress-strain relationship found from a simple tension test. The use of this approach allows the establishment of the conditions for subsequent yielding from a plastic state of stress and is given by:

$$\bar{\sigma} = m\ \sigma_o \qquad (4.15)$$

where σ_o is the initial effective stress and $\bar{\sigma}$ is the current effective or equivalent stress and is taken directly from the stress-strain relationship found in a simple tension test. Eq. 4.14 can then be written as follows for the case of a Von Mises' material:

$$f\ (\sigma_{ij},\ m) = \frac{1}{2}\ S_{ij}\ S_{ij} - \frac{1}{3}\ \bar{\sigma}^2 = 0 \qquad (4.16)$$

This equation represents the loading function, indicating further plastic straining if the equation is satisfied identically ($f = 0$), and elastic behavior if $f < 0$. Eq. 4.16 indicates that the effective stress is related to the stress components as follows:

$$\bar{\sigma} = (\sigma_x^2 + \sigma_y^2 - \sigma_x\sigma_y + 3\tau_{xy}^2)^{1/2} \qquad (4.17)$$

Furthermore, $\bar{\sigma}$ is dependent on the amount of plastic deformation that has taken place, as shown in Fig. 46. In incremental form this relationship is of the form:

$$\dot{\bar{\sigma}} = E_p\ \dot{\epsilon}^p \qquad (4.18)$$

where E_p is the slope of the equivalent stress versus equivalent plastic strain curve. An expression for the effective plastic strain rate can be derived as a function of the increments of the plastic strain components; thus:

$$\dot{\epsilon}^p = \left(\frac{2}{3}\ \dot{\epsilon}^p_{ij}\ \dot{\epsilon}^p_{ij}\right)^{1/2} \qquad (4.19)$$

The effective plastic strain $\bar{\epsilon}^p$ is found as the integral of Eq. 4.19, taken along the loading path so that all of the increments of plastic strain are included.

The yield condition and the loading function serve to establish criteria for yielding from elastic or plastic states of stress, respectively. The remaining problem is to establish relations for predicting the increments in the plastic strain components knowing what the increments in stress and the total stresses are. In order to arrive at plastic strain increments, it is assumed for the purpose of this work that the Prandtl-Reuss flow rule (Ref. 74), which is often used in connection with the Von Mises yield condition, is applicable. This constitutive relation, often termed flow rule, is based on Drucker's postulate for strain hardening material (Ref. 76), and can be written as:

$$\dot{\epsilon}^p_{ij} = \lambda \frac{\partial f}{\partial \sigma_{ij}} = \lambda \frac{\partial f}{\partial S_{ij}} = \lambda S_{ij} \qquad (4.20)$$

where λ is a positive scalar quantity, which can be found from a knowledge of the mechanical behavior of the material. Eq. 4.20 states that the increments of plastic strain depend on the current values of the deviatoric stress components and not on the stress increments to reach this state. Furthermore, it can be shown that the plastic strain increment vector is normal to the yield surface, as indicated in Fig. 44. To determine the unknown multiplier λ, use is made of the Von Mises' yield condition given by Eq. 4.16, and of the consistency equation:

$$\dot{f} = S_{ij}\,\dot{S}_{ij} - \frac{2}{3}\,\bar{\sigma}\,\dot{\bar{\sigma}} = 0 \qquad (4.21)$$

which expresses that the stress increment vector can only be tangential to the yield surface. As shown in Ref. 74, for example, λ is given by

$$\lambda = \frac{3}{2}\,\frac{\dot{\bar{\epsilon}}^p}{\bar{\sigma}} \qquad (4.22)$$

Combining Eq. 4.20 and Eq. 4.22 and using the strain hardening law, given by Eq. 4.18, leads to:

$$\dot{\epsilon}^p_{ij} = \frac{3}{2}\,\frac{S_{ij}\,\dot{\bar{\sigma}}}{\bar{\sigma}\;E_p} \qquad (4.23\,a)$$

or written explicitely in terms of stress components in the Cartesian stress space:

$$\{\dot{\epsilon}^p\} = \begin{bmatrix} \dot{\epsilon}^p_x \\ \dot{\epsilon}^p_y \\ \dot{\gamma}^p_{xy} \end{bmatrix} = \frac{\dot{\bar{\sigma}}}{\bar{\sigma}\;E_p} \begin{bmatrix} \sigma_x - \sigma_y/2 \\ \sigma_y - \sigma_x/2 \\ 3\tau_{xy} \end{bmatrix} \qquad (4.23\,b)$$

Eq. 4.23 establishes the relationships for predicting the increments in the plastic strain components in terms of the current state of stress, the anticipated increments in effective stress, and E_p, the slope of the effective stress versus effective plastic strain curve as shown in Fig. 46

4.3.4 Elastic-Plastic Stress Matrix for a Layer

For the purpose of deriving the element stiffness matrices used in the finite element displacement approach, which due to the nonlinear nature of the problem, is to be formulated in incremental form, the relationship is sought between the increments in stress and the increments in total strain. A step-by-step method is suited to follow the process of plastification in a structure for which the entire load-deformation history is desired. Having presented the fundamental constitutive relations in the previous section, the elastic-plastic stress matrix needed to generate the element stiffness matrices must now be derived. In order to be able to treat the limiting case of perfect plasticity, as well as the case of work hardening material, with the same general procedure, the following formulation, as described by Felippa (Ref. 77), is adapted. Starting with Eq. 4.17, one finds by implicit differentation:

$$2\bar{\sigma}\dot{\bar{\sigma}} = 2\sigma_x\dot{\sigma}_x - \sigma_y\dot{\sigma}_x + 2\sigma_y\dot{\sigma}_y - \sigma_x\dot{\sigma}_y + 6\tau_{xy}\dot{\tau}_{xy} \qquad (4.24)$$

The rate of effective stress, which is a scalar quantity, is derived from this expression, and can be written as follows:

$$\dot{\bar{\sigma}} = [A]^T \{\dot{\sigma}\} \qquad (4.25)$$

where the vector of stress rates is defined as:

$$\{\dot{\sigma}\}^T = < \dot{\sigma}_x \quad \dot{\sigma}_y \quad \dot{\tau}_{xy} > \qquad (4.26)$$

and [A] is a matrix connecting the rate of effective stress to the rates of total stress, given by:

$$[A] = \begin{bmatrix} (\sigma_x - \sigma_y/2)/\bar{\sigma} \\ (\sigma_y - \sigma_x/2)/\bar{\sigma} \\ 3\tau_{xy}/\bar{\sigma} \end{bmatrix} \tag{4.27}$$

Using Hooke's law, given by Eq. 4.6, and making use of the fact that elastic and plastic strain components can be separated, the vector of stress rates can be written as:

$$\{\dot{\sigma}\} = [D] \left\{ \{\dot{\epsilon}\} - \{\dot{\epsilon}^p\} \right\} \tag{4.28 a}$$

which, when using the constitutive equation 4.23 b, leads to:

$$\{\dot{\sigma}\} = [D] \left\{ \{\dot{\epsilon}\} - [A]\ \dot{\bar{\epsilon}}^p \right\}. \tag{4.28 b}$$

Therefore, the rate of effective stress, as given by Eq. 4.25, can be written as:

$$\dot{\bar{\sigma}} = [A]^T\ \{\dot{\sigma}\} = [A]^T\ [D] \left\{ \{\dot{\epsilon}\} - [A]\ \dot{\bar{\epsilon}}^p \right\} \tag{4.29}$$

Making use of Eq. 4.18, the rate of incremental effective plastic strain can be found from the above expression as follows:

$$\dot{\bar{\epsilon}}^p = \frac{[A]^T\ [D]\ \{\dot{\epsilon}\}}{E_p + [A]^T\ [D]\ [A]} \tag{4.30}$$

Substituting Eq. 4.30 for $\dot{\bar{\epsilon}}^p$ in Eq. 4.29 leads to the desired

relationship between the increments of stress and the rates of total strain:

$$\{\dot{\sigma}\} = \left[[D] - \frac{[D]\,[A]\,[A]^T\,[D]}{E_p + [A]^T\,[D]\,[A]} \right] \{\dot{\epsilon}\} \qquad (4.31\ a)$$

which can be written simply as:

$$\{\dot{\sigma}\} = [D_e]\,\{\dot{\epsilon}\} \qquad (4.31\ b)$$

The matrix $[D_e]$, defined as:

$$[D_e] = \left[[D] - \frac{[D]\,[A]\,[A]^T\,[D]}{E_p + [A]^T\,[D]\,[A]} \right] \qquad (4.32)$$

provides for the new relationship between the increments of stress and the increments of total strain. Matrix $[D_e]$ is called the elastic-plastic stress matrix, and is applicable to any layer which is stressed into the plastic range. Using this approach, the degenerate case of perfect plasticity ($E_p = 0$) can be handled with ease. This is in contrast to the initial stiffness approach, which breaks down for this special but frequently occurring case. Furthermore, it should be observed that matrix $[D_e]$ is now fully populated, and must be evaluated for each layer separately. Its elements take on new values for each cycle of iteration. The above derived elastic-plastic stress matrix is the key to the derivation of the element stiffness matrices used in the proposed incremental finite element tangent stiffness approach.

4.4 Incremental Elastic-Plastic Solution Procedure

4.4.1 Assembly of the System Tangent Stiffness Matrix

The essential elements needed in the formulation of the proposed elastic-plastic finite element solution have been derived in Section 4.3. In view of a future extension of this approach to include non-linearity due to geometry, an incremental type formulation is desired in which solutions are obtained by solving a sequence of linear problems associated with an incremental application of the loading. A step-by-step procedure in connection with a small incremental loading is needed for this elastic-plastic analysis, since the relationship between stresses and strains and hence the systems stiffness matrix is nonlinear.

In this step-by-step analysis, the effect of the non-linear material behavior of a structure subjected to the load vector $\{F\}$ is approximated by the sum of a series of linear structures, each subjected to the load increment $\{\dot{F}\}$ and assuming that the deformations during each load increment are essentially linear. In the tangent stiffness approach, taken here as the basis for this inelastic analysis, the systems stiffness matrix $[K]$ of the entire structure at any stage of loading is a function of the existing values of stresses in the structure, and thus needs to be modified for each load increment. For each step, this effective, or often called instantaneous stiffness matrix $[K_e]$, must be assembled for the entire structure taking into account plastification in the plate structure. To simplify this task,

each finite plate element is further subdivided into a number of layers, as discussed in Section 4.3. The stiffness contribution of each layer is then computed separately since the stiffness of any layer depends on the current state of stress; i.e. on the extent of plastification in a layer. The incremental displacement vector $\{\dot{\delta}\}$ resulting from the applied load increment $\{\dot{F}\}$ is then obtained by solving the basic stiffness relationship, which can be written in incremental form as:

$$\{\dot{F}\} = [K_e]\ \{\dot{\delta}\} \qquad (4.33)$$

in which $[K_e]$ is the tangent stiffness matrix for the entire structure, the coefficients of which are recomputed for each load increment by using appropriate incremental stress-strain relations.

As given in Appendix III, the stiffness matrix for a homogeneous anisotropic rectangular plate element, as originally described by Adini, Clough and Melosh (Ref. 34), was rederived in suitable form for the purpose of the present analysis. Three degrees of freedom per nodal point were introduced for this element; namely the lateral deflection w and the two slopes of the deflected plate surface θ_x and θ_y. Taking any layer K of the layered plate model for the inelastic analysis of plates, as shown in Fig. 43, the stiffness contribution for this layer can immediately be derived from the expression for the stiffness matrix given in Appendix III:

$$[K]^k = \frac{1}{12}\left[(z_k^a)^3 - (z_k^i)^3 \right] [C^{-1}]^T \Big[D_{11}[K_1] + D_{12}[K_2] + D_{13}[K_3] + D_{22}[K_4] + D_{23}[K_5] + D_{33}[K_6] \Big] [C^{-1}] \qquad (4.34)$$

in which $[K_i]$, where $i = 1, \cdots 6$ are component stiffness matrices and $[C]$ is a transformation matrix as given in Appendix III.

The process of assembling the systems stiffness matrix follows exactly the procedure outlined in Section 2.3, except that instead of treating a finite plate element at a time, a layer at a time must be considered. Depending on whether a layer is found to be elastic or plastic, appropriate stress-strain relationships, here formulated in incremental form as given by Eq. 4.6 or Eq. 4.31, must be used. The coefficients D_{ij} of the stress matrix for an elastic layer are always constant and given by Eq. 4.7, whereas the coefficients D_{ij} for a plastic layer take on different values for subsequent states of platification and must be evaluated for each cycle of iteration. These coefficients depend on the current state of stress σ_{ij} in a layer as well as on its effective stress $\bar{\sigma}$ given by Eq. 4.17, and the strain hardening parameter E_p.

Explicitly, these coefficients can be evaluated using Eq. 4.32 since at the start of an iteration cycle the current state of stress in a layer and all other needed quantities are known. The procedure for evaluating the stiffness of a plastic layer is as follows:

1. Evaluate the coefficients of matrix [A].

2. Evaluate the coefficients of matrix $[D_e]$.

3. Find the stiffness contribution of the layer in consideration by evaluating Eq. 4.34 and add it to the already accumulated stiffness.

The total stiffness of a finite plate element must be assembled by considering each layer separately and summing up all stiffness contributions. In the case of transversely loaded plates neglecting in-plane deformation, a pair of layers lying symmetric with respect to the middle plane of the plate can be treated at a time. Performing this process for all layers and considering all plate elements leads to the instantaneous or tangent systems stiffness matrix for the entire structure. As this is true for all presently known approaches capable of handling inelastic problems, the availability of a high-speed digital computer is essential for a successful implementation of this approach.

4.4.2 The Iterative Solution Technique

The iterative solution technique used for the solution of inelastic plate problems is summarized graphically by the flowchart shown in Fig. 47. A unit load is applied first to the initially assumed stress-free structure and the associated elastic stress distribution is obtained. The applied loads are then scaled up so as to cause initial yielding in the most stressed layer. This is done by comparing for each layer the effective stress representing the elastic limit of the material in

consideration. Since in the elastic range, and assuming first order theory, stresses and deformations are directly proportional to the applied load, the values of these field quantities can be equally found by scaling up the appropriate values found for the applied unit load.

The structure ceases to behave linearly elastic for loads higher than the elastic limit load. Thus, an incremental procedure must be used to find its response in the non-linear range. Since the final state of stress is not known in advance for each applied load increment added to the accumulated load, an iterative solution is needed to find the new equilibrium configuration corresponding to the applied load increment. Starting out with known values of all involved field quantities at the elastic limit load level, an increment of load $\{\dot{F}\}$ is applied to the structure first. To arrive at the new equilibrium configuration corresponding to this load increment an iterative procedure is started, described here for the i-th cycle of iteration.

For this i-th cycle of the current iteration, the following quantities are known specifically for each layer: First, $\{\sigma\}^{i-1}$, the accumulated stresses as computed at the end of the (i-1)-th cycle are known and hence, $\bar{\sigma}^{i-1}$, the total effective stress can be found. In addition, the maximum effective stress $\bar{\sigma}_{max}^{i-1}$ recorded during the entire loading history is stored. The iteration proceeds as described by the following steps:

1. Assume all layers to be in the same state of stress as

found in the previous cycle; or, if the iteration is started, as found in the last cycle of the previous load increment.

2. For any plastic layer, compute the coefficients of matrix [A]. This step is omitted if a layer is found to be elastic.

3. Compute the coefficients of matrix $[D_e]$ for any plastic layer. For elastic layers use matrix [D], the elements of which always remain constant.

4. Compute the stiffness contribution of this layer as outlined in Section 4.4.1.

5. Add the stiffness contributions of all layers appropriately and establish in this fashion the systems tangent stiffness matrix $[K_e]$ for the entire structure.

6. Solve the system of incremental equilibrium equations $\{\dot{F}\} = [K_e]\ \{\dot{\delta}\}$ for the unknown incremental nodal displacement vector $\{\dot{\delta}\}^i$.

7. Compute the rates of curvature $\{\dot{\emptyset}\}^i$ at the centroid of each plate element using the curvature-displacement relations as given in Appendix III.

8. Compute the total strain rates $\{\dot{\epsilon}\}^i$ at the centroid of each layer using the strain-curvature relations.

9. Find the stress rates $\{\dot{\sigma}\}^i$ at the centroid of each layer

using the incremental stress-strain relations given by Eq. 4.31 b for a plastic layer, or by Eq. 4.6 for a layer found to be elastic, respectively.

10. Find the total stresses $\{\sigma\}^i$ at the centroid of each layer by adding the stress increments to the previously accumulated stresses; i.e. $\{\sigma\}^i = \{\sigma\} + \{\dot{\sigma}\}^i$.

11. Check whether layers which were originally elastic are still elastic. Also check the computed effective stress $\bar{\sigma}^i$ against the assumed effective stress $\bar{\sigma}^{i-1}$ for all plastic layers. If $\bar{\sigma}^i$ is within a specified tolerance of $\bar{\sigma}^{i-1}$, then the iteration is terminated and the next load increment is applied to the structure. If $\bar{\sigma}^i$ is not within a tolerance of $\bar{\sigma}^{i-1}$, then the newly computed values for stresses $\{\sigma\}^i$ and effective stress $\bar{\sigma}^i$ are used as new initial guesses for cycle (i + 1). Steps 1 through 11 are then repeated until either $\bar{\sigma}$ is found within a certain tolerance or a specified number of cycles is exhausted. Accumulated values for all needed field quantities can then be computed and printed out if desired.

The analysis proceeds exactly in the same way for the next load increment. Basically, arbitrary values for $\{\dot{F}\}$ could be assigned; however, the present investigation was restricted to the case of proportional loading. It should be mentioned here that

the effect of different values of $\{\dot{F}\}$ on the convergence and accuracy of the involved field quantities can be studied easily by specifying different values for the incremental load and observing the convergence behavior. The effect of the chosen tolerance for the effective stress in a layer can be studied similarly as will be discussed in the presentation of the numerical examples.

4.4.3 Unloading and Neutral Loading of a Layer

By definition, a layer is termed elastic if its effective stress $\bar{\sigma}$ computed at the centroid of the layer is less than the current yield stress of the material. A plastic layer is characterized by the fact that its effective stress is equal to the current effective stress of the material. For such a layer the total strain is composed of an elastic and a plastic part. In the preceeding section it was assumed that those layers which were assumed plastic are being stressed further into the plastic range as the applied loads increase. This assumption must be checked in the analysis by computing the effective stress corresponding to the total stresses in each layer and comparing it to its previous value. If the computed value for the effective stress in the i-th cycle is found to be greater than the stored value, found in cycle (i-1), then the layer in consideration is being further loaded plastically.

On the other hand, if the newly computed value for the effective stress is less than the previously found value, elastic

unloading has taken place. When this occurs, the elastic stress-strain relations must be used and the analysis proceeds as outlined above. It should be mentioned that unloading can occur even though the externally applied loads are monotonically increasing. During unloading the stress path moves inside the current yield surface. Mathematically speaking, unloading from a plastic state which is characterized by Eq. 4.16, occurs if

$$\dot{f} = S_{ij}\dot{S}_{ij} - \frac{2}{3}\bar{\sigma}\dot{\bar{\sigma}} < 0 \qquad (4.35)$$

As this is usually done, it is assumed that elastic straining does not change the yield surface and subsequent loading follows the unloading path as indicated in Fig. 46.

Neutral loading is defined as loading from one plastic state to another plastic state in such away as to cause no plastic straining. In this case the stress path is moving tangential to the yield surface and in the analysis the elastic or elastic-plastic stress-strain relations can be used.

4.4.4 Yield Surface Correction

In the iterative procedure as described in Section 4.4.2 it is advantageous to find improved values for the state of stress in a layer before entering the next cycle of a given iteration. Convergence is then obtained faster resulting in considerable savings in computer time. Depending on the type of material used, different approaches can be taken to improve the initial guesses

for stresses and for the effective stress. Although the outlined tangent stiffness approach is valid for the more general case of elastic-linearly strain hardening material, the problems treated in this chapter and chosen for the purpose of demonstrating the application of this method are confined to materials exhibiting elastic perfectly-plastic material behavior.

The method of arriving at new improved guesses for stresses in a layer, outlined in this section, is limited to materials exhibiting elastic perfectly-plastic material behavior. A similar approach could be taken for the more general case of linearly-strain hardening material. As mentioned earlier, the incremental stress vector as shown in Fig. 48 is restricted to lie in the tangential plane to the current yield surface which, in the case of a perfectly-plastic material, is always identical with the initial yield surface. However, for any finite increment of load the stress rate vector will be of finite length and hence cannot remain on the yield surface. The state of stress must therefore be corrected in order to conform with the assumptions associated with perfectly-plastic material. This can be done by adding a correction vector to the incremental stress vector as shown in Fig. 48. This yield surface correction is best done in the deviatoric stress space and the following quantities are to be defined for this derivation:

$\{S'\} = (S'_x, S'_y, S'_{xy})$ = The uncorrected deviatoric stress vector

$\{S\} = (S_x, S_y, S_{xy})$ = The corrected deviatoric stress vector

$\{CB\}$ = The correction vector defined by

$$\{S\} = \{S'\} + \{CB\} \tag{4.36}$$

J'_2 = The second invariant of the deviatoric stresses computed from uncorrected stresses

J_2 = The second invariant of the deviatoric stresses computed from corrected stresses

These two quantities can be evaluated if the respective stresses are known; they are related by

$$J'_2 = J_2 + \xi^2 \tag{4.37}$$

where ξ^2 is defined as the error in J'_2. The correction vector is defined to be normal to the yield surface in the deviatoric stress space and is of unknown length c. It follows from the requirement of normality:

$$\{CB\} = c \frac{\text{grad}J_2}{|\text{grad}J_2|} = c \frac{\nabla J_2}{|\nabla J_2|} \tag{4.38}$$

For perfectly-plastic Von Mises' material, J_2 is given by:

$$J_2 = \frac{1}{2} S_{ij} S_{ij} = \frac{1}{3} \sigma_o^2 = k^2 \tag{4.39}$$

where k is the yield stress in pure shear. Proceeding now with the evaluation of the length of the gradient vector to the yield surface, one finds:

$$|\nabla J_2| = \sqrt{2J_2} = \sqrt{2k^2} \tag{4.40}$$

Substituting Eq. 4.38 and Eq. 4.40 into Eq. 4.36, and observing that $\nabla J_2 = \{S\}$ leads to

$$\{S'\} = \left[1 - \frac{c}{\sqrt{2k^2}}\right] \{S\} \tag{4.41}$$

Since J_2 and J_2' are quadratic functions of the deviatoric stresses it follows directly:

$$J_2' = \left[1 - \frac{c}{\sqrt{2k^2}}\right]^2 J_2 \tag{4.42}$$

Substituting Eq. 4.37 and Eq. 4.39 into Eq. 4.42 yields:

$$c = k\sqrt{2}\left[1 \pm \sqrt{1 + \xi^2/k^2}\right] \tag{4.43}$$

Linearizing the expression for the square root in Eq. 4.43, leads finally to:

$$\{S'\} = \left(1 + \frac{\xi^2}{2k^2}\right) \{S\} \tag{4.44}$$

Introducing now:

$$\delta = \frac{\xi^2}{2k^2} \tag{4.45}$$

the corrected deviatoric stress vector is found to be

$$\{S\} = \frac{\{S'\}}{1 + \delta} \tag{4.46}$$

and hence, the corrected stresses are given by:

$$\sigma_{ij} = \frac{\sigma'_{ij}}{1 + \delta} \tag{4.47}$$

The stresses computed in each plastic layer are to be corrected according to Eq. 4.47 before entering into the next cycle of the iteration. Finally, the evaluation of δ, given by Eq. 4.45, leads to:

$$\delta = \frac{1}{2}\left[\frac{\bar{\sigma}^2}{\sigma_o^2} - 1\right] \tag{4.48}$$

4.5 Numerical Results

The following examples have been selected to illustrate the application of the proposed finite element tangent stiffness approach for solving inelastic plate problems. A general computer program has been written for the implementation of this approach. This program allows the tracing of the entire load-deformation behavior of arbitrarily shaped and loaded plates. The approach was outlined in the previous sections of this chapter for the case of isotropic elastic, linearly-strain hardening material. An extension to include orthotropic material behavior can be easily made if the associated constitutive relations are known.

The validity of the proposed method is demonstrated on a few example solutions giving an indication of the reliability of the approach. To simplify comparisons with analytic solutions, the material was restricted to behave elastic perfectly-plastic ($E_p = 0$) and Von Mises' yield criterion in connection with the Prandtl-Reuss' flow rule were used in the solution of all example problems. However, other types of yield conditions could easily be incorporated as well in the present approach.

For the purpose of this investigation all example structures are thought to be made of structural steel with the following numerical values for the material behavior assumed in the analysis:

$$E = 30{,}000 \text{ ksi} \qquad E_p = 0$$

$$\sigma_o = 36 \text{ ksi} \qquad \nu = 0.30$$

The results are presented in non-dimensional form in terms of

$\bar{p} = p/p_y$ = Actual load divided by p_y, where

p_y = The load level at which yielding is initiated

δ_y = The deflection of a point representative for the behavior of the structure at first yielding

M_p = Moment capacity per unit width of plate

All other assumptions made concerning discretization and the geometry of the example structures chosen are listed in the

accompanying figures presented for each problem. The general computer program developed to implement the proposed approach yields the incremental and accumulated values of all involved field quantities; thus it allows the study of the complete elastic-plastic behavior of complex shaped plates.

4.5.1 Simply Supported and Clamped Plate Strip

The proposed method of analysis was first applied to a few simple problems for which the exact solution can be found from the theorems of limit analysis. Fig. 49 shows the load-deflection behavior of a simply supported and uniformly loaded plate strip of unit width. Sixteen elements were used in the idealization of a half-span of the plate strip. Results are plotted for different numbers of layers: k = 6, 8 and 10. It is recognized that an increase in numbers of layers used for the discretization of the plate elements leads to a better approximation of the collapse load. In addition, closer results would be obtained for a finer discretization of the plate strip. For the same example, the propagation of the elastic-plastic boundary for k = 10 (k = number of layers) is depicted in Fig. 50. The elastic-plastic boundary is in general a space surface and difficult to determine analytically. The error introduced in the present approach will be reduced if a finer mesh is used and the number of layers is increased at the locations of greater rate of change of curvature in the plate strip. It is worth noting here, that for the continuous

plate strip, collapse would occur as soon as the center section is fully plastic. In the finite element analysis, however, collapse does not occur until the two innermost layers closest to the center-line of the plate strip yield. In the numerical analysis, this state is indicated by a sudden, rapid increase in deflection. Mathematically speaking, the system stiffness matrix has become singular.

Similarly, the load-deflection behavior of a clamped plate strip of unit width is shown in Fig. 51. As predicted by simple plastic beam theory, this structure can withstand substantial additional loads after first yielding has taken place. The analysis was again performed for different numbers of layers; i.e. for k = 6, 8 and 10 and the respective response is plotted in the same figure. Closer results would again be obtained if a finer mesh size were used. The propagation of the elastic-plastic boundary and the extent of plastification is shown in Fig. 52. The structure becomes unstable as soon as the two innermost layers closest to the center-line of the plate strip exhibit plastic behavior. Fig. 53 is drawn to demonstrate the redistribution of plate moments M_x and M_y along the length of the clamped plate strip. The variation of all other stress and deformation components could be studied in a similar way. It should be noted that the theorems of limit analysis can be used to compute the exact collapse load for these two introductory examples. However, the calculation of the exact collapse load is possible in but a few simple cases.

4.5.2 Simply Supported Square Plate

The behavior of plates of various shapes subject to various boundary conditions and loading is of special interest to the designer and is considered a difficult problem if the elastic-plastic response of such structures is sought. The response of a few typical plate structures stressed into the inelastic range will be presented next in order to demonstrate the versatility of the proposed finite element approach. The load-deflection behavior of the center point of a simply supported and uniformly loaded square plate is illustrated in Fig. 54, along with the best upper and lower bound found in the literature. Sixteen rectangular plate elements were used for the discretization of one quadrant of the plate and six layers were chosen for each finite plate element. It is recognized from this figure that, despite the relatively rough mesh chosen, an already satisfactory solution is obtained. The propagation of yielded regions for different load levels is shown in Fig. 55. Plastification begins at the corners of the square plate and slowly spreads toward the center of the plate. The progression of yielding is in agreement with the solution given by Ang and Lopez (Ref. 44), which is based on a discrete element approach, as discussed in Section 4.2. However, the load-deflection curve found in the present approach is considerably different from the curve obtained by the cited authors due to their assumption of a two layer sandwich-type plate model used in their work.

As this is usually done, the collapse load of this structure is defined as the value of the load at which the pattern of fully plastic elements is such that the structure becomes a mechanism. It is seen from Fig. 54 that substantial deformations must take place before this stage is reached and a small deflection analysis is in fact not capable of predicting the correct collapse load for certain types of structures. Nevertheless, a value of $0.982\ (24\ M_p/L^2)$, where L is the span of the square plate, is estimated for the present example and this value can now be compared with available solutions. This comparison is made in Table 20, where the estimated limit load is compared with available upper and lower bound, finite difference and finite element solutions. An improved solution would be obtained for a finer mesh.

4.5.3 Clamped Square Plate

The elastic-plastic behavior of a uniformly loaded square plate is shown in Fig. 56 along with the best known upper and lower bound solution found in the literature. It is seen that the assumed discretization of sixteen elements per quarter of the plate leads to a slightly higher collapse load than predicted by the best known upper-bound solution. This is due to the fact that the chosen rough discretization cannot properly account for the high stress gradients occurring in the vicinity of the clamped edges. Performing the analysis with the next finer mesh, which

contains thirty-six elements per quadrant of the plate, leads to an improved result as seen from this figure. Fig. 57 depicts the sequence of yielding and the extent of plastification for the same problem. A comparison of this sequence of yielding, which agrees again with the one given by Lopez and Ang (Ref. 44), with the propagation of yielded regions of the simply supported plate reveals some interesting differences. Fig. 58 shows the redistribution of deflections as a result of the plastic flow. In Table 21, a comparison is made between the estimated limit load for this problem and the values found from different other approaches.

4.5.4 Square Plate with Three Edges Simply Supported and One Edge Free

The load-deflection behavior of a uniformly loaded square plate with three simply supported edges and one free edge is shown in Fig. 59. Due to symmetry in loading and geometry only one-half of the plate needs to be analyzed. The curve shown in Fig. 59 applies to the mid-point P of the free edge. No lower bound solution is known for this problem and it cannot be said with assurance how close the given upper bound solution found by Hodge (Ref. 78) is to the true solution. Fig. 60 depicts the propagation of yielded regions for increasing load and Fig. 61 demonstrates how the plate moments are redistributed as a result of plastic flow.

4.5.5 Plate Supported by Rows of Equidistant Columns (Flat Slab)

The load-deflection behavior of the center of a uniformly loaded square plate supported by rows of equidistant columns is illustrated in Fig. 62, along with a lower bound solution found by Wolfensberger (Ref. 65) and an upper bound solution given in (Ref. 61). Attention should be focused to the large additional strength that can be carried by this structure beyond first yielding. The sequence of yielding for this structure is shown in Fig. 63.

4.6 Convergence and Accuracy of Solutions

The presented examples show the validity of the proposed numerical technique from which approximate solutions to complex elastic-plastic plate problems can be obtained. No formal proof of the correctness of the solution method was attempted in this investigation and hence the reliability of the numerical solutions can only be shown on the basis of known solutions found by the theorems of limit analysis or by other types of analysis. This comparison was made whenever possible and the solutions found by the present approach are strongly supported by solutions derived from the theorems of limit analysis. All problems chosen in this investigation were analyzed using a relatively rough discretization. Improved results would be obtained if the mesh size is reduced or the number of layers is increased. This is demonstrated in Figs. 49, 50 and 54. A tolerance of 5% was usually specified

for the effective stress leading to two or three cycles per iteration for each applied load increment. A smaller value for this tolerance increases the number of cycles needed for convergence; thus, increasing the computer time considerably.

4.7 Summary

A finite element analysis capable of predicting the elastic-plastic behavior of complex shaped plates has been presented in this chapter. The approach is formulated in incremental form and is based on linear geometry. Hence, it is applicable to problems where the structure experiences significant plasticity before the deformations become excessive. A layered model is used to aid in the description of the elastic-plastic behavior of each finite plate element since the process of plastification is mathematically difficult to describe. The approach is based on the tangent stiffness concept and an iterative solution technique is needed to find the new equilibrium configuration corresponding to each applied load increment. For each cycle of iteration, the effective or instantaneous stiffness matrix of the entire structure is recomputed and the governing linear system of equilibrium equations is solved repeatedly. A few example solutions prove the validity of the proposed numerical technique which is applicable to plates of arbitrary geometry and loading and can be extended to more complex material behavior.

5. ELASTIC-PLASTIC ANALYSIS OF STIFFENED PLATES

5.1 Introduction

The behavior of eccentrically stiffened plate structures in the inelastic range is required to assess the effects of overloading and to compute the ultimate load-carrying capacity of such structures as a whole as well as that of its components. The most commonly used methods of elastic analysis for stiffened plate structures were discussed in Chapter 3, along with their possible extension to include the inelastic behavior of such structures. From an extensive literature survey it was concluded that the classical methods of elastic analysis are not suitable to study the inelastic response of beam-slab type structures and the application of the finite element method was again found to be the best suited. The reliability of the finite element tangent stiffness approach in solving elastic-plastic plate problems was demonstrated in Chapter 4. This approach will be extended to stiffened plates in this chapter making use of a layered beam model which is attached to the layered plate model described in the previous chapter. In-plane behavior must be considered and an incremental analysis is again required to solve this mathematically difficult problem.

5.2 A Finite Element Approach Using a Layered Model

5.2.1 Description of the Layered Beam-Plate Model

The finite element tangent stiffness approach described

in Chapter 4 for the elastic-plastic analysis of plates is extended in this chapter to eccentrically stiffened plates of arbitrary shape and loading. This problem being complex and not amenable to analytic solution, a numerical solution is worked out based on a layered system of beam and plate elements. A layered beam model is attached to layered plate elements in order to be able to describe the process of yielding in the actual beam-plate structure. It is assumed that the structure experiences significant plasticity before the deformations become excessive permitting the formulation of the outlined approach to be based on the first order theory. In-plane deformations and forces must be considered in the present analysis because both quantities are of prime interest in a stiffened plate structure. In view of a future inclusion of nonlinearities due to geometry, the tangent stiffness approach was preferred to the initial stiffness approach. As in the case of the analysis of inelastic plates, the load is applied incrementally, the stiffness matrix of the system must be derived and solved repeatedly for each load increment. The approach allows the tracing of the entire load-deformation relationship for any point of interest in the structure and the study of the process of plastification of complex shaped stiffened plates. The method is developed for an isotropic elastic linearly-strain hardening material; however, it can be easily extended to cope with arbitrary material behavior.

Plate elements are subdivided into a number of layers,

as described in Chapter 4, in order to be able to follow the process of plastification in the plate. Each layer is assumed to be in a state of plane stress and the state of stress at the centroid of a layer is taken as representative for the entire layer. Any layer is considered either elastic or elastic-plastic depending on the magnitude of effective stress present in this layer at a given load level. In the present analysis, the increments of total strain are computed as the sum of strain increments resulting from in-plane and out-of-plane behavior. In-plane strains in any layer k are computed at the centroid of this layer using the basic relationships derived in Appendix IV:

$$\{\dot{\epsilon}_i\}^k = [B]\ \{\dot{\delta}_i\}^e \qquad (5.1)$$

where [B] is the matrix connecting strains to nodal displacements as derived in Appendix IV and $\{\dot{\delta}_i\}^e$ is the nodal displacement vector made up of the consistent listing of in-plane displacement components. The strains in any layer k associated with out-of-plane deformations of the plate are given by Eq. 4.1 b:

$$\{\dot{\epsilon}_0\}^k = [H^k]\ \{\dot{\emptyset}\} \qquad (5.2)$$

The curvature terms listed in $\{\dot{\emptyset}\}$ are again defined at the centroid of a plate element and are computed as shown in Appendix III. Having found the displacement field by the proposed analysis based on a trial stiffness matrix associated with the previous load

increment, the in-plane displacement components and the curvatures at the centroid of a plate element can be computed. The total strain increments can be evaluated by adding the strain increments resulting from in-plane and out-of-plane action:

$$\{\dot{\epsilon}\}^k = \{\dot{\epsilon}_i\}^k + \{\dot{\epsilon}_0\}^k \qquad (5.3)$$

Depending on the current magnitude of the effective stress in a layer, the stress increments are evaluated using basic relationships: Eq. 4.6 being valid for an elastic layer, and Eq. 4.31 b, if the layer is found to be plastic. It is seen that for the purpose of computing stress increments in an elastic-plastic layer, Eq. 4.31 b is still valid, if the current total stresses resulting from in-plane and out-of-plane action are substituted.

Yielding starts often at the bottom fiber of a stiffener element in an eccentrically stiffened plate and successively spreads across the entire beam cross section. In order to study the process of plastification in a beam, a stiffener element is subdivided into a number of layers as shown in Fig. 64. An approach based on the plastic hinge concept would grossly oversimplify the actual behavior. The interaction of all involved stress resultants acting on a beam element stressed into the plastic range is difficult to describe mathematically if one ceases to accept the yield hinge concept. In the most general case, two shear forces and the bending moment about the y-axis interact with the axial force and the twisting moment in a beam. In order to

avoid obscuring the overall analysis with this interaction problem, it is assumed for the present approach that the beams are slender. It is also assumed that the shear force as well as the twisting moment do not significantly affect yielding in a layer and can be neglected in the yield condition. It is further assumed that GK_T, the torsion constant of the stiffener remains unchanged. The effect of these assumptions could be studied in a more refined analysis. It is assumed in the present analysis that the elastic-plastic behavior of the beams can adequately be described by the proposed layered finite beam model. Due to the above stated assumptions a beam layeris seen to be in a state of uniaxial stress for consideration of yielding and hence the yield condition reduces to its simplest form. The state of stress at the centroid of a layer is taken as representative for the entire beam layer. Stresses in beam layers are computed based on a linear distribution of strain extending to the bottom fiber of the stiffener. Basically, an arbitrary stress-strain relationship could be specified for each stiffener layer. The problems solved in this chapter are confined to isotropic elastic perfectly-plastic behavior of the material. It is expected that this approach can be extended to beams made of reinforced concrete by appropriate consideration of the material behavior of each layer made of concrete or reinforcing steel.

In the present analysis, any layer must be specified by its width, thickness and its distance to the plane of reference,

which is defined to coincide with the middle plane of the plate. As defined in Chapter 3, a beam element is bounded by two nodal points I and K, lying in the middle plane of the plate as shown in Fig. 64. Due to the incremental nature of the analysis proposed, the axial strain increments in any beam layer K due to bending moment and axial force can be evaluated separately using basic relationships. The total strain can then be obtained by adding the two parts. The axial strain component in any layer K is given by:

$$\dot{\epsilon}_s^k = \frac{1}{L}\left[(\dot{u}_k - \dot{u}_i) + Z_k(\dot{\theta}_{yk} - \dot{\theta}_{yi}) \right] \qquad (5.4)$$

Using this expression, the strain can be computed at the centroid of any layer K if the displacement components, as defined in Chapter 3, are known. Having determined the strain increment, the associated stress increment is found from the stress-strain relationship specified for the beam layer in consideration. The stress resultants acting on a beam element are defined at the plane of reference and are found by adding up the contribution of each layer:

$$\dot{M}_s = \sum_{k=1}^{\ell} \dot{\sigma}_x^k \, z_k \, t_k \, b_k \qquad (5.5)$$

$$\dot{N}_s = \sum_{k=1}^{\ell} \dot{\sigma}_x^k \, t_k \, b_k \qquad (5.6)$$

where ℓ is the number of beam layers, t_k is the thickness and b_k is the width of beam layer K.

5.2.2 Elastic-Plastic Stress-Strain Relations

The elastic-plastic response of beam and plate layers must be known in order to be able to formulate the proposed analysis. Plate layers are treated exactly as discussed in Chapter 4, which deals with the inelastic analysis of transversely loaded plates. In the presently discussed incremental elastic-plastic analysis of unsymmetrically stiffened plates, the stresses resisted by a layer due to in-plane and out-of-plane action must be considered. These stress increments are computed from incremental total strains which are found from appropriate strain-displacement relations. The same equations as derived in Sections 4.3.2 and 4.3.3, governing the elastic-plastic behavior of a layer, are applicable if the total stresses resulting from in-plane and out-of-plane action are substituted into these equations. No restrictions must be placed on the loading path, since the plastic stress-strain relations derived from the flow theory are themselves incremental. In the present analysis, Von Mises' yield condition in connection with Prandtl-Reuss' flow rule is adapted and the derivation of the stress-strain relations given in Section 4.3.3 for an elastic linearly-strain hardening material shall apply. If the computed effective stress in a plate layer is less than the specified value, the layer is termed elastic and Eq. 4.6 is applicable. For an elastic-plastic layer in which the total strains are composed of elastic and plastic parts, the incremental stress-strain relations given by Eq. 4.32, are used. Neutral loading and

unloading are treated as discussed in Chapter 4. From these stress-strain relations the increments of stresses for given increments of total strain resulting from in-plane and out-of-plane behavior of the stiffened plate are determined. The elastic-plastic stress matrix found in this manner is required to generate the element stiffness matrices associated with in-plane and out-of-plane behavior of the finite plate element.

Due to the assumption made that the twisting moment as well as the shear forces are small and need not be considered in the yield condition, each beam layer is stressed uniaxially. Furthermore, it is assumed that the beams are made of elastic linearly-strain hardening material of the type shown in Fig. 46. If the total stress is less than the current yield stress, a beam layer K is considered elastic and the increment of stress is found from the increment of strain by:

$$\{\dot{\sigma}_s\}^k = [D_s]\ \{\dot{\epsilon}_s\}^k \tag{5.7}$$

where $[D_s]$ is a matrix consisting of one element of value E_s, the modulus of elasticity of the beam material. If the current total stress is equal to the current yield stress, the layer is considered to be elastic-plastic and the increment of stress is given by:

$$\{\dot{\sigma}_s\}^k = [D_{se}]\ \{\dot{\epsilon}_s\}^k \tag{5.8}$$

where $[D_{se}]$ is identical with the strain-hardening modulus E_{ps}.

5.2.3 Generation of Element Stiffness Matrices

The instantaneous element stiffness matrices are established in a similar manner as described in Chapter 3, which presents an elastic finite element analysis of eccentrically stiffened plate structures. The elastic-plastic analysis of eccentrically stiffened plates requires again a step-by-step iterative procedure. The fact that first order theory is assumed to be adequate and hence, the structure is assumed to behave linearly elastic for each increment of load allows computing of the in-plane and out-of-plane stiffness matrices separately and to construct the system stiffness matrix from the component stiffness matrices.

The in-plane stiffness matrix for any plate element is found by summing up the in-plane stiffness contributions of each layer of the plate element. Separate consideration is to be given to each layer because the state of stress and hence, the effective stress is different in each layer. The in-plane stiffness matrix for a plate element is derived in Appendix IV. The same matrix can be used in the incremental elastic-plastic analysis, if the plate thickness h is replaced by the thickness of the layer in consideration. The elements D_{ij} of the stress matrix [D] depend on the state of stress in a layer and must be computed as outlined in Section 5.2.2.

The assumptions made for the derivation of the stiffness matrix governing the out-of-plane behavior of a plate element were discussed in Section 3.3.2. This matrix is derived in Appendix III.

In the present elastic-plastic analysis each layer must be treated separately, since the state of stress is different in each layer and the distance of the centroid of the layer to the plane of reference must be accounted for. For any plate layer, the same stress matrix [D] as generated for the in-plane stiffness matrix is applicable in evaluating the stiffness matrix governing the out-of-plane behavior of the plate element. As shown in Section 4.4.1, the contribution of each layer is found by applying Eq. 4.34. The stiffness contributions of all layers are then added.

In a similar fashion, the stiffness matrix for the stiffener element is formed by considering a stiffener layer at a time. This stiffness matrix is derived in Section 3.3.6 and can be applied in the elastic-plastic analysis if the cross-sectional properties of the stiffener layer in consideration are substituted. For a stiffener layer found to be elastic, the stress matrix $[D_s]$ in Eq. 5.7 reduces to E_s, the modulus of elasticity of the beam layer. In an elastic-plastic layer, the strain-hardening modulus E_{ps} is used instead of E_s.

5.3 The Incremental Elastic-Plastic Solution Procedure

5.3.1 Assembly of the System Stiffness Matrix

The incremental finite element displacement approach derived in Chapter 4 for the solution of elastic-plastic plate problems is extended in this chapter to elastic-plastic eccentrically stiffened plate structures. A step-by-step incremental

procedure which follows closely the procedure discussed in Chapter 4 forms the basis of this inelastic analysis. The tangent stiffness matrix $[K_e]$ of the structure must be reassembled at any stage of loading. This key matrix is a function of the geometry and of the existing state of stress in each plate and beam layer and must be modified for each load increment to account for plastification in the structure. The incremental displacement vector $\{\dot{\delta}\}$ resulting from the applied load increment $\{\dot{F}\}$ is obtained by solving the stiffness relationship:

$$\{\dot{F}\} = [K_e] \{\dot{\delta}\} \qquad (5.9)$$

in which $[K_e]$ is the tangent stiffness matrix of the entire structure which is discretized by an assemblage of beam and plate elements. The displacement vector of the structure is a listing of displacement components consistent with the force vector components. Five displacement components are introduced at each nodal point as in the case of the elastic analysis of stiffened plates, presented in Chapter 3. The process of assembling the overall tangent stiffness matrix is done in the computer. The out-of-plane and in-plane stiffness matrices are computed for the plate elements framing into a nodal point by appropriate addition of the component stiffness matrices listed in the appendices. For this purpose, the contributions of all plate layers involved are added. Finally, the stiffness of the stiffener elements framing into the nodal point in consideration are computed and added to the already

accumulated stiffness. A stiffener layer or plate layer at a time must be considered since the state of stress is different in each layer and its stiffness is a function of this state of stress. Depending on the magnitude of effective stress in a plate layer which is computed from total stresses resulting from in-plane and out-of-plane action, it is determined first whether the layer is elastic or elastic-plastic. The appropriate stress matrix must be used in computing the stiffness matrices. Stiffener layers are treated alike and their contribution is added to the present stiffness. No fundamental difficulties are encountered whether one deals with elastic linearly-strain hardening or with a more general material behavior of the beams.

It is seen that the process of assembling the system tangent stiffness matrix follows closely the procedure outlined in Chapter 4. The essential difference lies in the fact that in the present analysis the in-plane behavior must be considered and the effect of the beam elements must properly be accounted for. Appropriate stress-strain relationships must be used depending on the state of stress found in a layer. These relationships were derived in Chapter 4 and are equally valid in the present analysis if the total stresses due to in-plane and out-of-plane action are considered. The evaluation of the coefficients of the stress matrix proceeds as discussed in Section 4.2.1.

5.3.2 The Iterative Solution Technique

The iterative solution technique used in the analysis of elastic-plastic eccentrically stiffened plates is schematically illustrated in Fig. 65. The approach taken in the present analysis follows closely the procedure outlined in Chapter 4 used in the analysis of inelastic plates except that the in-plane behavior of the plate and the behavior of beam elements must be included. A unit load is applied first to the structure. Based on an assumed elastic behavior of every plate and beam layer, the overall stiffness matrix is assembled and the displacement vector corresponding to the applied unit load is found by solving the governing system of simultaneous equations. The applied loads are then scaled to cause initial yielding in the most highly stressed layer. Depending on the dimensions of the beam and plate components yielding will initiate in either a beam or a plate layer. All other field quantities are scaled similarly.

After the initiation of first yielding the behavior of the structure is non-linear and the incremental iterative technique is started. Steps 1 through 11, as discussed in Section 4.4.2 for the i-th cycle of iteration constitute again the iterative procedure taken in the present analysis. The structure is assumed to behave linearly elastic for any given cycle within the iteration designed to find the response of the structure for the load increment applied. Hence, strain and stress increments resulting from in-plane and out-of-plane deformation of the beam and plate

elements can be evaluated separately. The strain increments caused by the in-plane and the out-of-plane behavior of the plate elements are computed using the strain-displacement relations listed in Appendices III and IV.

The strain increments in beam layers, caused by axial and bending deformation, are evaluated using Eq. 5.4. Depending on the total accumulated stress in a stiffener layer or the total accumulated effective stress in a plate layer, the layer is assumed elastic or elastic-plastic. Appropriate stress-strain relations must be used to find the increment of stress corresponding to the strain increment evaluated. All plate and stiffener layers must be considered when it is checked in cycle i whether the assumed effective stress is within a specified tolerance of the computed value for the effective stress. Improved guesses on total stresses and on effective stresses in elastic-plastic layers are obtained by the procedure outlined in Section 4.4.4. The tolerance specified for the effective stress should not be kept too small since a small value can significantly increase the overall computation time. A value of 5 to 10% was used in the present analysis. If desired, different values could be assigned to beam and plate layers. Unloading and neutral loading are treated as outlined in Section 4.4.3.

5.4 Numerical Results

Two example structures have been chosen to demonstrate

the application of the described incremental finite element approach, which is capable of analyzing complex shaped eccentrically stiffened plate structures in the elastic-plastic range. A general computer program has been written to implement this procedure allowing to trace the entire load-deflection behavior of a transversely loaded stiffened plate structure, to describe the sequence of plastification and the redistribution of stresses in all beam and plate layers. Elastic perfectly-plastic material behavior is assumed for both the plate and the stiffener material.

The two examples chosen to verify the presented approach have purposely been kept simple in order to be able to check the results by some other method. Von Mises yield condition in connection with the Prandtl-Reuss' flow rule are assumed to be valid. For the purpose of this investigation, all example structures are thought to be made of structural steel. The following material properties were assumed in the analysis:

Parameter	Plate Layers	Beam Layers
E	30,000 ksi	30,000 ksi
σ_o	36 ksi	36 ksi
E_p	0	0
ν	0.30	--

The results are presented in a non-dimensionalized form. Other assumptions associated with the discretization and the

geometry of the example structures are shown in the figures, which present some results of this investigation. The computer program provides a complete listing of all important field quantities at any chosen stage of loading and hence, permits a detailed study of the elastic-plastic response of complex shaped eccentrically stiffened plate structures.

5.4.1 Simply Supported Three-Beam Bridge Model

The bridge model investigated to illustrate the application of the proposed finite element stiffness approach capable of finding the elastic-plastic response of eccentrically stiffened plates, is shown in Fig. 66. The uniformly loaded structure is discretized by sixteen plate elements and twelve beam elements. Each plate element is further subdivided into six plate layers, and similarly each beam element into five beam layers. Fig. 67 shows the load-deflection behavior at the center beam at midspan of this structure. As illustrated in this figure, simple plastic theory underestimates the ultimate load by approximately 10%. This can be attributed to the fact that the plate is stressed biaxially. The propagation of yielded regions across the cross section at midspan is shown in Fig. 68. As expected, the lower most layer of the center beam plastifies first, and yielding is restricted to beams up to a load of 1.70 times the yield load. The load-carrying capacity of the structure is reached shortly after yielding in the top most plate layer is initiated. Fig. 69

demonstrates clearly the dependency of the lateral distribution of load on the state of plastification in the structure. At the midspan section, the load is shared equally by all beams when the failure stage is approached. On the other hand, the lateral distribution of load does not change any more at the quarter point section for loads greater than 1.50 times the yield load. Fig. 70 depicts the bending moment carried by the center beam in function of the non-dimensionalized center deflection. Similarly, the variation of the axial force in the center beam is shown in Fig. 71. Though yielding in beams occurs at the quarter point section as this would not be expected from a consideration of simple plastic theory, the moment and axial force values corresponding to a fully plastic cross section are nowhere reached. Fig. 72 depicts deflection profiles for the cross section located at midspan and at quarter point for different load levels. These figures demonstrate that the deflections remain small up to a load of 1.40 times the yield load. It can also be observed that the deflection curve changes its shape from a concave to a convex form during the load history.

5.4.2 Continuous Three-Beam Bridge Model

A continuous uniformly loaded bridge model of the dimensions shown in Fig. 64 was investigated next. The structure was discretized exactly in the same way as the simply supported model described in Section 5.4.1. The load-deflection behavior at the

center beam at midspan is depicted in Fig. 73. The figure shows clearly the large additional strength available after initiation of yielding which occured at the support, again in the lower most layer of the center beam. Indicated in Fig. 73 is also the collapse load of the structure found by simple plastic theory. It can also be observed that the center deflection associated with the collapse load is only approximately one-sixtieth of the span length; thus the first order theory seems to be adequate for the present analysis. The propagation of yielding through the cross sections located at midspan and at the quarter point is illustrated in Fig. 74. Yielding is restricted to the support cross section up to a load of 1.45 times the yield load. The outermost plate layers at this cross-section plastify at a load of 2.20 times the yield load. At the midspan cross section, the layers close to the center start yielding at 2.42 times the yield load. Such plots are instructive and help in the understanding of the elastic-plastic behavior of stiffened plate structures. The lateral distribution of load for different stages of plastification is depicted in Fig. 75. It is interesting to observe that the lateral distribution of load does not change significantly at both the support and the midspan cross-section up to a load of $\bar{p} = 1.50$. As expected, the load is shared equally by all beams when the state of collapse is approached. Fig. 76 shows the variation of the center beam bending moment at the support and at the midspan cross section as a function of the non-dimensionalized deflection

at midspan. Similarly, the variation of the axial force in the center beam is shown in Fig. 77. The deflected shape of the midspan and the quarter span cross section is shown in Fig. 78 for different load levels. It can be observed that the deflections remain small up to a load $\bar{p} = 2.00$. No change in shape of the transverse deflection profile is recognizable at the midspan section in this example as in the case of the simply supported three-beam bridge model.

5.5 Summary

A finite element analysis capable of determining the elastic-plastic response of complex shaped eccentrically stiffened plate structures is presented in this chapter. The approach is formulated in incremental form and is based on linear geometry and the tangent stiffness concept. A layered beam-plate model is adopted to aid in the desciption of the elastic-plastic behavior of the structure. The iterative solution technique outlined in Chapter 4 for the elastic-plastic analysis of plates is extended to account for the in-plane behavior of the plate elements and the behavior of the stiffener elements. Two example structures were analyzed to demonstrate the validity of the proposed approach. The response of two three-beam bridge models could be closely predicted using the outlined approach. The computer program developed to implement the presented analysis yields the state of stress and deformation in every beam and plate layer used in the discretization

of the structure. The analysis shows clearly that the lateral distribution of load at any section depends on the amount of plastification the structure has undergone. It was found that simple plastic theory considerably underestimates the load-carrying capacity of the continuous three-beam bridge model and hence, a more refined analysis is clearly advisable.

6. SUMMARY AND CONCLUSIONS

6.1 Summary

This dissertation presents four different types of finite element analyses of transversely loaded plates and eccentrically stiffened plates:

1. A finite element analysis of elastic plates based on a new, refined plate bending element.
2. A finite element analysis of elastic, eccentrically stiffened plates subjected to transverse loading.
3. A finite element analysis of elastic-plastic transversely loaded plates.
4. A finite element analysis of elastic-plastic eccentrically stiffened plates subjected to transverse loading.

The formulations of these methods, which are all based on linear geometry, are described in detail in Chapters 2, 3, 4 and 5. For each type of analysis, a general computer program has been developed and was applied in the analysis of several sample structures.

In Chapter 2, a refined plate bending element for use in a finite element displacement analysis of arbitrarily shaped elastic plates is described. Along with the three basic nodal displacement parameters: w, θ_x and θ_y, three curvature terms are entered as unknowns in the vector of generalized displacements at each nodal point. A higher-order polynomial expression is assumed

for the displacement field within an element and based on this expression, the stiffness matrix of the refined element is derived in a systematic way. The method adopted in solving the system of simultaneous equations makes efficient use of the bandedness of the overall stiffness matrix. The accuracy and convergence of solutions obtained with this new element is demonstrated on a few example problems analyzed in this chapter.

In Chapter 3, a method of analysis based on the finite element displacement approach, and capable of analyzing complex shaped eccentrically stiffened plates is presented. The discretization of such a structure into an assemblage of plate and beam elements is first discussed. The stiffness matrices associated with the in-plane and out-of-plane behavior of a plate element and with the behavior of a beam element are derived and the assembly of the overall stiffness matrix is described. Longitudinal as well as transverse stiffeners can be taken into account in this analysis. A variation of the thickness of the slab and its orthotropic nature can be accounted for as well as a variable beam cross section. The power of the proposed method lies in its versatility and in the fact that forces occurring in beam and plate elements can be separated. The approach is applied to the analysis of I-beam bridges in this dissertation and is verified with the aid of field test results. An extensive study of most of the parameters governing the behavior of I-beam bridges is included in this chapter. In addition, a new approach capable of determing the St. Venant torsion

constant K_T of arbitrarily shaped solid cross-sections is presented in this chapter. This method is based on the fact that the differential equations governing the torsional behavior of a solid cross section and that of the corresponding transversely loaded plate problem of the same shape are formally identical. A solution can therefore be accomplished by solving the analogous plate problem using the finite element method.

In Chapter 4, a general finite element displacement analysis capable of determining the complete elastic-plastic behavior of complex shaped plates is presented. The approach is formulated in incremental form and is based on the tangent stiffness concept. A layered plate model is adopted to aid in the description of the elastic-plastic behavior of the plate since the process of plastification in a plate element is mathematically difficult to describe. The analysis is developed for an elastic linearly-strain hardening material and can easily be extended to more general material behavior. A few example solutions demonstrate the validity of the described numerical technique which is applicable to plates of arbitrary loading and geometry. The computer program written to implement the approach computes and lists the entire stress and displacement field in the structure at any desired stage of loading. Therefore, it allows to study the complete elastic-plastic behavior of complex shaped transversely loaded plates.

In Chapter 5, a method of analysis of eccentrically stiffened plates in the elastic-plastic range is described. An

incremental finite element displacement approach is used to find the elastic-plastic response of such structures. Layered beam elements are attached to the described layered plate elements in order to be able to describe the process of plastification. In-plane behavior of the plate as well as the behavior of the stiffeners are considered. The developed approach allows studying of the entire load-deformation behavior of complex shaped eccentrically stiffened plate structures and permits the design of such structures more rationally.

6.2 Conclusions

The methods of analysis presented in this dissertation are of a general nature and can be applied to a variety of plate structures. Each of the methods discussed has been implemented with the aid of a general finite element program.

a. The following conclusions can be drawn based on the finite element analysis of elastic plates using the refined plate element:

   1. The refined plate bending element yields better accuracy for displacements and internal moments than most of the presently known rectangular plate bending elements for any given number of degrees of freedom. The actual displacement field is approximated more closely by the chosen higher-order polynomial.

2. Internal moments need not be computed separately since the associate curvature terms are introduced as unknown parameters in the displacement vector.

3. For the examples studied, it was found that the enforcement of known curvature terms at boundary points does not, in general, improve the displacement field; it does, however, improve internal moments in the vicinity of the boundary points where the curvature terms were enforced.

b. Based on the elastic analysis of eccentrically stiffened plates, presented in Chapter 3 and applied in this dissertation to I-beam bridges, the following conclusions can be drawn:

1. The developed approach provides a powerful tool for the analysis of complex shaped longitudinally and transversely stiffened plate structures.

2. The introduced model consisting of beam and plate elements approximates the actual behavior of the structure more closely than the methods used today for the analysis of I-beam bridges. It allows the separation of the forces acting in the beam and plate elements and the computation of more reliable plate stresses.

3. Due to the versatility of the method a number of important variables governing the lateral distribution of load can be studied. Diaphragms and the orthotropic nature of the bridge deck can be included in the analysis.

4. The most significant variables governing the lateral distribution of load in an I-beam bridge are seen to be the span length of the bridge, the deck thickness, the spacing of the beams and the type of beam used. The type of loading applied to the bridge is also important as well as the support conditions of the bridge.

5. The following variables found to have less effect on the lateral distribution of load are: curb and parapet of the cross-section, torsional stiffness of beams, Poisson's ratio and the modular ratio between beam and slab material.

c. Based on the numerical examples processed to demonstrate the proposed numerical technique for the elastic-plastic analysis of arbitrarily shaped plates, presented in Chapter 4, the following conclusions can be drawn:

1. The analyzed examples prove the validity of the described incremental approach from which approximate solutions to complex elastic-plastic plate problems can be obtained.

2. The chosen layered plate model together with the iterative technique adopted allows the adequate description of the elastic-plastic behavior of transversely loaded plates. The approach allows the study of the entire load-deformation behavior, the process of plastification and the redistribution of stresses in complex shaped plates.

d. The following conclusions can be drawn from the incremental finite element approach developed to determine the elastic-plastic response of eccentrically stiffened plates:

1. The adopted layered beam-plate model used to aid in the description of the elastic-plastic behavior of eccentrically stiffened plates adequately predicts their elastic-plastic behavior.

2. The approach allows the description of the entire load-deformation behavior, the process of plastification and the redistribution of stresses in complex shaped eccentrically stiffened plates.

3. Based on the two examples processed in this investigation, it is evident that the lateral distribution of load is a function of the extent of plastification in the structure and all beams are stressed equally when the ultimate load is approached. The approach allows the study of the behavior of bridges under any given overload.

6.3 Future Research

Based on the work done in this dissertation, the following suggestions can be made for future work:

1. Extensive use should be made of the developed general finite element program to study the lateral distribution of load in I-beam bridges in order to arrive at a more rational design.

2. The approach presented for the elastic-plastic analysis of stiffened plate structures should be extended to account for non-linearities due to geometry.

3. The proposed layered approach should be applied to study the inelastic behavior of reinforced concrete plates and stiffened plates.

7. APPENDICES

APPENDIX I

7.1 Derivation of Stiffness Matrix of the Refined Plate Bending Element

This appendix presents the stiffness matrix for the refined plate bending element, discussed in Chapter 2, under the assumption of homogeneous orthotropic material behavior. The assumed displacement field represented by Eq. 2.24 was discussed in Section 2.4.1. The unknown displacement components at node i are listed in the nodal displacement vector as:

$$\{\delta_i\}^T = < w \quad \theta_x \quad \theta_y \quad \emptyset_x \quad \emptyset_y \quad \emptyset_{xy} > \tag{A1.1}$$

Element displacements are given as the listing of nodal displacements:

$$\{\delta^e\}^T = < \delta_i^T \quad \delta_j^T \quad \delta_k^T \quad \delta_\ell^T > \tag{A1.2}$$

The consistent element force vector is given by:

$$\{F^e\}^T = < F_i^T \quad F_j^T \quad F_k^T \quad F_\ell^T > \tag{A1.3}$$

The vector of generalized coordinates was derived as:

$$\{\alpha\} = [\bar{C}]^{-1} [T_1] \{\delta^e\} = [C]^{-1} \{\delta^e\} \tag{A1.4}$$

The connection matrix $[\bar{C}]$ consists of numbers only and is listed

in this appendix, whereas the matrix $[T_1]$ is given in Section 2.4.2. The stress matrix relates generalized stresses to generalized strains:

$$\{M\} = [D]\ \{\emptyset\} \tag{A1.5}$$

in which:

$$[D] = \begin{bmatrix} D_x & D_1 & 0 \\ D_1 & D_y & 0 \\ 0 & 0 & D_{xy} \end{bmatrix} \tag{A1.6}$$

$$\{M\}^T = < M_x \quad M_y \quad M_{xy} > \tag{A1.7}$$

and

$$\{\emptyset\}^T = < -\frac{\partial^2 w}{\partial x^2} \quad -\frac{\partial^2 w}{\partial y^2} \quad 2\frac{\partial^2 w}{\partial x \partial y} > \tag{A1.8}$$

Generalized strains can be expressed in terms of nodal displacements as shown in Section 2.4.1

$$\{\emptyset\} = [Q]\ [C]^{-1}\ \{\delta^e\} = [B]\ \{\delta^e\} \tag{A1.9}$$

The magnitude of nodal forces, given by Eq. A1.3, can be found by applying the principle of virtual work, which leads to:

$$\{\delta^e\}^T\ \{F^e\} = \iint_A \{\emptyset\}^T\ \{M\}\ dA \tag{A1.10}$$

where the integration is to be taken over the area A of the rectangular plate element. When Eq. A1.5 and Eq. A1.9 are substituted

into Eq. A1.10, and account is taken of the fact that the last equation must be valid for any arbitrary virtual displacement vector; i.e. also for the actual displacement pattern, the following equation results:

$$\{F^e\} = \left[\iint_A [B]^T [D] [B] \, dxdy \right] \{\delta^e\} \qquad \text{(A1.11)}$$

This is the element force-deformation relationship, and hence, the stiffness matrix is given by:

$$[K^e]_{24x24} = \iint_A [B]^T [D] [B] \, dxdy \qquad \text{(A1.12)}$$

The introduction of non-dimensionalized coordinates, as explained in Section 2.4.2, leads to a particularly simple integration and is best done by considering one term of the stress matrix [D] at a time. The result can be given in the form:

$$[K^e]_{24x24} = [C^{-1}]^T \left[D_x[K_1] + D_1[K_2] + D_y[K_3] + D_{xy}[K_4] \right] [C^{-1}] \qquad \text{(A1.13)}$$

Carrying out the necessary operations yields the component matrices as listed below. The final stiffness matrix is assembled in the digital computer.

Matrix $[\bar{C}]$

$$
\begin{bmatrix}
1 & -1 & 1 & 1 & -1 & 1 & -1 & 1 & -1 & 1 & 1 & -1 & 1 & -1 & 1 & -1 & 1 & -1 & 1 & -1 & 1 & -1 & -1 & -1 \\
0 & 0 & 1 & 0 & -1 & 2 & 0 & 1 & -2 & 3 & 0 & -1 & 2 & -3 & 4 & 0 & 1 & -2 & 3 & -4 & 5 & -1 & -3 & -5 \\
0 & -1 & 0 & 2 & -1 & 0 & -3 & 2 & -1 & 0 & 4 & -3 & 2 & -1 & 0 & -5 & 4 & -3 & 2 & -1 & 0 & -5 & -3 & -1 \\
0 & 0 & 0 & -2 & 0 & 0 & 6 & -2 & 0 & 0 & -12 & 6 & -2 & 0 & 0 & 20 & -12 & 6 & -2 & 0 & 0 & 20 & 6 & 0 \\
0 & 0 & 0 & 0 & 0 & -2 & 0 & 0 & 2 & -6 & 0 & 0 & -2 & 6 & -12 & 0 & 0 & 2 & -6 & 12 & -20 & 0 & 6 & 20 \\
0 & 0 & 0 & 0 & 1 & 0 & 0 & -2 & 2 & 0 & 0 & 3 & -4 & 3 & 0 & 0 & -4 & 6 & -6 & 4 & 0 & 5 & 9 & 5 \\
1 & -1 & -1 & 1 & 1 & 1 & -1 & -1 & -1 & -1 & 1 & 1 & 1 & 1 & 1 & -1 & -1 & -1 & -1 & -1 & -1 & 1 & 1 & 1 \\
0 & 0 & 1 & 0 & -1 & -2 & 0 & 1 & 2 & 3 & 0 & -1 & -2 & -3 & -4 & 0 & 1 & 2 & 3 & 4 & 5 & -1 & -3 & -5 \\
0 & -1 & 0 & 2 & 1 & 0 & -3 & -2 & -1 & 0 & 4 & 3 & 2 & 1 & 0 & -5 & -4 & -3 & -2 & -1 & 0 & 5 & 3 & 1 \\
0 & 0 & 0 & -2 & 0 & 0 & 6 & 2 & 0 & 0 & -12 & -6 & -2 & 0 & 0 & 20 & 12 & 6 & 2 & 0 & 0 & -20 & -6 & 0 \\
0 & 0 & 0 & 0 & 0 & -2 & 0 & 0 & 2 & 6 & 0 & 0 & -2 & -6 & -12 & 0 & 0 & 2 & 6 & 12 & 20 & 0 & -6 & -20 \\
0 & 0 & 0 & 0 & 1 & 0 & 0 & -2 & -2 & 0 & 0 & 3 & 4 & 3 & 0 & 0 & -4 & -6 & -6 & -4 & 0 & 5 & 9 & 5 \\
1 & 1 & 1 & 1 & 1 & 1 & 1 & 1 & 1 & 1 & 1 & 1 & 1 & 1 & 1 & 1 & 1 & 1 & 1 & 1 & 1 & 1 & 1 & 1 \\
0 & 0 & 1 & 0 & 1 & 2 & 0 & 1 & 2 & 3 & 0 & 1 & 2 & 3 & 4 & 0 & 1 & 2 & 3 & 4 & 5 & 1 & 3 & 5 \\
0 & -1 & 0 & -2 & -1 & 0 & -3 & -2 & -1 & 0 & -4 & -3 & -2 & -1 & 0 & -5 & -4 & -3 & -2 & -1 & 0 & -5 & -3 & -1 \\
0 & 0 & 0 & -2 & 0 & 0 & -6 & -2 & 0 & 0 & -12 & -6 & -2 & 0 & 0 & -20 & -12 & -6 & -2 & 0 & 0 & -20 & -6 & 0 \\
0 & 0 & 0 & 0 & 0 & -2 & 0 & 0 & -2 & -6 & 0 & 0 & -2 & -6 & -12 & 0 & 0 & -2 & -6 & -12 & -20 & 0 & -6 & -20 \\
0 & 0 & 0 & 0 & 1 & 0 & 0 & 2 & 2 & 0 & 0 & 3 & 4 & 3 & 0 & 0 & 4 & 6 & 6 & 4 & 0 & 5 & 9 & 5 \\
1 & 1 & -1 & 1 & -1 & 1 & 1 & -1 & 1 & -1 & 1 & -1 & 1 & -1 & 1 & 1 & -1 & 1 & -1 & 1 & -1 & -1 & -1 & -1 \\
0 & 0 & 1 & 0 & 1 & -2 & 0 & 1 & -2 & 3 & 0 & 1 & -2 & 3 & -4 & 0 & 1 & -2 & 3 & -4 & 5 & 1 & 3 & 5 \\
0 & -1 & 0 & -2 & 1 & 0 & -3 & 2 & -1 & 0 & -4 & 3 & -2 & 1 & 0 & -5 & 4 & -3 & 2 & -1 & 0 & 5 & 3 & 1 \\
0 & 0 & 0 & -2 & 0 & 0 & -6 & 2 & 0 & 0 & -12 & 6 & -2 & 0 & 0 & -20 & 12 & -6 & 2 & 0 & 0 & 20 & 6 & 0 \\
0 & 0 & 0 & 0 & 0 & -2 & 0 & 0 & -2 & 6 & 0 & 0 & -2 & 6 & -12 & 0 & 0 & -2 & 6 & -12 & 20 & 0 & 6 & 20 \\
0 & 0 & 0 & 0 & 1 & 0 & 0 & 2 & -2 & 0 & 0 & 3 & -4 & 3 & 0 & 0 & 4 & -6 & 6 & -4 & 0 & 5 & 9 & 5
\end{bmatrix}
$$

Matrix $[K_1]$

Multiplier $\frac{16b}{105a^3}$

0																															
0	0																														
0	0	0																													
0	0	0	105																												
0	0	0	0	0																											
0	0	0	0	0	0																										
0	0	0	0	0	0	315																									
0	0	0	0	0	0	0	35																								
0	0	0	0	0	0	0	0	0																							
0	0	0	0	0	0	0	0	0	0																						
0	0	0	210	0	0	0	0	0	0	756																					
0	0	0	0	0	0	0	0	0	0	0	105																				
0	0	0	35	0	0	0	0	0	0	70	0	21																			
0	0	0	0	0	0	0	0	0	0	0	0	0	0																		
0	0	0	0	0	0	0	0	0	0	0	0	0	0	0																	
0	0	0	0	0	0	630	0	0	0	0	0	0	0	0	1500																
0	0	0	0	0	0	0	70	0	0	0	0	0	0	0	0	252															
0	0	0	0	0	0	105	0	0	0	0	0	0	0	0	210	0	63														
0	0	0	0	0	0	0	21	0	0	0	0	0	0	0	0	42	0	15													
0	0	0	0	0	0	0	0	0	0	0	0	0	0	0	0	0	0	0	0												
0	0	0	0	0	0	0	0	0	0	0	0	0	0	0	0	0	0	0	0	0											
0	0	0	0	0	0	0	0	0	0	0	210	0	0	0	0	0	0	0	0	0	500										
0	0	0	0	0	0	0	0	0	0	0	63	0	0	0	0	0	0	0	0	0	126	45									
0	0	0	0	0	0	0	0	0	0	0	0	0	0	0	0	0	0	0	0	0	0	0	0								

Symmetric

Matrix $[K_2]$

Multiplier $\frac{16}{1575ab}$

Symmetric

0																							
0	0																						
0	0	0																					
0	0	0	0																				
0	0	0	0	0																			
0	0	0	1575	0	0																		
0	0	0	0	0	0	0																	
0	0	0	0	0	0	0	0																
0	0	0	0	0	0	1575	0	0															
0	0	0	0	0	0	0	1575	0	0														
0	0	0	0	0	3150	0	0	0	0	0													
0	0	0	0	0	0	0	0	0	0	0	0												
0	0	0	525	0	525	0	0	0	0	1890	0	350											
0	0	0	0	0	0	0	0	0	0	0	1575	0	0										
0	0	0	3150	0	0	0	0	0	0	6300	0	1890	0	0									
0	0	0	0	0	0	0	0	3150	0	0	0	0	0	0	0								
0	0	0	0	0	0	0	0	0	3150	0	0	0	0	0	0	0							
0	0	0	0	0	0	945	0	525	0	0	0	0	0	0	2250	0	630						
0	0	0	0	0	0	0	525	0	945	0	0	0	0	0	0	1890	0	630					
0	0	0	0	0	0	3150	0	0	0	0	0	0	0	0	6300	0	1890	0	0				
0	0	0	0	0	0	0	3150	0	0	0	0	0	0	0	0	6300	0	2250	0	0			
0	0	0	0	0	0	0	0	0	0	0	0	0	3150	0	0	0	0	0	0	0	0		
0	0	0	0	0	0	0	0	0	0	0	945	0	945	0	0	0	0	0	0	0	2250	1134	
0	0	0	0	0	0	0	0	0	0	0	3150	0	0	0	0	0	0	0	0	0	6300	2250	0

Matrix $[K_3]$

Multiplier $\frac{16a}{105b^3}$

0																											
0	0																										
0	0	0																									
0	0	0	0																								
0	0	0	0	0																							
0	0	0	0	0	105																						
0	0	0	0	0	0	0																					
0	0	0	0	0	0	0	0																				
0	0	0	0	0	0	0	0	35																			
0	0	0	0	0	0	0	0	0	315																		
0	0	0	0	0	0	0	0	0	0	0																	
0	0	0	0	0	0	0	0	0	0	0	0																
0	0	0	0	0	35	0	0	0	0	0	0	21															
0	0	0	0	0	0	0	0	0	0	0	0	0	105														
0	0	0	0	0	210	0	0	0	0	0	0	70	0	756													
0	0	0	0	0	0	0	0	0	0	0	0	0	0	0	0												
0	0	0	0	0	0	0	0	0	0	0	0	0	0	0	0	0											
0	0	0	0	0	0	0	0	21	0	0	0	0	0	0	0	0	15										
0	0	0	0	0	0	0	0	0	105	0	0	0	0	0	0	0	0	63									
0	0	0	0	0	0	0	0	70	0	0	0	0	0	0	0	0	42	0	252								
0	0	0	0	0	0	0	0	0	630	0	0	0	0	0	0	0	0	210	0	1500							
0	0	0	0	0	0	0	0	0	0	0	0	0	0	0	0	0	0	0	0	0	0						
0	0	0	0	0	0	0	0	0	0	0	0	0	63	0	0	0	0	0	0	0	0	45					
0	0	0	0	0	0	0	0	0	0	0	0	0	210	0	0	0	0	0	0	0	0	126	500				

Symmetric

Matrix $[K_4]$

Multiplier $\frac{16}{1575ab}$

0																							
0	0																						
0	0	0																					
0	0	0	0																				
0	0	0	0	1575																			
0	0	0	0	0	0																		
0	0	0	0	0	0	0																	
0	0	0	0	0	0	0	2100																
0	0	0	0	0	0	0	0	2100															
0	0	0	0	0	0	0	0	0	0														
0	0	0	0	0	0	0	0	0	0	0													
0	0	0	0	1575	0	0	0	0	0	0	2835												
0	0	0	0	0	0	0	0	0	0	0	0	2800											
0	0	0	0	1575	0	0	0	0	0	0	1575	0	2835										
0	0	0	0	0	0	0	0	0	0	0	0	0	0	0									
0	0	0	0	0	0	0	0	0	0	0	0	0	0	0	0								
0	0	0	0	0	0	0	2520	0	0	0	0	0	0	0	0	3600							
0	0	0	0	0	0	0	0	2100	0	0	0	0	0	0	0	0	3780						
0	0	0	0	0	0	0	2100	0	0	0	0	0	0	0	0	2520	0	3780					
0	0	0	0	0	0	0	0	2520	0	0	0	0	0	0	0	0	2520	0	3600				
0	0	0	0	0	0	0	0	0	0	0	0	0	0	0	0	0	0	0	0	0			
0	0	0	0	1575	0	0	0	0	0	0	3375	0	1575	0	0	0	0	0	0	0	4375		
0	0	0	0	1575	0	0	0	0	0	0	2835	0	2835	0	0	0	0	0	0	0	3375	5103	
0	0	0	0	1575	0	0	0	0	0	0	1575	0	3375	0	0	0	0	0	0	0	1575	3375	4375

Symmetric

APPENDIX II

7.2 Consistent Force Vector for Uniformly Distributed Load On a Refined Plate Element

In this section, the kinematically consistent force vector for uniformly distributed loads $p(x,y)$, defined as acting on a unit area of the refined plate element, is derived. The equivalent concentrated forces in the directions of the element displacements, as defined in Section 2.4.3, are represented by the vector $\{F\}_p^e$. These concentrated nodal forces must be made statically equivalent to the distributed loads $p(x,y)$ acting on an element.

The simplest procedure to achieve this equivalence is to impose an arbitrary virtual nodal displacement and to equate the external and internal work done by the distributed loads and the equivalent concentrated nodal forces. Let such a displacement be $\{\delta^e\}$ at the nodes. Using Eq. 2.26 b, and denoting virtual by a tilde, the displacement within an element is given by:

$$\tilde{w} = \langle P \rangle \{\tilde{\alpha}\} \qquad \text{(A2.1)}$$

or making use of Eq. 2.33 b, by:

$$\tilde{w} = \langle P \rangle [C^{-1}] \{\tilde{\delta}^e\} \qquad \text{(A2.2)}$$

Equating the internal work to the external one leads to

$$\{\tilde{\delta}^e\}^T \{F\}_p^e = -\iint_A p(x,y)\ \tilde{w}(x,y)\ dxdy \qquad (A2.3)$$

or:

$$\{\tilde{\delta}^e\}^T \{F\}_p^e = \{\tilde{\delta}^e\}^T \left[-[C^{-1}]^T \iint_A <P>^T p(x,y)\ dxdy \right]$$

From this equation it follows that:

$$\{F\}_p^e = -[C^{-1}]^T \iint_A <P>^T p(x,y)\ dxdy \qquad (A2.4)$$

It should be noted that any distribution of load $p(x,y)$ can be treated using this approach. The integration is performed explicitely for a uniformly distributed load

$$q = p(x,y) = \text{constant} \qquad (A2.5)$$

The result is listed below. The final load vector is generated in the digital computer. In a similar way, the force vector for any other distribution of load or for a concentrated load acting within the element could be derived. In the same way, force vectors corresponding to distributed edge loads can be derived.

Force vector for uniformly distributed load:

$$\{F\}_p^e = -[C^{-1}]^T \, q\,a\,b \int_{-1}^{+1}\int_{-1}^{+1} \begin{bmatrix} 1 \\ \xi \\ \eta \\ \xi^2 \\ \xi\eta \\ \eta^2 \\ \xi^3 \\ \xi^2\eta \\ \xi\eta^2 \\ \eta^3 \\ \xi^4 \\ \xi^3\eta \\ \xi^2\eta^2 \\ \xi\eta^3 \\ \eta^4 \\ \xi^5 \\ \xi^4\eta \\ \xi^3\eta^2 \\ \xi^2\eta^3 \\ \xi\eta^4 \\ \eta^5 \\ \xi^5\eta \\ \xi^3\eta^3 \\ \xi\eta^5 \end{bmatrix} d\eta d\xi = -[C^{-1}]^T \frac{4qab}{45} \begin{bmatrix} 45 \\ 0 \\ 0 \\ 15 \\ 0 \\ 15 \\ 0 \\ 0 \\ 0 \\ 0 \\ 9 \\ 0 \\ 5 \\ 0 \\ 9 \\ 0 \\ 0 \\ 0 \\ 0 \\ 0 \\ 0 \\ 0 \\ 0 \\ 0 \end{bmatrix}$$

APPENDIX III

7.3 Derivation of Stiffness Matrix of the ACM Plate Bending Element

As discussed in Section 3.3.2, the polynomial expression representing the displacement field within an element is given by Eq. 3.1. The displacement components introduced at node i of the finite plate element are:

$$\{\delta_i\}^T = < w \quad \theta_x \quad \theta_y > \tag{A3.1}$$

Element displacements are given as the listing of the following nodal displacements:

$$\{\delta^e\}^T = < \delta_i^T \quad \delta_j^T \quad \delta_k^T \quad \delta_\ell^T > \tag{A3.2}$$

Similarly, element forces are given by:

$$\{F^e\}^T = < F_i^T \quad F_j^T \quad F_k^T \quad F_\ell^T > \tag{A3.3}$$

The derivation of the stiffness matrix proceeds exactly as described for the refined plate element, shown in Appendix I. First, the vector of generalized coordinates is expressed as:

$$\{\alpha\} = [\bar{C}]^{-1} [T_1] \{\delta^e\} = [C]^{-1} \{\delta^e\} \tag{A3.4}$$

in which $[T_1]$ is a (12 x 12) transformation matrix relating the modified element displacement vector to the actual displacement vector, defined by Eq. A3.2. Matrix $[\bar{C}]$ is a connection matrix consisting of numbers only; both matrices are listed in this appendix. The relationship between generalized stresses and generalized strains is given by:

$$\{M\} = [D]\ \{\emptyset\} \tag{A3.5}$$

where

$$[D] = \begin{bmatrix} D_{11} & D_{12} & D_{13} \\ D_{21} & D_{22} & D_{23} \\ D_{31} & D_{32} & D_{33} \end{bmatrix} \tag{A3.6}$$

$$\text{with } D_{ij} = D_{ji} \text{ for } i \neq j$$

$$\{M\}^T = < M_x \quad M_y \quad M_{xy} > \tag{A3.8}$$

and

$$\{\emptyset\}^T = < -\frac{\partial^2 w}{\partial x^2} \quad -\frac{\partial^2 w}{\partial y^2} \quad 2\frac{\partial^2 w}{\partial x \partial y} > \tag{A3.9}$$

All terms of the stress matrix [D] must be considered in this derivation, since for the elastic-plastic analysis, the stiffness matrix will be used in its complete form. Generalized strains can be expressed in terms of element displacements by:

$$\{\emptyset\} = [Q]\ [C]^{-1}\ \{\delta^e\} = [B]\ \{\delta^e\} \tag{A3.10}$$

Minimization of the total potential energy leads to the stiffness relation governing the out-of-plane behavior of the plate element:

$$\{F^e\} = \left[\iint_A [B]^T [D] [B] \, dxdy \right] \{\delta^e\} \tag{A3.11}$$

Hence, the stiffness matrix is given by:

$$[K^e]_{12x12} = \iint_A [B]^T [D] [B] \, dxdy \tag{A3.12}$$

where the integration is to be taken over the area of the plate element. Carrying out the necessary operations, the result can again be given in a form suitable for the elastic-plastic analysis:

$$[K^e]_{12x12} = [C^{-1}]^T \Big[D_{11}[K_1] + D_{12}[K_2] + D_{13}[K_3] + D_{22}[K_4] + D_{23}[K_5] + D_{33}[K_6] \Big] [C^{-1}] \tag{A3.13}$$

The component matrices are listed subsequently and the final assembly of the stiffness matrix is again performed with the aid of the digital computer.

$$[T_1] = \begin{bmatrix} 1 & 0 & 0 & & & & & & & & & \\ 0 & b & 0 & & & & & & & & & \\ 0 & 0 & a & & & & & & & & & \\ & & & 1 & 0 & 0 & & & & & & \\ & & & 0 & b & 0 & & & & & & \\ & & & 0 & 0 & a & & & & & & \\ & & & & & & 1 & 0 & 0 & & & \\ & & & & & & 0 & b & 0 & & & \\ & & & & & & 0 & 0 & a & & & \\ & & & & & & & & & 1 & 0 & 0 \\ & & & & & & & & & 0 & b & 0 \\ & & & & & & & & & 0 & 0 & a \end{bmatrix}$$

$$[\bar{C}] = \begin{bmatrix} 1 & -1 & 1 & 1 & -1 & 1 & -1 & 1 & -1 & 1 & -1 & -1 \\ 0 & 0 & 1 & 0 & -1 & 2 & 0 & 1 & -2 & 3 & -1 & -3 \\ 0 & -1 & 0 & 2 & -1 & 0 & -3 & 2 & -1 & 0 & -3 & -1 \\ 1 & -1 & -1 & 1 & 1 & 1 & -1 & -1 & -1 & -1 & 1 & 1 \\ 0 & 0 & 1 & 0 & -1 & -2 & 0 & 1 & 2 & 3 & -1 & -3 \\ 0 & -1 & 0 & 2 & 1 & 0 & -3 & -2 & -1 & 0 & 3 & 1 \\ 1 & 1 & 1 & 1 & 1 & 1 & 1 & 1 & 1 & 1 & 1 & 1 \\ 0 & 0 & 1 & 0 & 1 & 2 & 0 & 1 & 2 & 3 & 1 & 3 \\ 0 & -1 & 0 & -2 & -1 & 0 & -3 & -2 & -1 & 0 & -3 & -1 \\ 1 & 1 & -1 & 1 & -1 & 1 & 1 & -1 & 1 & -1 & -1 & -1 \\ 0 & 0 & 1 & 0 & 1 & -2 & 0 & 1 & -2 & 3 & 1 & 3 \\ 0 & -1 & 0 & -2 & 1 & 0 & -3 & 2 & -1 & 0 & 3 & 1 \end{bmatrix}$$

$$[K_1] = \frac{16b}{15a^3}\begin{bmatrix}
0 & & & & & & & & & & & \\
0 & 0 & & & & & & & & & & \\
0 & 0 & 0 & & & & & & & & & \\
0 & 0 & 0 & 15 & & & & & & & & \\
0 & 0 & 0 & 0 & 0 & & & & & & & \\
0 & 0 & 0 & 0 & 0 & 0 & & & & & & \\
0 & 0 & 0 & 0 & 0 & 0 & 45 & & & & & \\
0 & 0 & 0 & 0 & 0 & 0 & 0 & 5 & & & & \\
0 & 0 & 0 & 0 & 0 & 0 & 0 & 0 & 0 & & & \\
0 & 0 & 0 & 0 & 0 & 0 & 0 & 0 & 0 & 0 & & \\
0 & 0 & 0 & 0 & 0 & 0 & 0 & 0 & 0 & 0 & 15 & \\
0 & 0 & 0 & 0 & 0 & 0 & 0 & 0 & 0 & 0 & 0 & 0
\end{bmatrix}$$

Symmetric

$$[K_2] = \frac{16}{15ab}\begin{bmatrix}
0 & & & & & & & & & & & \\
0 & 0 & & & & & & & & & & \\
0 & 0 & 0 & & & & & & & & & \\
0 & 0 & 0 & 0 & & & & & & & & \\
0 & 0 & 0 & 0 & 0 & & & & & & & \\
0 & 0 & 0 & 15 & 0 & 0 & & & & & & \\
0 & 0 & 0 & 0 & 0 & 0 & 0 & & & & & \\
0 & 0 & 0 & 0 & 0 & 0 & 0 & 0 & & & & \\
0 & 0 & 0 & 0 & 0 & 0 & 15 & 0 & 0 & & & \\
0 & 0 & 0 & 0 & 0 & 0 & 0 & 15 & 0 & 0 & & \\
0 & 0 & 0 & 0 & 0 & 0 & 0 & 0 & 0 & 0 & 0 & \\
0 & 0 & 0 & 0 & 0 & 0 & 0 & 0 & 0 & 0 & 15 & 0
\end{bmatrix}$$

Symmetric

$$[K_3] = \frac{16}{15a^2}$$

$$\begin{bmatrix}
0 & & & & & & & & & & & \\
0 & 0 & & & & & & & & & & \\
0 & 0 & 0 & & & & & & & & & \\
0 & 0 & 0 & 0 & & & & \text{Symmetric} & & & & \\
0 & 0 & 0 & -15 & 0 & & & & & & & \\
0 & 0 & 0 & 0 & 0 & 0 & & & & & & \\
0 & 0 & 0 & 0 & 0 & 0 & 0 & & & & & \\
0 & 0 & 0 & 0 & 0 & 0 & -30 & 0 & & & & \\
0 & 0 & 0 & 0 & 0 & 0 & 0 & -10 & 0 & & & \\
0 & 0 & 0 & 0 & 0 & 0 & 0 & 0 & 0 & 0 & & \\
0 & 0 & 0 & -15 & 0 & 0 & 0 & 0 & 0 & 0 & 0 & \\
0 & 0 & 0 & -15 & 0 & 0 & 0 & 0 & 0 & 0 & 0 & 0
\end{bmatrix}$$

$$[K_4] = \frac{16a}{15b^3}$$

$$\begin{bmatrix}
0 & & & & & & & & & & & \\
0 & 0 & & & & & & & & & & \\
0 & 0 & 0 & & & & & & & & & \\
0 & 0 & 0 & 0 & & & & \text{Symmetric} & & & & \\
0 & 0 & 0 & 0 & 0 & & & & & & & \\
0 & 0 & 0 & 0 & 0 & 15 & & & & & & \\
0 & 0 & 0 & 0 & 0 & 0 & 0 & & & & & \\
0 & 0 & 0 & 0 & 0 & 0 & 0 & 0 & & & & \\
0 & 0 & 0 & 0 & 0 & 0 & 0 & 0 & 5 & & & \\
0 & 0 & 0 & 0 & 0 & 0 & 0 & 0 & 0 & 45 & & \\
0 & 0 & 0 & 0 & 0 & 0 & 0 & 0 & 0 & 0 & 0 & \\
0 & 0 & 0 & 0 & 0 & 0 & 0 & 0 & 0 & 0 & 0 & 15
\end{bmatrix}$$

$$[K_5] = \frac{16}{15b^2}$$

0											
0	0										
0	0	0									
0	0	0	0								
0	0	0	0	0							
0	0	0	0	-15	0						
0	0	0	0	0	0	0					
0	0	0	0	0	0	0	0				
0	0	0	0	0	0	0	-10	0			
0	0	0	0	0	0	0	0	-30	0		
0	0	0	0	0	-15	0	0	0	0	0	
0	0	0	0	0	-15	0	0	0	0	0	0

Symmetric

$$[K_6] = \frac{16}{15ab}$$

0											
0	0										
0	0	0									
0	0	0	0								
0	0	0	0	15							
0	0	0	0	0	0						
0	0	0	0	0	0	0					
0	0	0	0	0	0	0	20				
0	0	0	0	0	0	0	0	20			
0	0	0	0	0	0	0	0	0	0		
0	0	0	0	15	0	0	0	0	0	27	
0	0	0	0	15	0	0	0	0	0	15	27

Symmetric

APPENDIX IV

7.4 Derivation of In-Plane Stiffness Matrix

The displacement field representing in-plane behavior of the plate element was discussed in Section 3.3.2 and is given by Eq. 3.2 and Eq. 3.3. The nodal displacement vector is defined as:

$$\{\delta_i\}^T = < u_i \quad v_i > \tag{A4.1}$$

and the corresponding element displacement vector as:

$$\{\delta^e\}^T = < u_i \quad v_i \quad u_j \quad v_j \quad u_k \quad v_k \quad u_\ell \quad v_\ell > \tag{A4.2}$$

The vector of generalized coordinates is found by enforcing compatibility of displacements at the four nodal points:

$$\{\alpha\} = [C]^{-1} \{\delta^e\} \tag{A4.3}$$

The connection matrix [C] can be inverted with ease in the present case. The vectors of strains and stresses are defined as:

$$\{\epsilon\} = \begin{Bmatrix} \epsilon_x \\ \epsilon_y \\ \gamma_{xy} \end{Bmatrix} = \begin{Bmatrix} \partial u/\partial x \\ \partial v/\partial y \\ \partial u/\partial y + \partial v/\partial x \end{Bmatrix} \tag{A4.4}$$

and

$$\{\sigma\}^T = < \sigma_x \quad \sigma_y \quad \tau_{xy} > \tag{A4.5}$$

The relationship between stresses and strains is given by

$$\{\sigma\} = [D]\ \{\epsilon\} \tag{A4.6}$$

where for an isotropic material:

$$[D] = \frac{E}{1-\nu^2} \begin{bmatrix} 1 & \nu & 0 \\ \nu & 1 & 0 \\ 0 & 0 & \frac{1-\nu}{2} \end{bmatrix} \tag{A4.7}$$

and for an anisotropic material, the stress matrix is of the form:

$$[D] = \begin{bmatrix} D_{11} & D_{12} & D_{13} \\ D_{21} & D_{22} & D_{23} \\ D_{31} & D_{32} & D_{33} \end{bmatrix} \tag{A4.8}$$

$$\text{with } D_{ij} = D_{ji} \text{ for } i \neq j$$

Strains can be expressed in terms of element displacements as:

$$\{\epsilon\} = [Q]\ \{\alpha\} = [Q]\ [C]^{-1}\ \{\delta^e\} = [B]\ \{\delta^e\} \tag{A4.9}$$

The force-deformation relationship governing the in-plane behavior of the plate element is derived from a minimization of the total potential energy:

$$\{F^e\} = \left[\iint [B]^T\ [D]\ [B]\ dxdy \right] \{\delta^e\} \tag{A4.10}$$

Hence, the stiffness matrix is given by:

$$[K^e]_{8x8} = t \iint_A [B]^T [D] [B] \, dxdy \qquad (A4.11)$$

The integration can be performed with ease, and the final result, given for the case of anisotropic material, and hence, suitable for the elastic-plastic analysis, is listed below.

$$
\begin{bmatrix}
16\beta D_{11} & -12D_{12} & 8\beta D_{11} & 12D_{12} & -16\beta D_{11} & -12D_{12} & -8\beta D_{11} & 12D_{12} \\
+16\alpha D_{33} & +16\alpha D_{23} & -16\alpha D_{33} & -16\alpha D_{23} & +8\alpha D_{33} & +8\alpha D_{23} & -8\alpha D_{33} & -8\alpha D_{23} \\
 & -12D_{33} & & -12D_{33} & & +12D_{33} & & +12D_{33} \\
 & 16\alpha D_{22} & -12D_{12} & -16\alpha D_{22} & 12D_{12} & 8\alpha D_{22} & 12D_{12} & -8\alpha D_{22} \\
 & -24D_{23} & -16\alpha D_{23} & +8\beta D_{33} & +8\alpha D_{23} & -16\beta D_{33} & -8\alpha D_{23} & +24D_{23} \\
 & +16\beta D_{33} & +12D_{33} & & -12D_{33} & & +12D_{33} & -8\beta D_{33} \\
 & & 16\beta D_{11} & 12D_{12} & -8\beta D_{11} & -12D_{12} & -16\beta D_{11} & 12D_{12} \\
 & & +16\alpha D_{33} & +16\alpha D_{23} & -8\alpha D_{33} & -8\alpha D_{23} & +8\alpha D_{33} & +8\alpha D_{23} \\
 & & & +12D_{33} & & -12D_{33} & & -12D_{33} \\
 & & & 16\alpha D_{22} & -12D_{12} & -8\alpha D_{22} & -12D_{12} & 8\alpha D_{22} \\
 & & & +24D_{23} & -8\alpha D_{23} & -24D_{23} & +8\alpha D_{23} & -16\beta D_{33} \\
 & & & +16\beta D_{33} & -12D_{33} & -8\beta D_{33} & +12D_{33} & \\
 & & & & 16\beta D_{11} & 12D_{12} & 8\beta D_{11} & -12D_{12} \\
 & & & & +16\alpha D_{33} & +16\alpha D_{23} & -16\alpha D_{33} & -16\alpha D_{23} \\
 & & & & & +12D_{33} & & +12D_{33} \\
 & & & & & 16\alpha D_{22} & 12D_{12} & -16\alpha D_{22} \\
 & & & & & +24D_{23} & -16\alpha D_{23} & +8\beta D_{33} \\
 & & & & & +16\beta D_{33} & -12D_{33} & \\
 & & & & & & 16\beta D_{11} & -12D_{12} \\
 & & & & & & +16\alpha D_{33} & +16\alpha D_{23} \\
 & & & & & & & -12D_{33} \\
 & & & & & & & 16\alpha D_{22} \\
 & & & & & & & -24D_{23} \\
 & & & & & & & +16\beta D_{33}
\end{bmatrix}
$$

Symmetric

Matrix $[K^e]$

Multiplier $\frac{h}{48}$ $\qquad \alpha = \frac{a}{b} \qquad \beta = \frac{b}{a}$

APPENDIX V

7.5 Evaluation of St. Venant Torsion Constant K_T for an Arbitrarily Shaped Solid Cross Section

Closed form solutions for the St. Venant torsion problem exist only for a few geometrically simple cross sections. An approximate solution based on the finite element concept is presented in this appendix. As shown in Ref. 3, the fundamental partial differential equation governing the behavior of a transversely loaded plate, given by Eq. 2.14, can be split into the two partial differential equations of the second order:

$$M = \frac{M_x + M_y}{1 + \nu} = -\left[\frac{\partial^2 w}{\partial x^2} + \frac{\partial^2 w}{\partial y^2}\right] \qquad \text{(A5.1)}$$

and

$$q = -\nabla^2 M = -\left[\frac{\partial^2 M}{\partial x^2} + \frac{\partial^2 M}{\partial y^2}\right] \qquad \text{(A5.2)}$$

when the plate rigidity is taken as unity. On the other hand, the stress function $\psi(x,y)$ introduced often to solve the problem of St. Venant torsion of a solid cross section, must satisfy the following differential equation:

$$\frac{\partial^2 \psi}{\partial x^2} + \frac{\partial^2 \psi}{\partial y^2} = -2G\emptyset' \qquad \text{(A5.3)}$$

where: $\psi(x,y)$ = Stress function introduced

ϕ' = Rate of twist

G = Shear modulus

The determination of the stress distribution over the cross section of a twisted bar consists in finding the function $\psi(x,y)$ which satisfies Eq. A5.3 and the given boundary conditions. Shear stresses are expressed as:

$$\tau_{xz} = \frac{\partial \psi}{\partial y} \tag{A5.4}$$

$$\tau_{yz} = -\frac{\partial \psi}{\partial x} \tag{A5.5}$$

and the twisting moment is given as:

$$T_{St.V.} = 2 \iint_A \psi dxdy = K_T G\phi' \tag{A5.6}$$

where: K_T = St. Venant torsion constant

The integration is to be taken over the area of the cross section. Recognizing that Eq. A5.2 is formally identical with Eq. A5.3, it can be concluded that the problems of solving the first equation for M or the second equation for ψ are analogous. Hence, instead of solving the torsion problem for a given cross section, one can solve the corresponding plate bending problem. Accordingly, a plate which is of the same shape as the cross section to be analyzed for torsion, is analyzed for a uniformly distributed transverse load

of unit intensity. Any conventional finite element program capable of analyzing plate bending problems can be used to find the moment field. The moment sum M defined by Eq. A5.1 can then be computed at each mesh point.

Pursuing this analogy, the St. Venant torsion moment is found to be:

$$T_{St.V.} = 2 \iint_A M \, dxdy = K_T G \frac{q}{2G} = K_T \frac{q}{2} \qquad (A5.7)$$

from which the St. Venant torsion constant is derived as:

$$K_T = 4 \iint_A M \, dxdy = 4V \qquad (A5.8)$$

where V is the volume under the surface created by plotting the moment sum values M at each mesh point. Having found the moment field, the integral in Eq. A5.8 can be evaluated using any conventional numerical integration procedure.

The shearing stresses in the twisted cross section correspond to the shear forces in the analogous plate bending problem.

$$\tau_{xz} = \frac{\partial M}{\partial y} = -\frac{\partial}{\partial y}\left[\frac{\partial^2 w}{\partial x^2} + \frac{\partial^2 w}{\partial y^2}\right] = Q_y \qquad (A5.9)$$

$$\tau_{yz} = -\frac{\partial M}{\partial x} = \frac{\partial}{\partial x}\left[\frac{\partial^2 w}{\partial x^2} + \frac{\partial^2 w}{\partial y^2}\right] = -Q_x$$

and can be evaluated once the displacement field is known.

A solid square cross section of unit width was analyzed to verify the proposed method for determining the St. Venant torsion constant K_T. According to this analogy, a square plate with four simple supports is to be analyzed for a uniformly distributed transverse load of unit intensity. The described refined plate element discussed in Chapter 2 was used to find the displacement field and the associated moment field. Simpson's rule was used for the numerical integration. Two meshes were processed and the following results were obtained:

Mesh	K_T (in.^{4})	Error in (%)
4 x 4	0.1382	-1.74%
8 x 8	0.1398	-0.57%
Exact Value	0.1406	Ref. 48

Due to the great versatility of the finite element method, this procedure can be applied to any arbitrary shape. Cross sections built-up of regions having varying material properties can be treated. This approach was taken in the evaluation of K_T for the AASHO Type III beam used in the investigation on lateral distribution of load, discussed in Chapter 3.

8. NOMENCLATURE

a.) Scalars

A_s	=	cross-sectional area of stiffener
a	=	half length of plate element
a_i	=	coefficients of polynomial expansion
b	=	half width of plate element
b_i	=	coefficients of polynomial expansion
c	=	length of correction vector
D	=	plate stiffness
D_x, D_y, D_{xy}, D_1	=	coefficients of stress matrix for orthotropic material
D_{ij}	=	coefficients of stress matrix for anisotropic material
E	=	modulus of elasticity of plate
E_p	=	strain-hardening modulus
E_s	=	modulus of elasticity of stiffener
f	=	function describing subsequent yielding
f^*	=	function describing initial yielding
G	=	shear modulus
h	=	plate thickness

I_s = moment of inertia of the stiffener area with respect to plane of reference

I_w = warping constant

J_2 = second invariant of stress deviator tensor

K_T = St. Venant torsional constant

k = yield stress in simple shear

L = length of stiffener element; or span length

ℓ = number of beam layers

M_x, M_y, M_{xy} = plate bending moments per unit width

M_s = bending moment in stiffener with respect to plane of reference

m = strain hardening parameter

N_s = axial force in stiffener

p = distributed load per unit area of finite element

Q_x, Q_y = plate shearing forces per unit width

q = distributed load per unit area of plate

S_s = first moment of the stiffener area with respect to plane of reference

S_{ij} = components of stress deviator tensor

T = total twisting moment in stiffener

$T_{St.V.}$ = St. Venant torsional moment

T_w = warping torsional moment

t = thickness of plate layer

U = in-plane displacement in x-direction of a point lying outside the middle plane of the plate

U^* = complementary strain energy

u = in-plane displacement in x-direction of a point lying in the middle plane of the plate

V = in-plane displacement in y-direction of a point lying outside the middle plane of the plate

v = in-plane displacement in y-direction of a point lying in the middle plane of the plate

w = lateral deflection in z-direction

Z = shear force in stiffener in z-direction

α_i = coefficients of polynomial expansion

β = non-dimensionalized parameter

γ_{xy} = shearing strain

δ = variation of functional

ϵ_x, ϵ_y = strain in x-direction and y-direction, respectively

ϵ_{ij} = components of strain tensor

η = non-dimensionalized coordinate

θ_x, θ_y = slope about x-axis and y-axis, respectively

λ = positive scalar

ν = Poisson's Ratio

ξ = non-dimensionalized coordinate

π = total potential energy functional

π^* = total complementary energy functional

σ_{ij} = components of stress tensor

σ_x, σ_y = normal stresses in x-direction and y-direction, respectively

σ_s = axial stress in stiffener

$\bar{\sigma}$ = current effective stress

σ_o = initial effective stress

τ_{xy} = shearing stress

ϕ_x, ϕ_y, ϕ_{xy} = curvatures of plate surface

ϕ' = rate of change of angle of twist

ψ = stress function

∇^2 = Laplace operator

b.) Vectors and Matrices

[A] = matrix relating the rate of effective stress to the stress rate vector

$[B]$ = matrix relating element displacements to generalized strains

$[C]$ = matrix relating element displacements to generalized coordinates

$[\bar{C}]$ = matrix relating modified element displacements to generalized coordinates

$[D]$ = stress matrix relating generalized strains to generalized stresses

$[D_e]$ = elastic-plastic stress matrix

$\{F\}$ = overall force vector of system

$\{F^e\}$ = vector of generalized element forces

$\{F_i\}$ = vector of generalized nodal forces

$[K]$ = overall structural stiffness matrix

$[K^e]$ = element stiffness matrix

$[K_e]$ = instantaneous overall stiffness matrix

$[K_i]$ = component stiffness matrix

$[L]$ = lower triangular matrix

$\{M\}$ = vector of plate bending moments

$\{M_s\}$ = vector of generalized forces acting on stiffener element

$< P >$ = row vector listing polynomial terms

$[Q]$ = matrix relating generalized coordinates to generalized strains

$\{R\}^e$ = vector of external forces

$[T_1]$ = transformation matrix relating element displacements to modified element displacements

$\{Y\}$ = auxiliary vector used in Choleski decomposition

$\{\alpha\}$ = vector of generalized coordinates

$\{\delta\}$ = overall displacement vector of system

$\{\delta^e\}$ = vector of generalized element displacements

$\{\delta_i\}$ = vector of generalized nodal displacements

$\{\epsilon\}$ = vector of total strains

$\{\epsilon^e\}$ = vector of elastic strains

$\{\epsilon^p\}$ = vector of plastic strains

$\{\epsilon_s\}$ = vector of generalized strains for beam element

$\{\emptyset\}$ = vector of curvatures of plate surface

$\{\sigma\}$ = vector of stresses referred to a cartesian coordinate system

9. TABLES

TABLE 1: CLAMPED SQUARE PLATE - PROBLEM P1

a.) Center Deflection Under Uniformly Distributed Unit Load

Source	Mesh 2 x 2	Mesh 4 x 4	Mesh 8 x 8	Mesh 16 x 16	Multiplier
New Element	0.001594	0.001325	0.001284	0.001266	$\frac{qL^4}{D}$
ACM (Ref. 6)	0.001480	0.001403	0.001304	0.001275	
Exact Value	0.00126				

b.) Center Deflection Under Single Concentrated Load

Source	Mesh 2 x 2	Mesh 4 x 4	Mesh 8 x 8	Mesh 16 x 16	Multiplier
New Element	0.005912	0.005634	0.005611	0.005607	$\frac{PL^2}{D}$
ACM (Ref. 6)	0.005919	0.006134	0.005803	0.005672	
Exact Value	0.00560				

TABLE 2: SIMPLY SUPPORTED SQUARE PLATE - PROBLEM P2

a.) Center Deflection Under Uniformly Distributed Unit Load

Source	Mesh 2 x 2	Mesh 4 x 4	Mesh 8 x 8	Mesh 16 x 16	Multiplier
New Element	0.004187	0.004076	0.004064	0.004063	$\frac{qL^4}{D}$
ACM (Ref. 6)	0.003446	0.003939	0.004033	0.004056	
Exact Value	0.004062				

b.) Center Deflection Under Single Concentrated Load

Source	Mesh 2 x 2	Mesh 4 x 4	Mesh 8 x 8	Mesh 16 x 16	Multiplier
New Element	0.011265	0.011497	0.011572	0.011593	$\frac{PL^2}{D}$
ACM (Ref. 6)	0.013784	0.012327	0.011829	0.011671	
Exact Value	0.01160				

TABLE 3: CENTER DEFLECTION - PROBLEMS P3 AND P4

Problem P3: Center Deflection Under Uniformly Distributed Unit Load

Source	Mesh 2 x 2	Mesh 4 x 4	Mesh 8 x 8	Mesh 16 x 16	Multiplier
New Element	0.005208	0.005671	0.005769	0.005793	$\frac{qL^4}{D}$
ACM (Ref. 6)	0.005208	0.005779	0.005843	0.005821	
Exact Value	0.00581				

Problem P4: Center Deflection Under Uniformly Distributed Unit Load

Source	Mesh 2 x 2	Mesh 4 x 4	Mesh 8 x 8	Mesh 16 x 16	Multiplier
New Element	0.025770	0.025544	0.025512	0.025507	$\frac{qL^4}{D}$
ACM (Ref. 6)	0.021790	0.024296	0.025178	0.025422	
Ref. 82	0.0265				

TABLE 4: DEFLECTION PROFILES -

UNIFORMLY LOADED PLATE

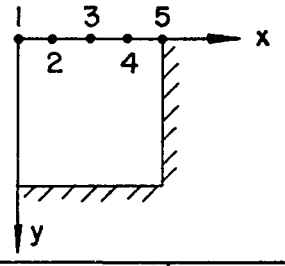

Multiplier $\frac{qL^4}{D}$

	Mesh	Point 1	Point 2	Point 3	Point 4	Point 5
Problem P1	4 x 4	0.001325		0.000805		0.
	8 x 8	0.001284	0.001145	0.000769	0.000283	0.
	16 x 16	0.001266	0.001131	0.000759	0.000279	0.
	Exact Value	0.001260				0.
Problem P2	4 x 4	0.004076		0.002948		0.
	8 x 8	0.004064	0.003778	0.002939	0.001624	0.
	16 x 16	0.004063	0.003776	0.002938	0.001623	0.
	Exact Value	0.004062	0.003776	0.002938	0.001623	0.
Problem P3	4 x 4	0.005671		0.004967		0.004228
	8 x 8	0.005769	0.005564	0.005058	0.004539	0.004319
	16 x 16	0.005793	0.005587	0.005081	0.004562	0.004343
	Exact Value	0.00581				
Problem P4	4 x 4	0.025544		0.023053		0.017791
	8 x 8	0.025512	0.024853	0.023018	0.020428	0.017754
	16 x 16	0.025507	0.024848	0.023013	0.020424	0.017750
	Ref. 82	0.0265				0.0170

TABLE 5: DEFLECTION PROFILES -

SINGLE CONCENTRATED LOAD

Multiplier $\frac{PL^2}{D}$

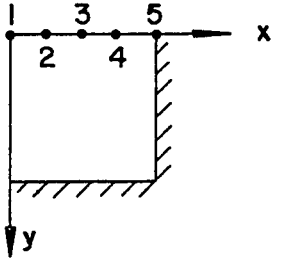

	Mesh	Point 1	Point 2	Point 3	Point 4	Point 5
Problem P1	4 x 4	0.005634		0.002573		0.
	8 x 8	0.005611	0.004417	0.002484	0.000781	0.
	16 x 16	0.005607	0.004404	0.002470	0.000771	0.
	Exact Value	0.00560				0.
Problem P2	4 x 4	0.011497		0.007144		0.
	8 x 8	0.011572	0.010066	0.007141	0.003670	0.
	16 x 16	0.011593	0.010068	0.007139	0.003669	0.
	Exact Value	0.01160	0.010066	0.007139	0.003668	0.
Problem P3	4 x 4	0.011341		0.008044		0.005671
	8 x 8	0.011538	0.010259	0.008153	0.006427	0.005769
	16 x 16	0.011585	0.010286	0.008176	0.006451	0.005793
	Exact Value					
Problem P4	4 x 4	0.039055		0.032957		0.022964
	8 x 8	0.039117	0.037131	0.032934	0.027859	0.022920
	16 x 16	0.039159	0.037128	0.032925	0.027850	0.022911
	Exact Value					

TABLE 6: PLATE MOMENTS M_x -

UNIFORMLY LOADED PLATE

Multiplier qL^2

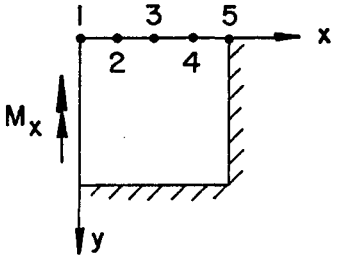

	Mesh	Point 1	Point 2	Point 3	Point 4	Point 5
Problem P1	4 x 4	0.0215		0.0109		-0.0574
	8 x 8	0.0230	0.0194	0.0104	-0.0102	-0.0515
	16 x 16	0.0229	0.0202	0.0108	-0.0102	-0.0515
	Exact Value	0.0231				-0.0513
Problem P2	4 x 4	0.0454		0.0383		0.
	8 x 8	0.0475	0.0454	0.0385	0.0248	0.
	16 x 16	0.0478	0.0457	0.0388	0.0248	0.
	Exact Value	0.0479	0.0458	0.0390	0.0250	0.
Problem P3	4 x 4	0.0254		0.0053		-0.0236
	8 x 8	0.0317	0.0250	0.0079	-0.0109	-0.0194
	16 x 16	0.0328	0.0261	0.0089	-0.0101	-0.0185
	Exact Value	0.0331				-0.0185
Problem P4	4 x 4	0.1069		0.0760		0.
	8 x 8	0.1101	0.1025	0.0803	0.0440	0.
	16 x 16	0.1112	0.1037	0.0814	0.0458	0.
	Ref. 82	0.109				0.

TABLE 7: PLATE MOMENTS M_x -

SINGLE CONCENTRATED LOAD

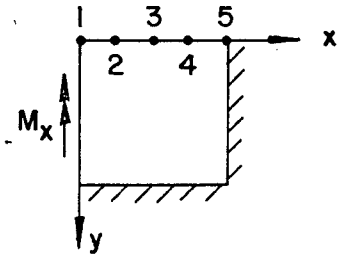

Multiplier P

	Mesh	Point 1	Point 2	Point 3	Point 4	Point 5
Problem P1	4 x 4			-0.0092		-0.1376
	8 x 8		0.0548	-0.0025	-0.0522	-0.1299
	16 x 16		0.0680	-0.0010	-0.0525	-0.1265
	Exact Value					-0.1257
Problem P2	4 x 4			0.0460		0.
	8 x 8		0.1093	0.0568	0.0242	0.
	16 x 16		0.1226	0.0586	0.0242	0.
	Exact Value		0.1231	0.0585	0.0251	0.
Problem P3	4 x 4			-0.0274		-0.0784
	8 x 8		0.0516	-0.0117	-0.0562	-0.0721
	16 x 16		0.0663	-0.0085	-0.0538	-0.0702
	Exact Value					
Problem P4	4 x 4			0.0926		0.
	8 x 8		0.1822	0.1094	0.0468	0.
	16 x 16		0.1974	0.1126	0.0500	0.
	Exact Value					0.

TABLE 8: PLATE MOMENTS M_y -

UNIFORMLY LOADED PLATE

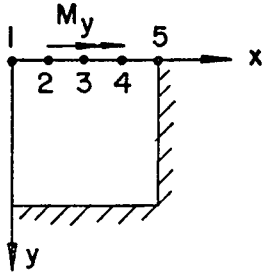

Multiplier qL^2

	Mesh	Point 1	Point 2	Point 3	Point 4	Point 5
Problem P1	4 x 4	0.0215		0.0098		-0.0214
	8 x 8	0.0230	0.0202	0.0121	-0.0015	-0.0176
	16 x 16	0.0229	0.0203	0.0125	-0.0001	-0.0158
	Exact Value	0.0231				-0.0154
Problem P2	4 x 4	0.0454		0.0350		0.
	8 x 8	0.0475	0.0444	0.0348	0.0205	0.
	16 x 16	0.0478	0.0447	0.0355	0.0203	0.
	Exact Value	0.0479	0.0448	0.0356	0.0204	0.
Problem P3	4 x 4	0.0254		0.0411		0.0548
	8 x 8	0.0317	0.0341	0.0406	0.0488	0.0527
	16 x 16	0.0328	0.0349	0.0410	0.0483	0.0517
	Exact Value	0.0331				0.0512
Problem P4	4 x 4	0.1069		0.1119		0.1706
	8 x 8	0.1101	0.1126	0.1208	0.1307	0.1617
	16 x 16	0.1112	0.1137	0.1214	0.1341	0.1570
	Ref. 82	0.109				0.140

TABLE 9: PLATE MOMENTS M_y -
SINGLE CONCENTRATED LOAD

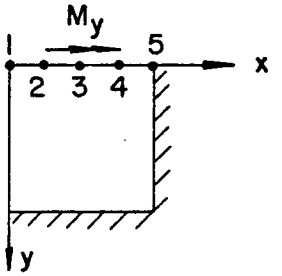

Multiplier P

	Mesh	Point 1	Point 2	Point 3	Point 4	Point 5
Problem P1	4 x 4			0.0489		-0.0532
	8 x 8		0.1232	0.0488	-0.0021	-0.0429
	16 x 16		0.1253	0.0478	-0.0016	-0.0379
	Exact Value					-0.0377
Problem P2	4 x 4			0.1040		0.
	8 x 8		0.1764	0.0999	0.0489	0.
	16 x 16		0.1784	0.0990	0.0456	0.
	Exact Value		0.1776	0.0982	0.0456	0.
Problem P3	4 x 4			0.0942		0.0784
	8 x 8		0.1433	0.0930	0.0755	0.0721
	16 x 16		0.1447	0.0917	0.0740	0.0702
	Exact Value					
Problem P4	4 x 4			0.2033		0.2272
	8 x 8		0.2645	0.2122	0.1941	0.2142
	16 x 16		0.3316	0.2292	0.1992	0.1962
	Exact Value					

TABLE 10: PLATE MOMENTS M_{xy} -
UNIFORMLY LOADED PLATE

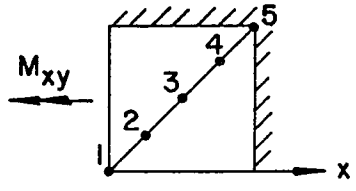

Multiplier qL^2

	Mesh	Point 1	Point 2	Point 3	Point 4	Point 5
Problem P1	4 x 4	0.		0.0105		0.
	8 x 8	0.	0.0036	0.0082	0.0097	0.
	16 x 16	0.	0.0027	0.0075	0.0076	0.
	Exact Value	0.				0.
Problem P2	4 x 4	0.		0.0133		0.0319
	8 x 8	0.	0.0037	0.0134	0.0252	0.0288
	16 x 16	0.	0.0038	0.0134	0.0252	0.0324
	Exact Value	0.	0.0037	0.0134	0.0252	0.0324
Problem P3	4 x 4	0.		0.0196		0.
	8 x 8	0.	0.0056	0.0176	0.0300	0.
	16 x 16	0.	0.0055	0.0174	0.0280	0.
	Exact Value	0.				0.
Problem P4	4 x 4	0.		0.0291		
	8 x 8	0.	0.0074	0.0290	0.0642	
	16 x 16	0.	0.0075	0.0289	0.0642	
	Exact Value	0.				

TABLE 11: EFFECT OF BOUNDARY CONDITIONS ON CENTER DEFLECTION - PROBLEM P1

a.) Center Deflection Under Uniformly Distributed Load

Bondary Conditions	Mesh 2 x 2	Mesh 4 x 4	Mesh 8 x 8	Mesh 16 x 16	Multi-plier
Type I	0.001594	0.001325	0.001284	0.001266	$\frac{qL^4}{D}$
Type II	0.001571	0.001322	0.001284	0.001266	
Exact Value	0.001260				

b.) Center Deflection Under Concentrated Load

Boundary Conditions	Mesh 2 x 2	Mesh 4 x 4	Mesh 8 x 8	Mesh 16 x 16	Multi-plier
Type I	0.005912	0.005634	0.005611	0.005607	$\frac{PL^2}{D}$
Type II	0.005895	0.005627	0.005611	0.005607	
Exact Value	0.00560				

TABLE 12: EFFECT OF BOUNDARY CONDITIONS ON CENTER DEFLECTION - PROBLEM P2

a.) Center Deflection Under Uniformly Distributed Load

Boundary Conditions	Mesh 2 x 2	Mesh 4 x 4	Mesh 8 x 8	Mesh 16 x 16	Multiplier
Type I	0.004187	0.004076	0.004064	0.004063	$\frac{qL^4}{D}$
Type II	0.004066	0.004063	0.004062	0.004062	
Type III	0.004065	0.004063	0.004062	0.004062	
Exact Value	0.004062				

b.) Center Deflection Under Concentrated Load

Boundary Conditions	Mesh 2 x 2	Mesh 4 x 4	Mesh 8 x 8	Mesh 16 x 16	Multiplier
Type I	0.011265	0.011497	0.011572	0.011593	$\frac{PL^2}{D}$
Type II	0.011184	0.011478	0.011570	0.011593	
Type III	0.011180	0.011478	0.011570	0.011593	
Exact Value	0.01160				

TABLE 13: EFFECT OF BOUNDARY CONDITIONS

ON PLATE MOMENTS M_x - PROBLEM P1

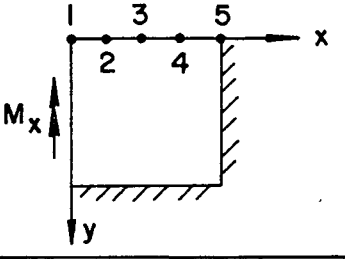

a.) Uniformly Distributed Load: Mesh 16 x 16

Boundary Conditions	Point 1	Point 2	Point 3	Point 4	Point 5	Multiplier
Type I	0.0229	0.0201	0.0108	-0.0102	-0.0509	qL^2
Type II	0.0229	0.0201	0.0108	-0.0102	-0.0515	
Exact Value	0.0231				-0.0513	

b.) Single Concentrated Load: Mesh 16 x 16

Boundary Conditions	Point 1	Point 2	Point 3	Point 4	Point 5	Multiplier
Type I		0.0684	-0.0008	-0.0525	-0.1247	P
Type II		0.0684	-0.0008	-0.0525	-0.1265	
Exact Value					-0.1257	

TABLE 14: EFFECT OF BOUNDARY CONDITIONS

ON PLATE MOMENTS M_x - PROBLEM P2

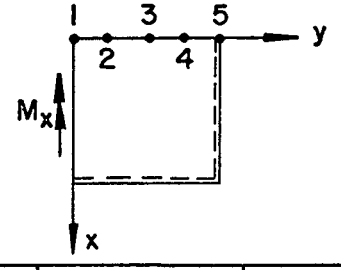

a.) Uniformly Distributed Load: Mesh 16 x 16

Boundary Conditions	Point 1	Point 2	Point 3	Point 4	Point 5	Multi-plier
Type I	0.0478	0.0457	0.0388	0.0248	-0.0010	
Type II	0.0478	0.0457	0.0387	0.0248	-0.0002	qL^2
Type III	0.0478	0.0457	0.0388	0.0248	0.	
Exact Value	0.0479	0.0458	0.0390	0.0250	0.	

b.) Single Concentrated Load: Mesh 16 x 16

Boundary Conditions	Point 1	Point 2	Point 3	Point 4	Point 5	Multi-plier
Type I		0.1230	0.0588	0.0244	-0.0025	
Type II		0.1230	0.0588	0.0245	-0.0004	P
Type III		0.1226	0.0586	0.0242	0.	
Exact Value		0.1231	0.0585	0.0251	0.	

TABLE 15: EFFECT OF ORTHOTROPY OF BRIDGE DECK ON DEFLECTION AND STRESS RESULTANTS IN BEAMS

Mesh 10 x 8 - Truck in Lane 4

Bartonsville Bridge - Cross-Section M

$\frac{D_y}{D_x}$	Deflection at Midspan			Bending Moment Section M			Axial-Force Section M		
	Beam A	Beam B	Beam C	Beam A	Beam B	Beam C	Beam A	Beam B	Beam C
1.0	0.03056	0.09168	0.13260	332.039	2679.252	4466.444	2.041	64.172	107.902
0.9	0.02933	0.09191	0.13491	292.709	2680.437	4537.636	1.067	64.156	109.758
0.8	0.02800	0.09210	0.13749	251.609	2678.925	4616.972	0.066	64.062	111.819
Units	in.			K. in.			K.		

TABLE 16: EFFECT OF MESH SIZE ON DEFLECTION AND STRESS RESULTANTS IN BEAMS

Truck in Lane 4

Bartonsville Bridge - Cross-Section M

Mesh	Deflection at Midspan			Bending Moment Section M			Axial-Force Section M		
	Beam A	Beam B	Beam C	Beam A	Beam B	Beam C	Beam A	Beam B	Beam C
10 x 4	0.02920	0.09053	0.13221	310.519	2728.905	4459.719	1.574	65.179	107.968
10 x 8	0.03056	0.09168	0.13260	332.039	2679.252	4466.444	2.041	64.172	107.902
10 x 16	0.03089	0.09193	0.13268	337.776	2668.198	4472.175	2.187	63.923	107.944
Test	0.035	0.086	0.129						
Units	in.			K. in.			K.		

TABLE 17: EFFECT OF MESH SIZE ON DEFLECTION AND STRESS RESULTANTS IN BEAMS

Truck in Lane 3

Bartonsville Bridge - Cross-Section M

Mesh	Deflection at Midspan			Bending Moment Section M			Axial-Force Section M		
	Beam A	Beam B	Beam C	Beam A	Beam B	Beam C	Beam A	Beam B	Beam C
10 x 4	0.05784	0.12160	0.11975	1236.754	3965.505	3955.342	23.877	94.797	95.166
10 x 8	0.06036	0.12253	0.12041	1235.371	3961.652	3950.800	23.880	94.362	94.798
10 x 16	0.06107	0.12278	0.12054	1233.704	3959.843	3948.402	23.853	94.250	94.704
Test	0.066	0.112	0.116						
Units	in.			K. in.			K.		

TABLE 18: EFFECT OF MESH SIZE ON DEFLECTION AND STRESS RESULTANTS IN BEAMS

Truck in Lane 2

Bartonsville Bridge - Cross-Section M

Mesh	Deflection at Midspan			Bending Moment Section M			Axial-Force Section M		
	Beam A	Beam B	Beam C	Beam A	Beam B	Beam C	Beam A	Beam B	Beam C
10 x 4	0.10492	0.13670	0.08981	2902.377	4492.236	2696.199	65.286	107.433	64.308
10 x 8	0.10832	0.13778	0.09097	2871.726	4506.656	2648.289	64.680	107.335	63.297
10 x 16	0.10934	0.13814	0.09122	2864.479	4515.217	2637.752	64.471	107.373	63.054
Test	0.110	0.123	0.089						
Units	in.			K. in.			K.		

TABLE 19: EFFECT OF MESH SIZE ON DEFLECTION AND STRESS RESULTANTS IN BEAMS

Truck in Lane 1

Bartonsville Bridge - Cross-Section M

Mesh	Deflection of Midspan			Bending Moment Section M			Axial Force Section M		
	Beam A	Beam B	Beam C	Beam A	Beam B	Beam C	Beam A	Beam B	Beam C
10 x 4	0.16964	0.12713	0.05654	5339.568	4000.892	1386.085	125.198	93.948	30.090
10 x 8	0.17356	0.12915	0.05796	5311.649	4018.698	1362.395	124.362	93.806	29.625
10 x 16	0.17481	0.12978	0.05828	5299.971	4023.451	1354.966	124.002	93.786	29.502
Test	0.156	0.113	0.065						
Units	in.			K. in.			K.		

TABLE 20: AVAILABLE SOLUTIONS FOR LIMIT LOAD - SIMPLY SUPPORTED SQUARE PLATE

Method	Author	Ref.	Yield Criterion			
			Johansen	Tresca	Von Mises	
Lower Bound	Wolfensberger	65	0.945			Multiplier $24\ M_p/L^2$
	Ranaweera and Leckie	79		0.920	0.995	
	Shull and Hu	63		0.826		
	Koopman and Lance	64		0.964		
	Hodge and Belytscho	78			1.036	
	Prager	80	1.000			
Upper Bound	Ranaweera and Leckie	79		0.961	1.044	
	Shull and Hu	63		1.000		
	Koopman and Lance	64		1.000		
	Hodge	56			1.106	
	Prager	80	1.000			
Finite Difference	Lopez and Ang	44			1.031	
	Bhaumik and Hanley	66	1.041	0.922	1.000	
Finite Element	Armen et al	67			1.137	
	Present Analysis Mesh: 8 x 8				0.982	

TABLE 21: AVAILABLE SOLUTIONS FOR LIMIT LOAD - CLAMPED SQUARE PLATE

Method	Author	Ref.	Yield Criterion			
			Johansen	Tresca	Von Mises	
Lower Bound	Wolfensberger	65	1.560			Multiplier $24\ M_p/L^2$
	Ranaweera and Leckie	79		1.553	1.710	
	Koopman and Lance	64		1.596		
	Hodge and Belytscho	78			1.786	
Upper Bound	Ranaweera and Leckie	79		1.682	1.844	
	Koopman and Lance	64		1.712		
	Hodge	56			2.052	
Finite Difference	Lopez and Ang	44			1.901	
	Bhaumik and Hanley	66	1.746	1.560	1.740	
Finite Element	Armen et al.	67			2.590	
	Present Analysis Mesh: 8 x 8 Mesh: 12 x 12				2.220 1.865	

10. FIGURES

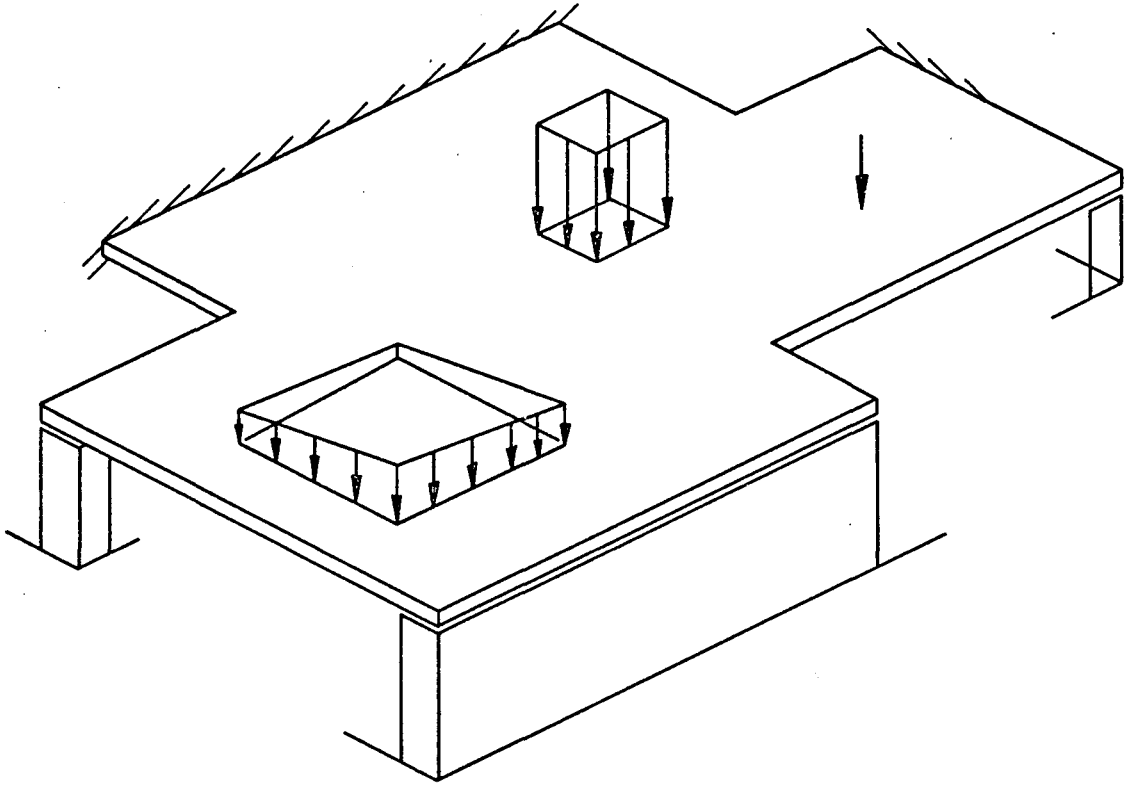

Fig. 1 Plate of Arbitrary Loading and Geometry

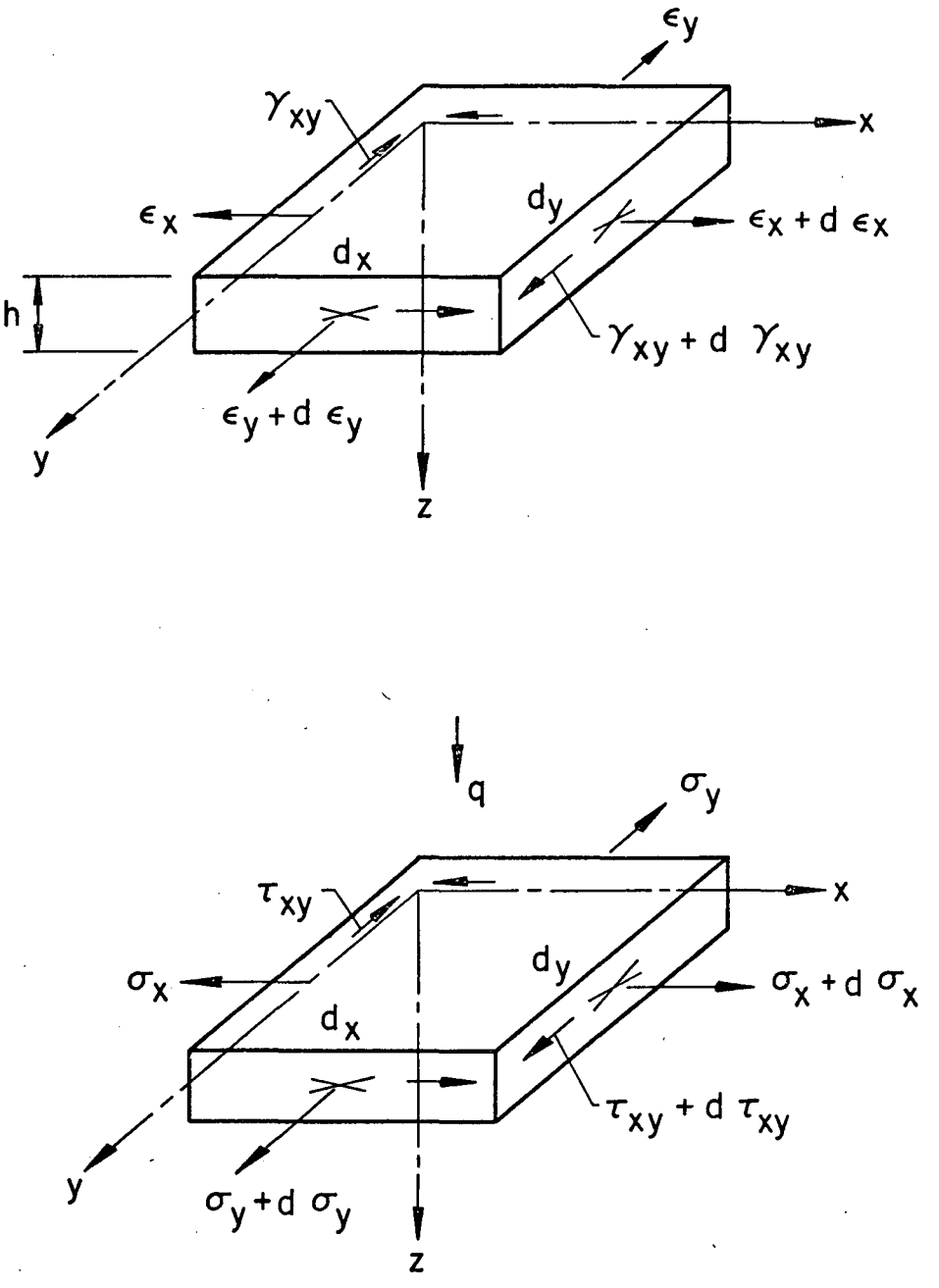

Fig. 2 Sign Convention for Stresses and Strains Acting on a Plate Element

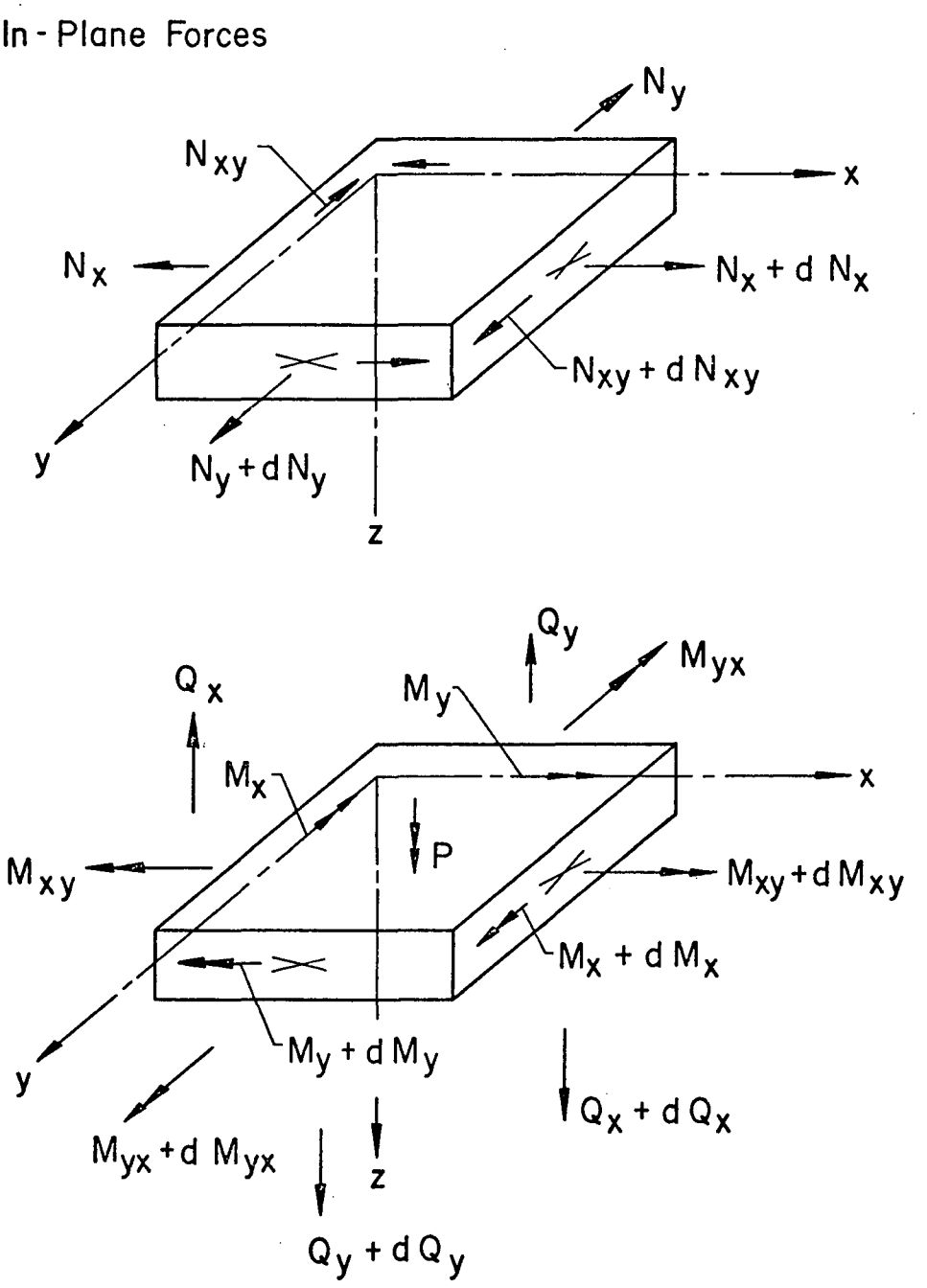

Fig. 3 Sign Convention for Stress Resultants Acting on a Plate Element

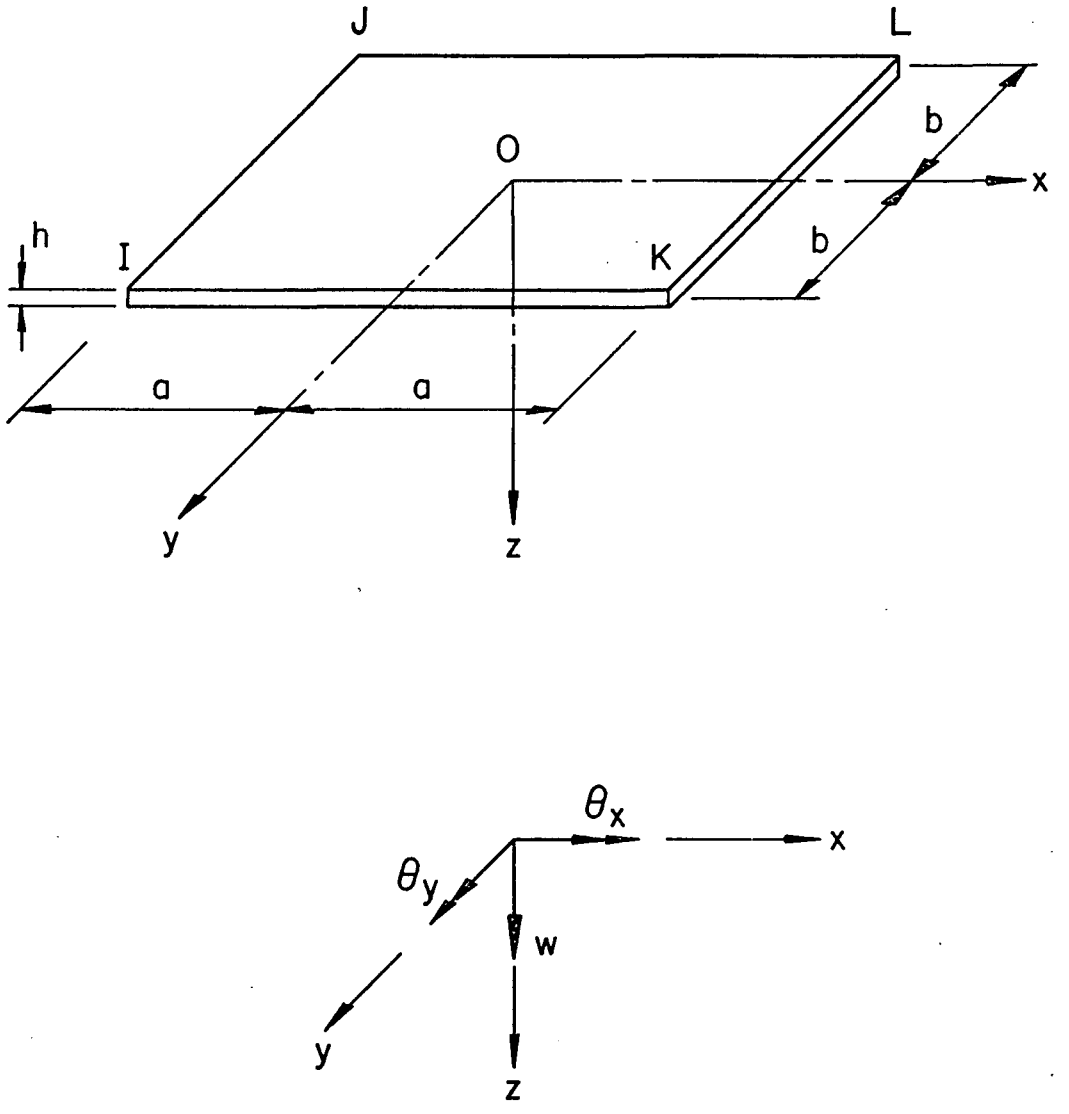

Fig. 4 Rectangular Plate Element and Basic Displacement Components

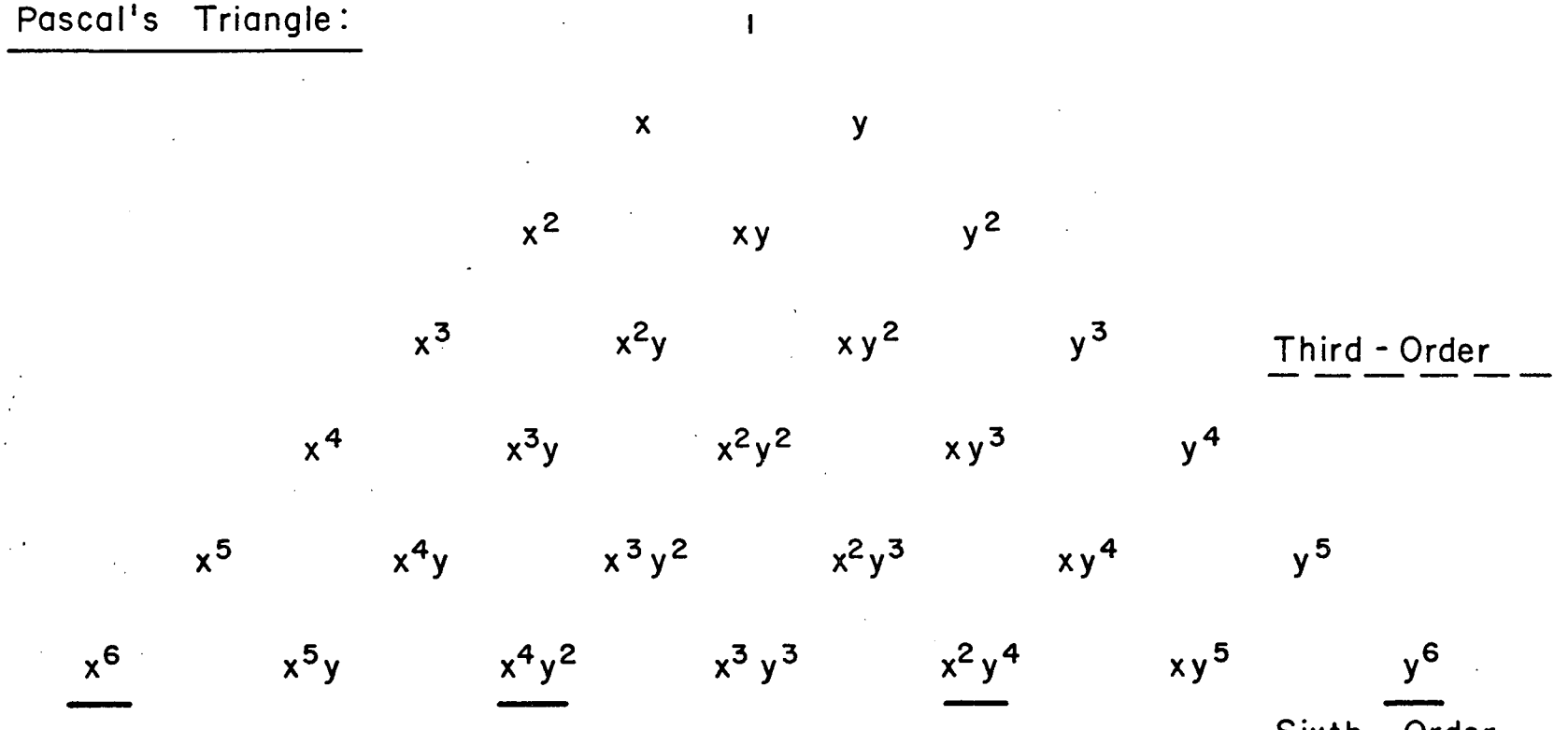

Fig. 5 Polynomial Expansion Represented by Pascal's Triangle

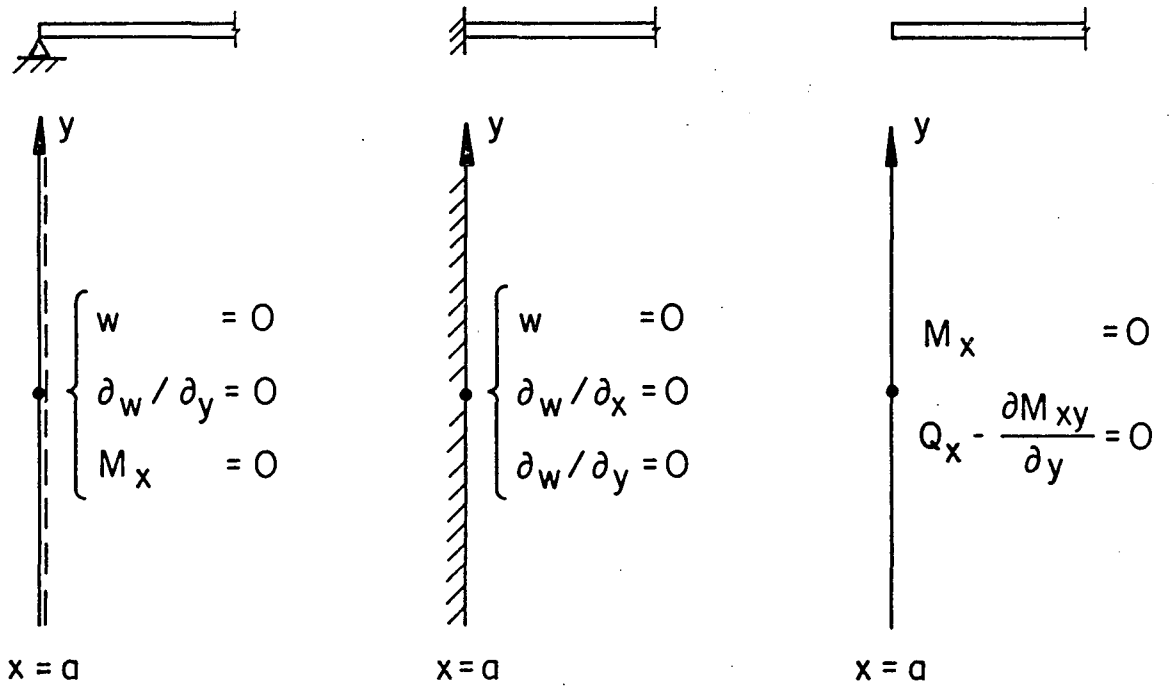

Conventional Plate Theory

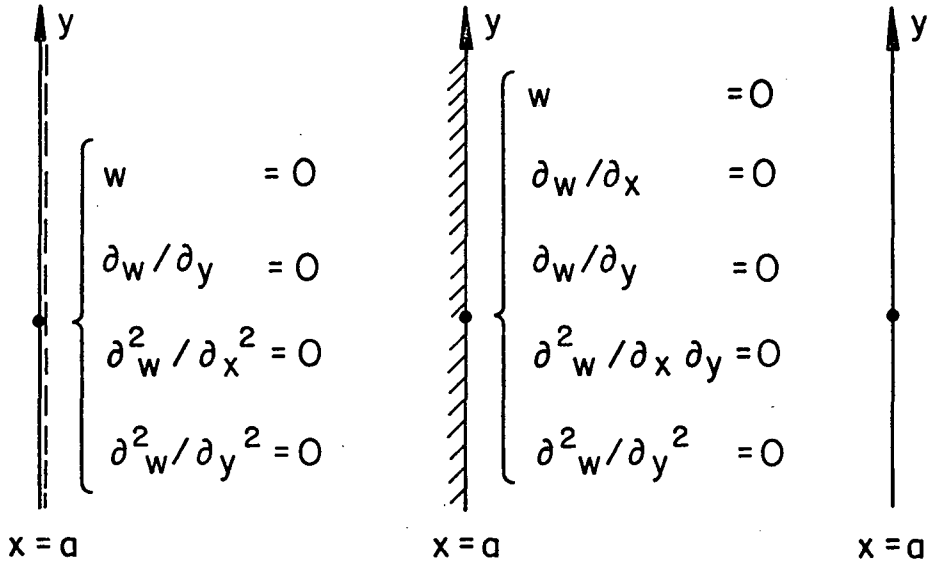

Finite Element Approach

Fig. 6 Typical Plate Boundary Conditions

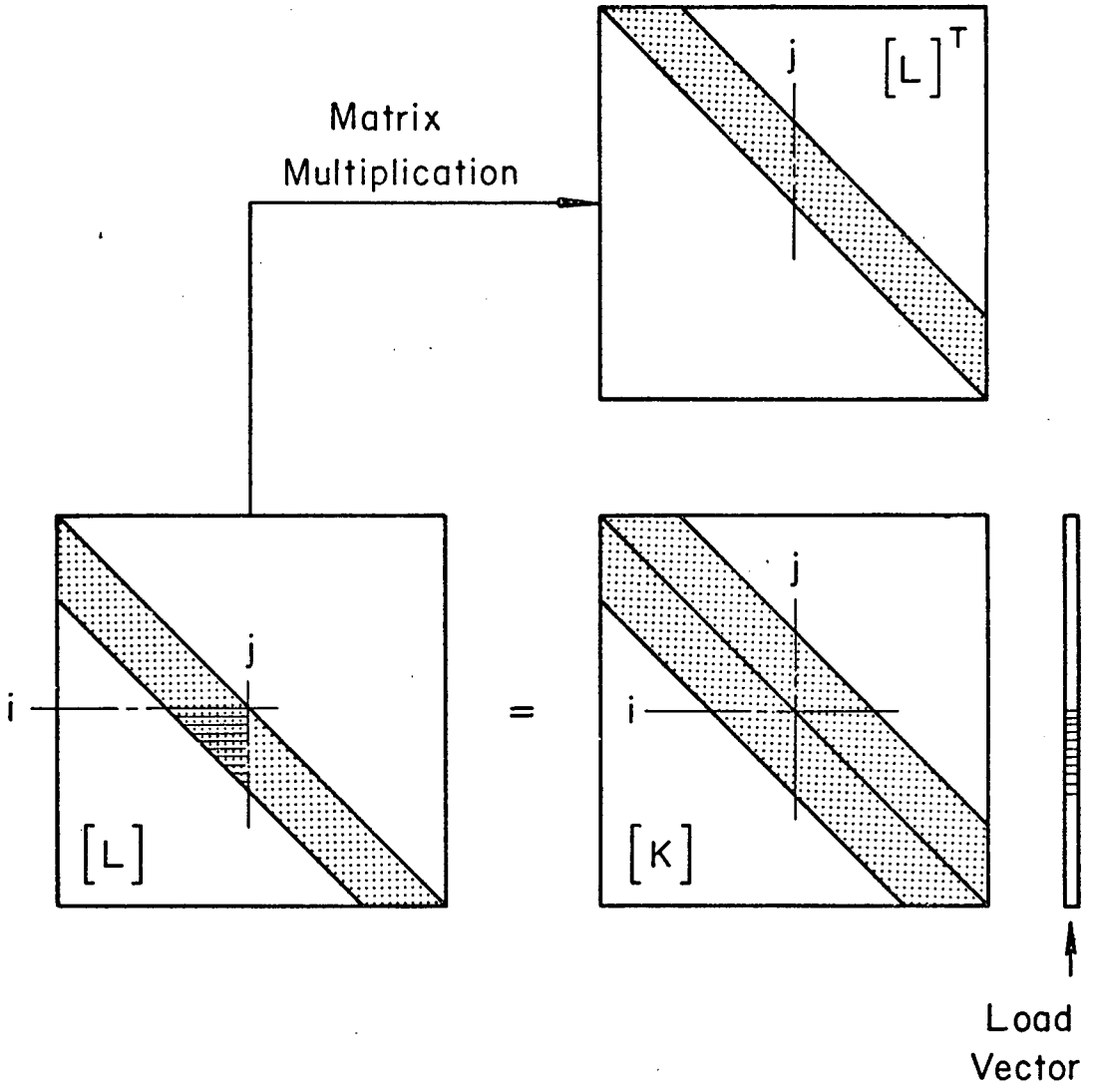

$$[K] = [L]\,[L]^{T}$$

Fig. 7 Banded Stiffness Matrix and its Choleski Decomposition

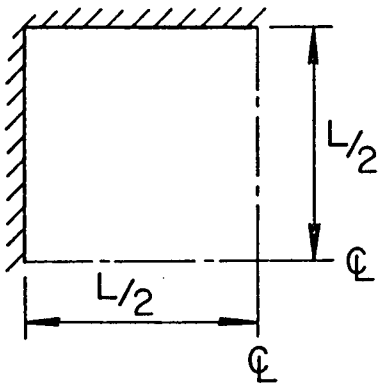

Problem P1:

Square Isotropic Plate
with Four Fixed Supports

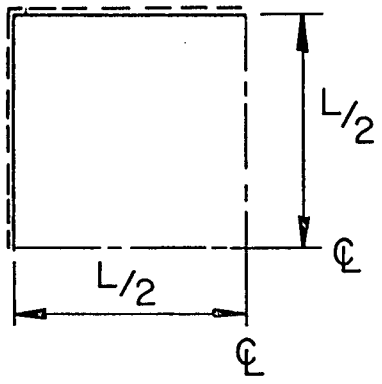

Problem P2:

Square Isotropic Plate
with Four Simple Supports

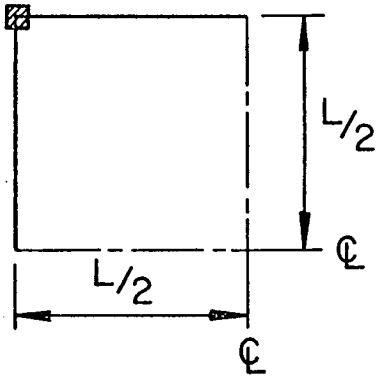

Problem P3:

Plate Supported by Rows
of Equidistant Columns
(Flat Plate)

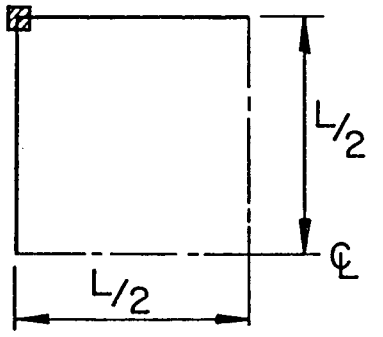

Problem P4:

Square Isotropic Plate
Supported at Corners

Fig. 8 Selected Example Structures for Testing the Refined Plate Element

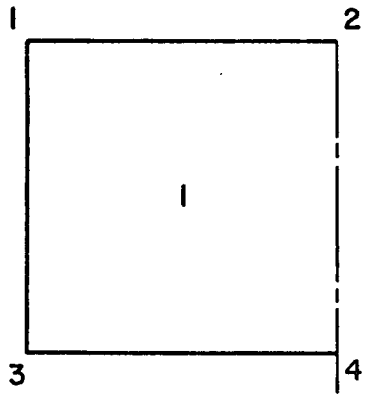

Mesh 2 x 2

1 Element

4 Nodal Points

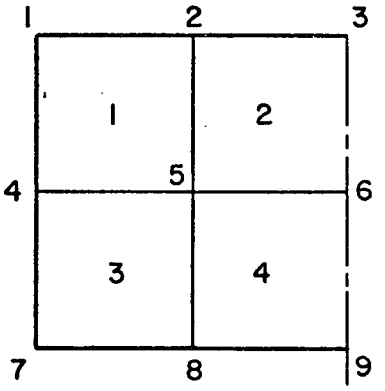

Mesh 4 x 4

4 Elements

9 Nodal Points

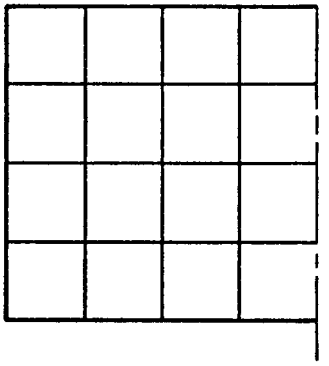

Mesh 8 x 8

16 Elements

25 Nodal Points

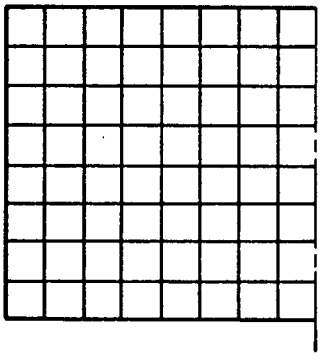

Mesh 16 x 16

64 Elements

81 Nodal Points

Fig. 9 Discretization of a Plate Quadrant

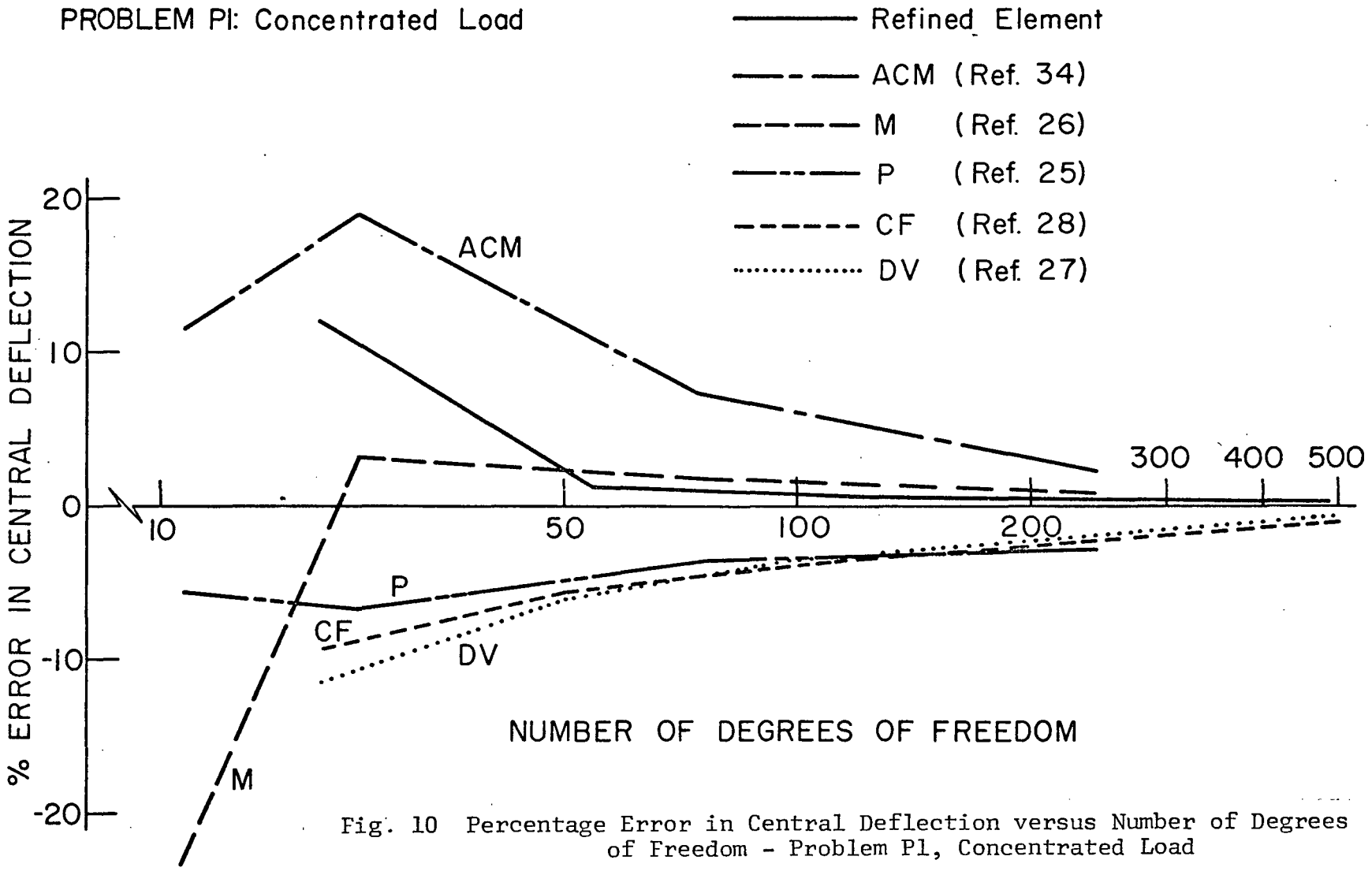

Fig. 10 Percentage Error in Central Deflection versus Number of Degrees of Freedom - Problem P1, Concentrated Load

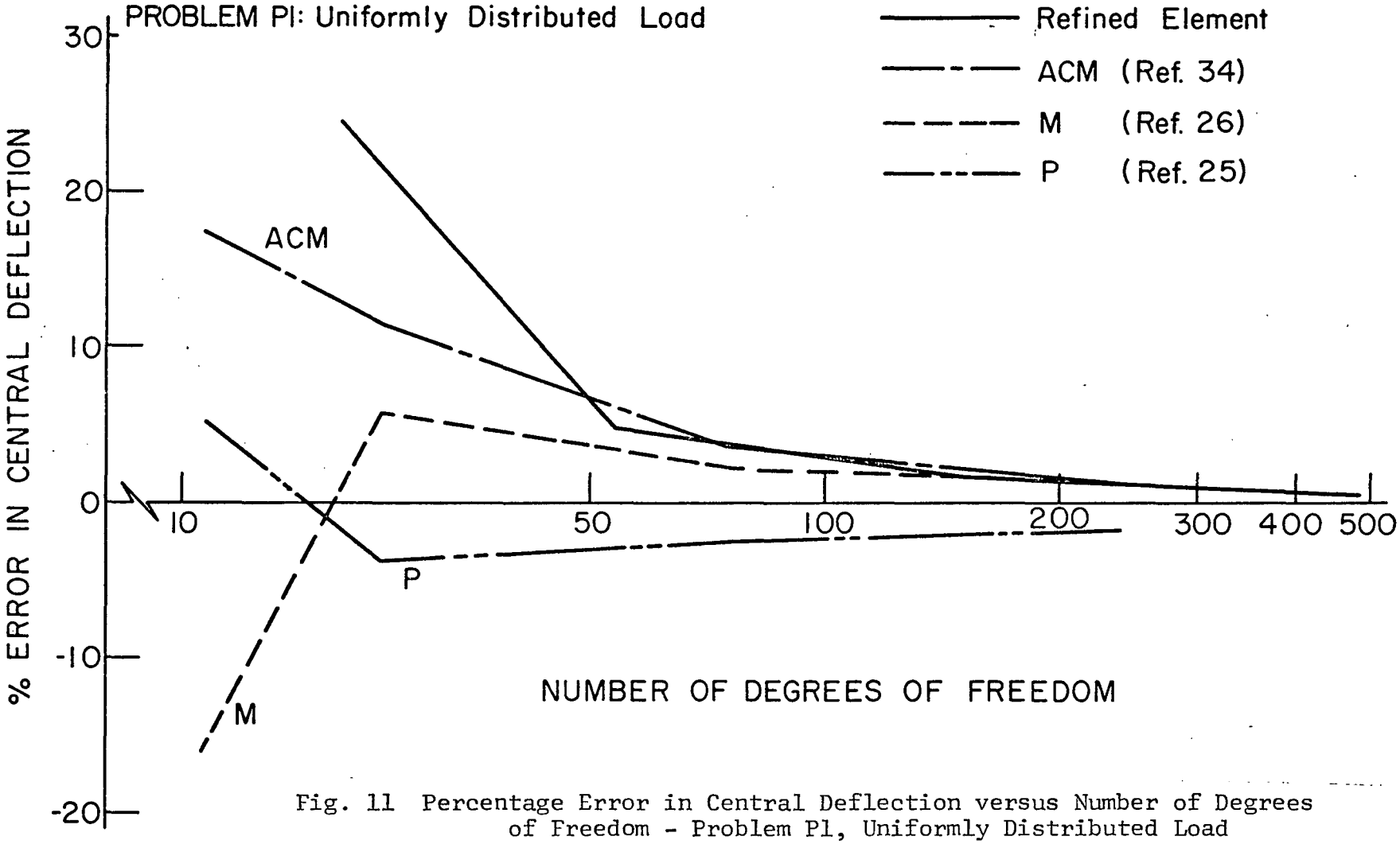

Fig. 11 Percentage Error in Central Deflection versus Number of Degrees of Freedom - Problem P1, Uniformly Distributed Load

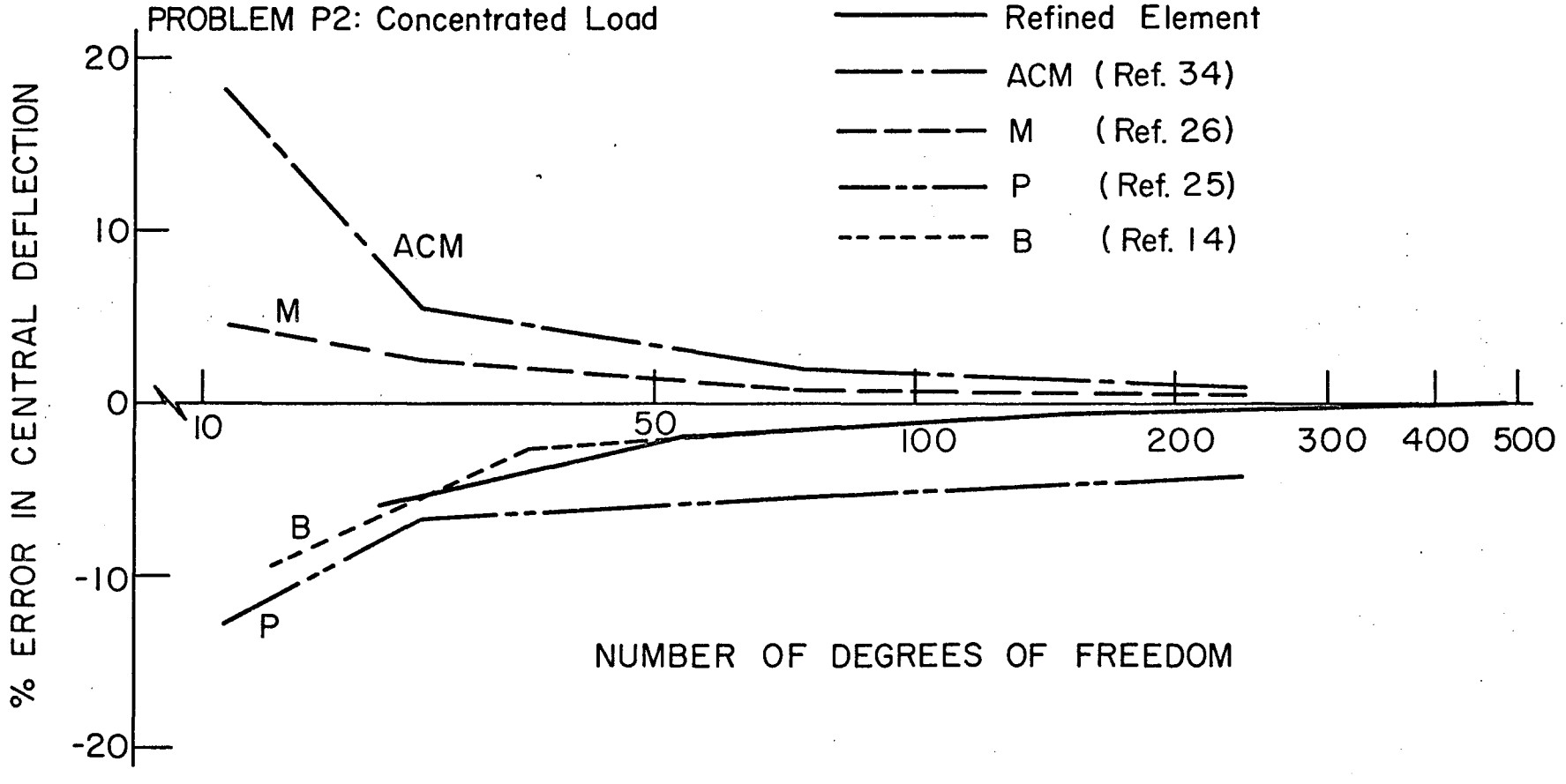

Fig. 12 Percentage Error in Central Deflection versus Number of Degrees of Freedom - Problem P2, Concentrated Load

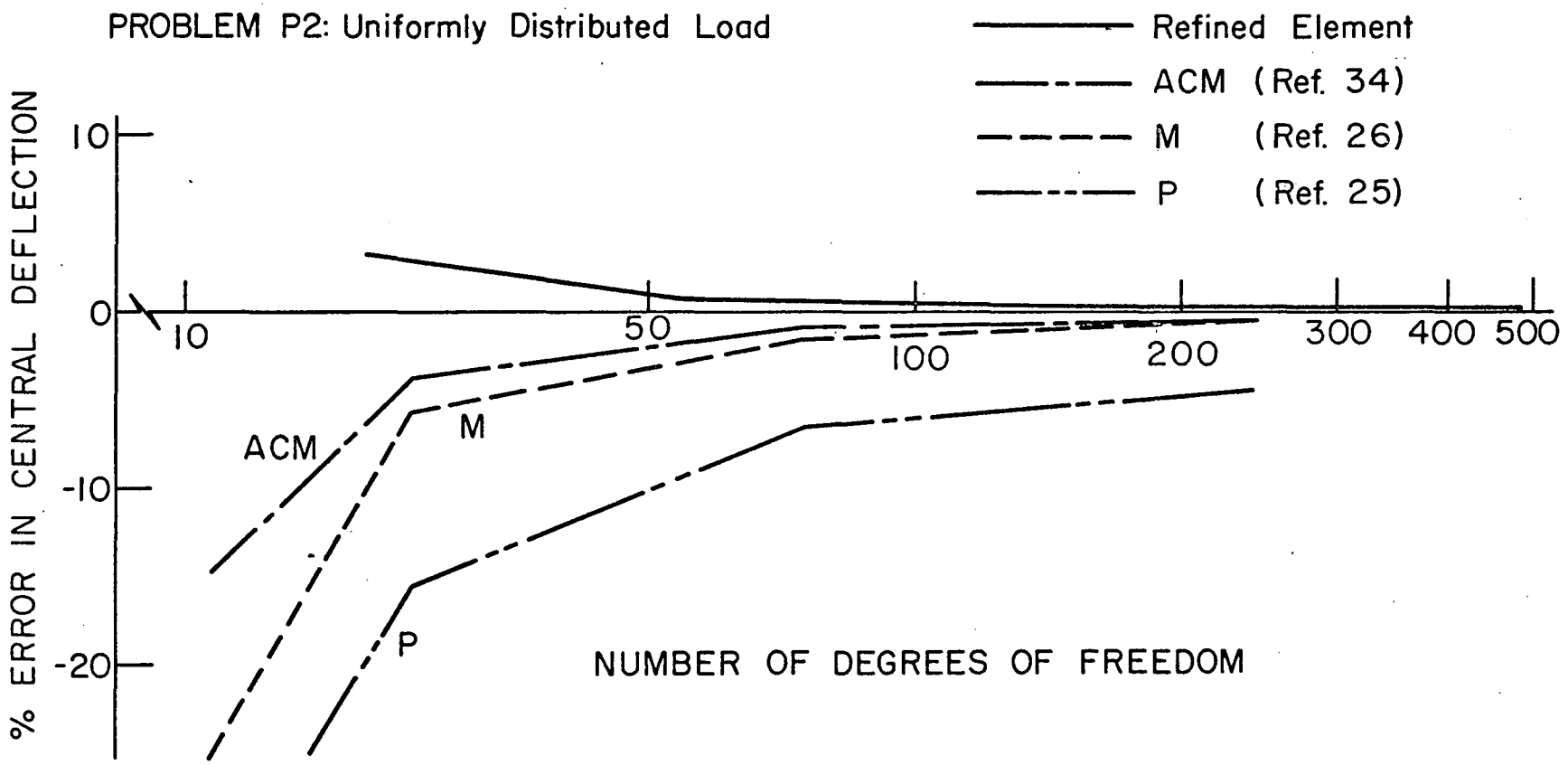

Fig. 13 Percentage Error in Central Deflection versus Number of Degrees of Freedom - Problem P2, Uniformly Distributed Load

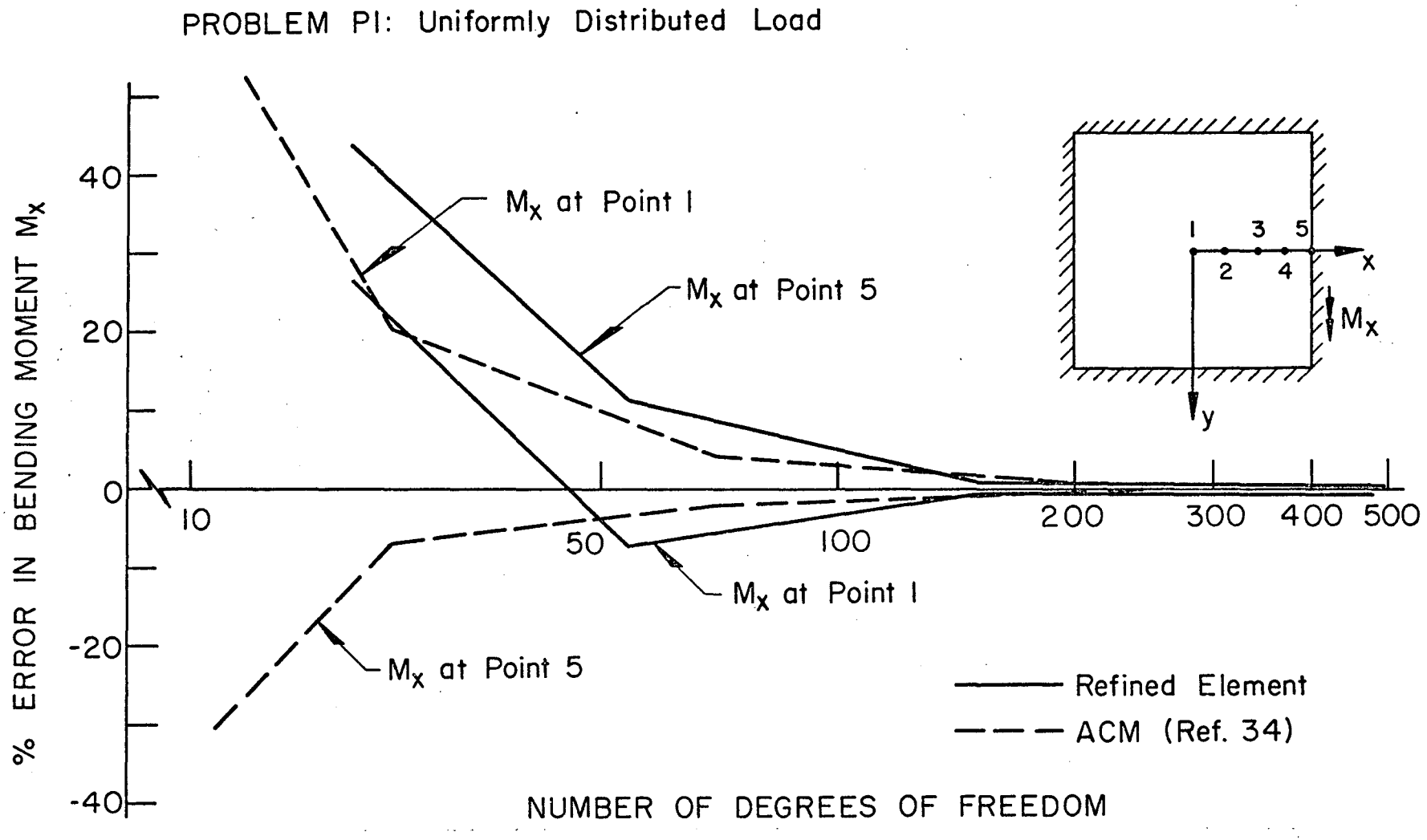

Fig. 14 Percentage Error in Plate Bending Moment M_x versus Number of Degrees of Freedom - Problem P1

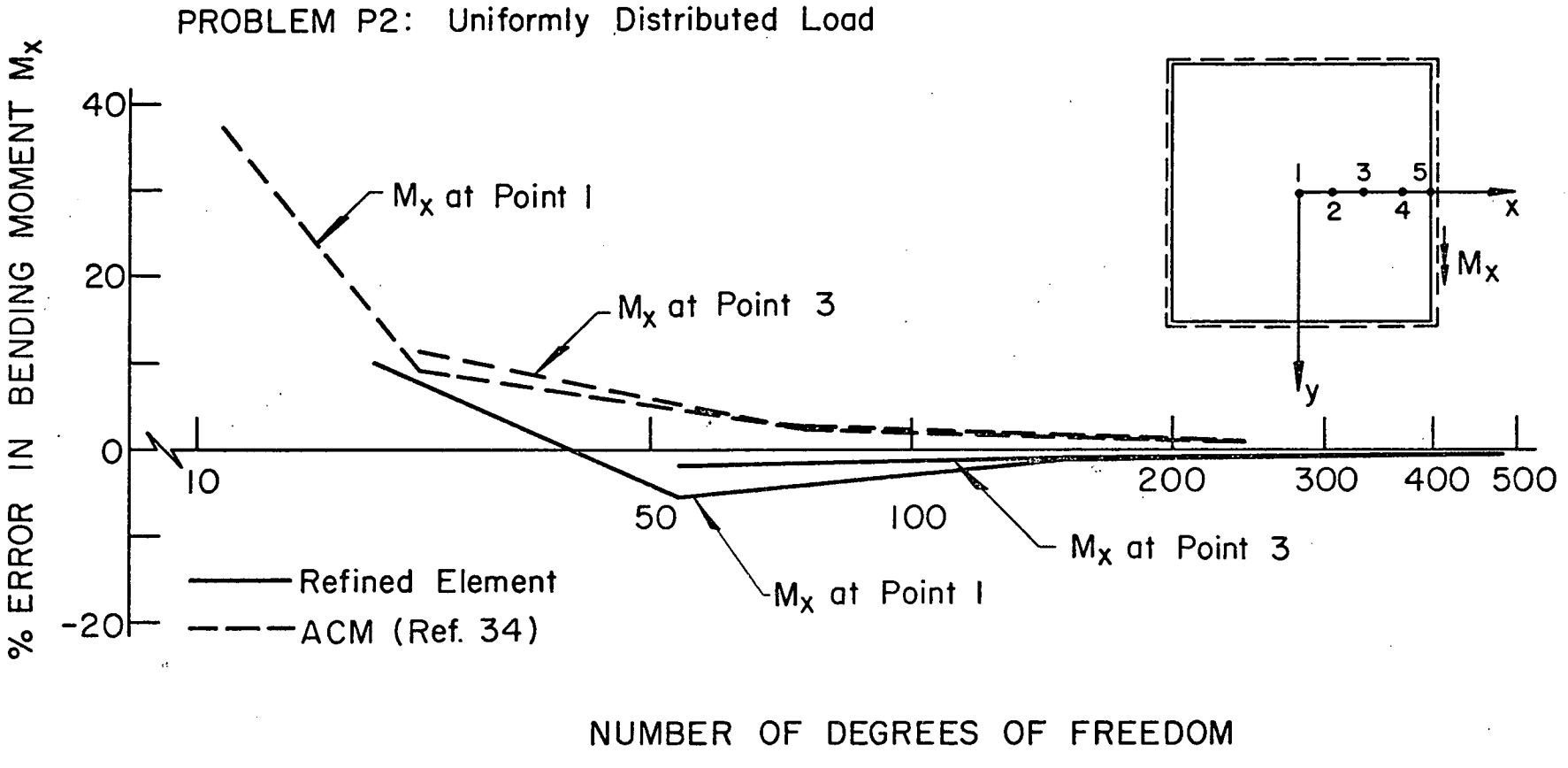

Fig. 15 Percentage Error in Plate Bending Moment M_x versus Number of Degrees of Freedom - Problem P2

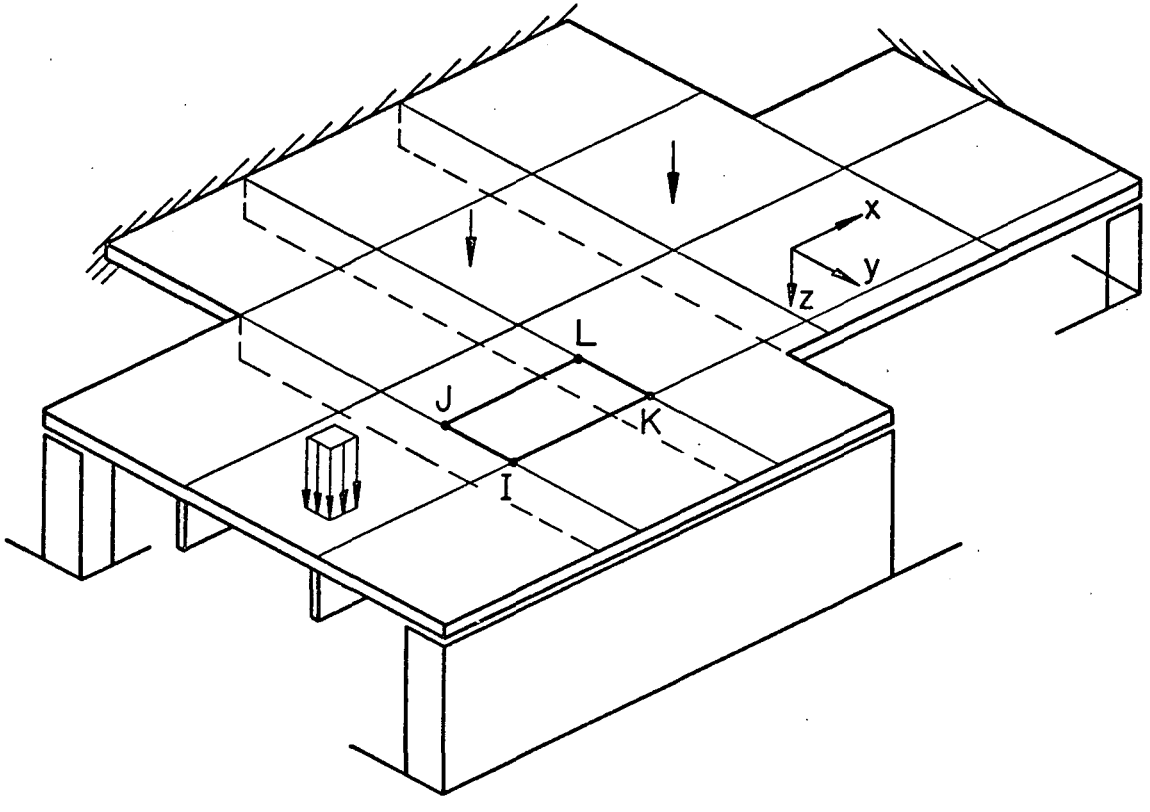

Fig. 16 Stiffened Plate of Arbitrary Loading and Geometry

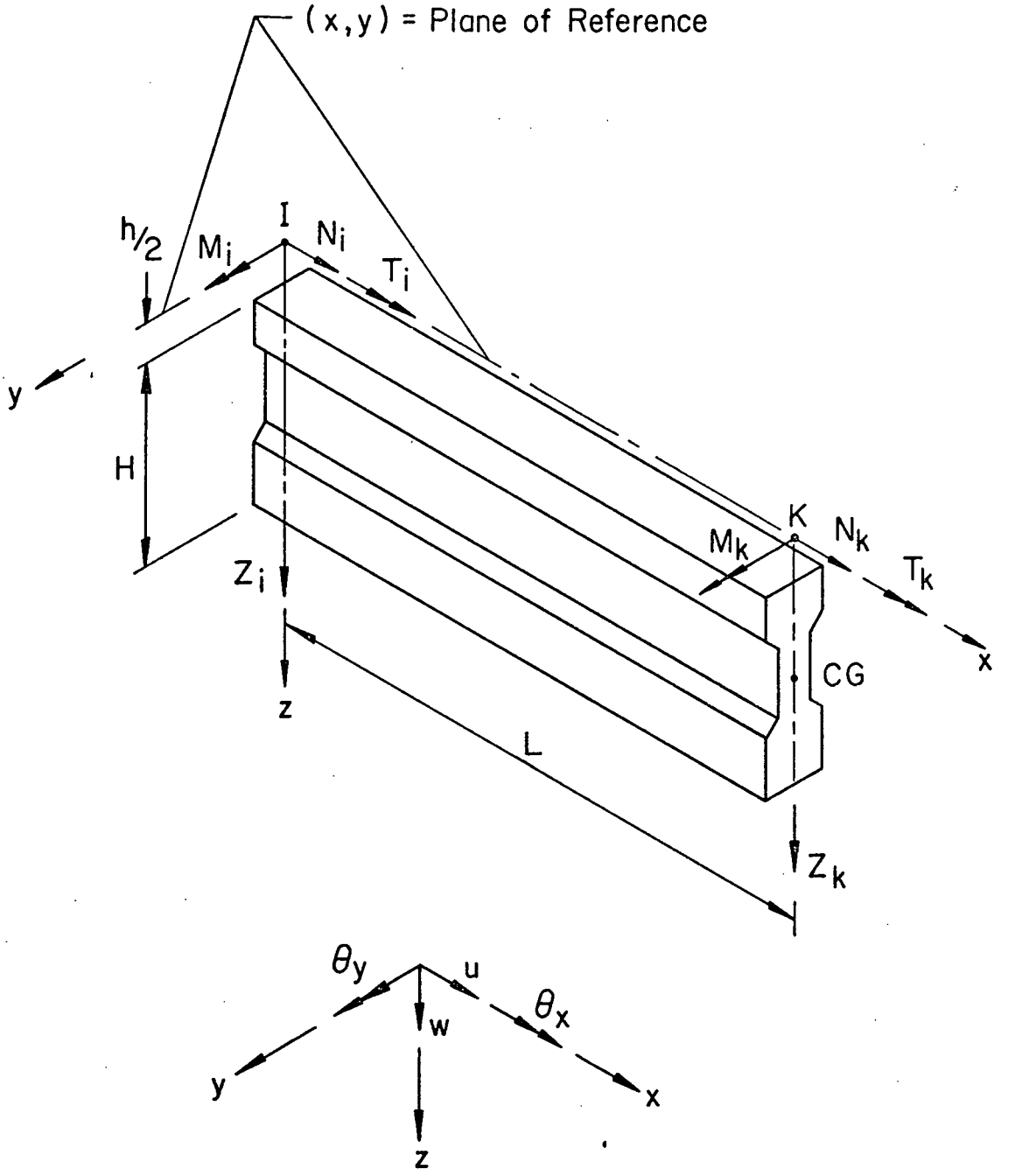

Fig. 17 Eccentrically Attached Stiffener Element

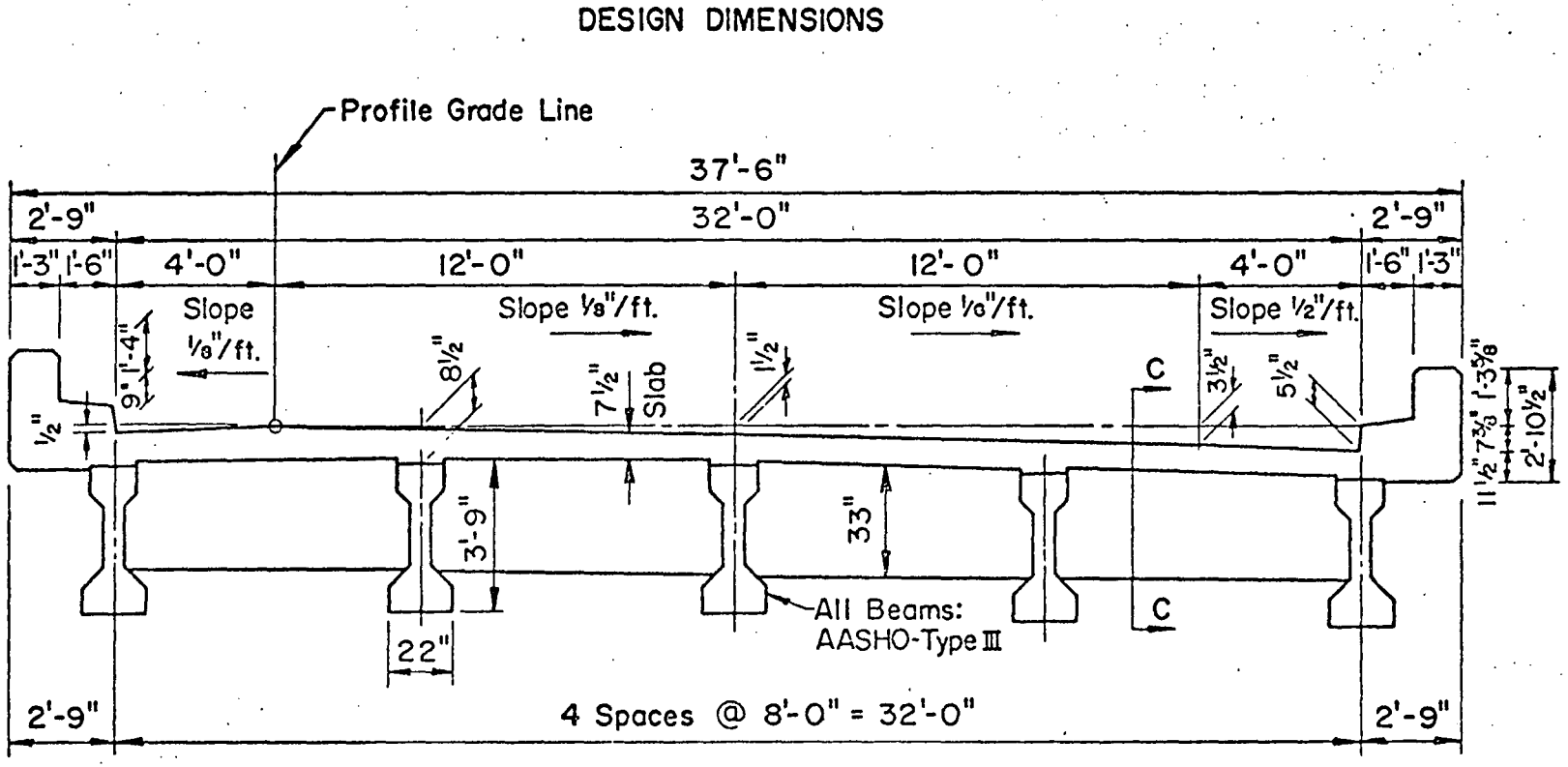

Fig. 18 Cross Section of Test Bridge

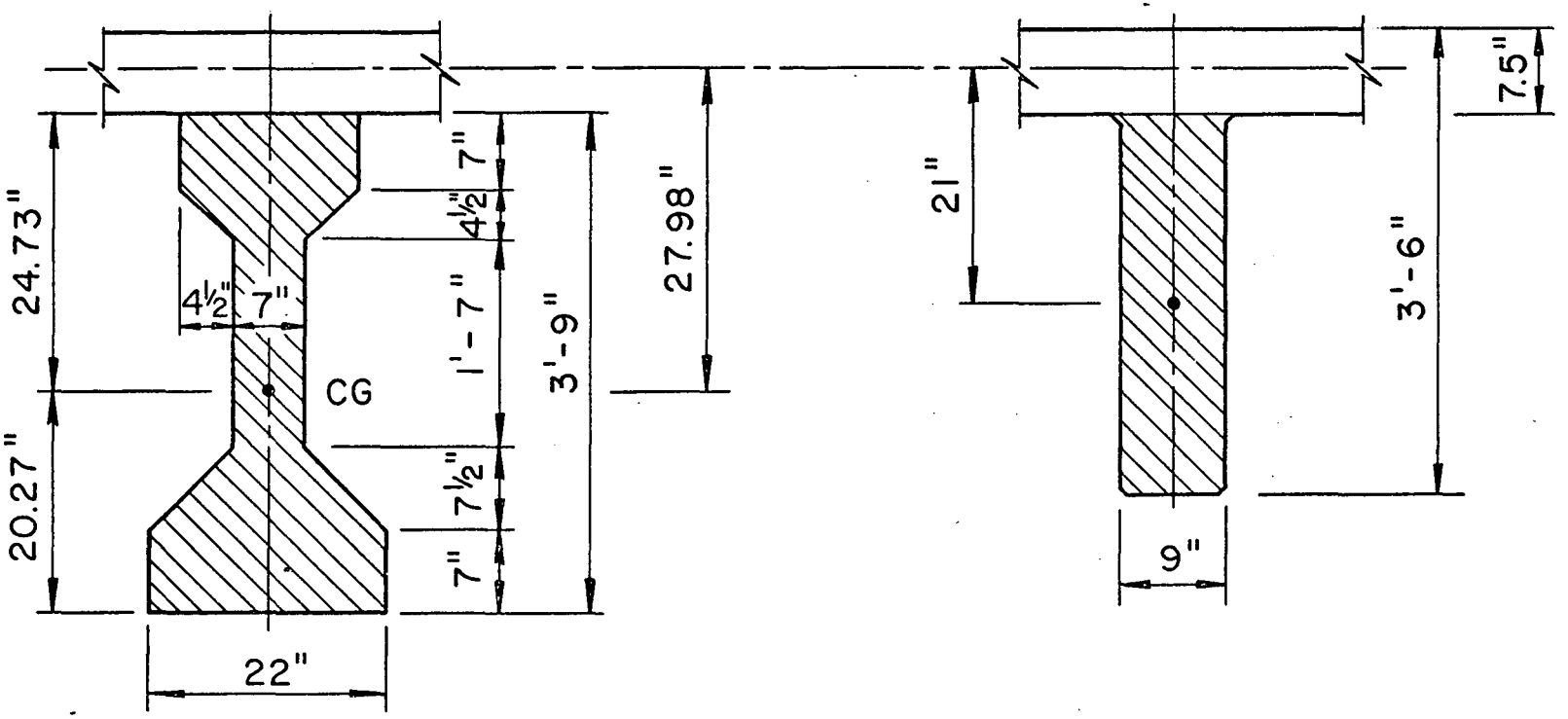

Fig. 19 Cross-Sectional Dimensions of Beams and Midspan Diaphragm

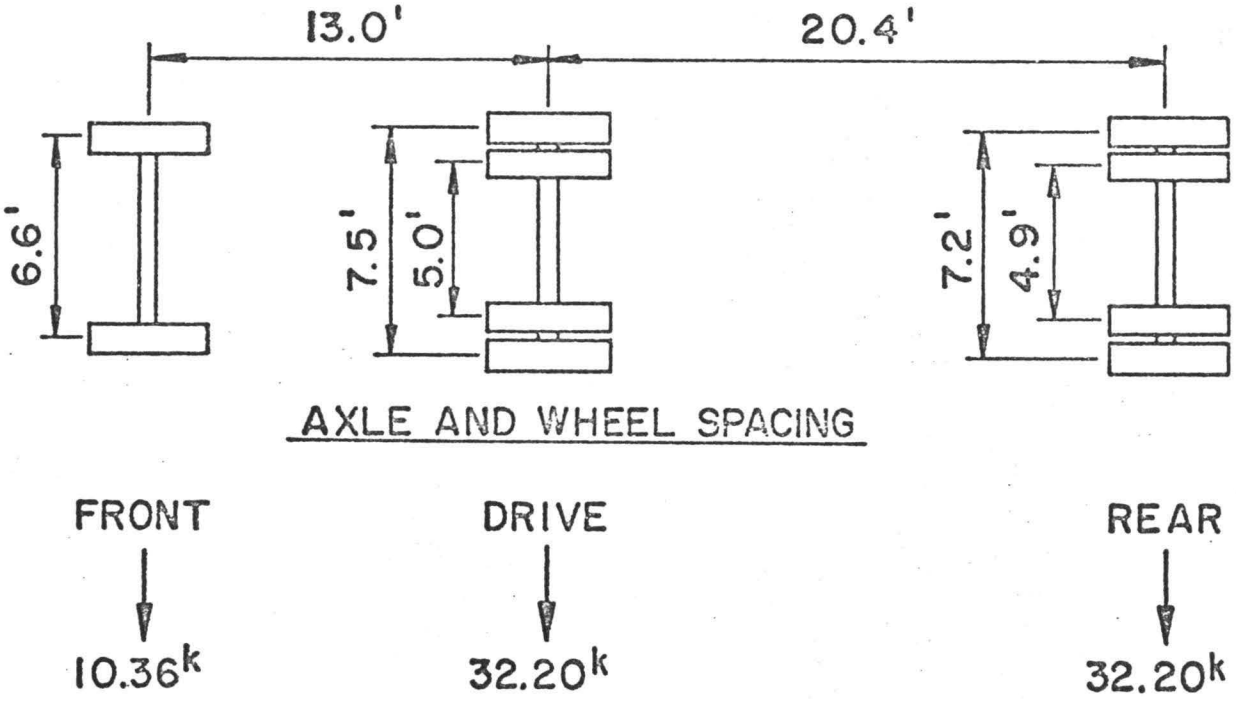

Fig. 20 Test Vehicle

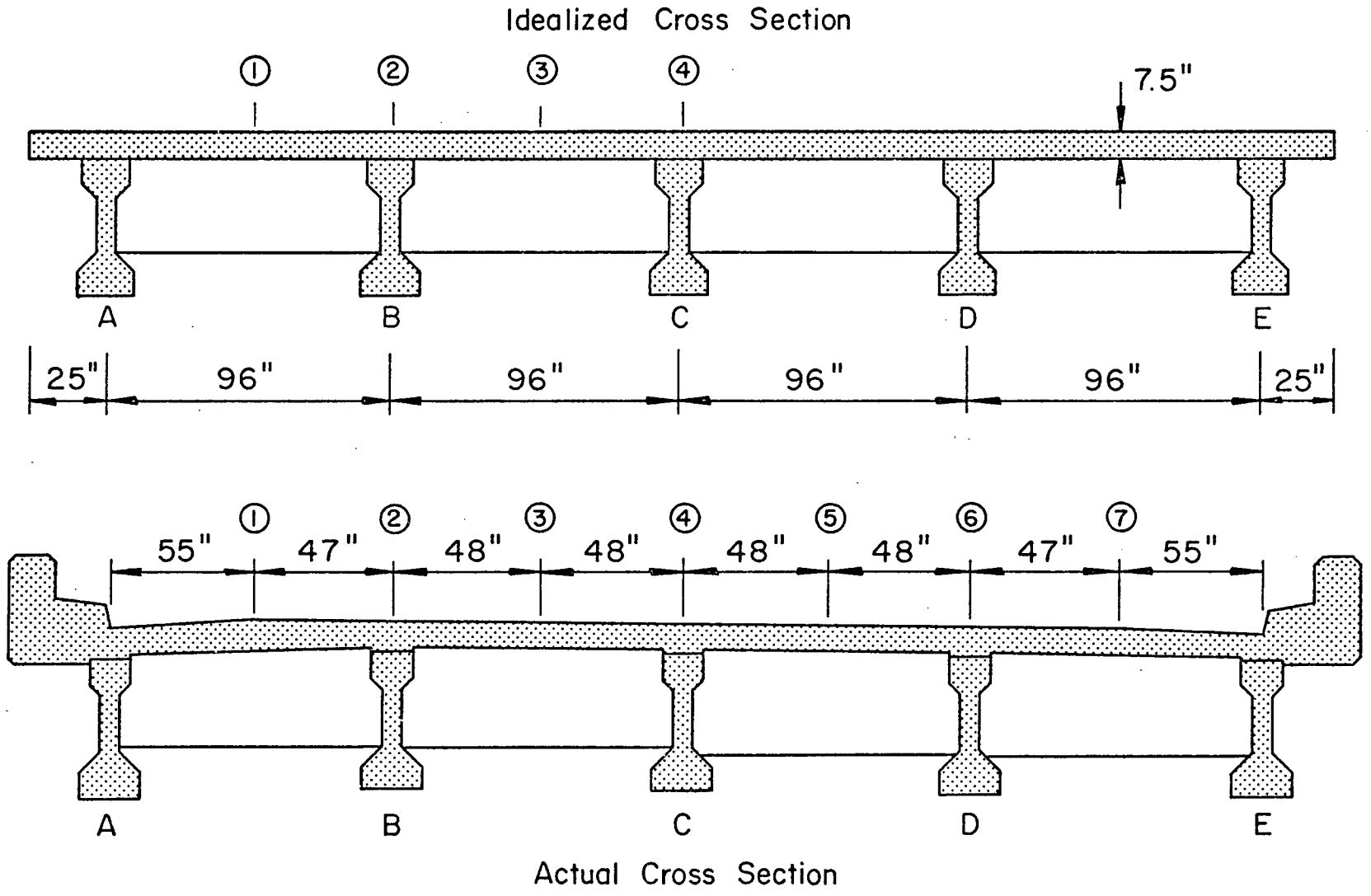

Fig. 21 Idealized and Actual Bridge Cross Section and Loading Lanes

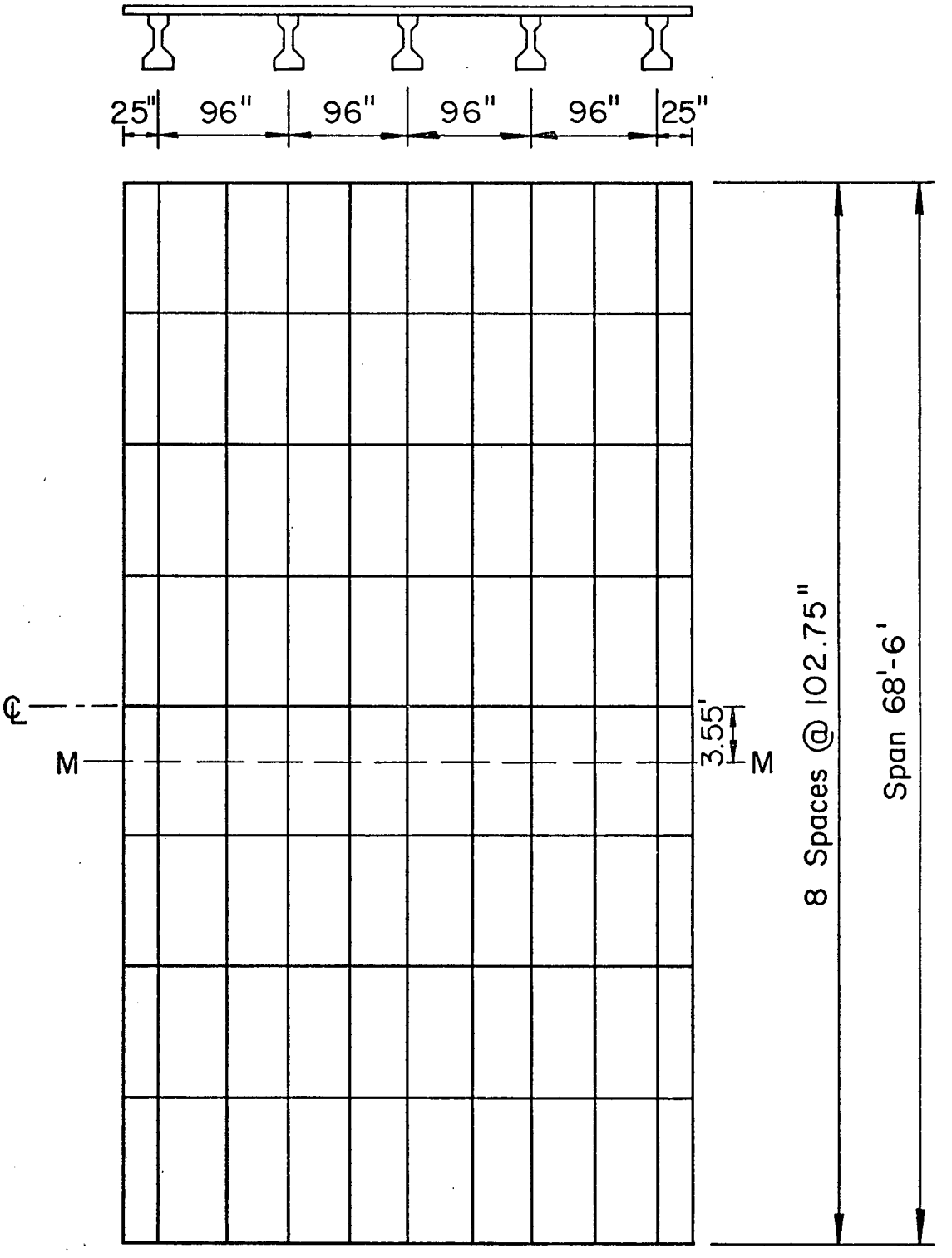

Fig. 22 Discretization of I-Beam Bridge: Mesh 10*8

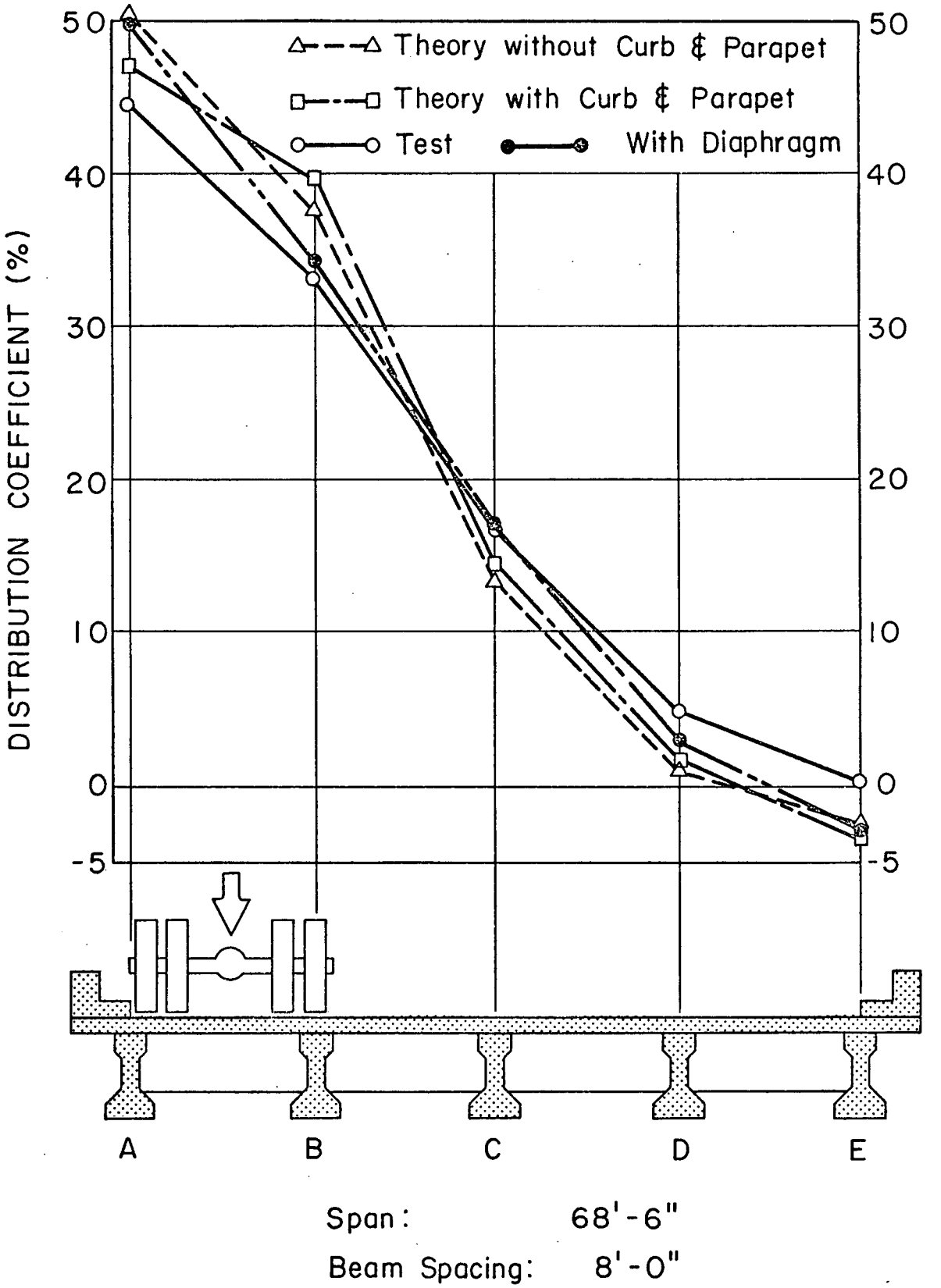

Fig. 23 Distribution Coefficients - Load in Lane 1

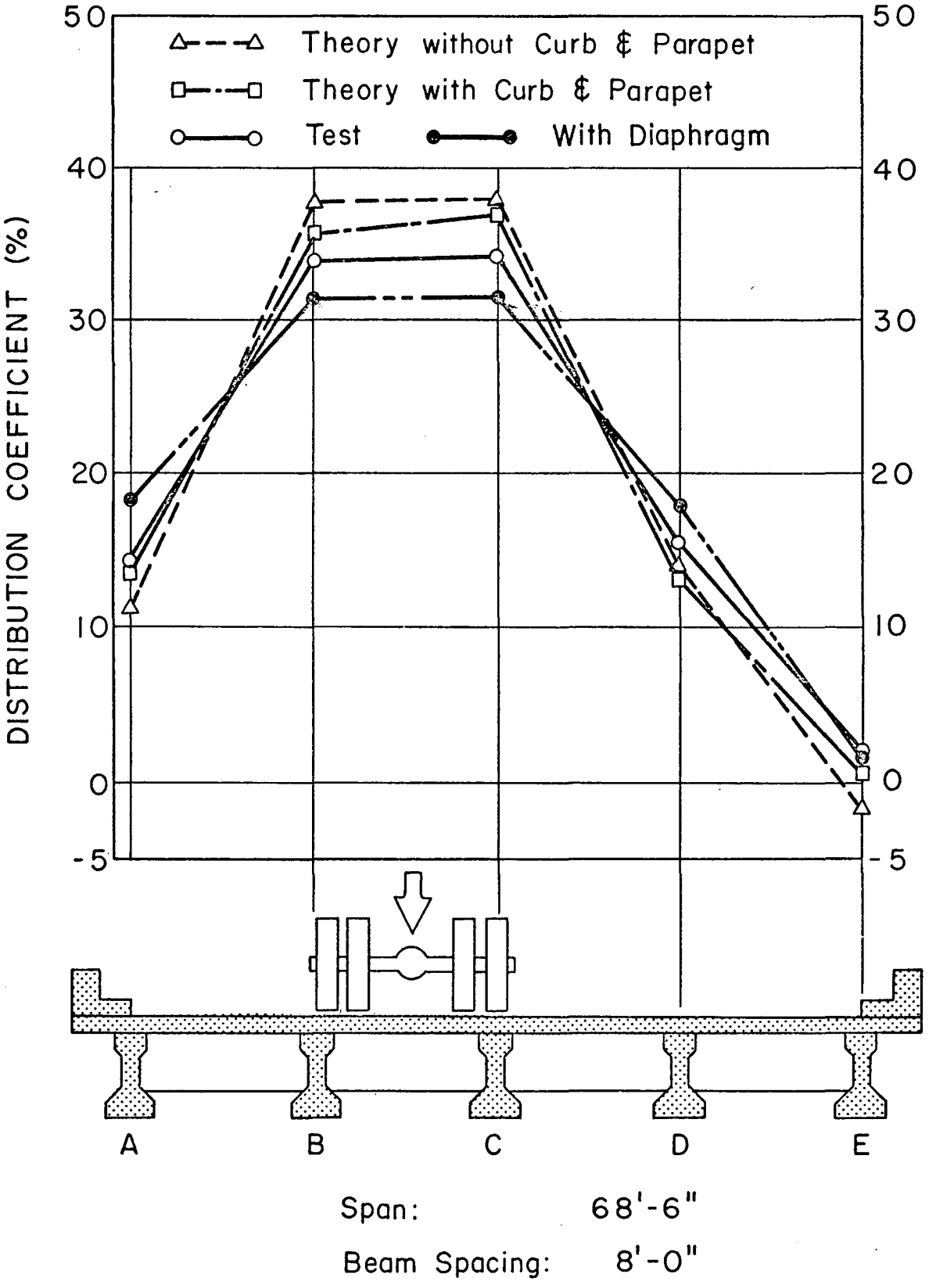

Fig. 24 Distribution Coefficients - Load in Lane 3

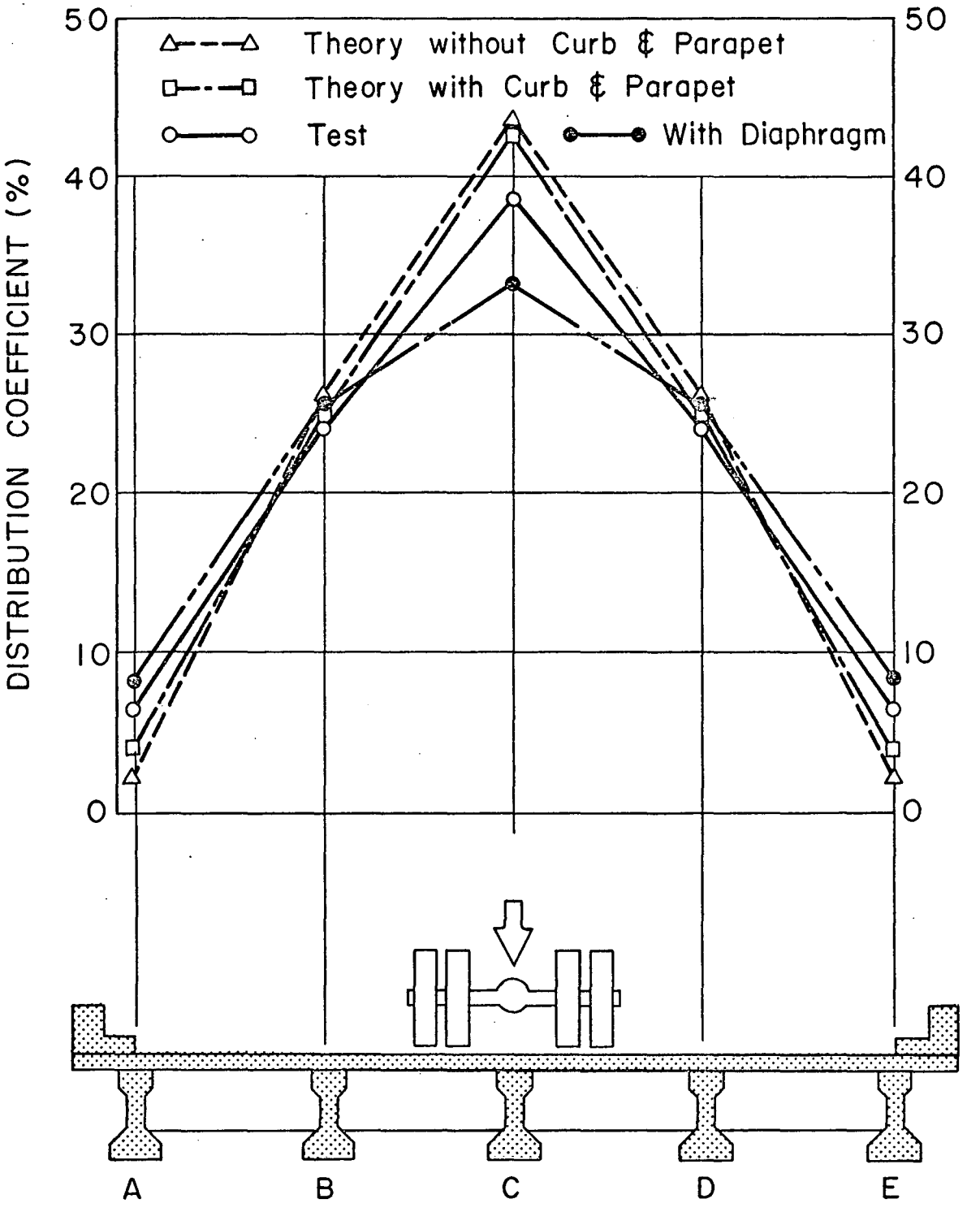

Fig. 25 Distribution Coefficients - Load in Lane 4

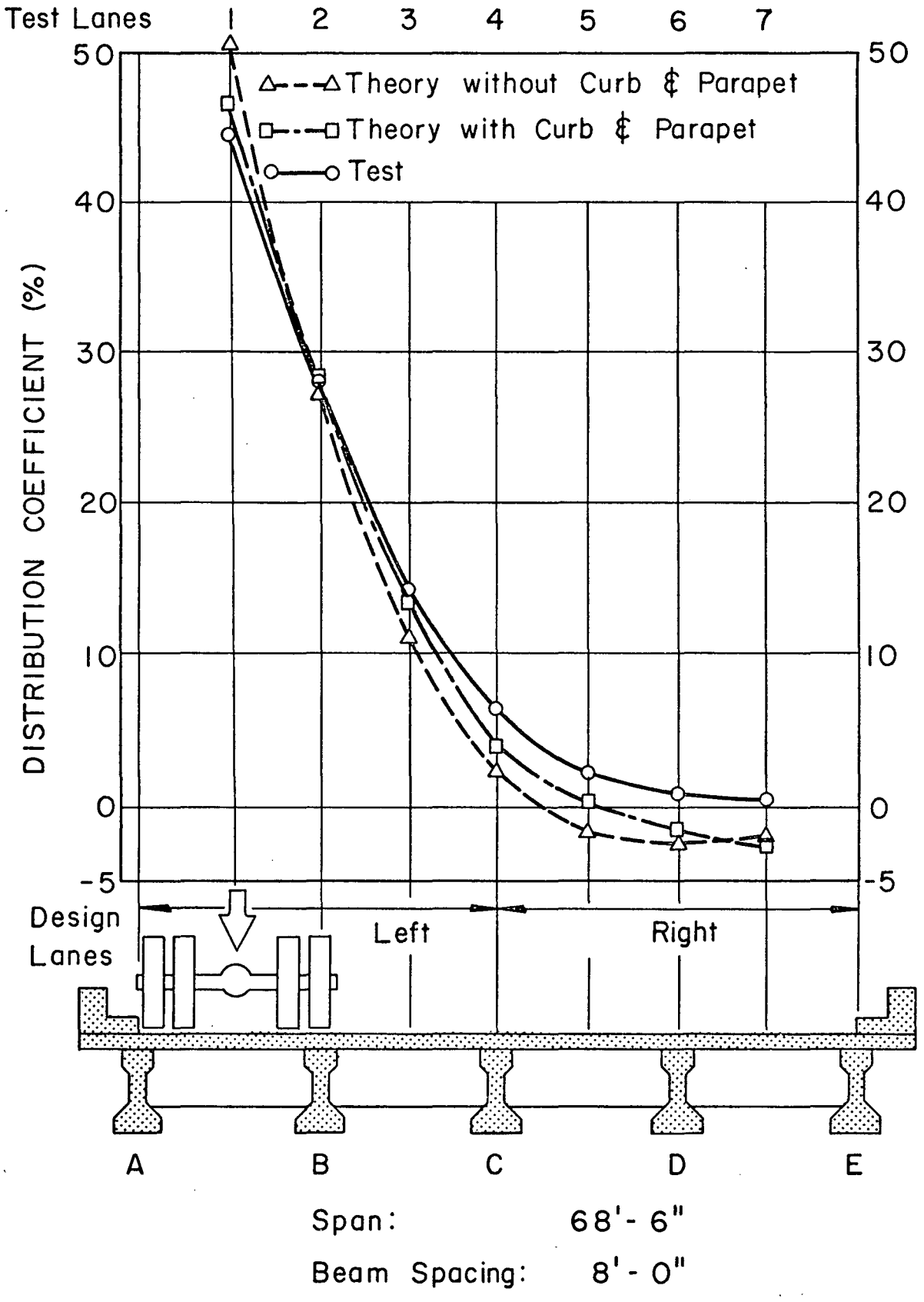

Fig. 26 Influence Line for Bending Moment - Beam A

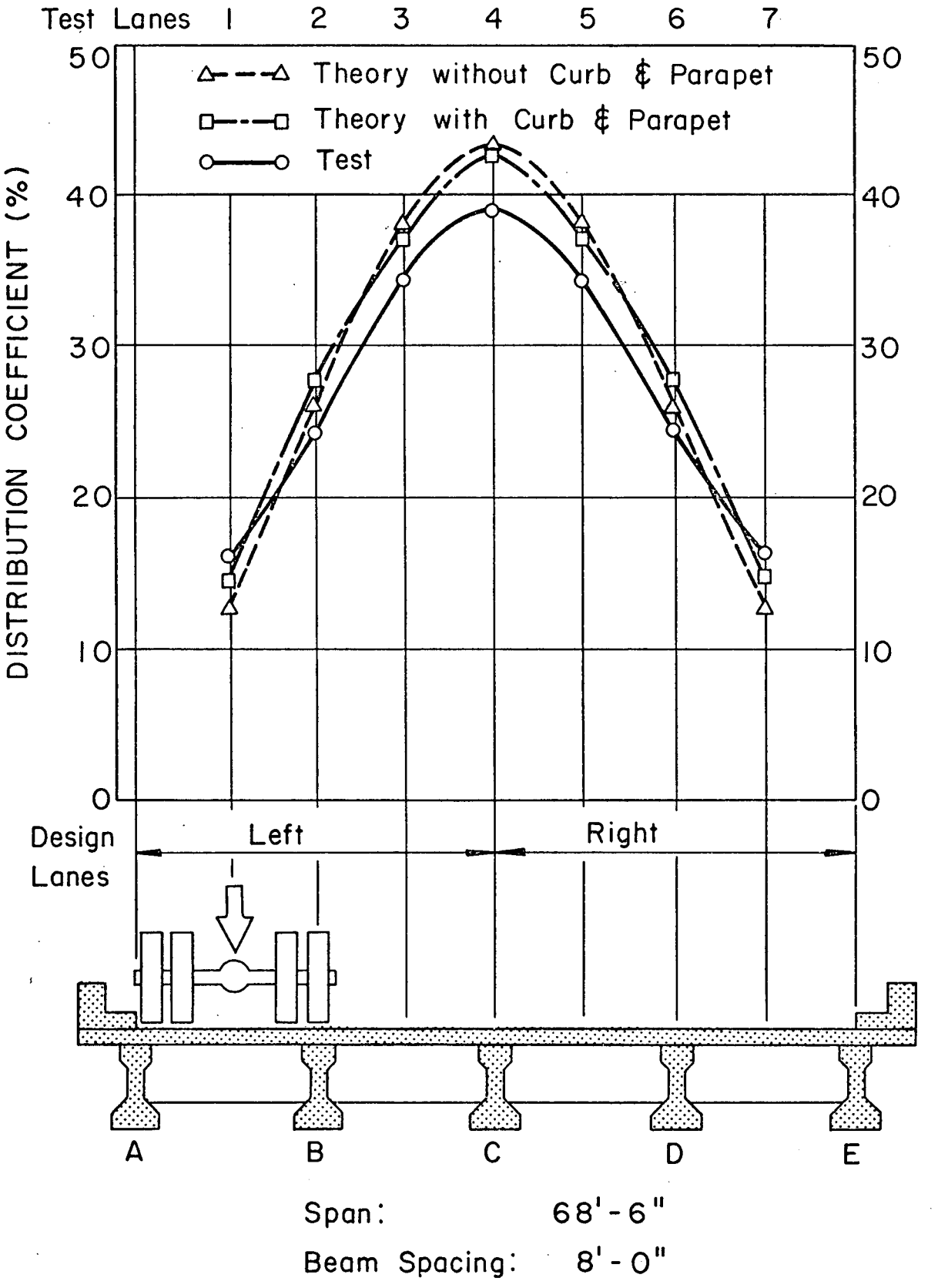

Fig. 27 Influence Line for Bending Moment - Beam C

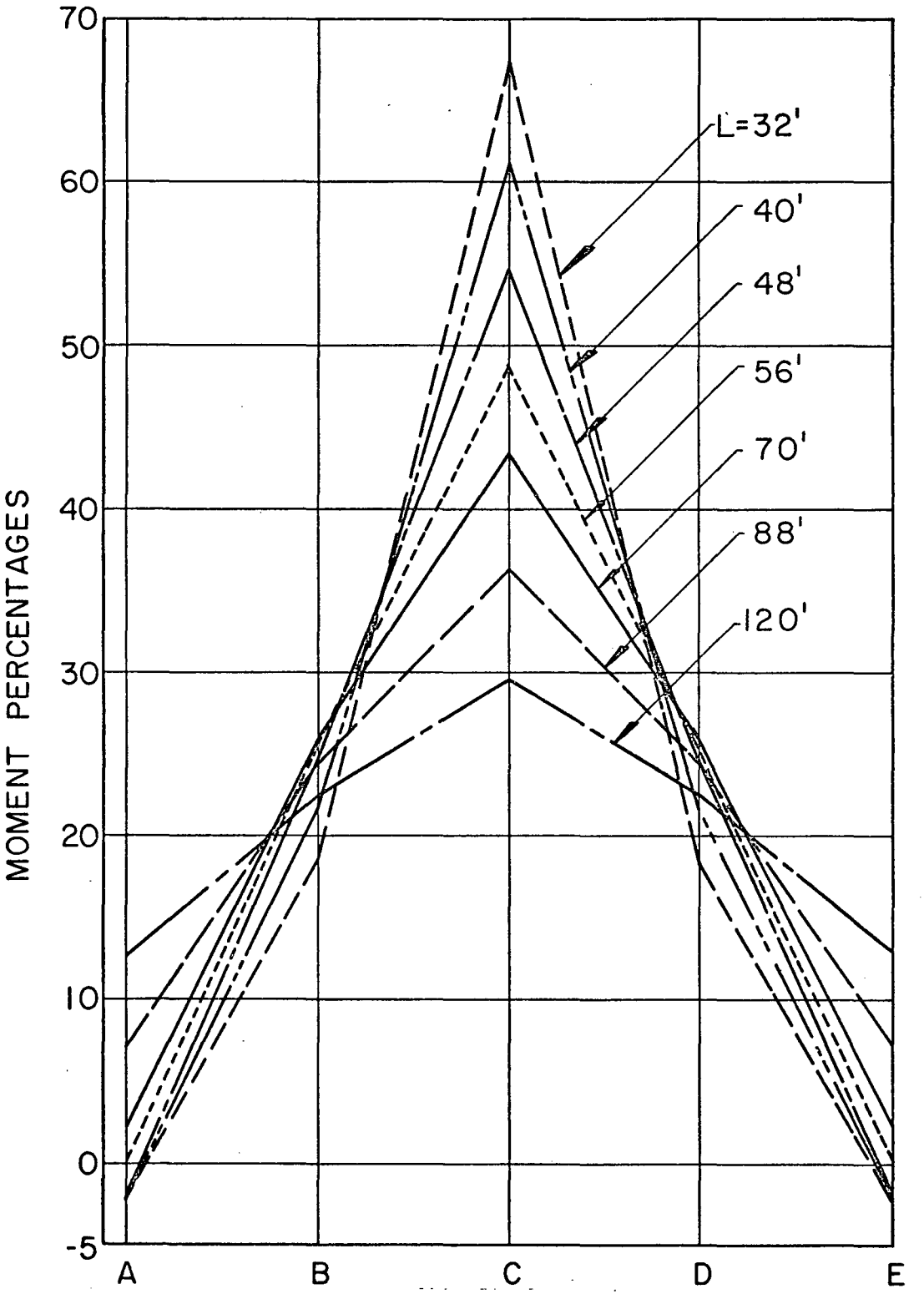

Fig. 28 Effect of Span Length on Load Distribution - Load in Lane 4

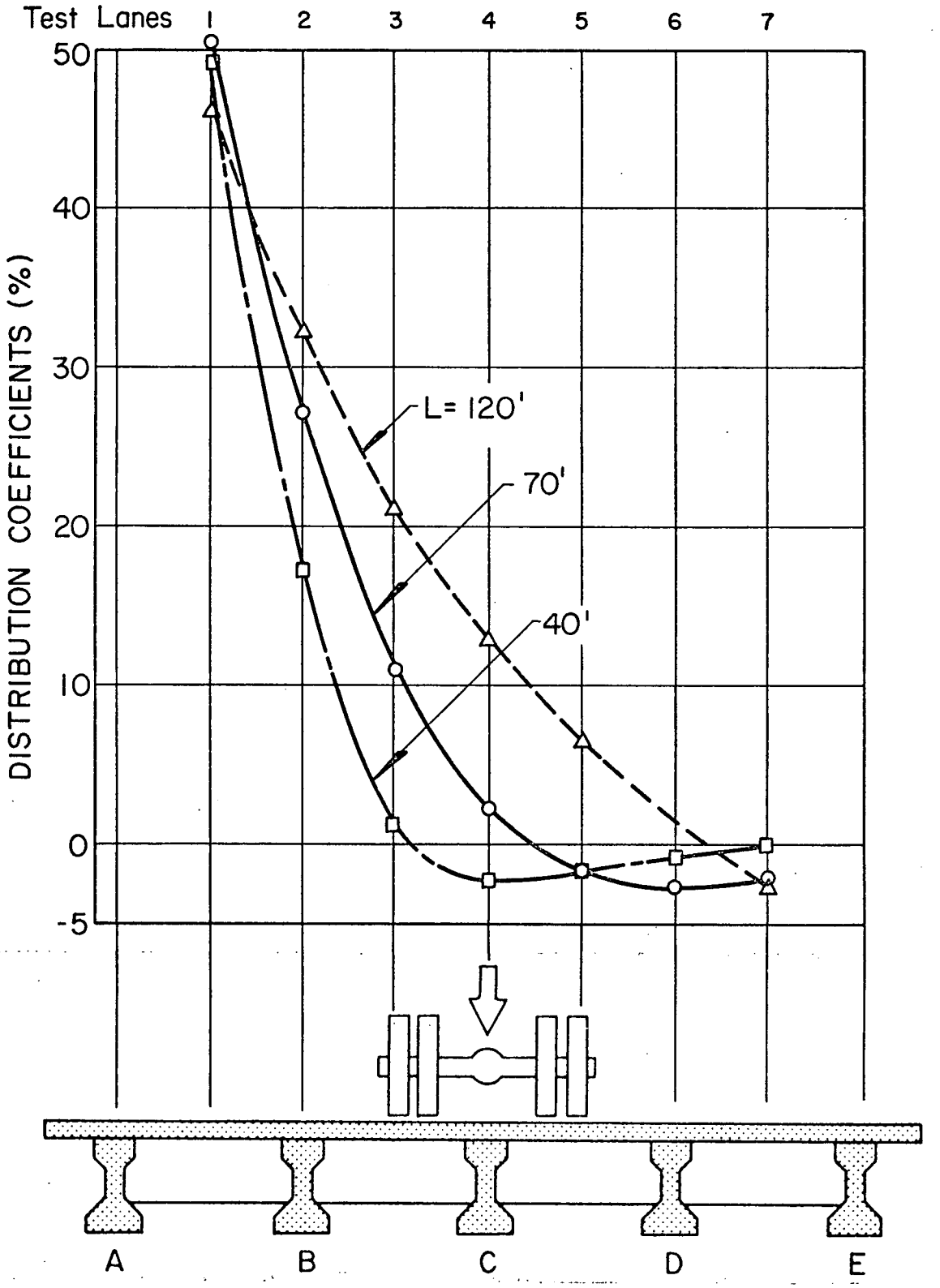

Fig. 29 Influence Lines for Bending Moment - Beam A
Effect of Span Length

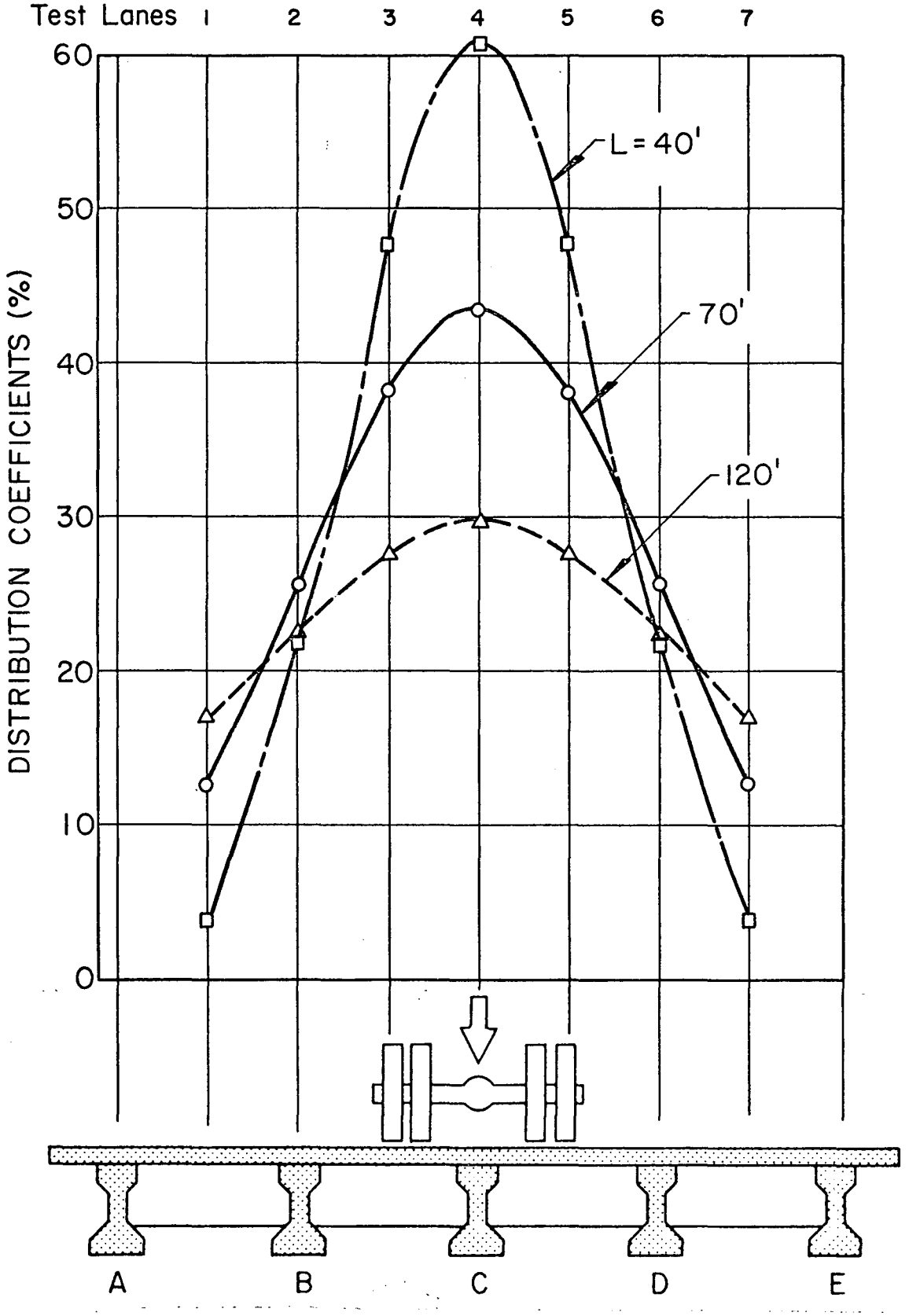

Fig. 30 Influence Lines for Bending Moment - Beam C
Effect of Span Length

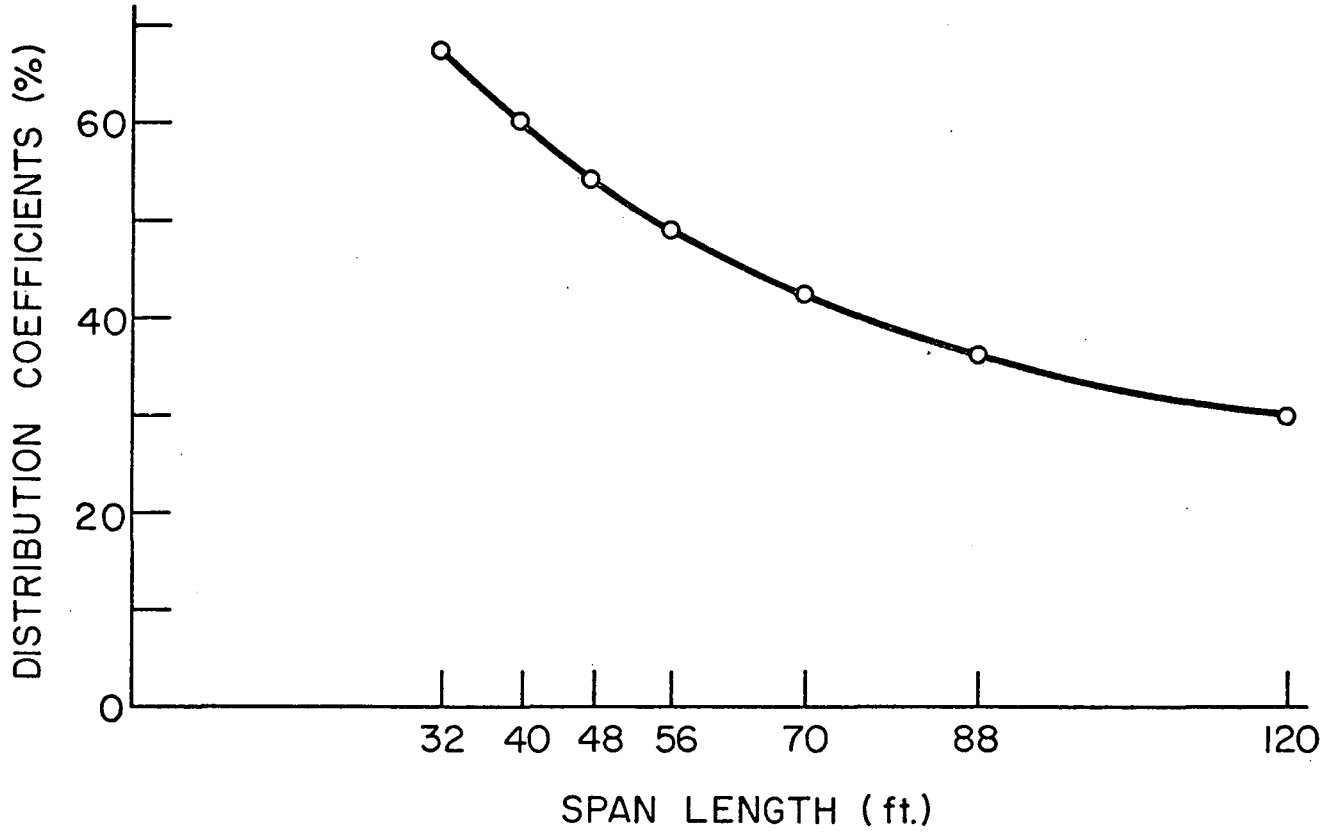

Fig. 31 Effect of Span Length on Center Beam Moment - Beam C

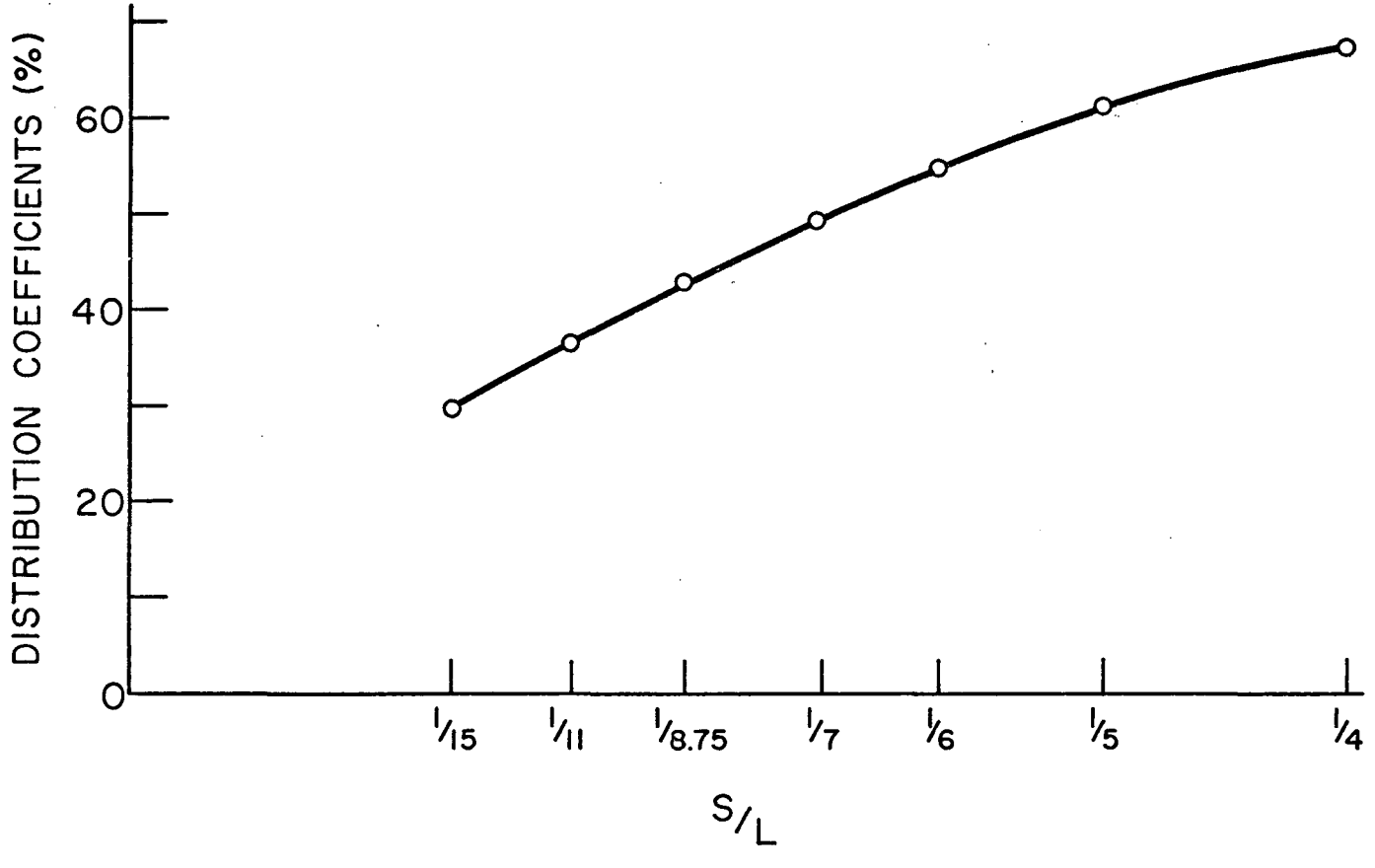

Fig. 32 Distribution Factor for Beam C versus s/L

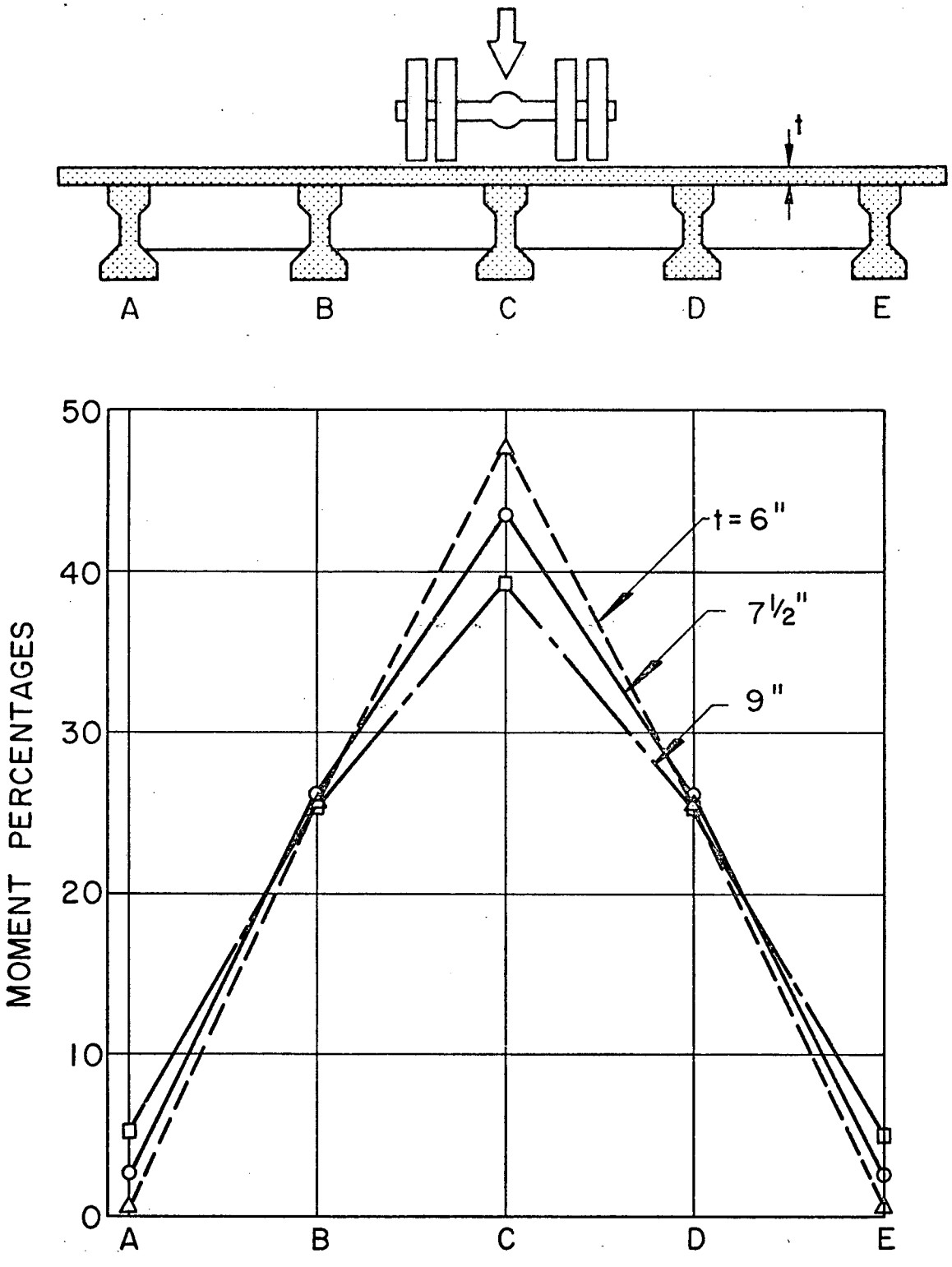

Fig. 33 Effect of Slab Thickness on Load Distribution

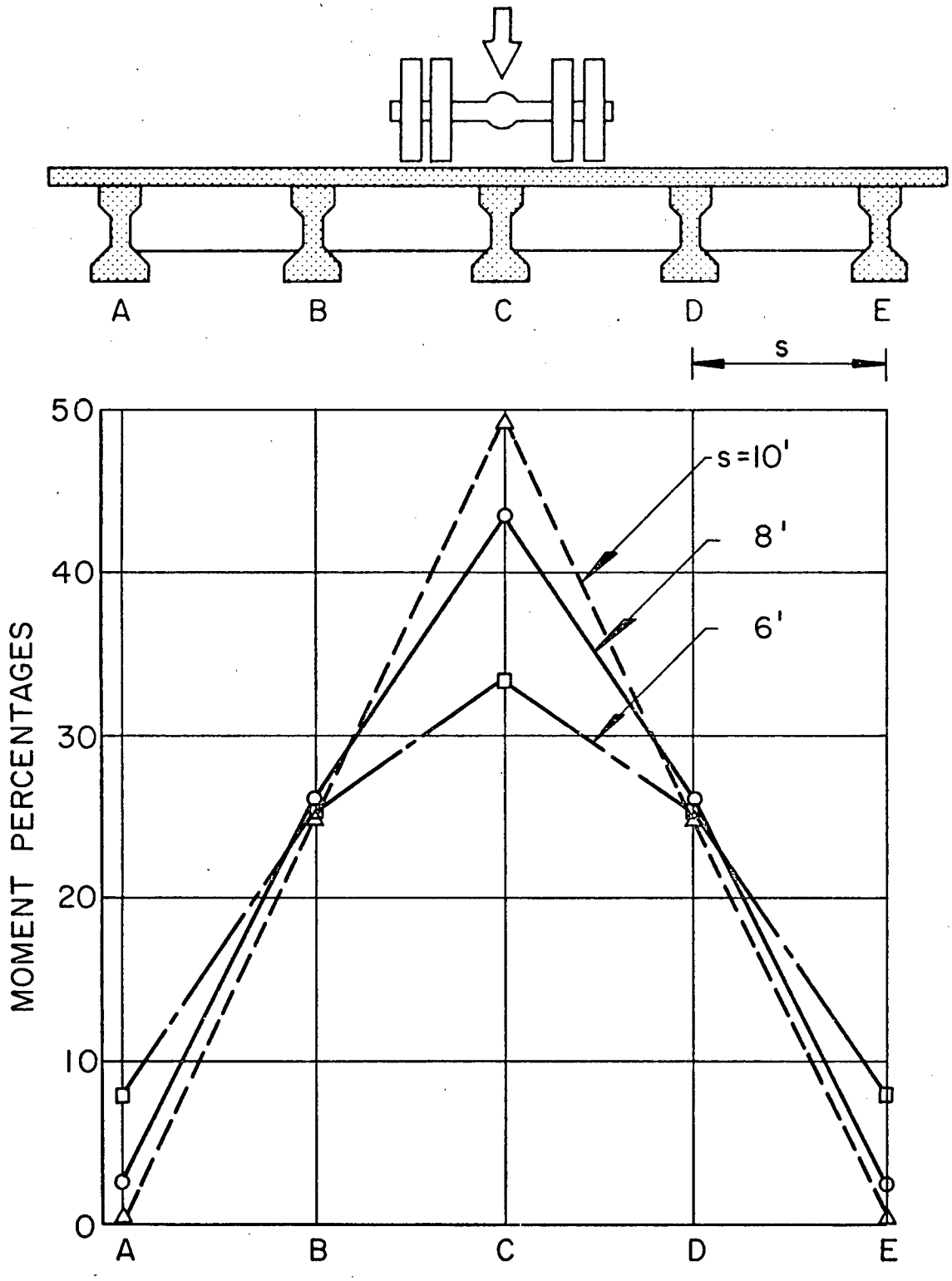

Fig. 34 Effect of Beam Spacing on Load Distribution

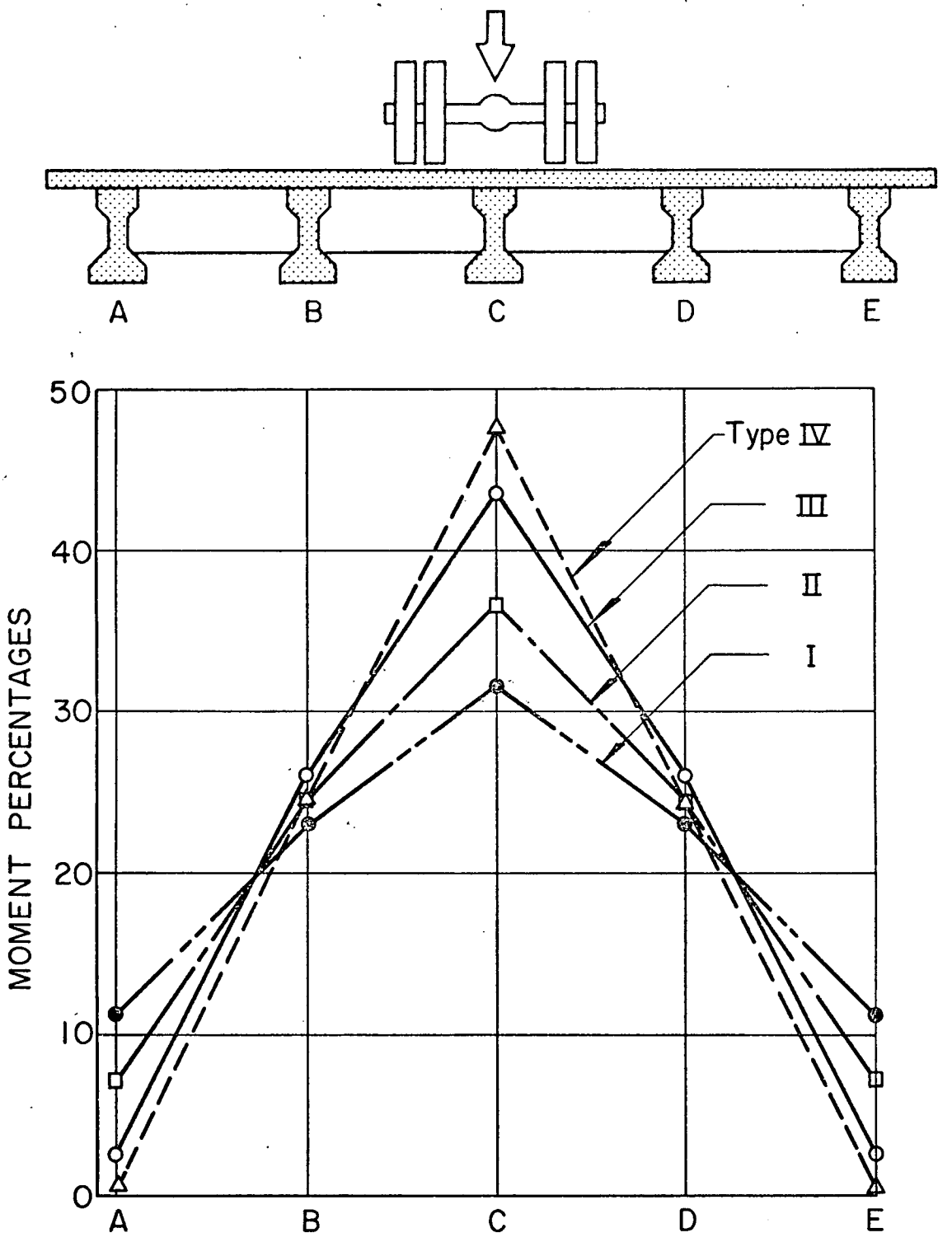

Fig. 35 Effect of Beam Size on Load Distribution

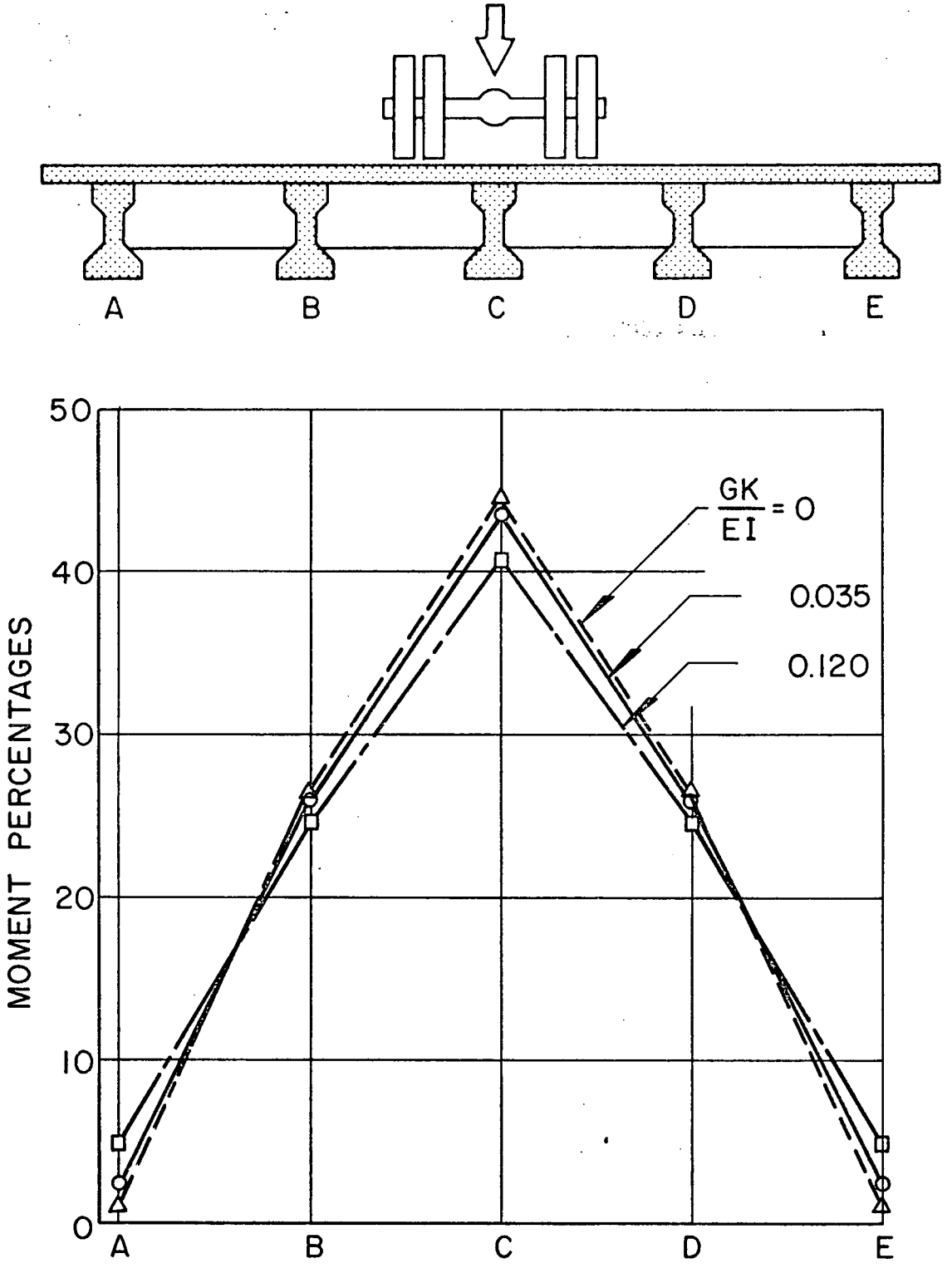

Fig. 36 Effect of Torsional Stiffness of Beams on Lateral Load Distribution

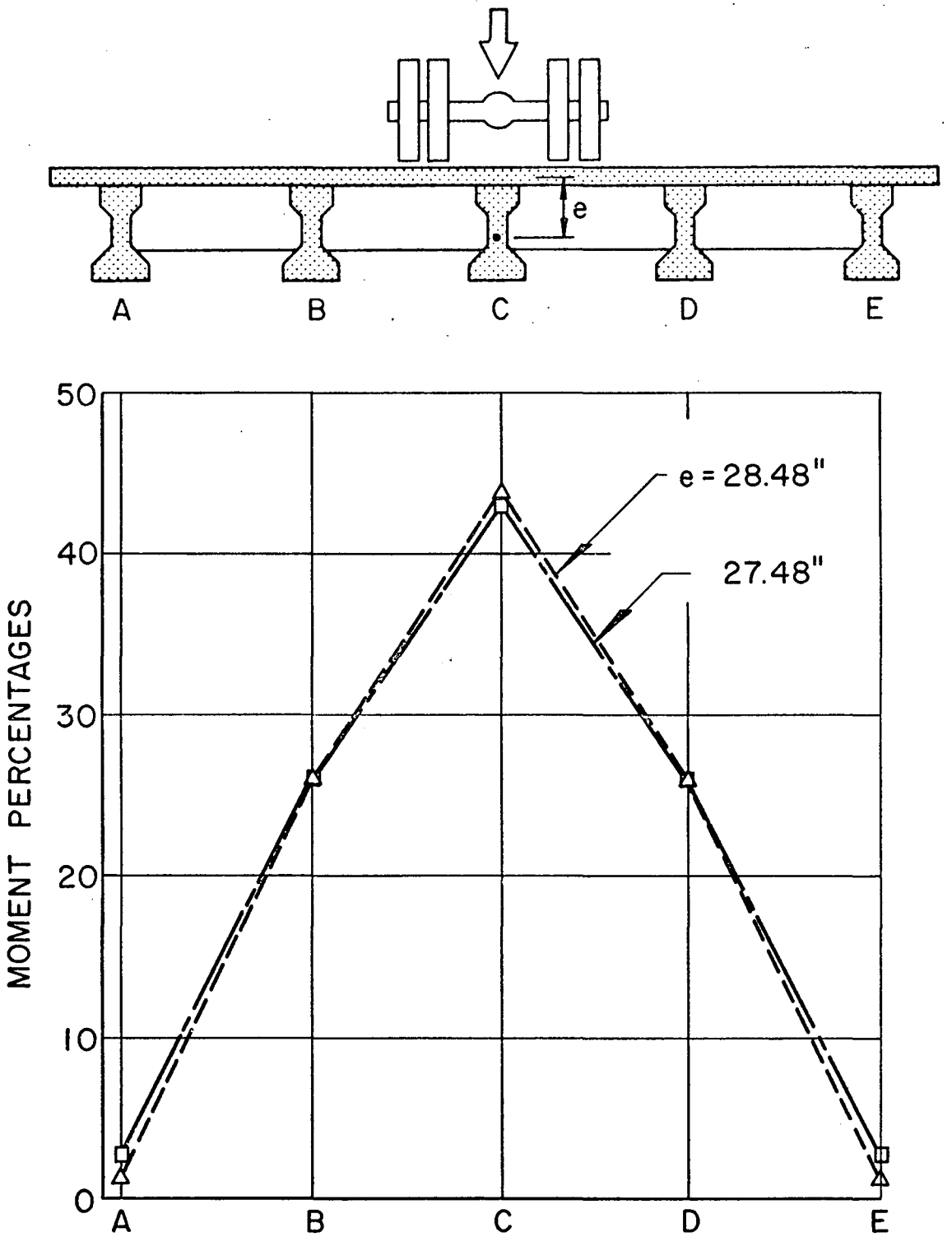

Fig. 37 Effect of Eccentricity of Beams on Lateral Load Distribution

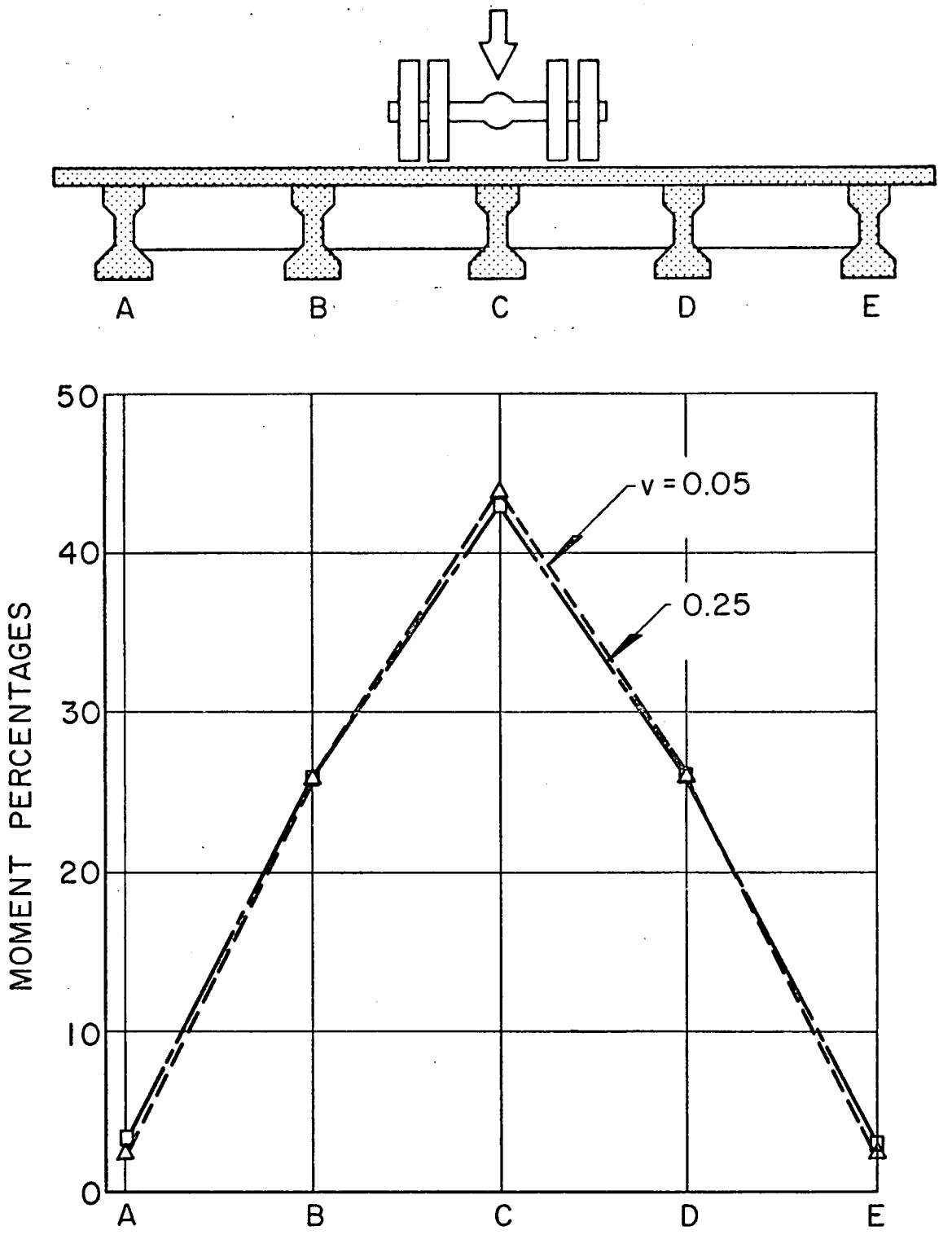

Fig. 38 Effect of Poisson's Ratio on Lateral Load Distribution

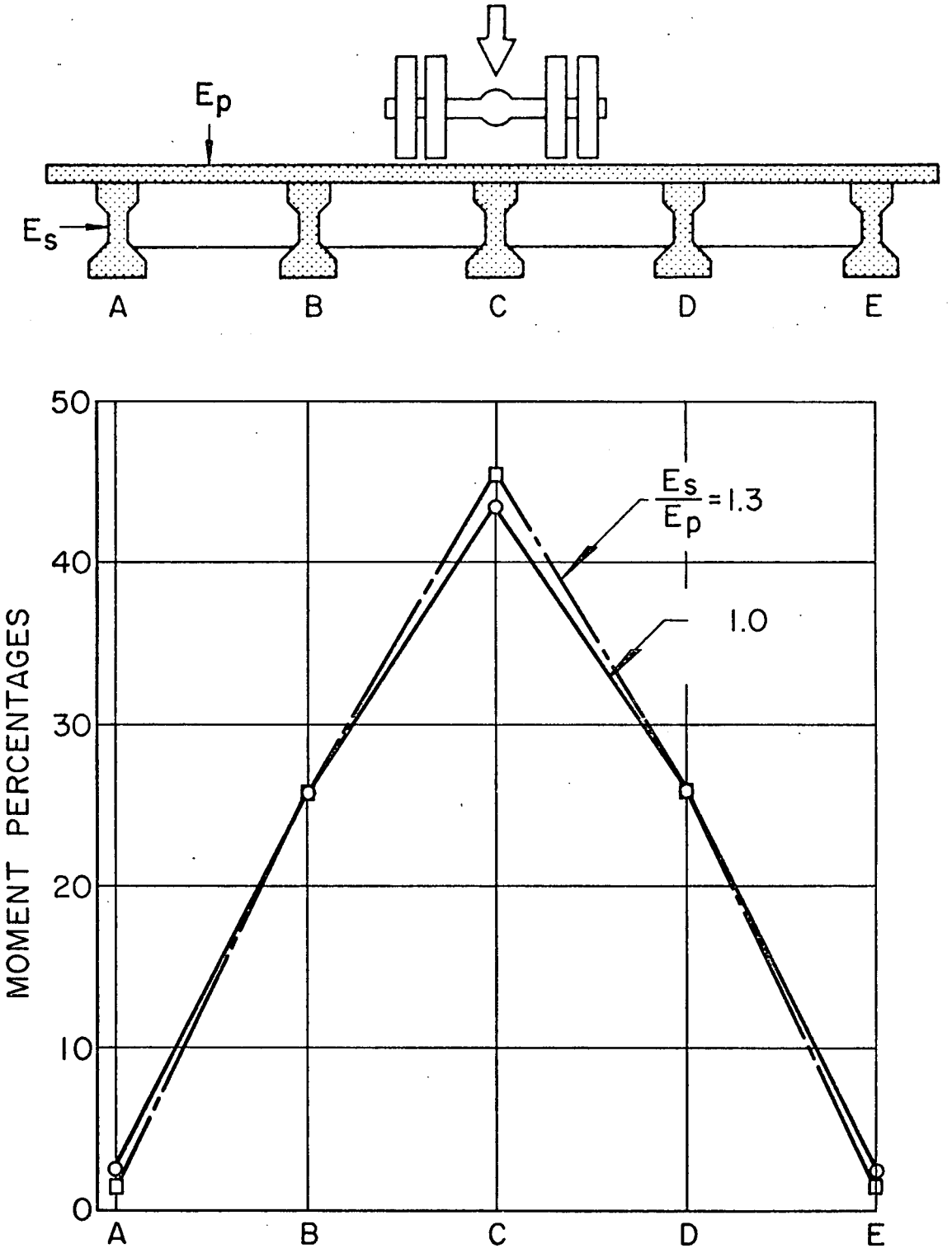

Fig. 39 Effect of Ratio of Moduli of Elasticity on Lateral Load Distribution

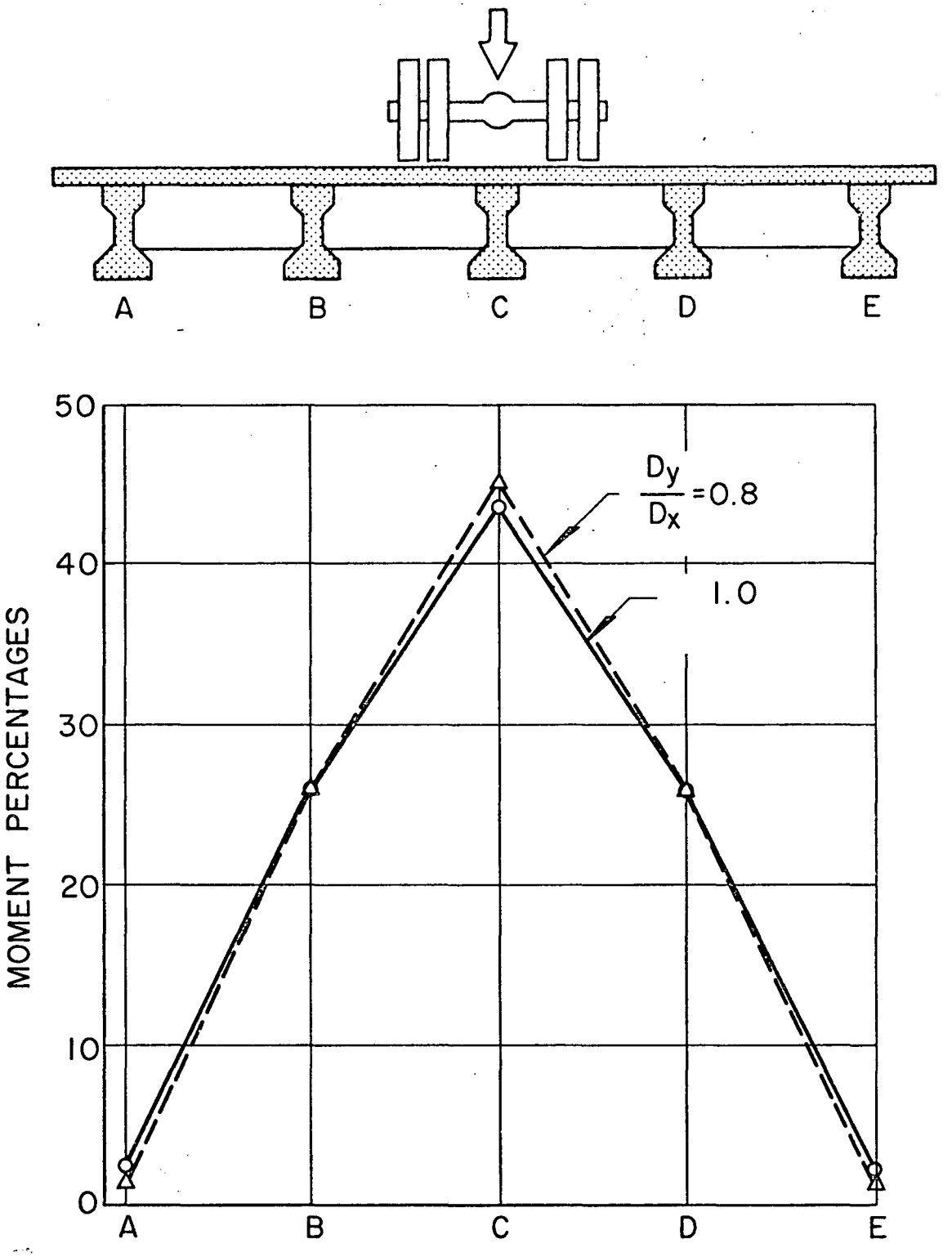

Fig. 40 Effect of Orthotropy of Deck on Lateral Load Distribution

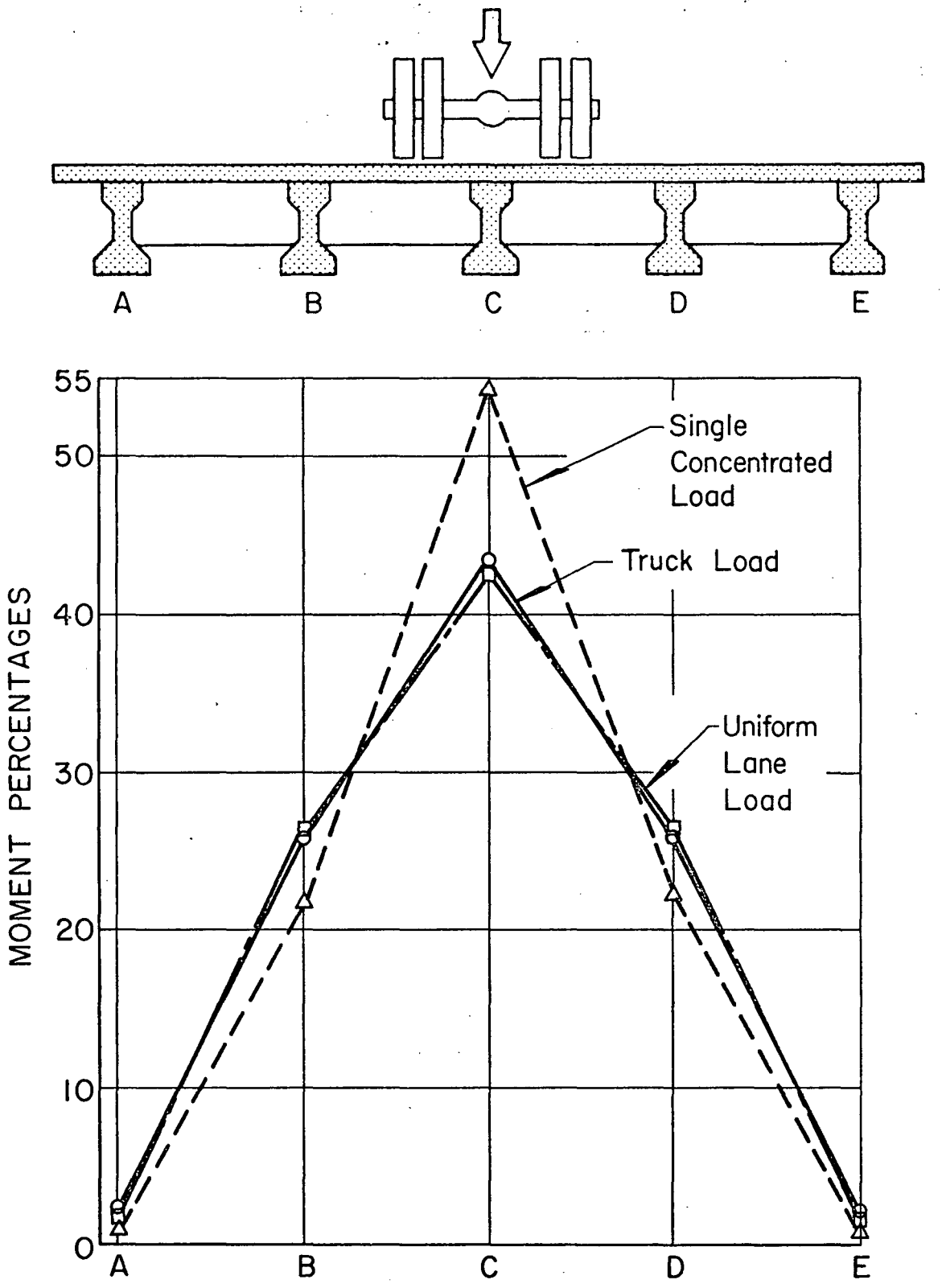

Fig. 41 Effect of Type of Load on Lateral Load Distribution

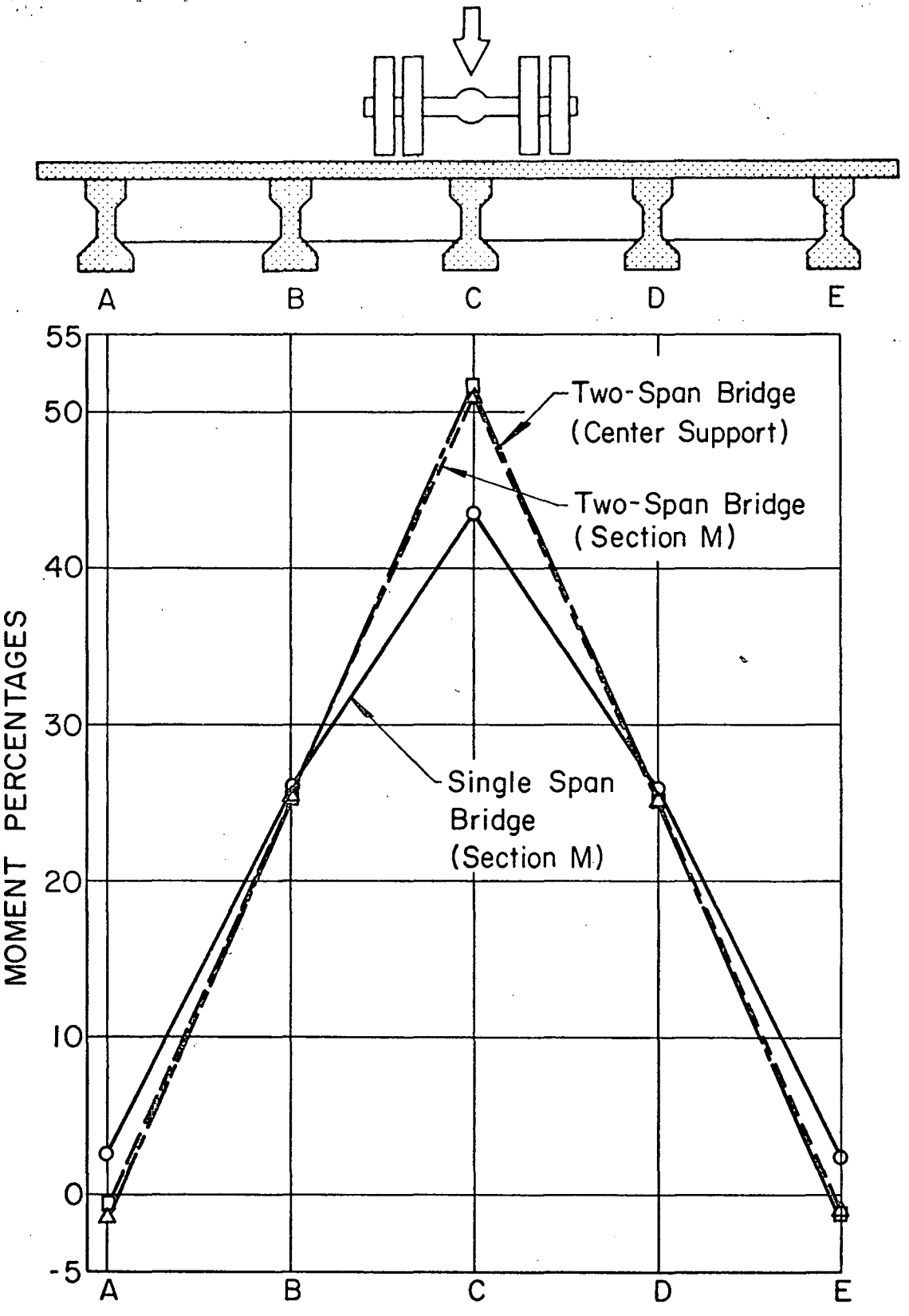

Fig. 42 Effect of Boundary Conditions on Lateral Load Distribution

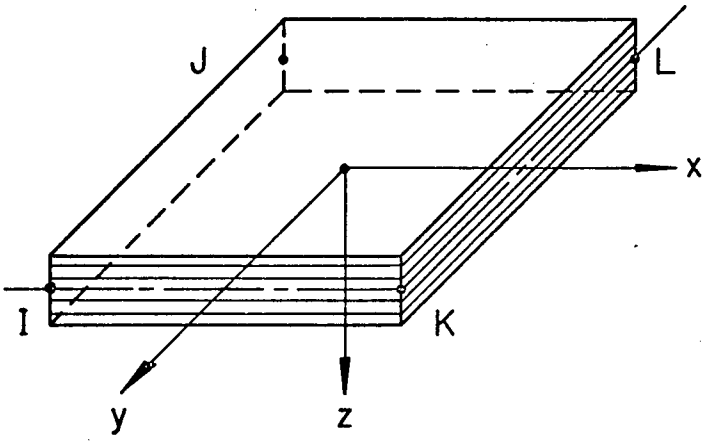

(a.) Layered Finite Plate Element

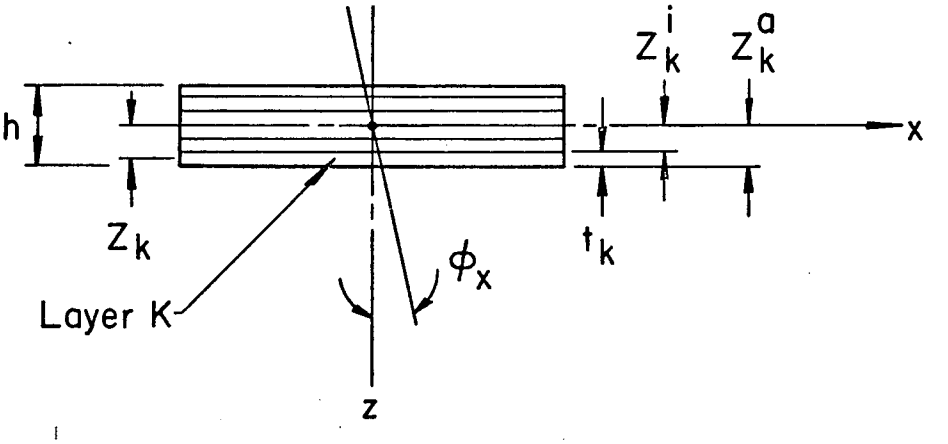

(b.) Cross Section of Layered Model

Fig. 43 Layered Plate Finite Element for Elastic-Plastic Analysis of Plates

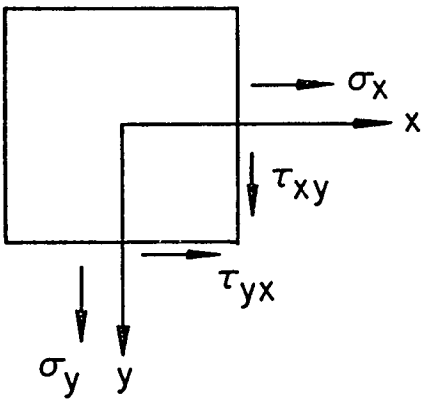

(a.) State of Stress in a Layer

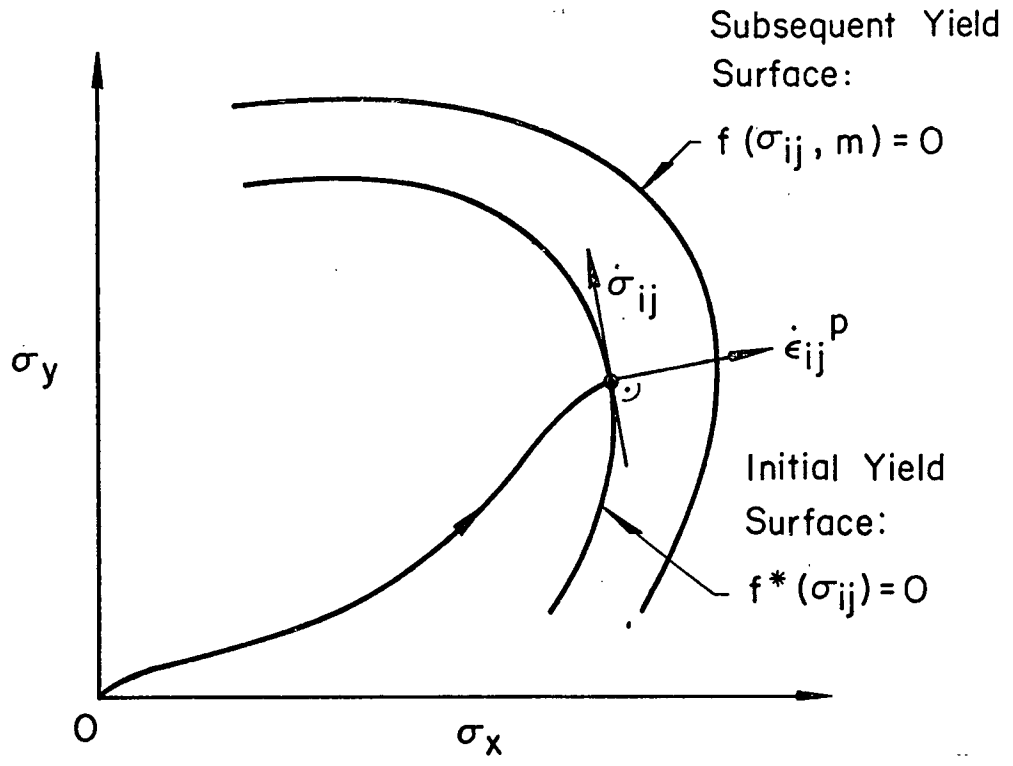

(b) Loading Path and Yield Surfaces

Fig. 44 Loading Path and Yield Surfaces for a Layer of the Finite Plate Element

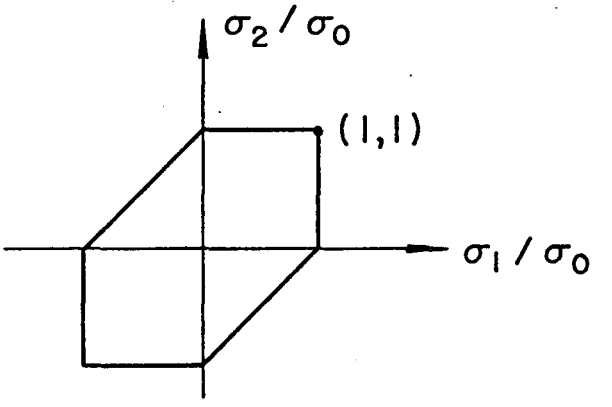

(a.) Tresca's Yield Condition

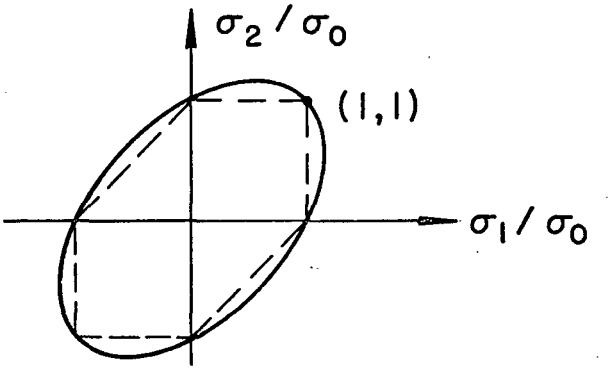

(b.) Von Mises' Yield Condition

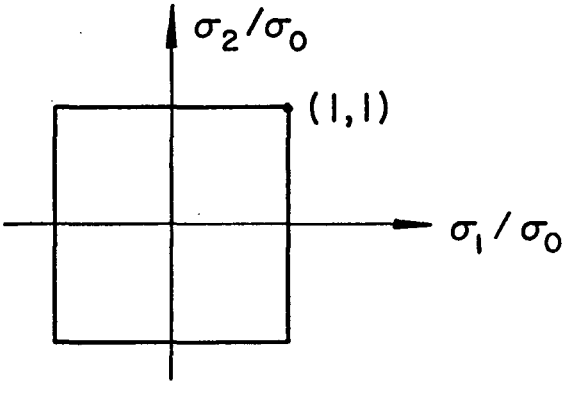

(c.) Johansen's Yield Condition

Fig. 45 Most Commonly Used Yield Criteria

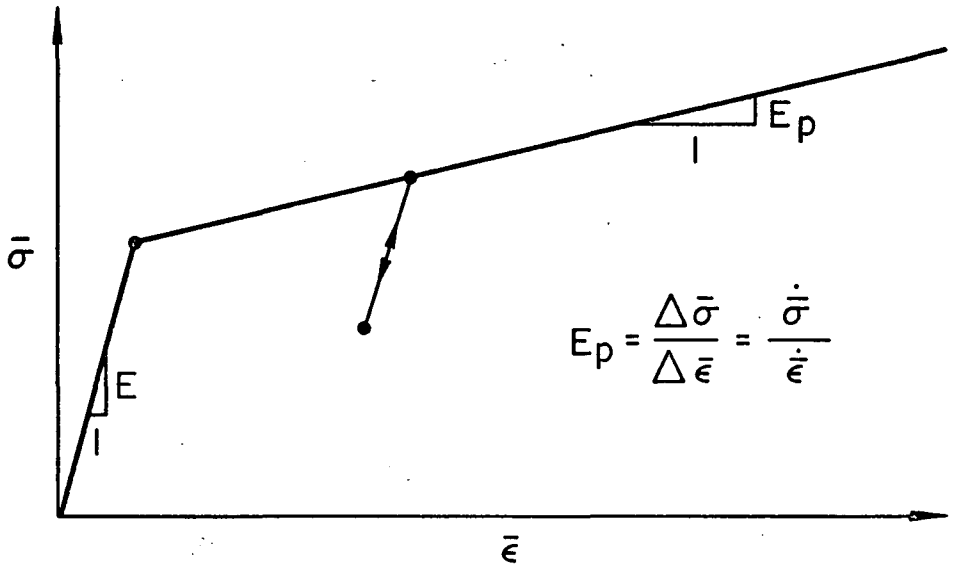

(a.) Effective Stress versus Effective Total Strain Curve

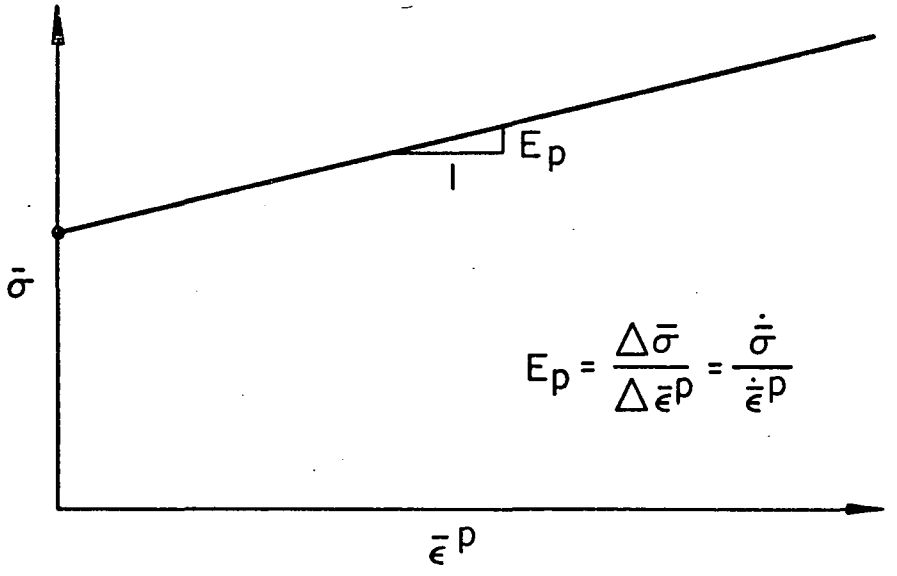

(b.) Effective Stress versus Effective Plastic Strain Curve

Fig. 46 Effective Stress versus Effective Strain Curves

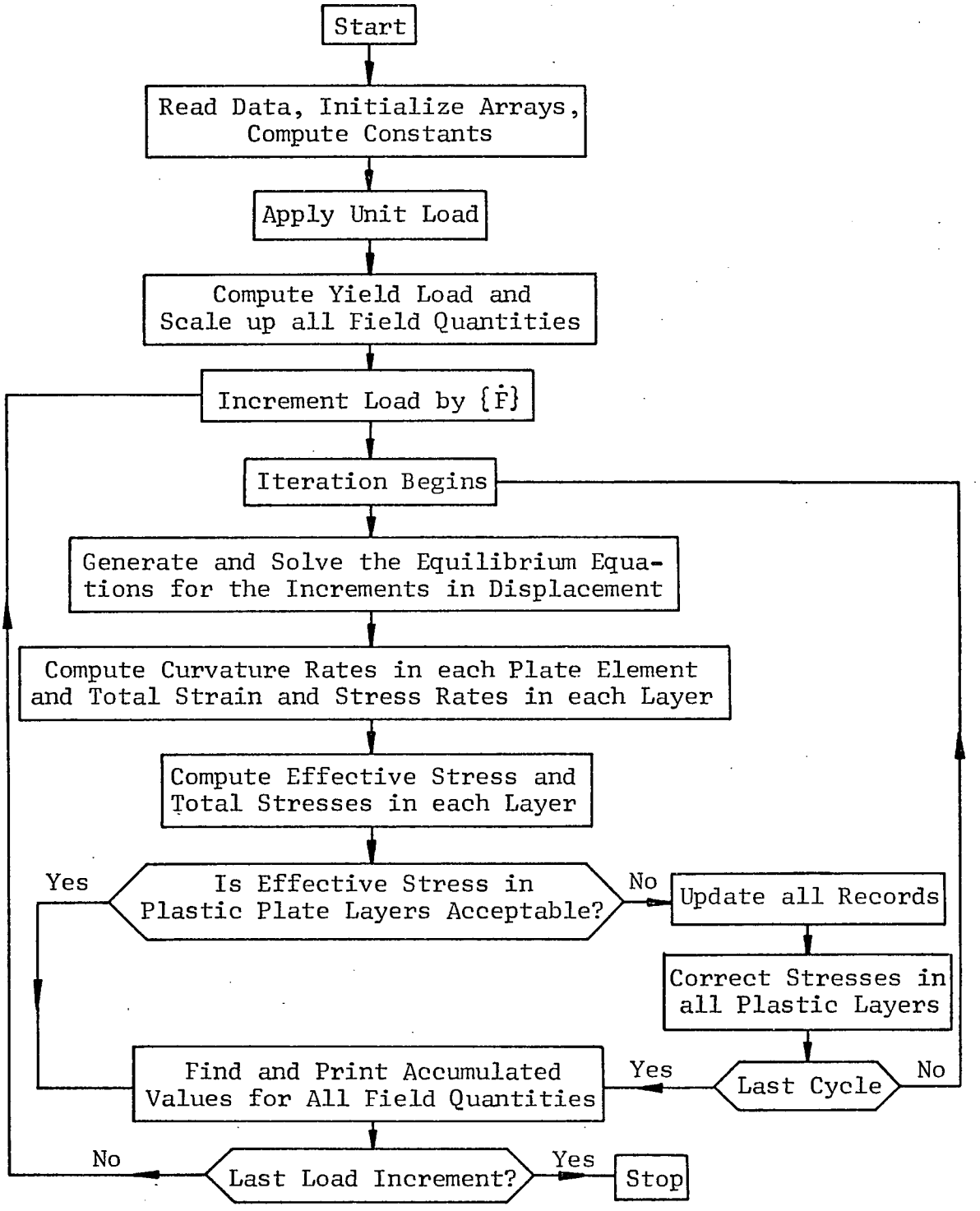

Fig. 47 Flow Diagram for Elastic-Plastic Plate Analysis

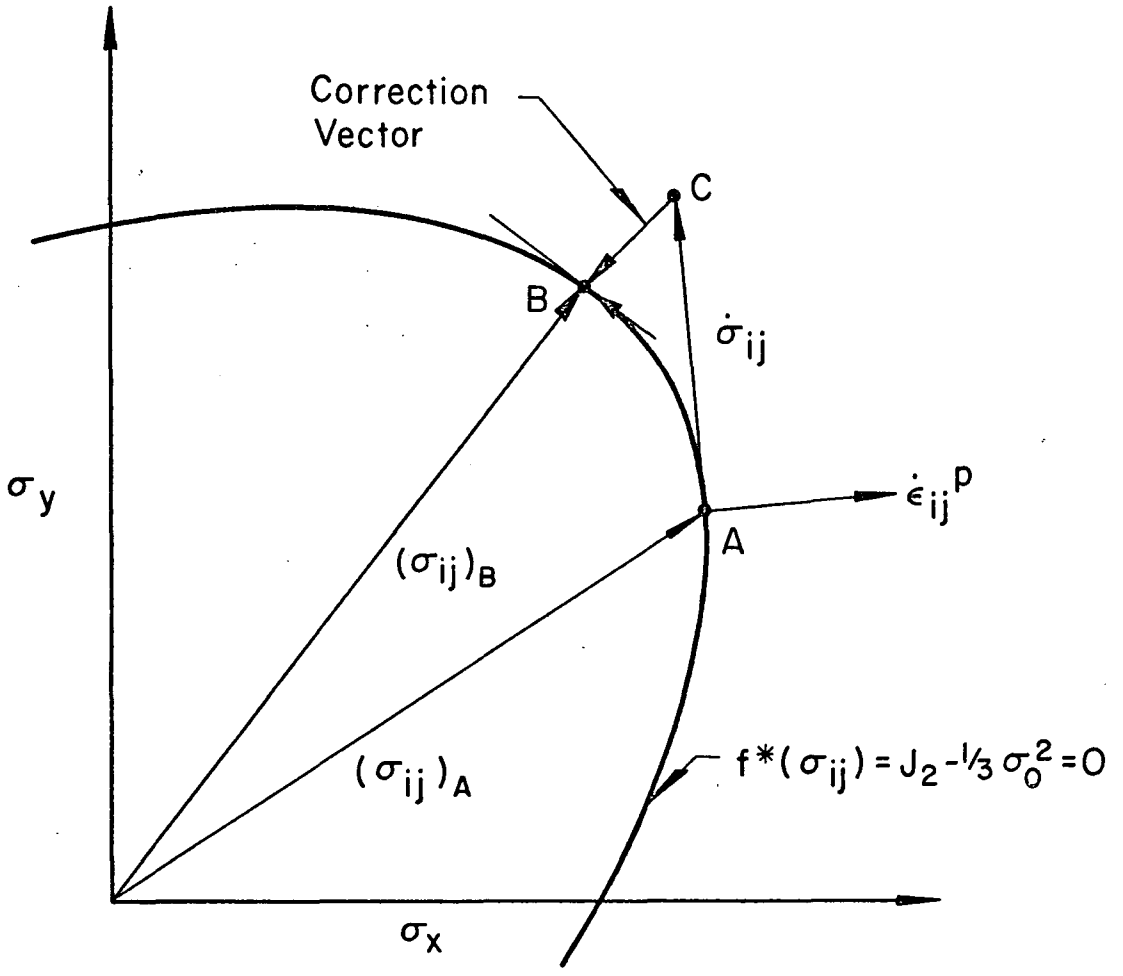

Fig. 48 Yield Surface Correction for Elastic Perfectly-Plastic Material

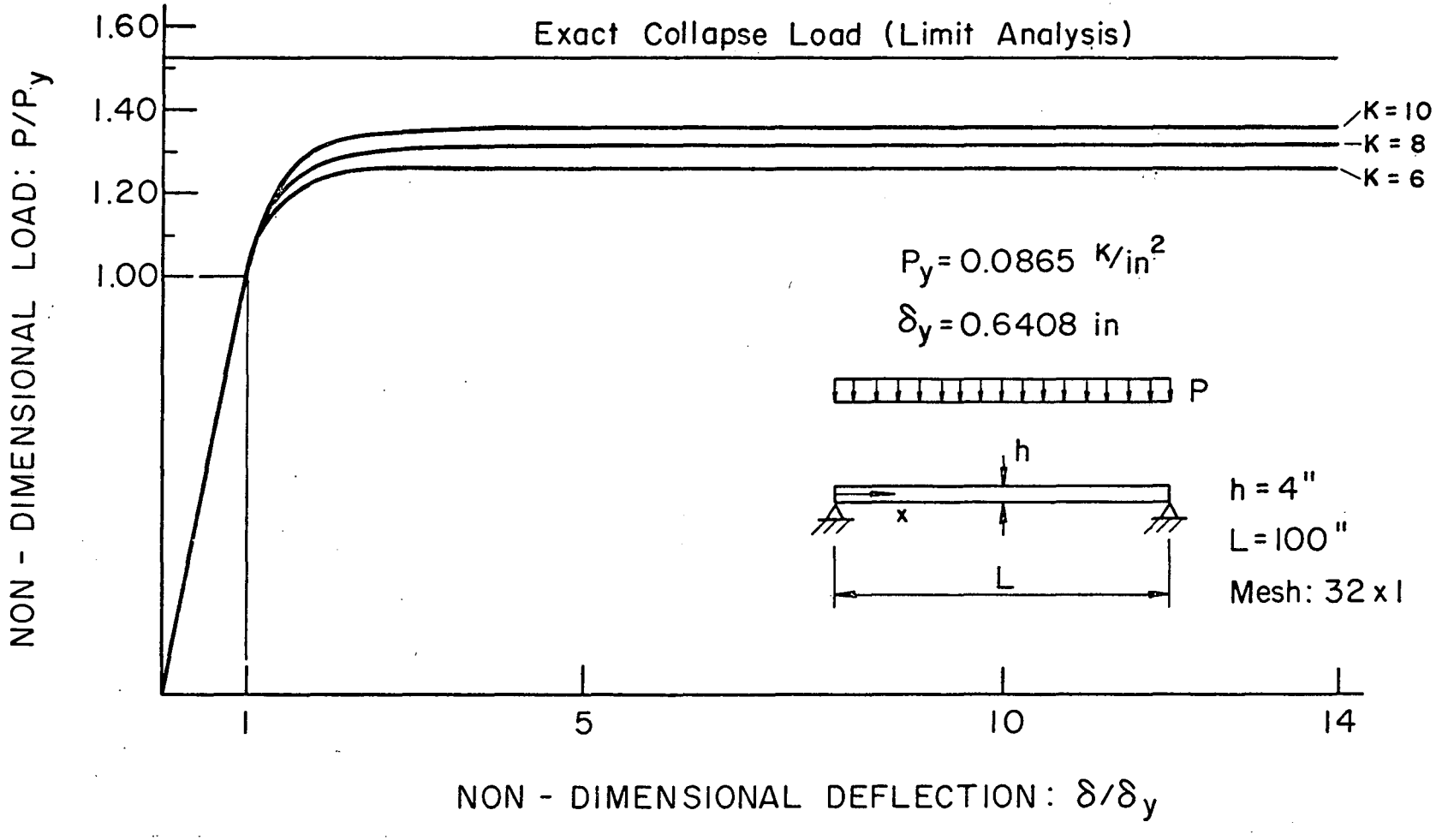

Fig. 49 Load-Deflection Curve at Center of Simply Supported Plate Strip

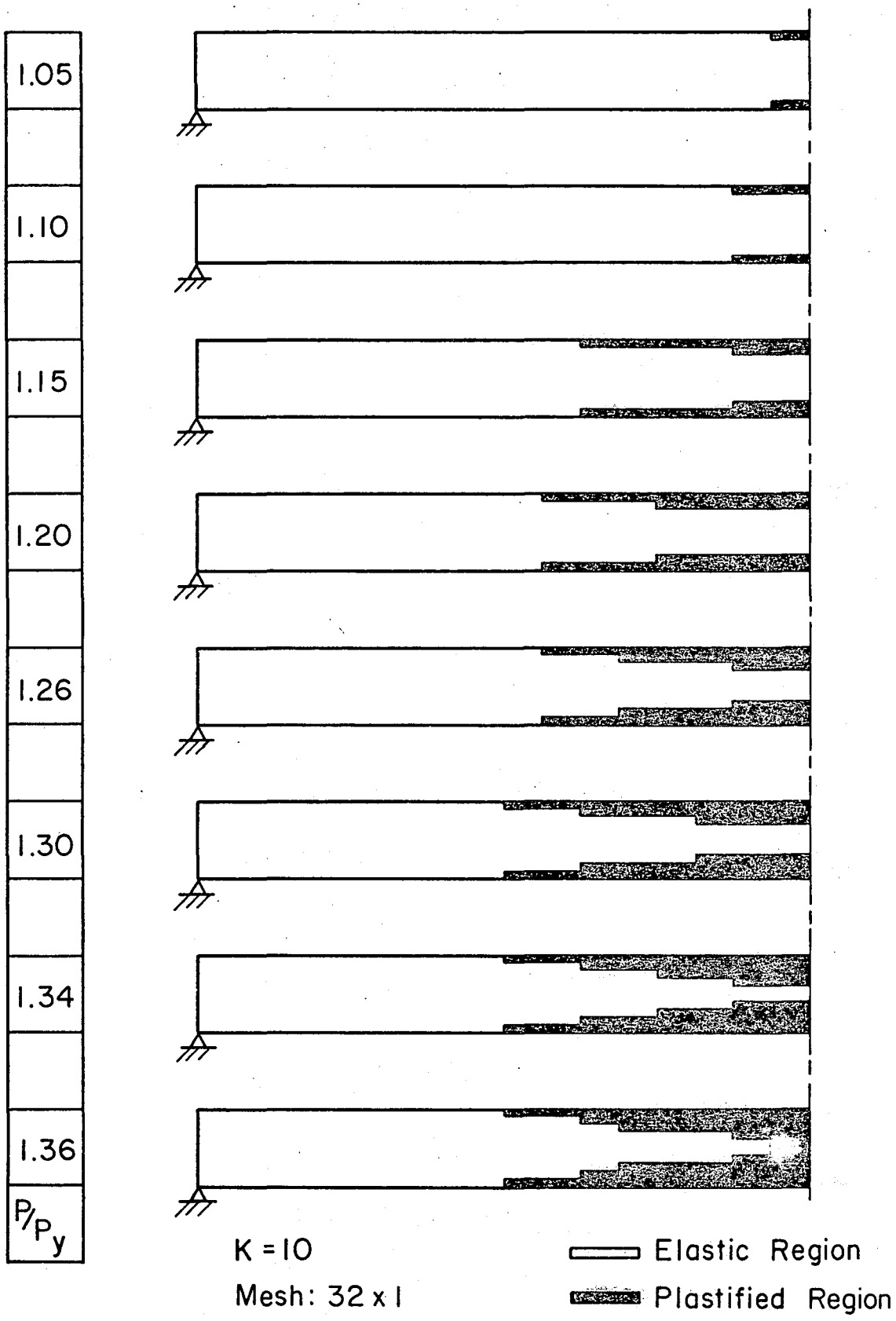

Fig. 50 Progression of Elastic-Plastic Boundary for Simply Supported Plate Strip

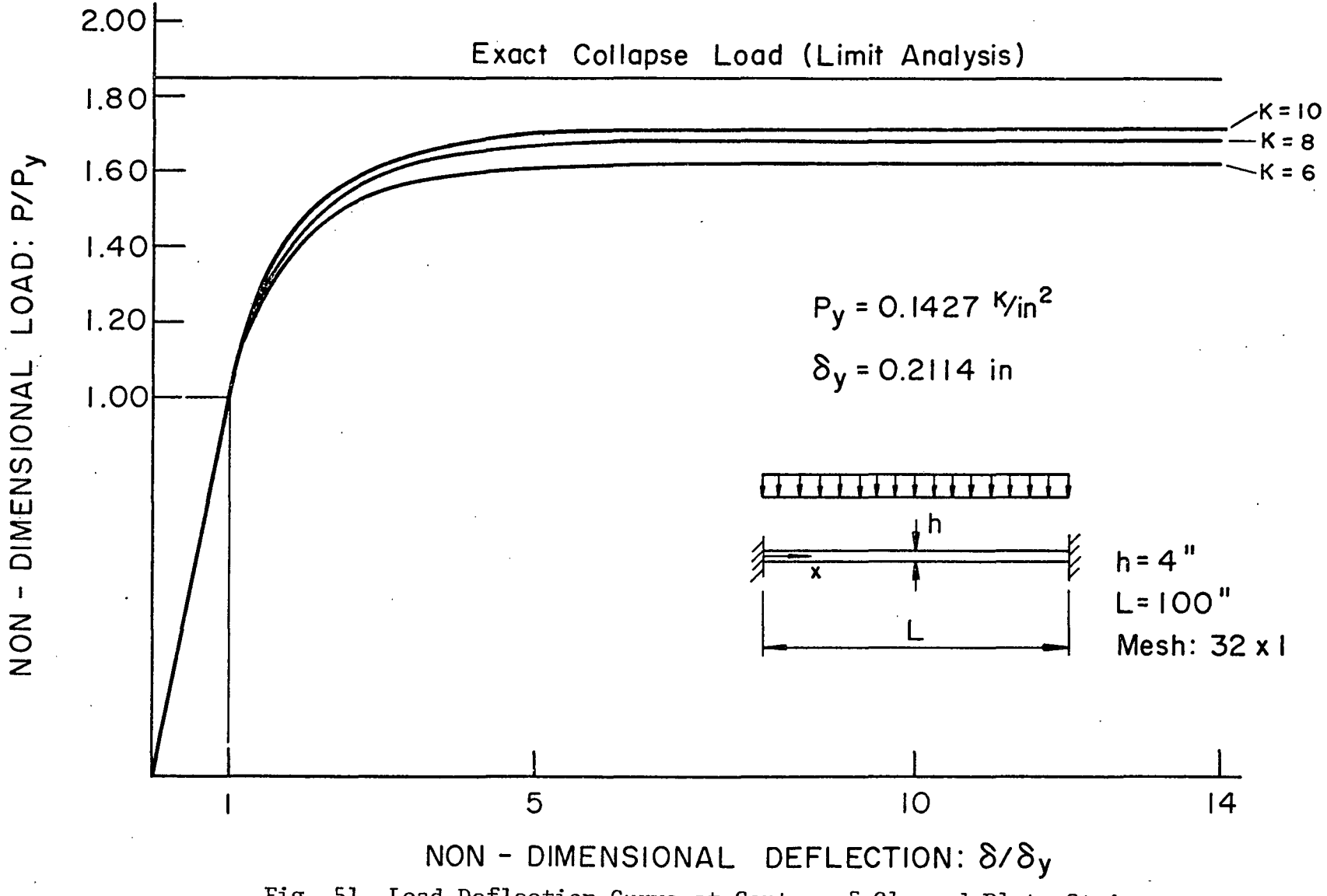

Fig. 51 Load-Deflection Curve at Center of Clamped Plate Strip

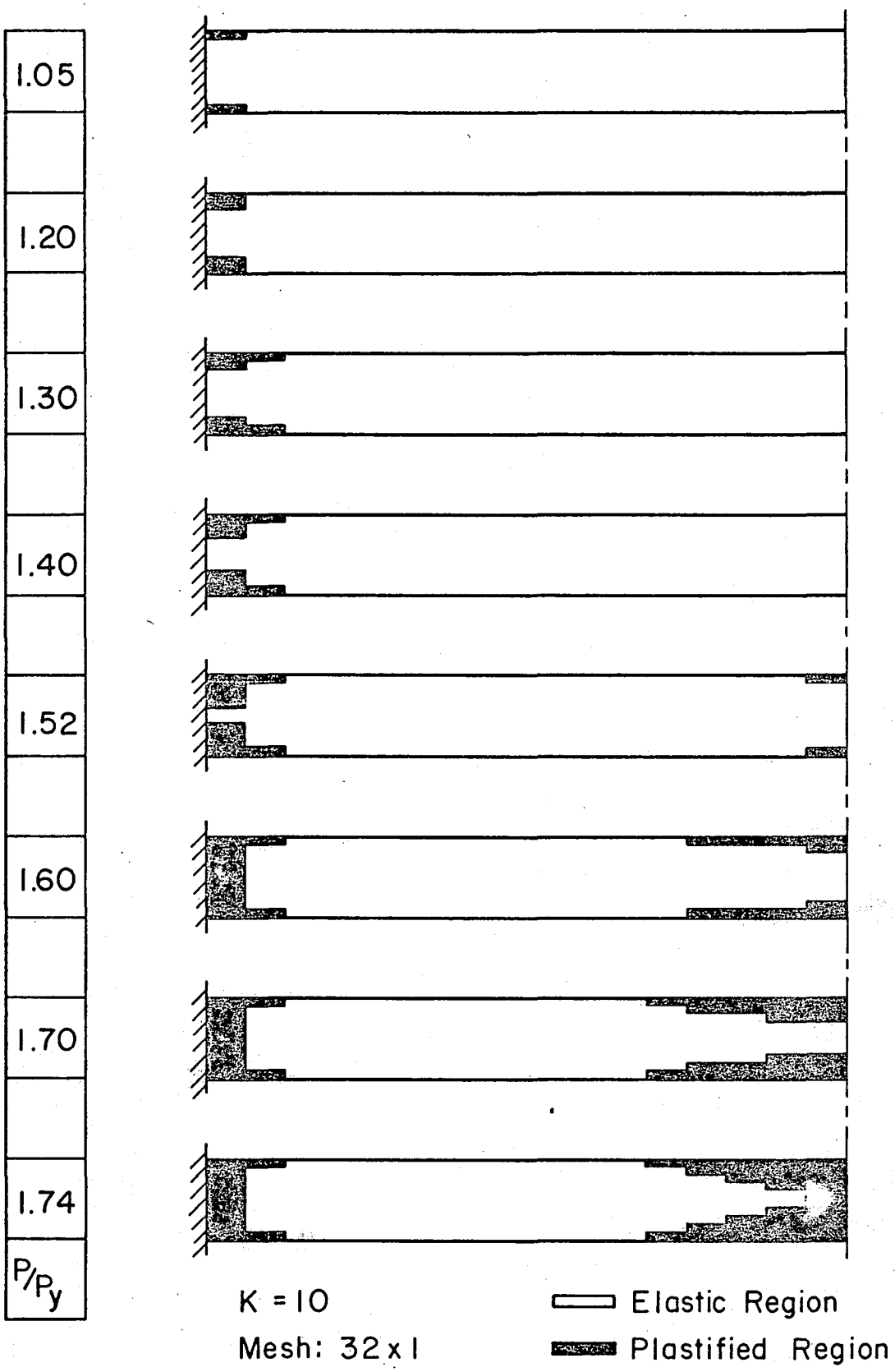

Fig. 52 Progression of Elastic-Plastic Boundary for Clamped Plate Strip

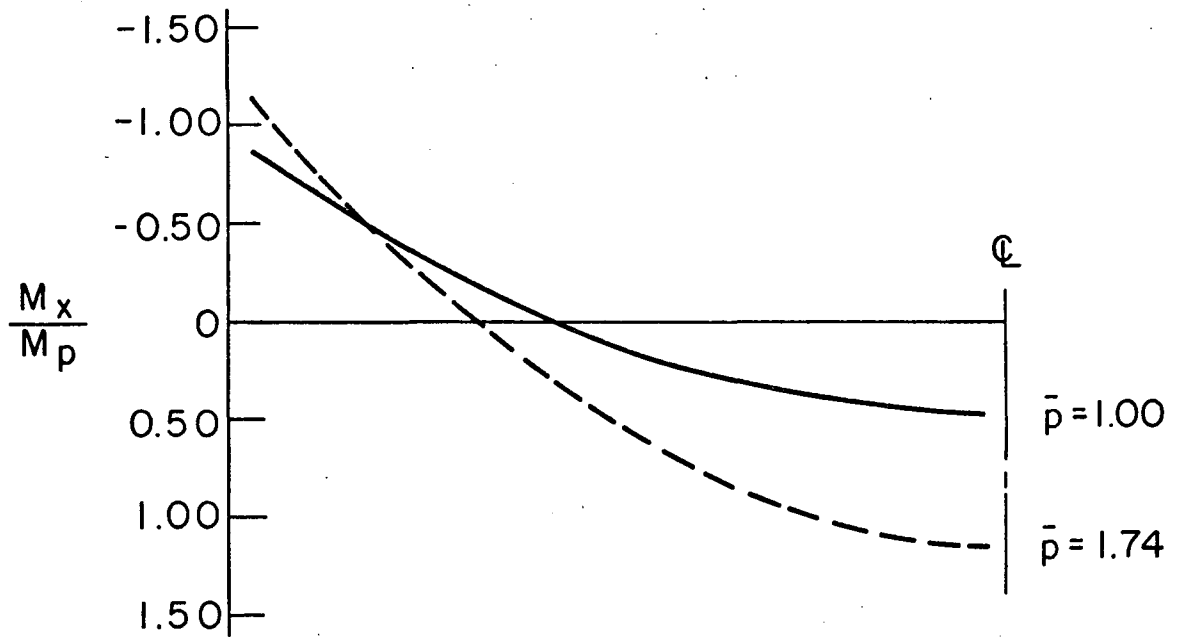

BENDING MOMENT M_x ALONG x-AXIS

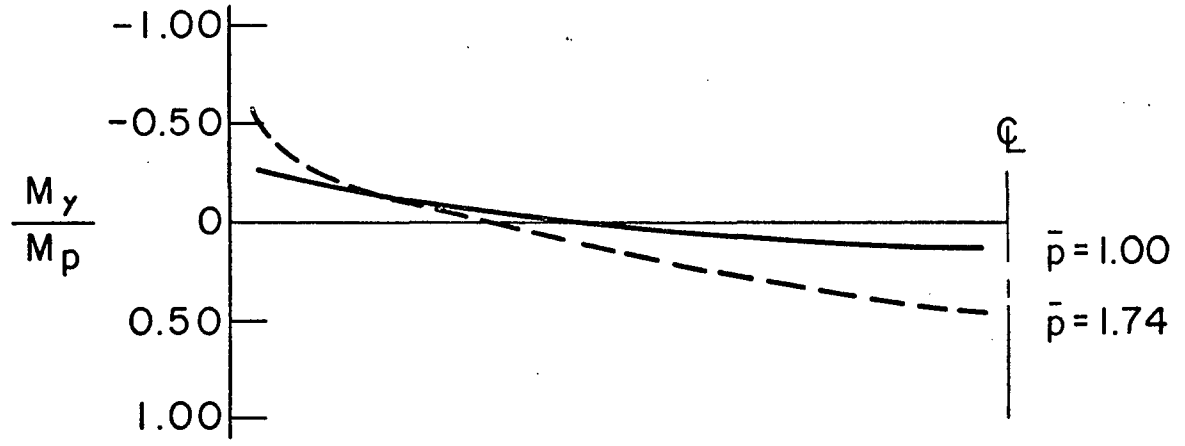

BENDING MOMENT M_y ALONG x-AXIS

Fig. 53 Redistribution of Moments in Clamped Plate Strip

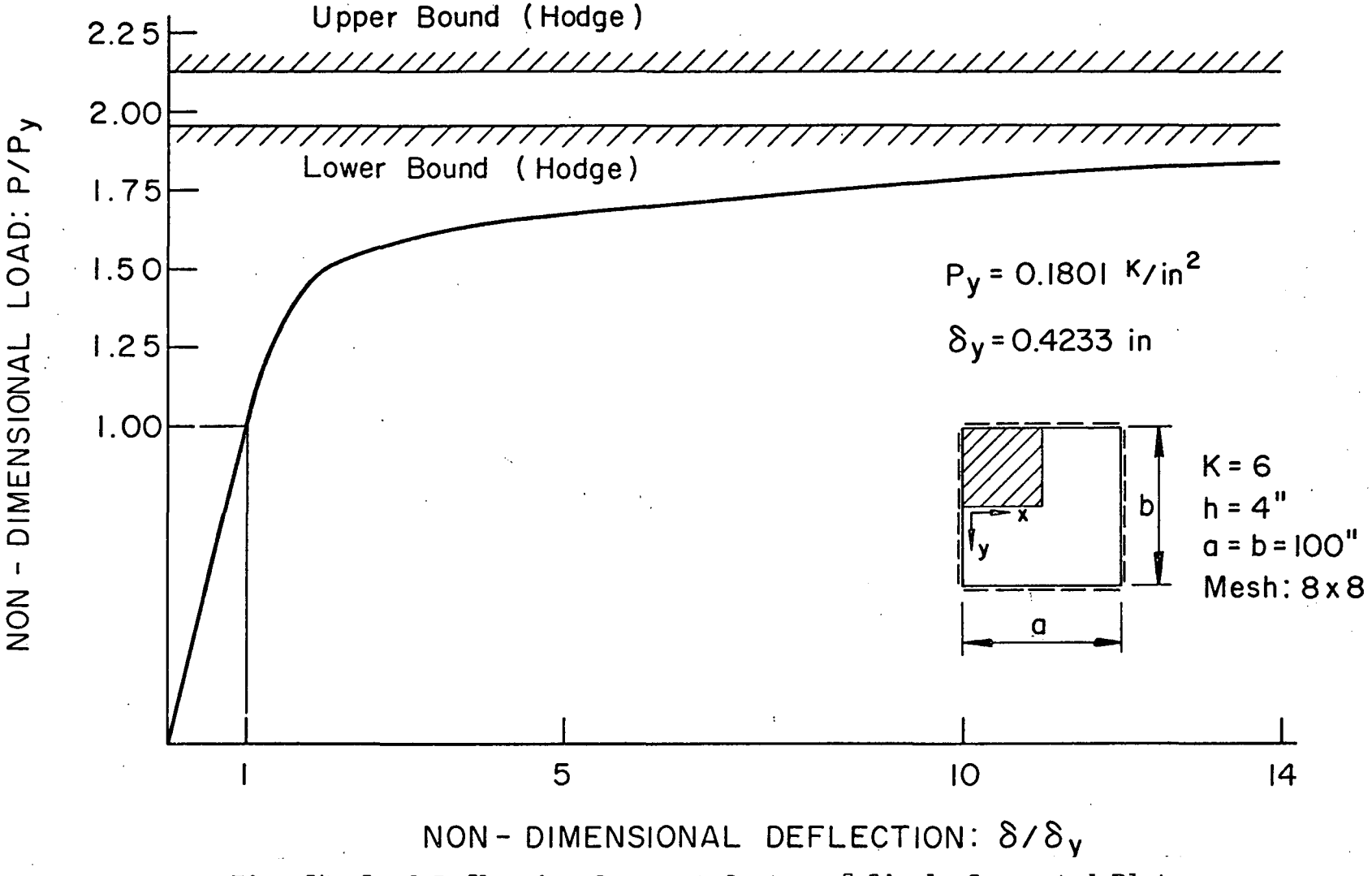

Fig. 54 Load-Deflection Curve at Center of Simply Supported Plate

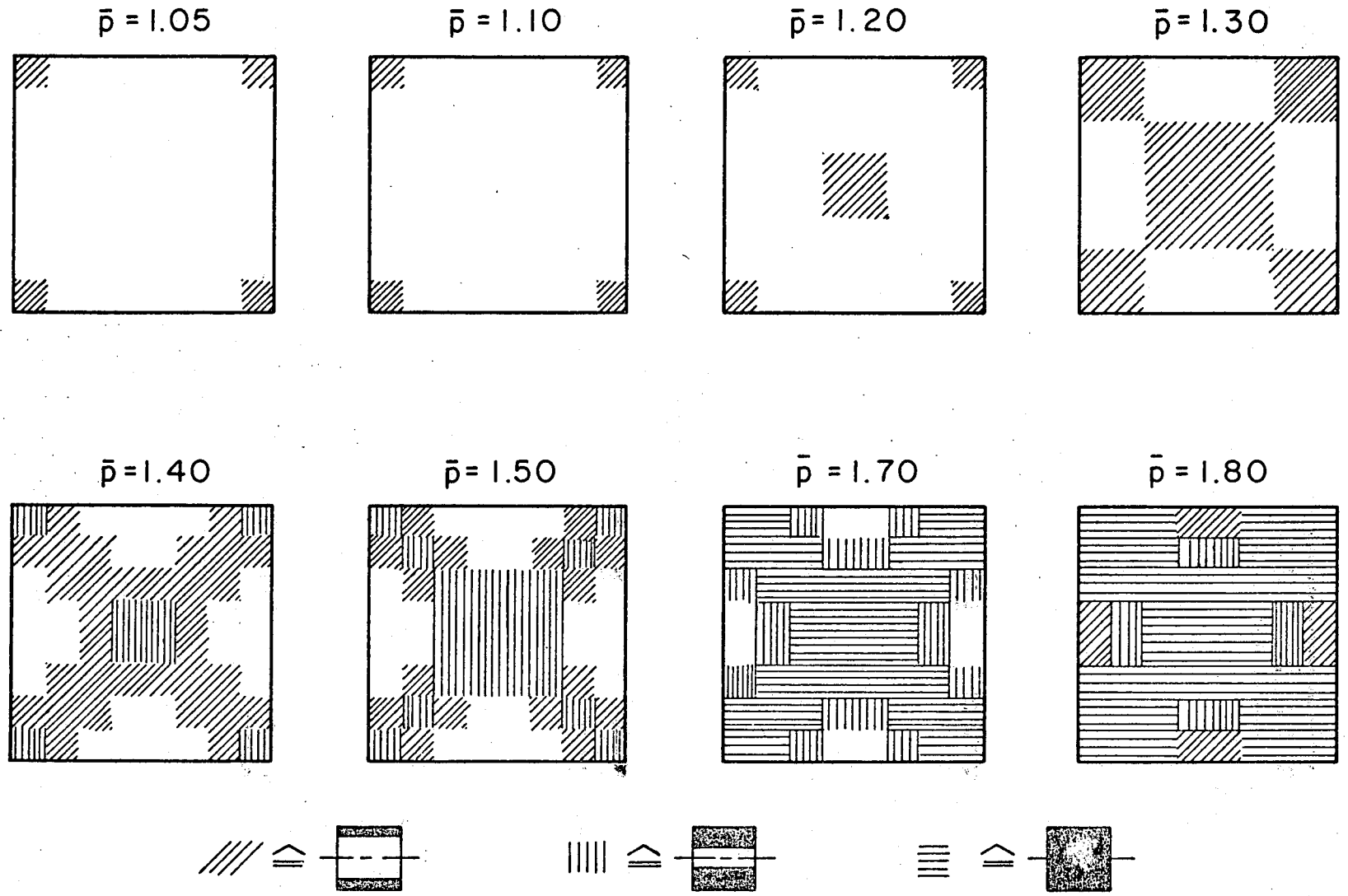

Fig. 55 Progression of Yielded Regions - Simply Supported Square Plate

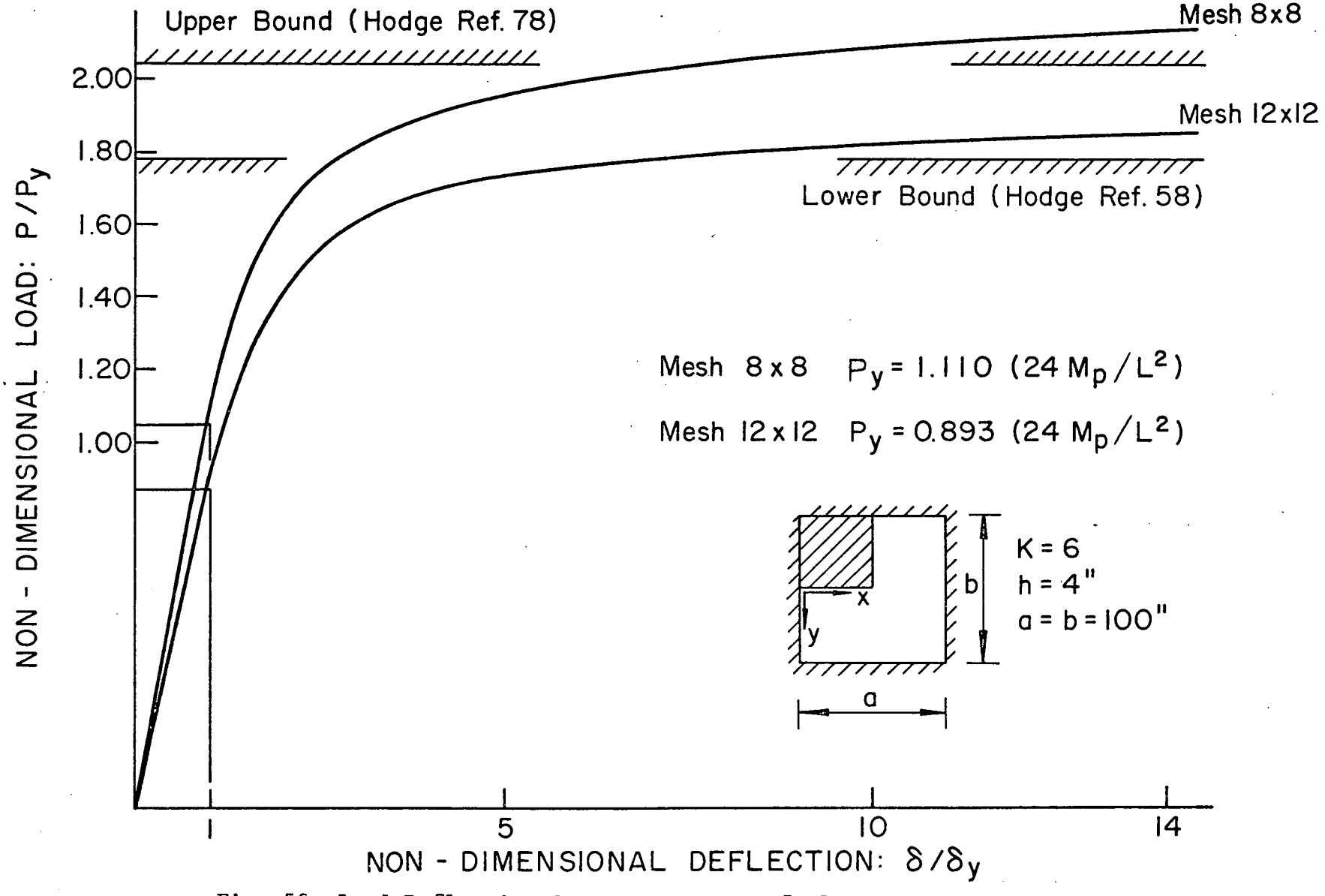

Fig. 56 Load-Deflection Curve at Center of Clamped Square Plate

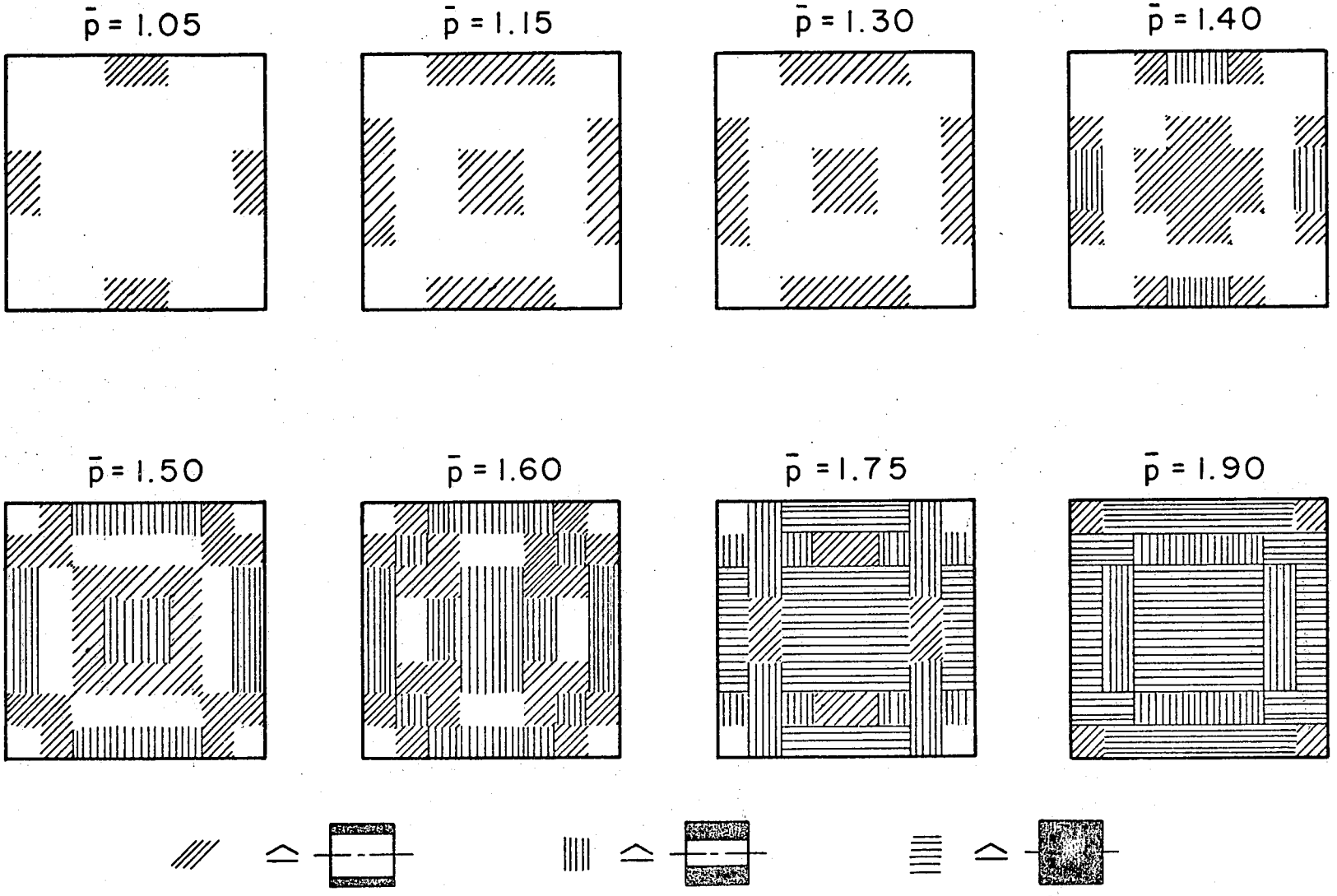

Fig. 57 Progression of Yielded Regions - Clamped Square Plate

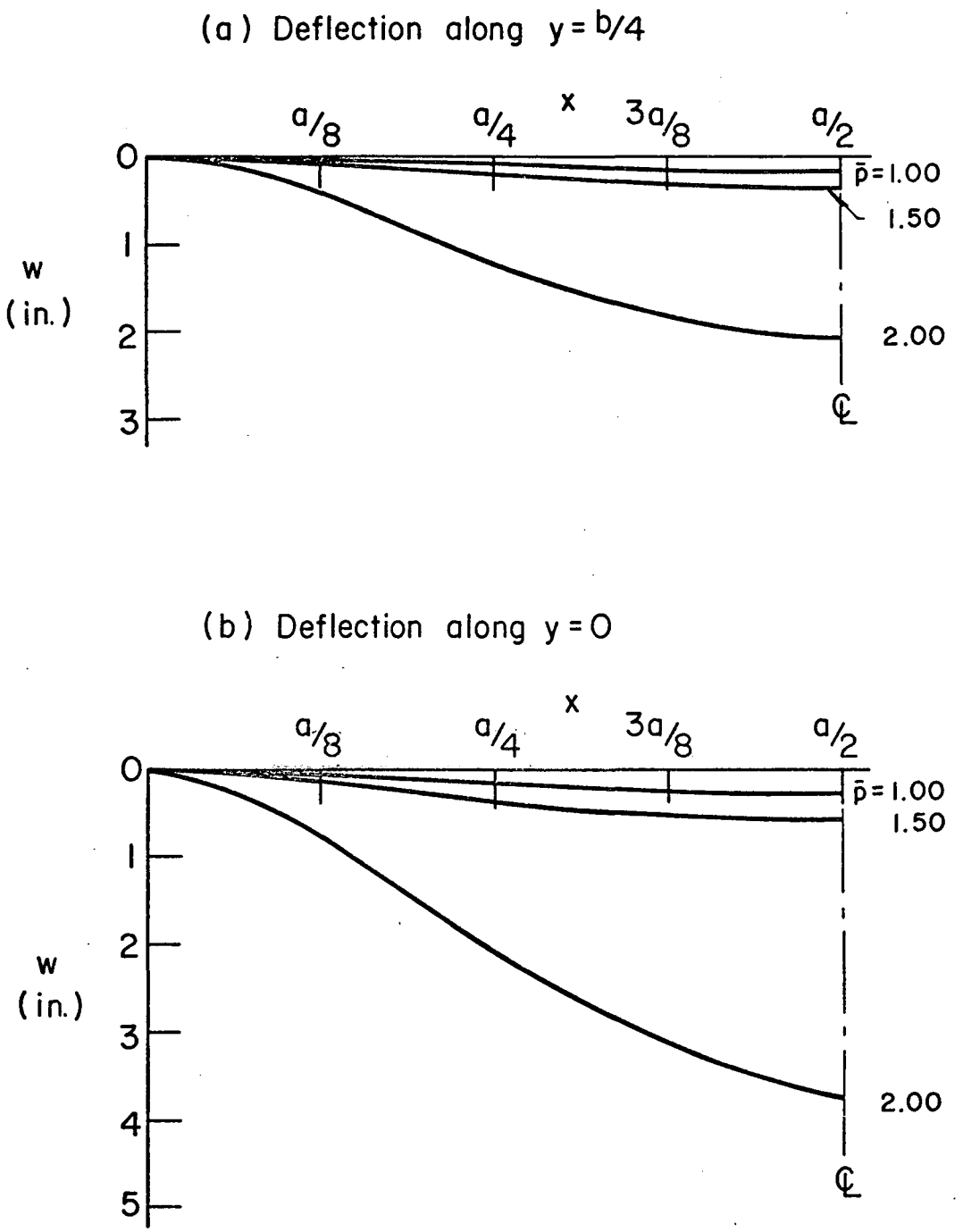

Fig. 58 Typical Displacement Contours - Clamped Plate

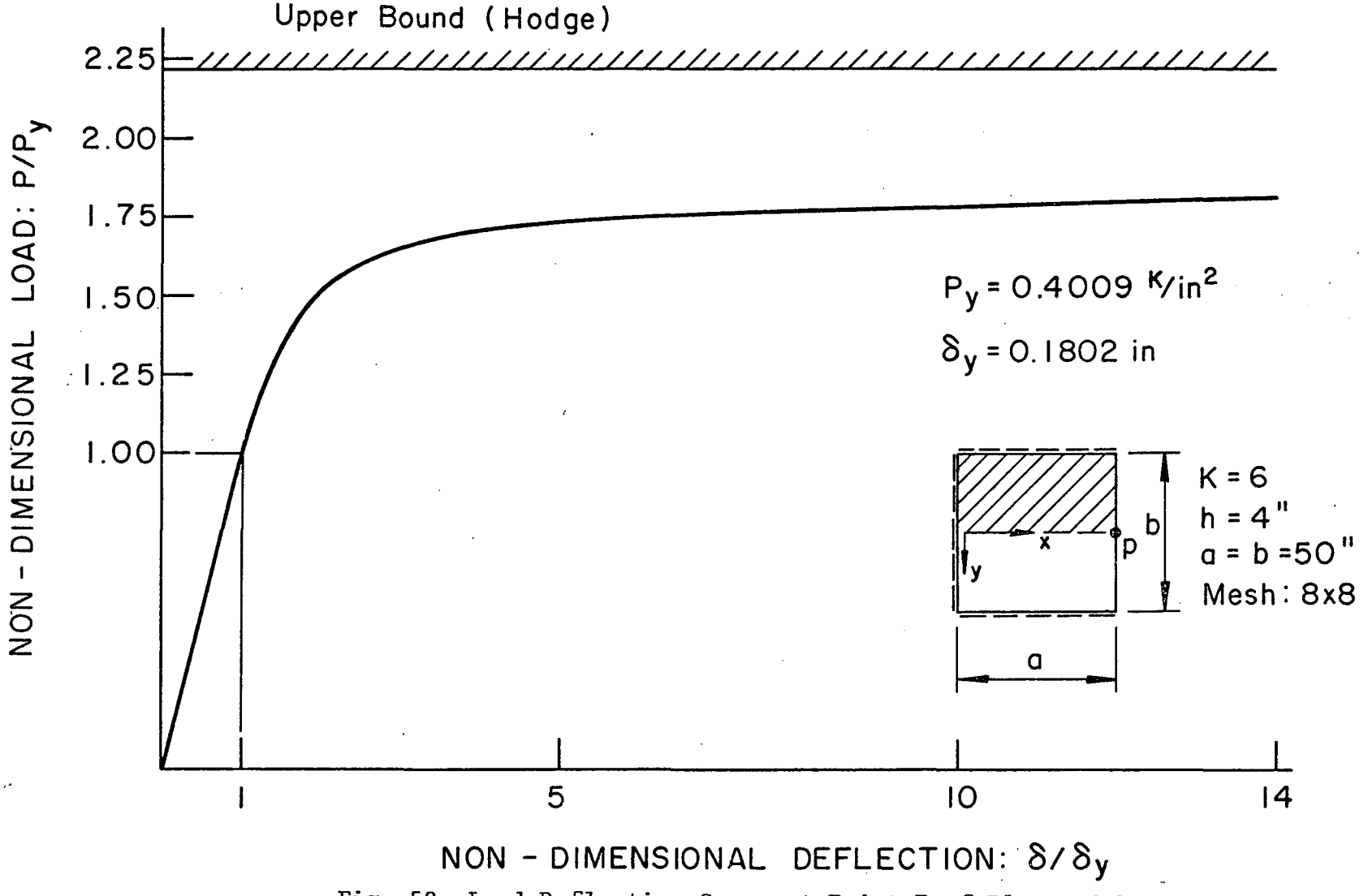

Fig. 59 Load-Deflection Curve at Point P of Plate with Three Simple Supports and One Free Edge

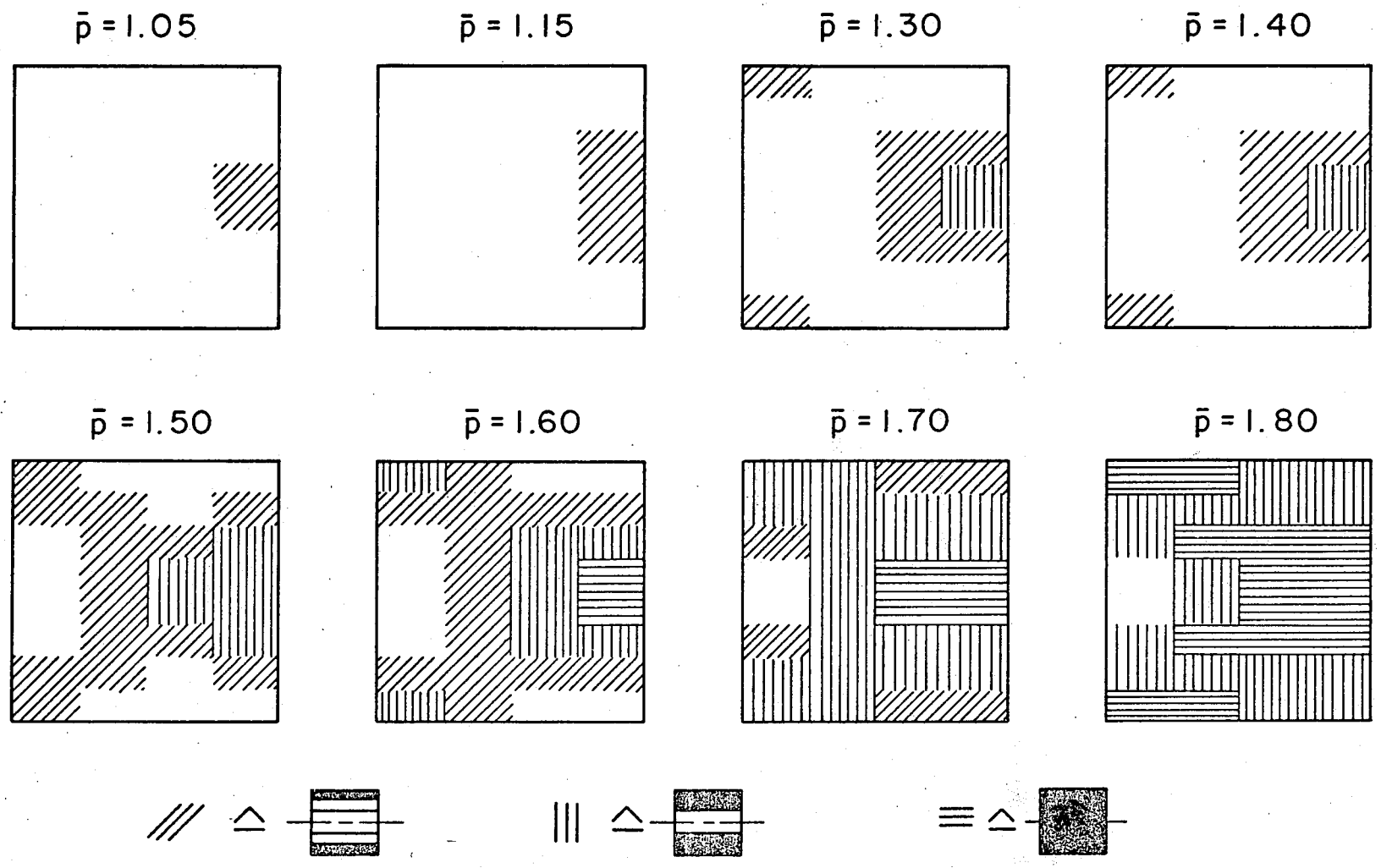

Fig. 60 Progression of Yielded Regions - Plate with Three Simple Supports and One Free Edge

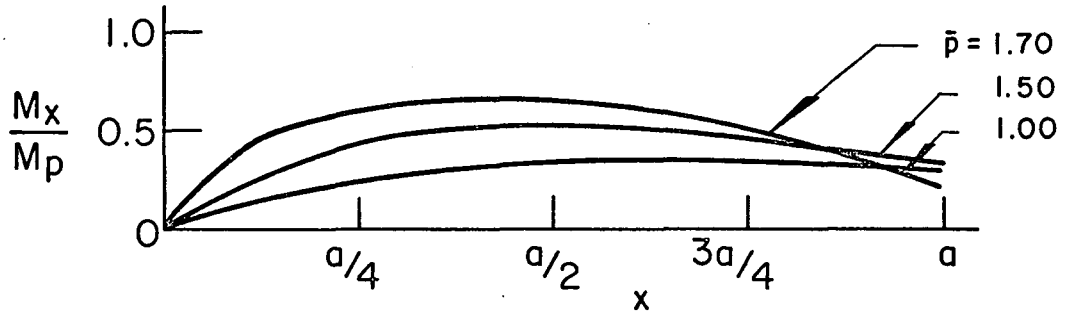

Bending Moment M_x along x-Axis

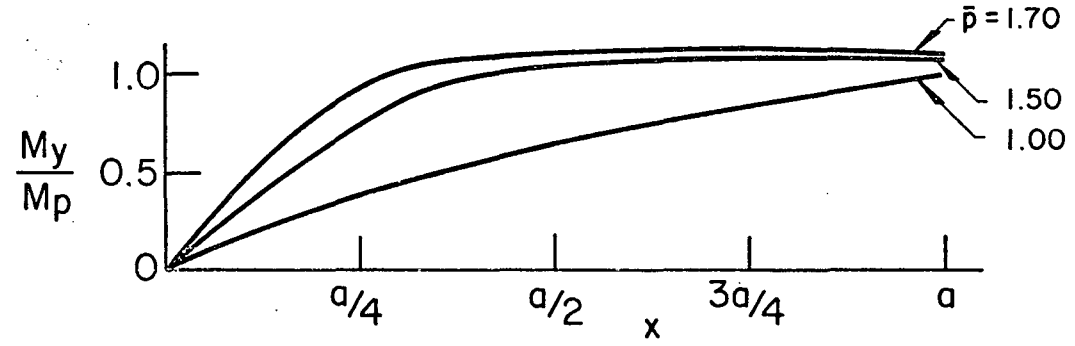

Bending Moment M_y along x-Axis

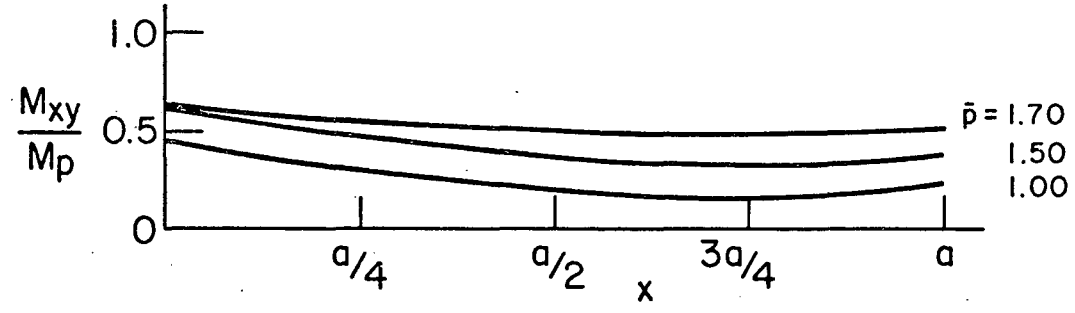

Twisting Moment M_{xy} along $y = 7/16\ b$

Fig. 61 Redistribution of Moments due to Plastic Flow - Plate with Three Simple Supports and One Free Edge

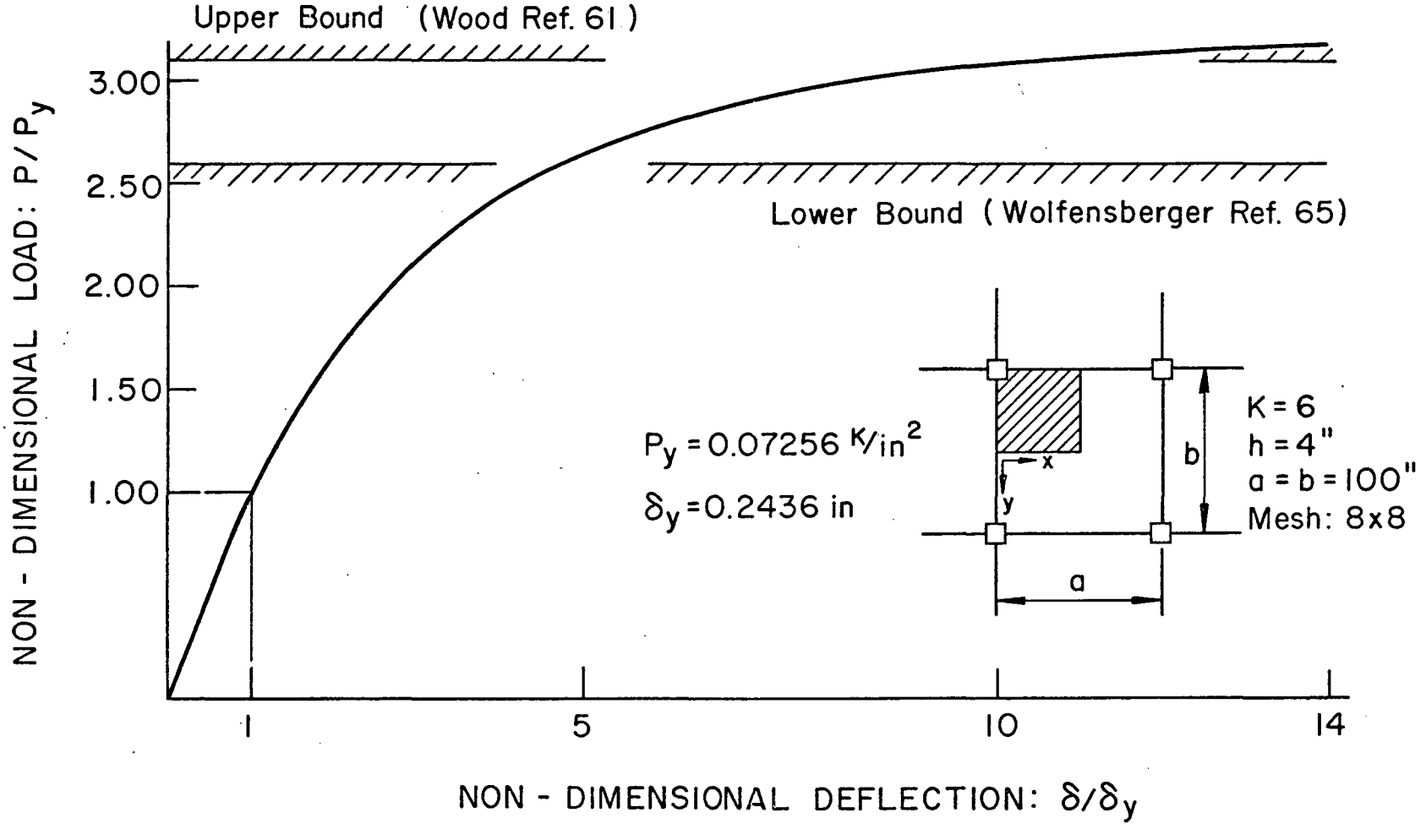

Fig. 62 Load-Deflection Curve at Center of Flat Slab Panel

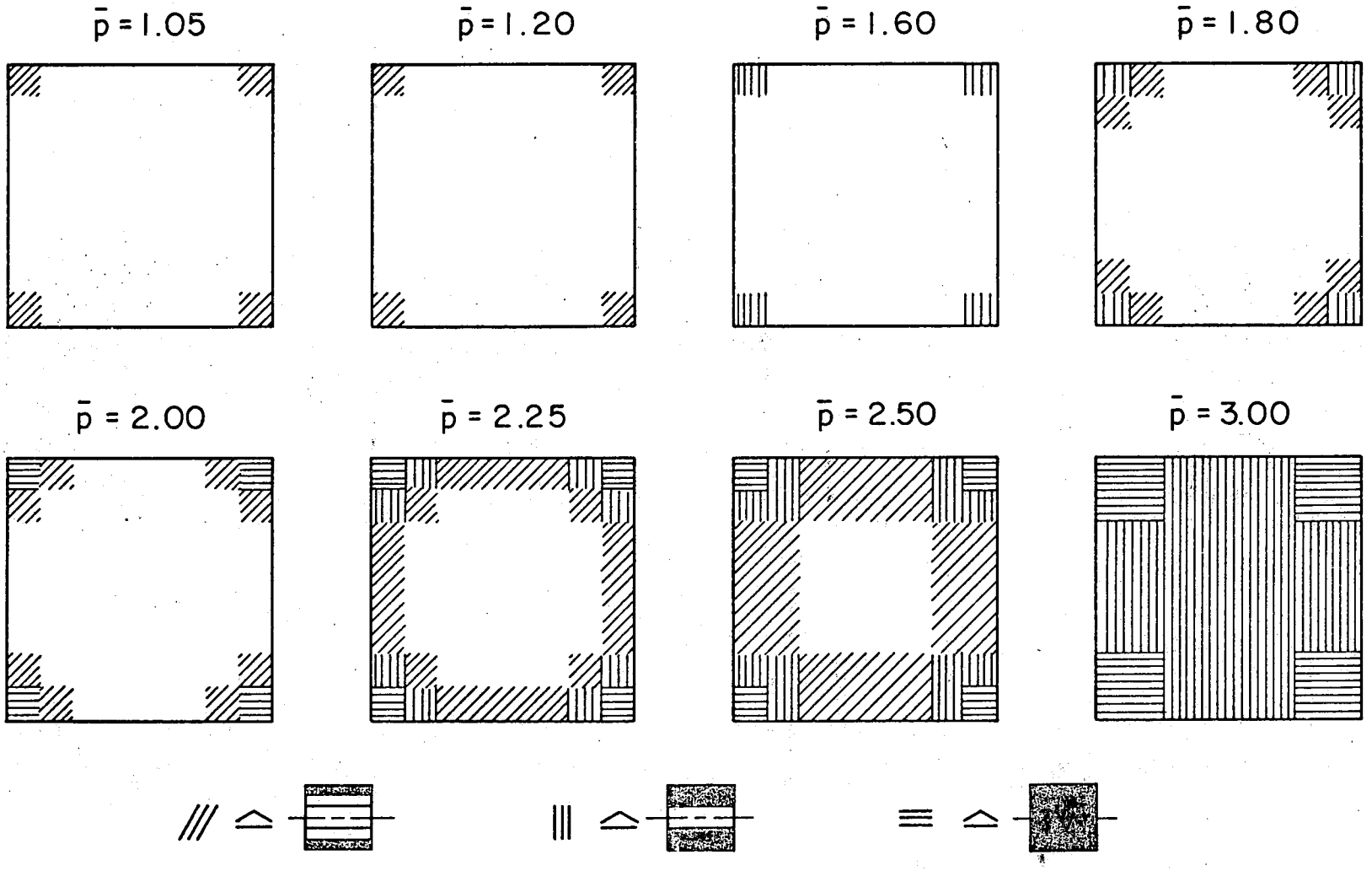

Fig. 63 Progression of Yielded Regions - Flat Slab Panel

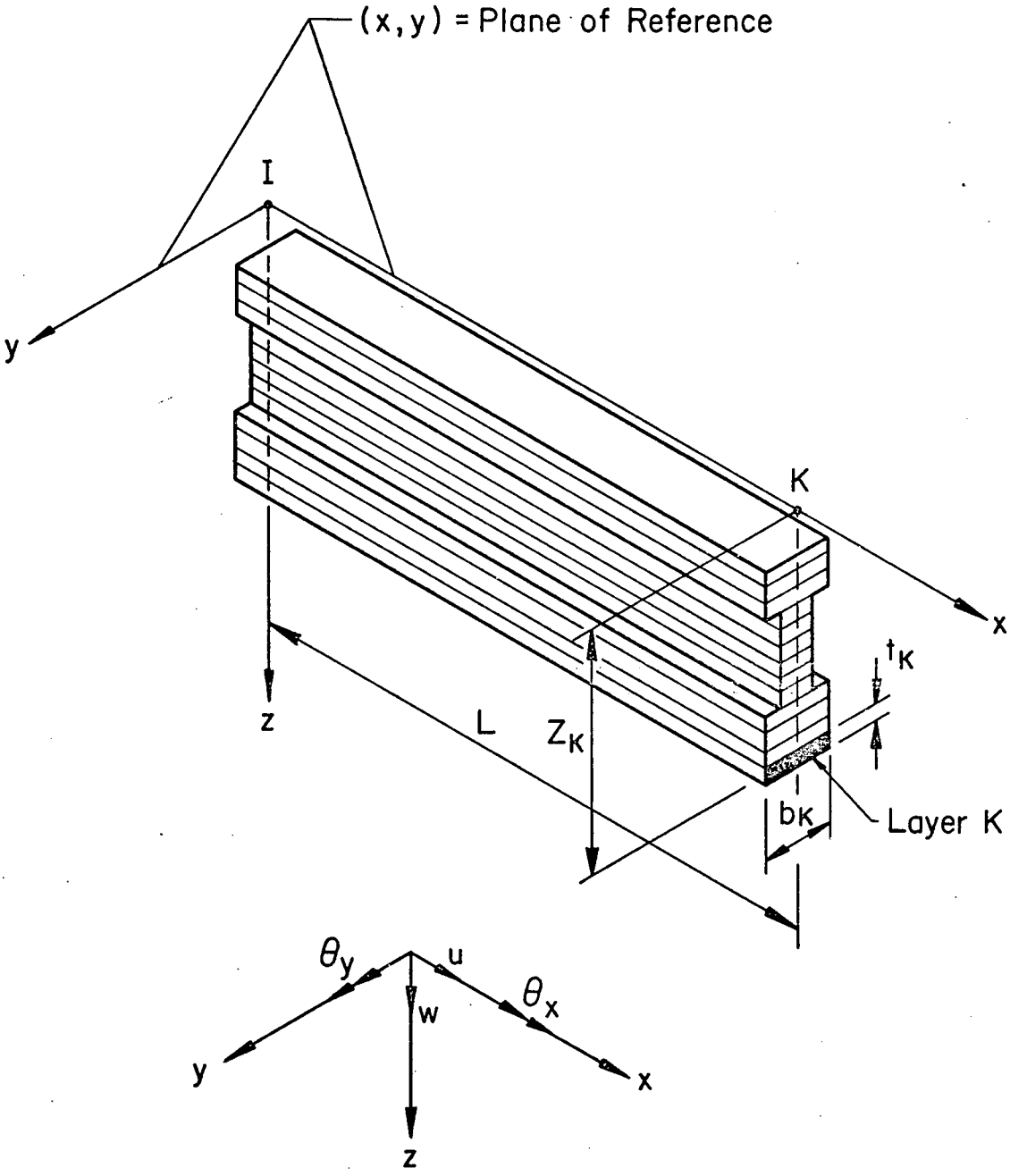

Fig. 64 Layered Finite Beam Element for Elastic-Plastic Analysis of Stiffened Plates

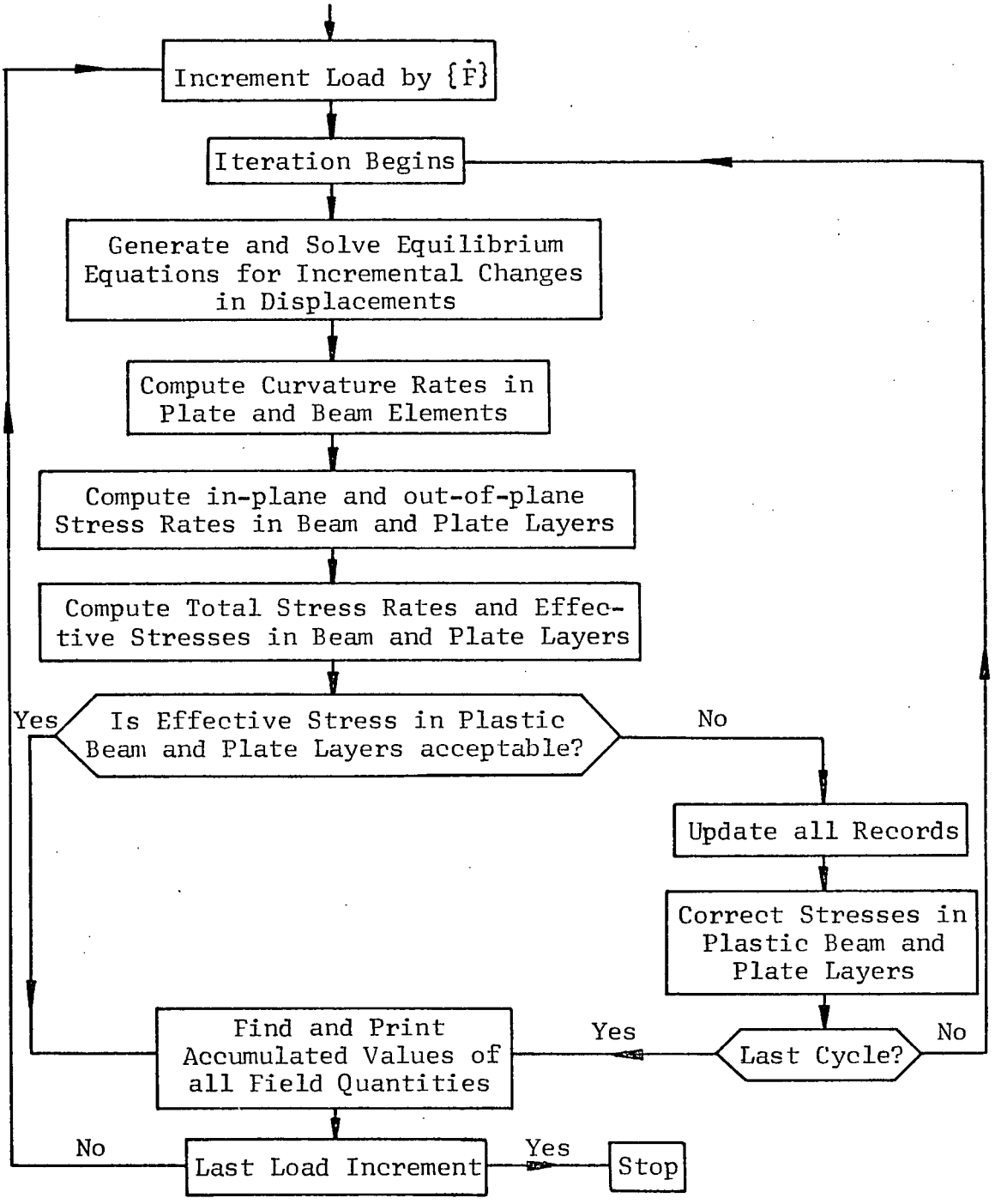

Fig. 65 Flow Diagram for Elastic-Plastic Eccentrically Stiffened Plate Analysis

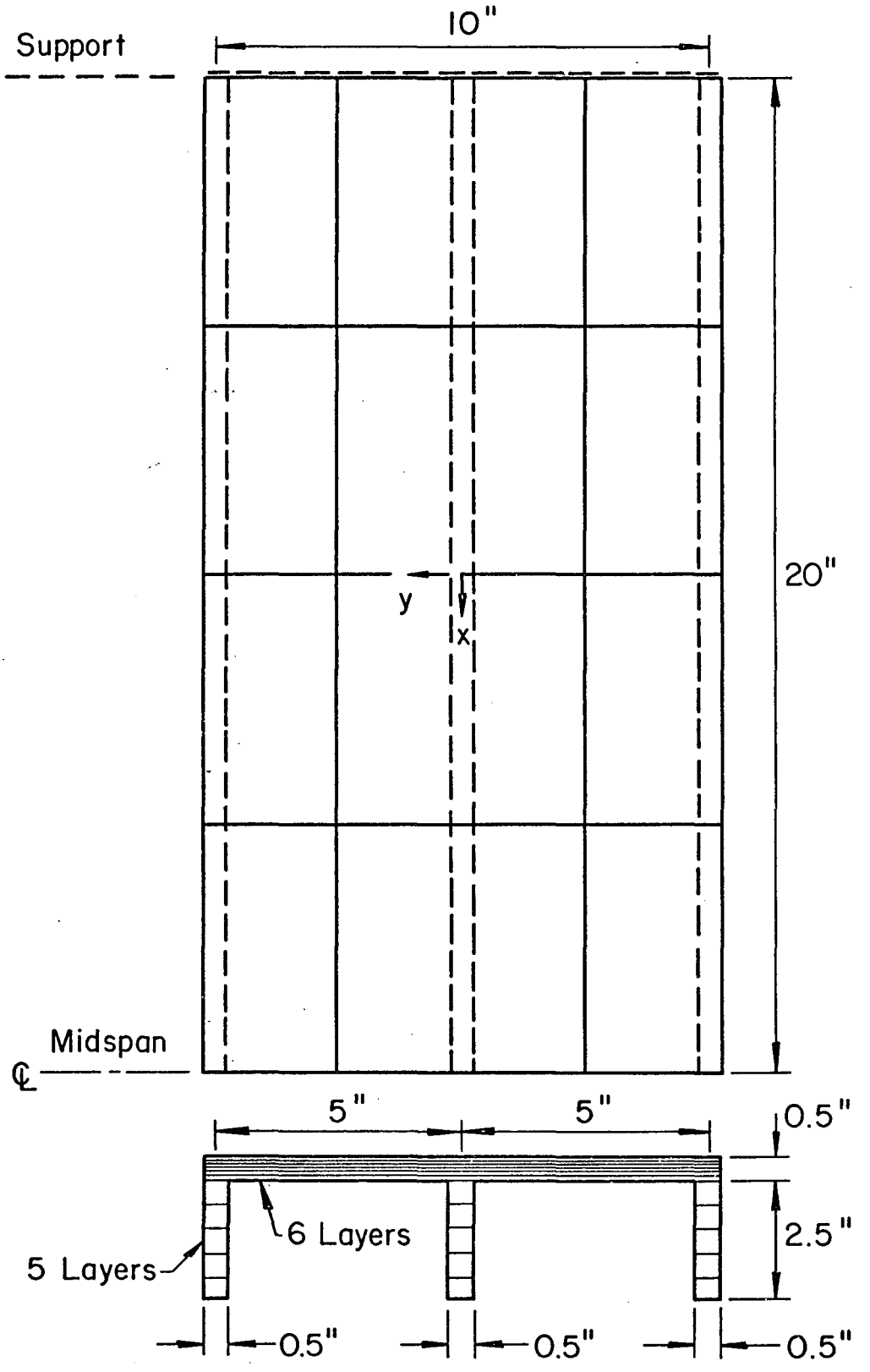

Fig. 66 Dimensions of Three-Beam Bridge Model

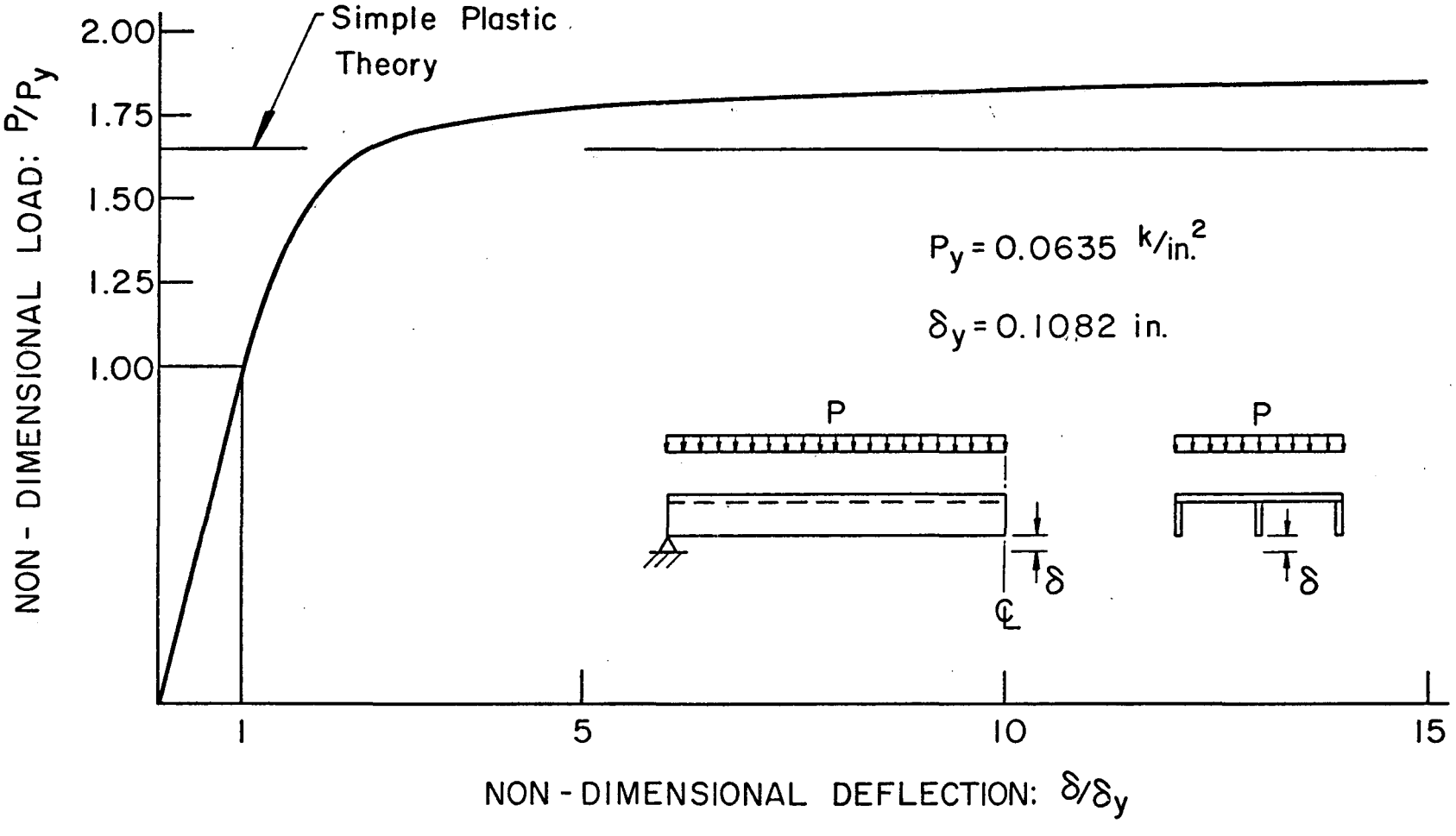

Fig. 67 Load-Deflection Curve at Center Point of Simply Supported Three-Beam Bridge Model

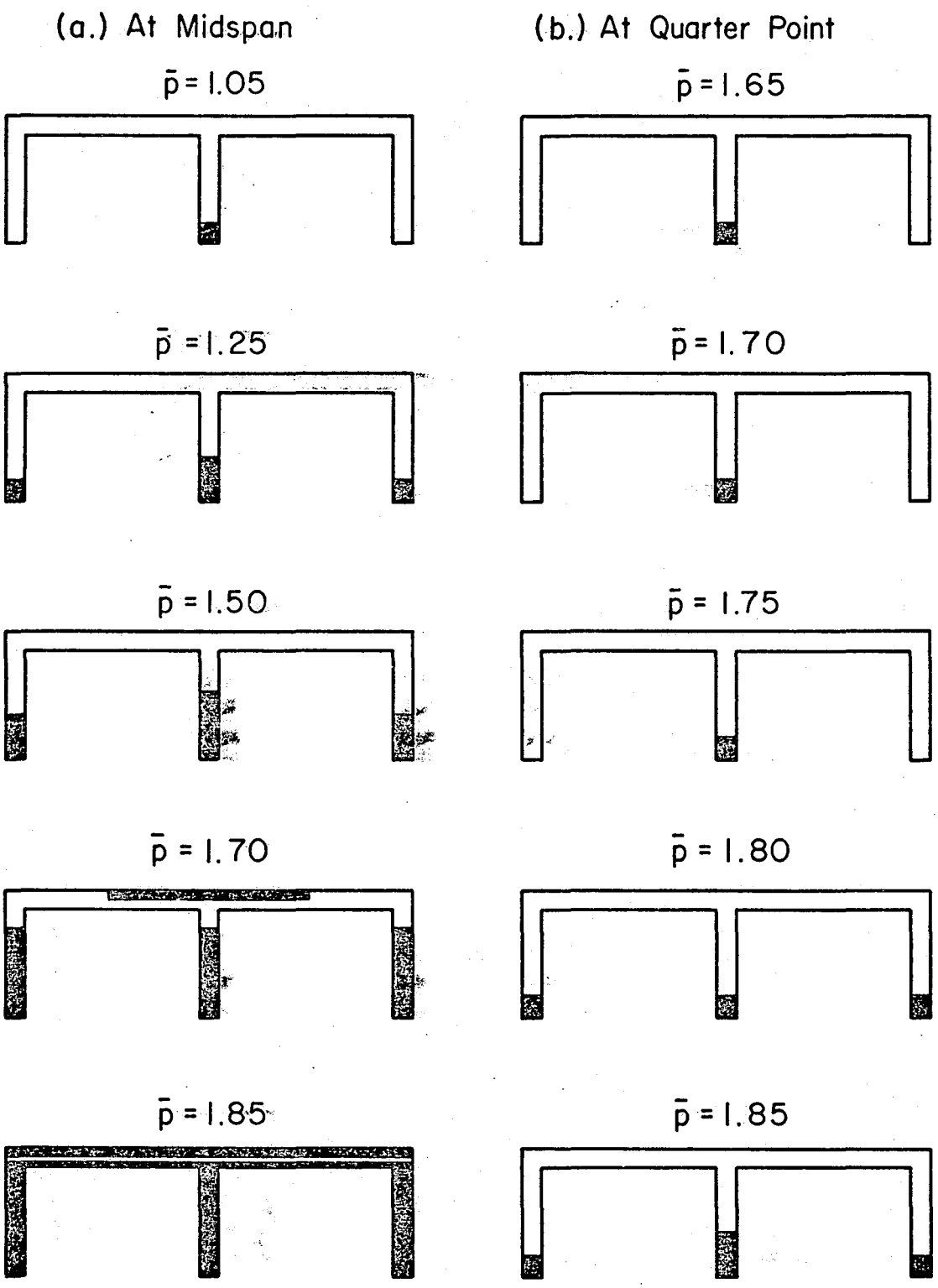

Fig. 68 Progression of Yielded Regions through Cross Section - Simply Supported Three-Beam Bridge Model

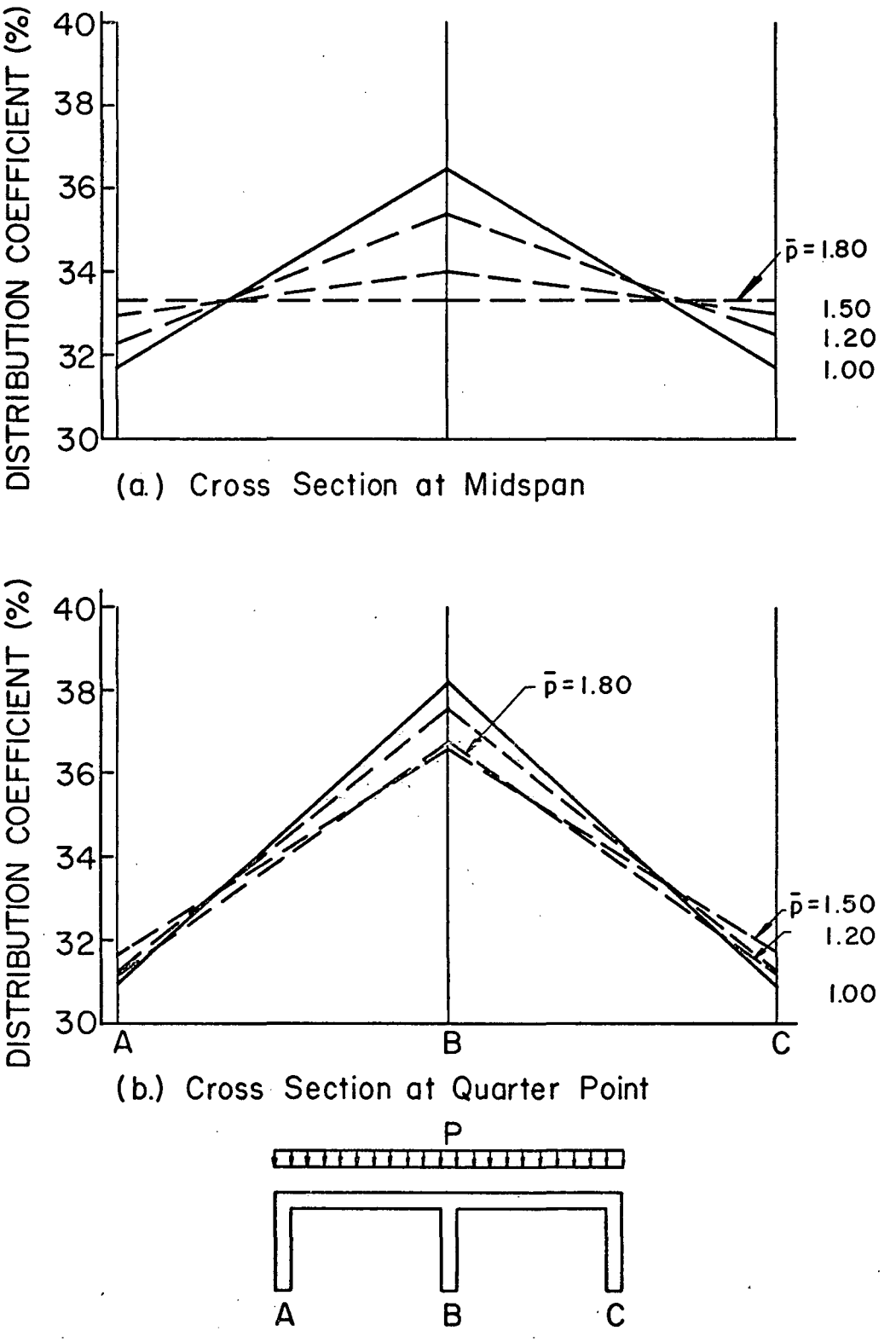

Fig. 69 Inelastic Lateral Distribution of Load - Simply Supported Three-Beam Bridge Model

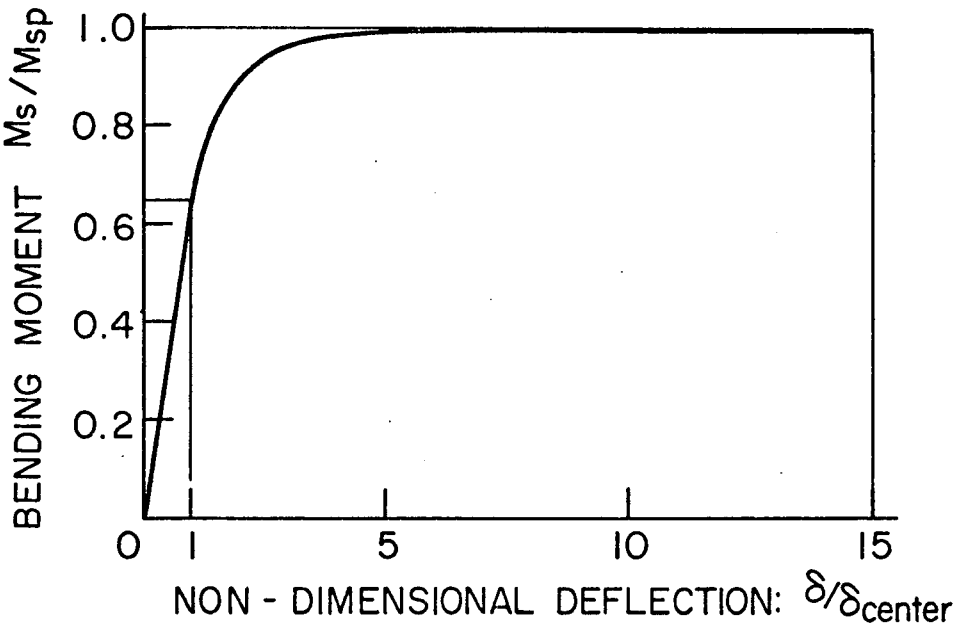

(a.) Center Beam - Midspan

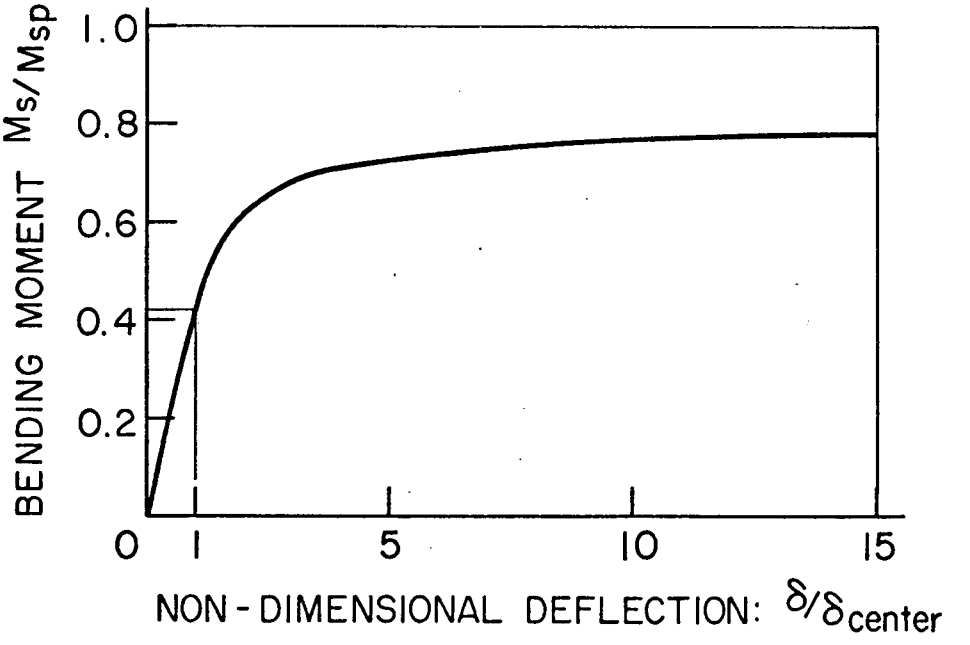

(b.) Center Beam - Quarter Point

Fig. 70 Bending Moment in Center Beam versus Deflection - Simply Supported Three-Beam Bridge Model

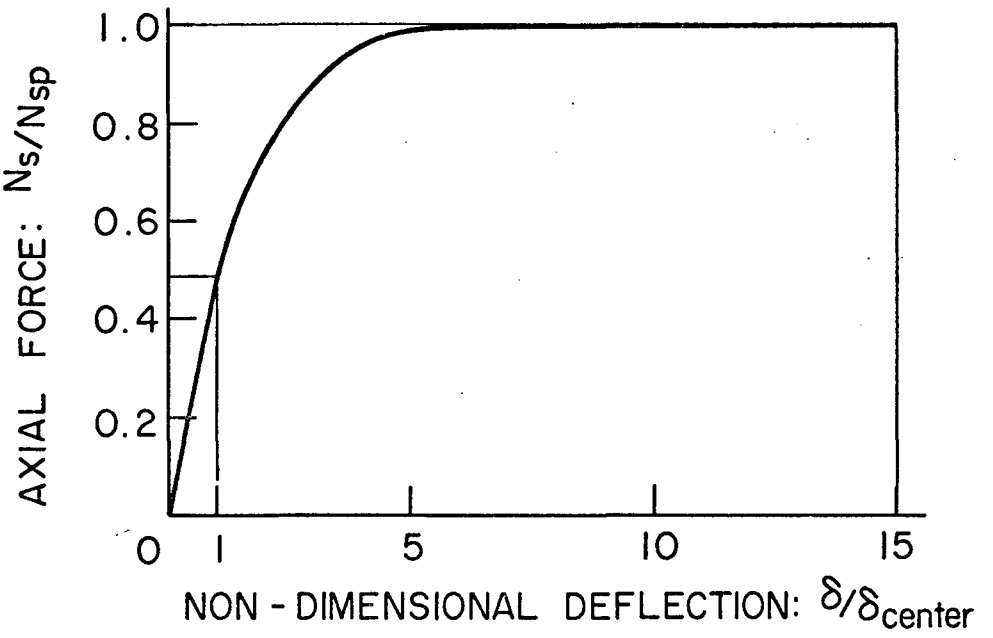

(a.) Center Beam - Midspan

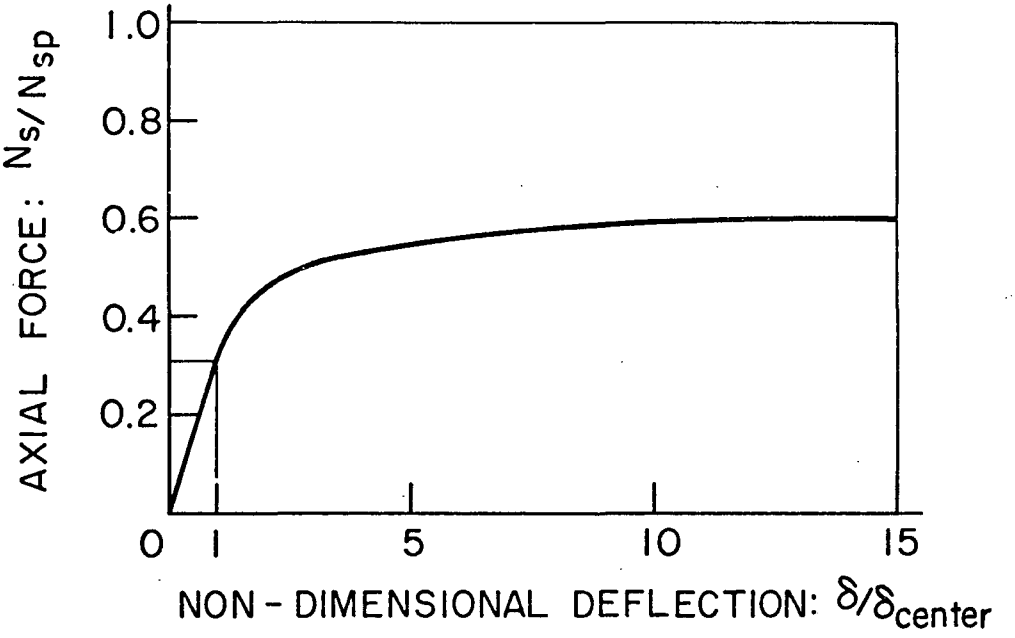

(b.) Center Beam - Quarter Point

Fig. 71 Axial Force in Center Beam versus Deflection - Simply Supported Three-Beam Bridge Model

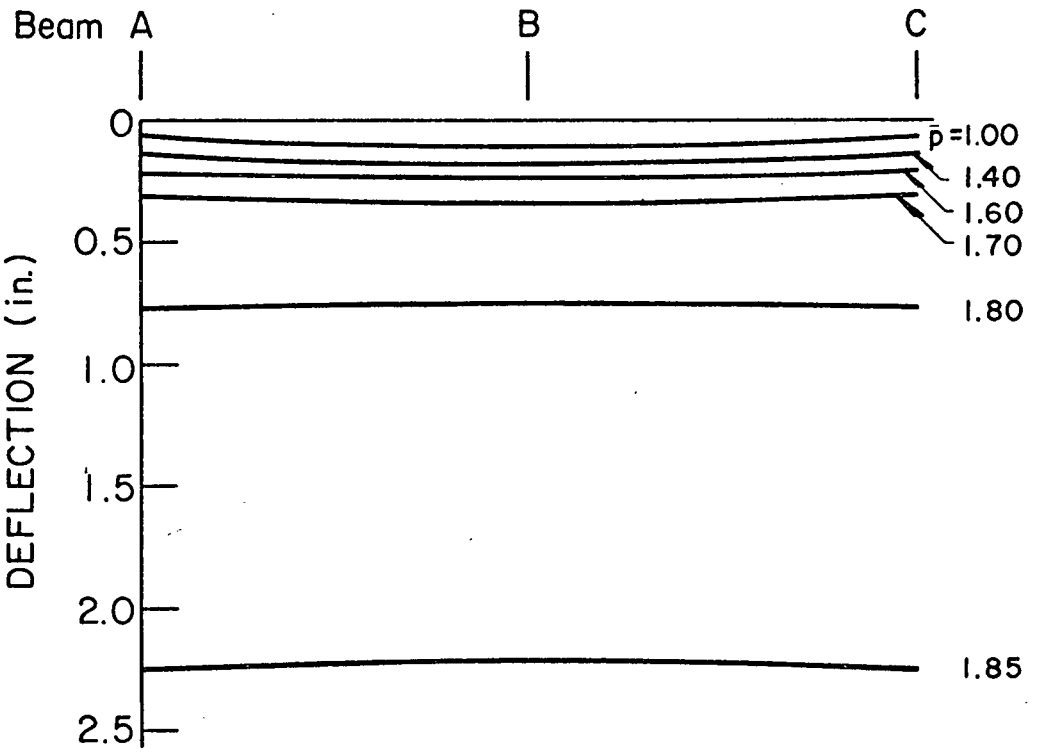

(a.) Cross Section at Midspan

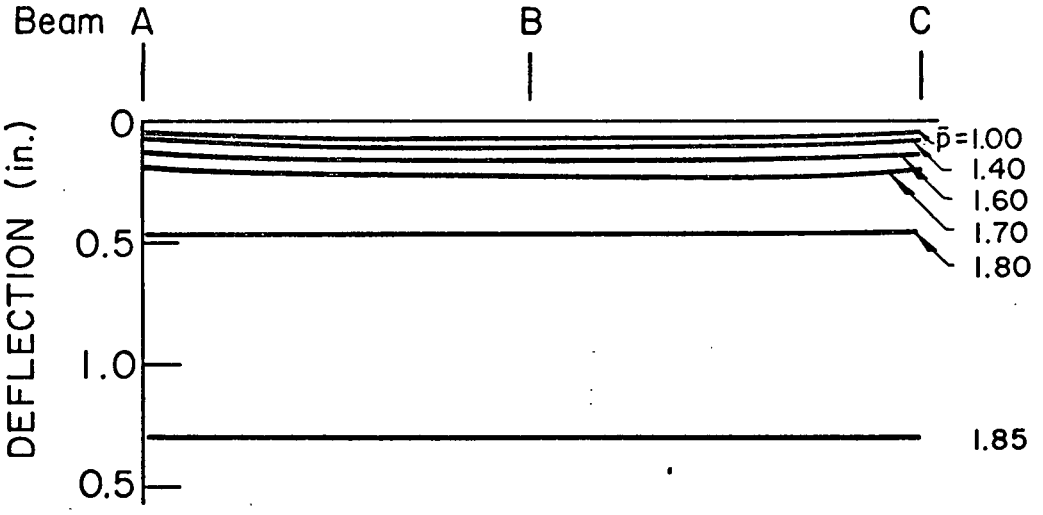

(b.) Cross Section at Quarter Point

Fig. 72 Transverse Deflection Profiles - Simply Supported Three-Beam Bridge Model

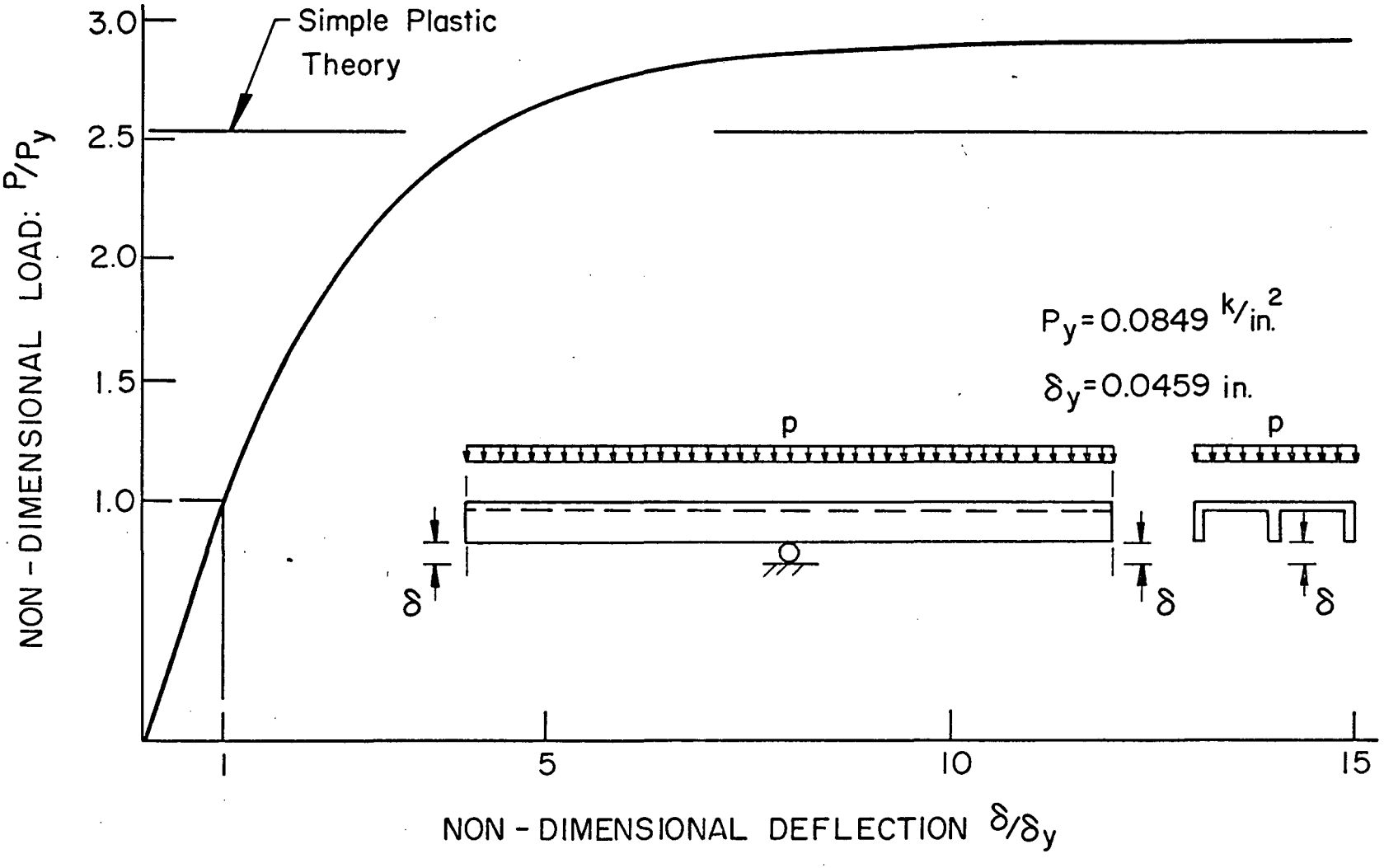

Fig. 73 Load-Deflection Curve at Center Point of Continuous Three-Beam Bridge Model

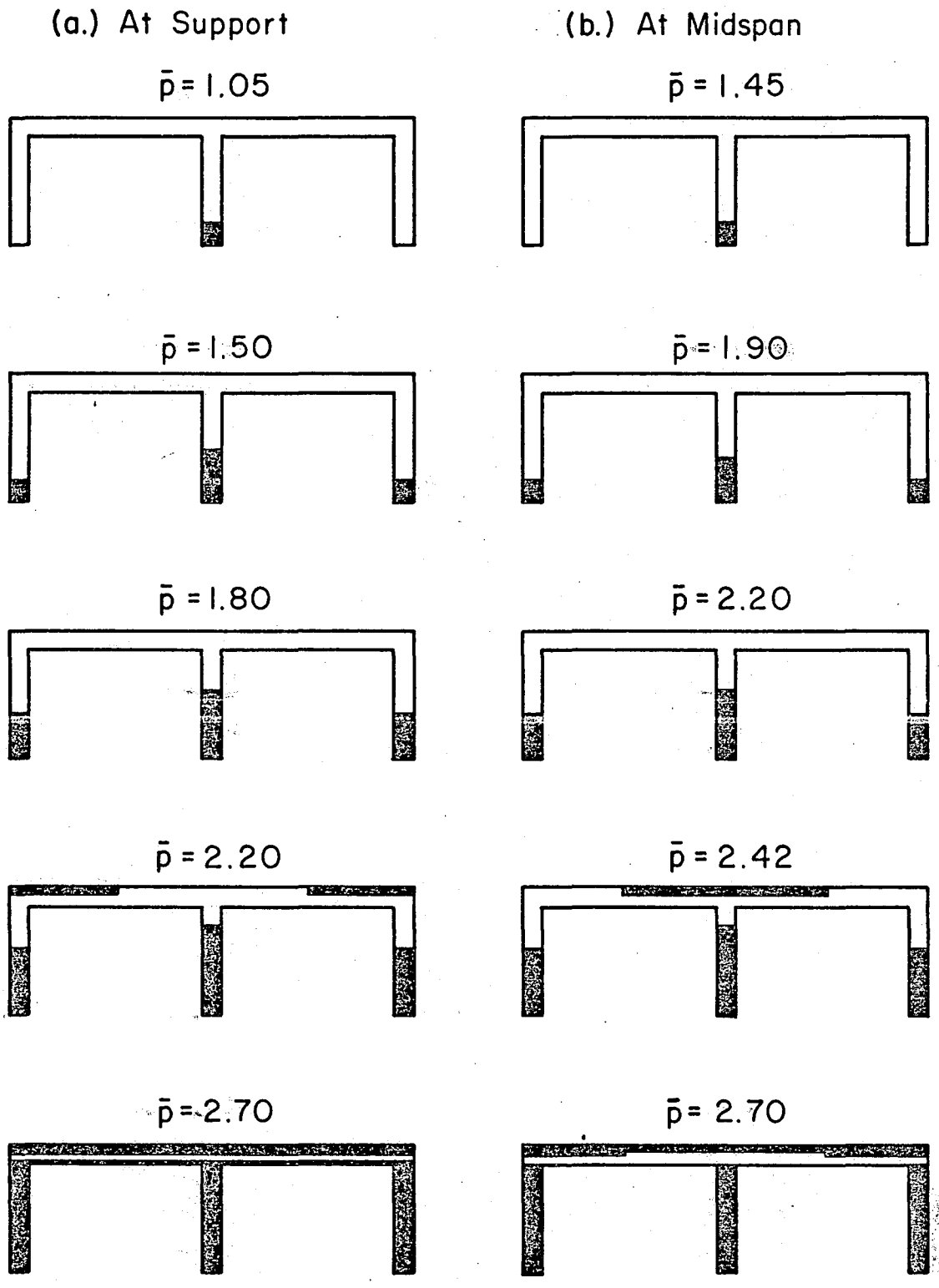

Fig. 74 Progression of Yielded Regions through Cross Section - Continuous Three-Beam Bridge Model

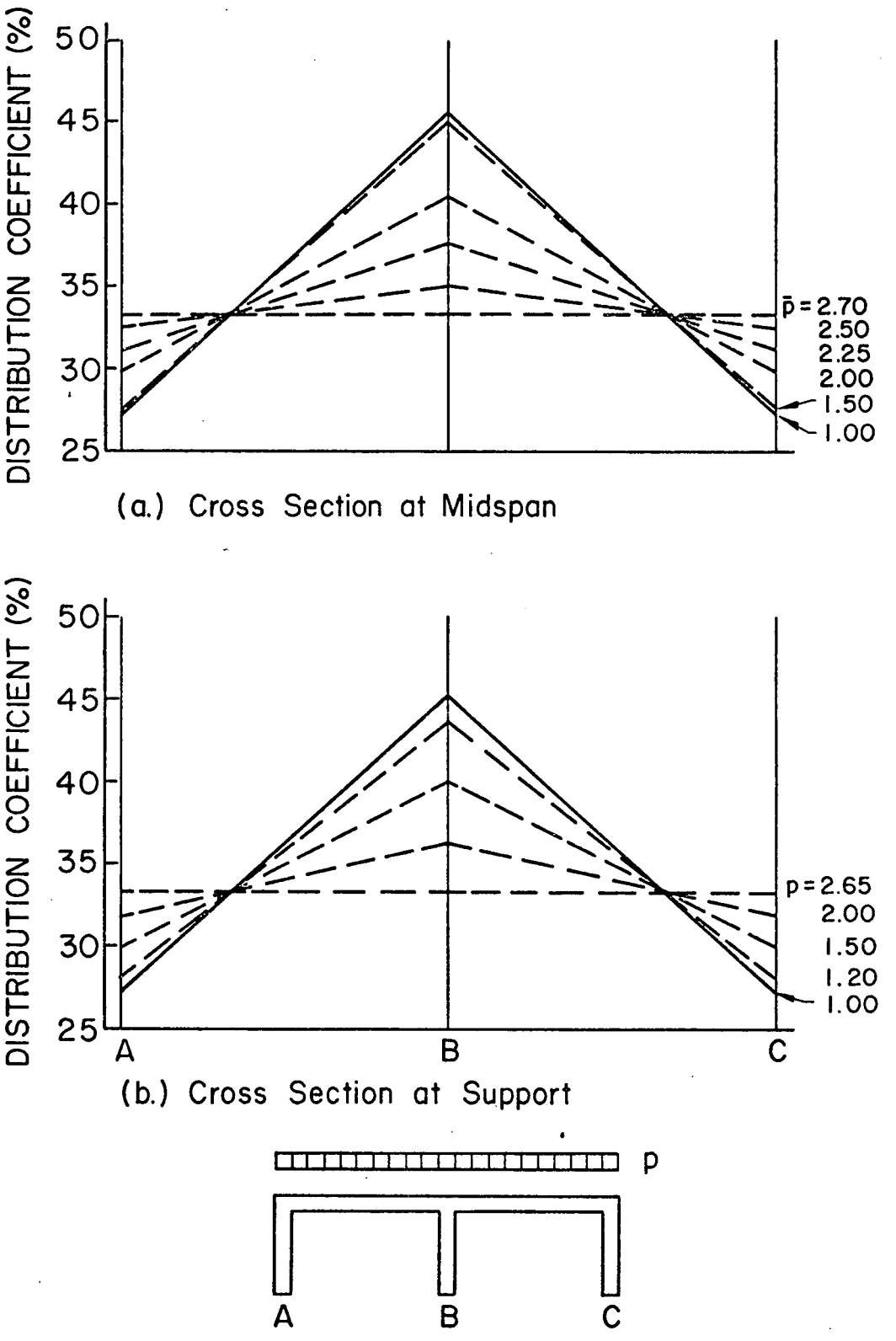

Fig. 75 Inelastic Lateral Distribution of Load - Continuous Three-Beam Bridge Model

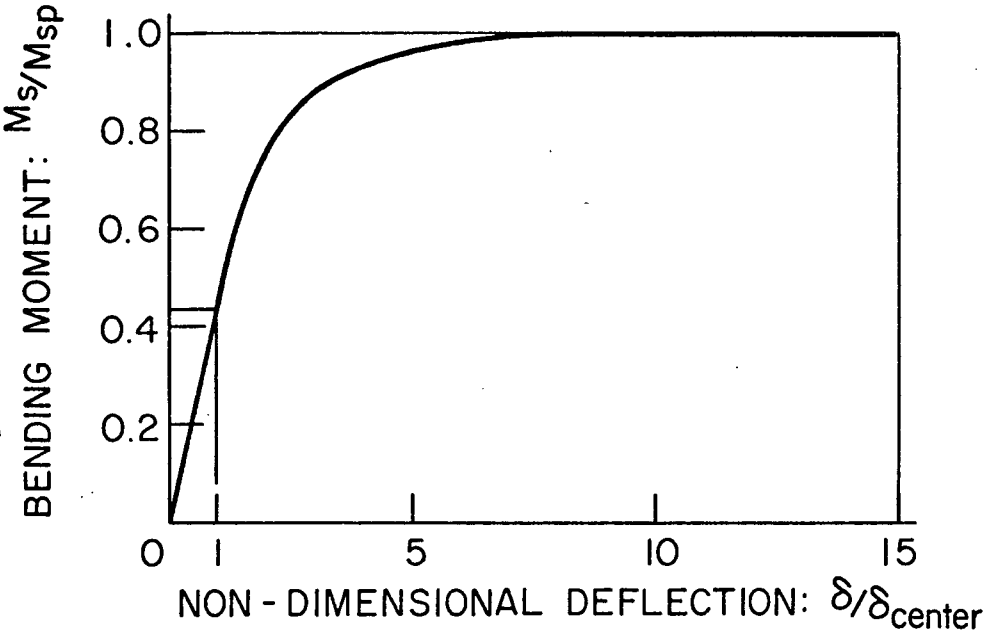

(a.) Center Beam - Midspan

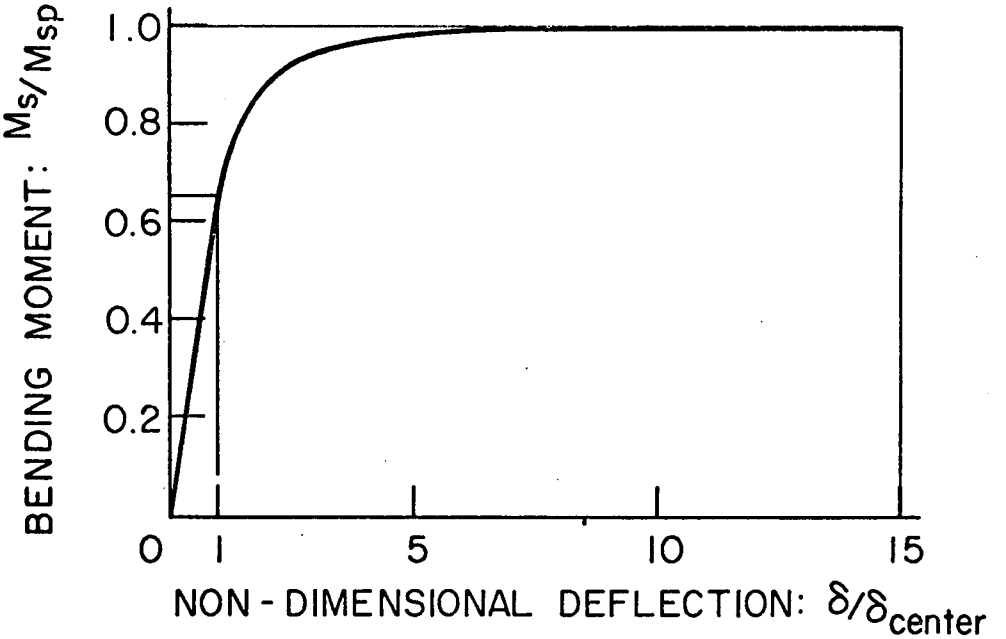

(b.) Center Beam - Support

Fig. 76 Bending Moment in Center Beam versus Deflection - Continuous Three-Beam Bridge Model

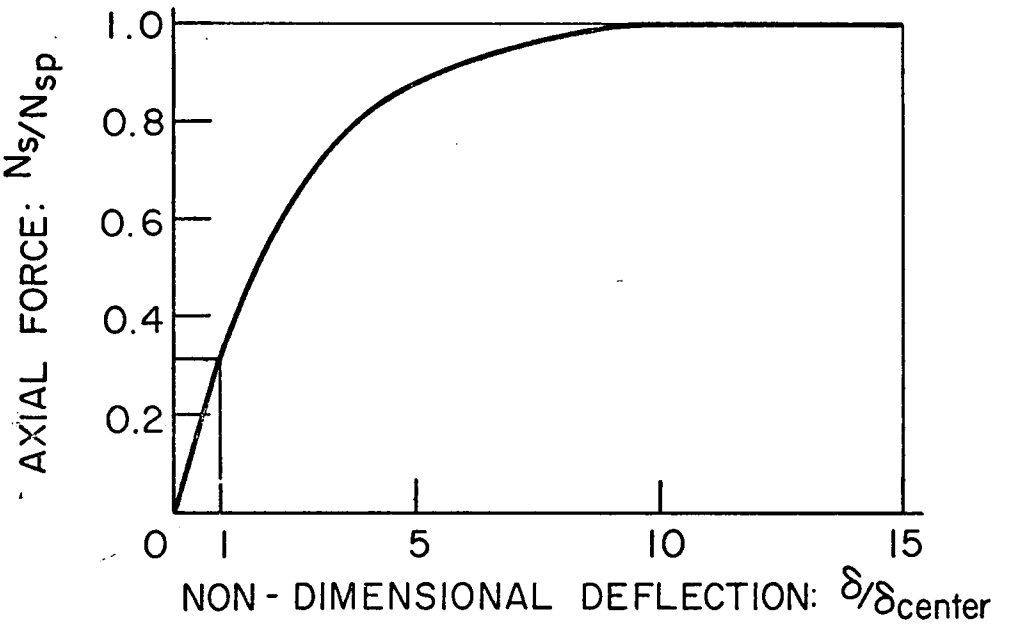

(a.) Center Beam - Midspan

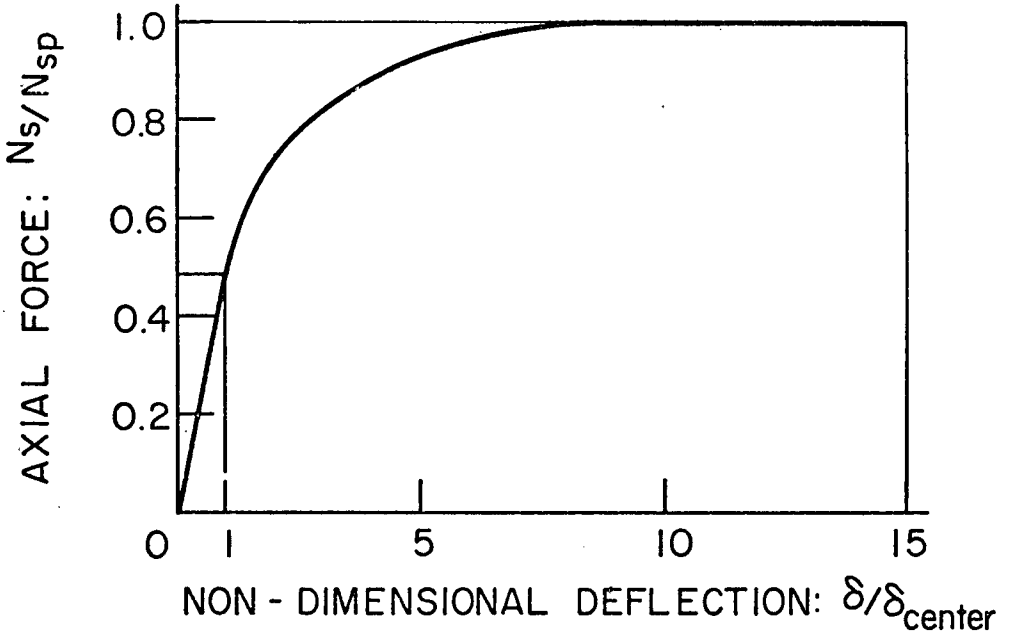

(b.) Center Beam - Support

Fig. 77 Axial Force in Center Beam versus Deflection - Continuous Three-Beam Bridge Model

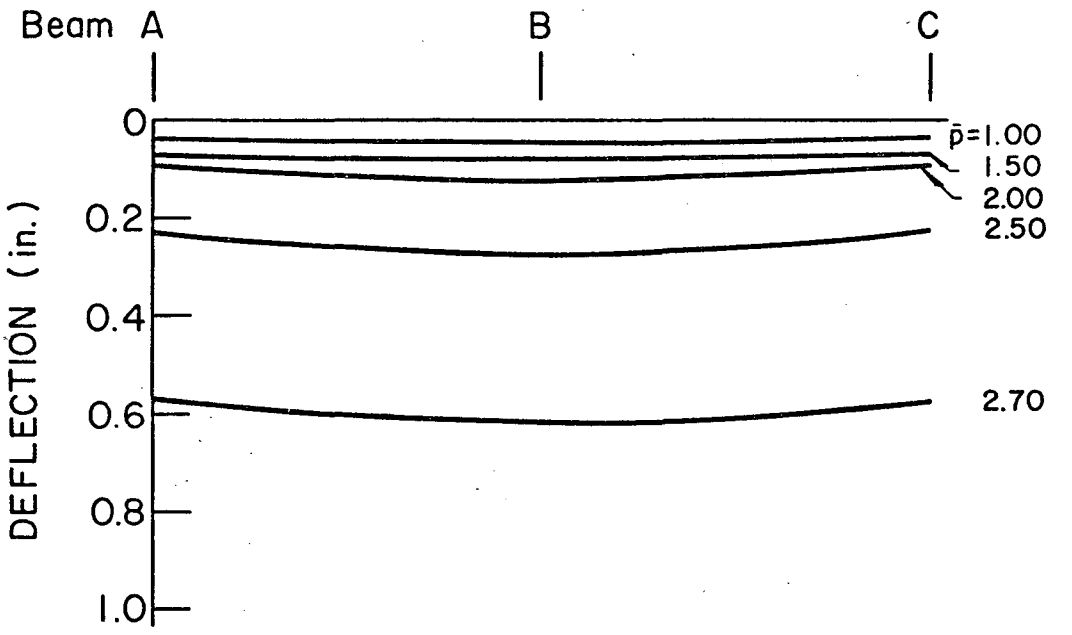

(a.) Cross Section at Midspan

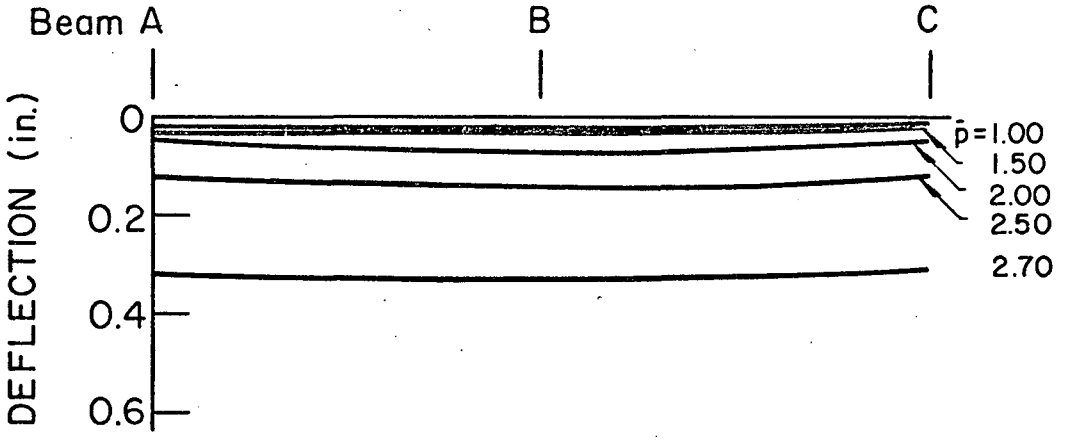

(b.) Cross Section at Quarter Point

Fig. 78 Transverse Deflection Profiles - Continuous Three-Beam Bridge Model

11. REFERENCES

1. American Concrete Institute
   BUILDING CODE REQUIREMENTS FOR REINFORCED CONCRETE (ACI 318-63), Detroit, Michigan, 1963.

2. American Association of State Highway Officials
   STANDARD SPECIFICATIONS FOR HIGHWAY BRIDGES, Ninth Edition, AASHO, Washington, D.C., 1965.

3. Timoshenko, S. P. and Woinowsky-Krieger, S.
   THEORY OF PLATES AND SHELLS, Second Edition, McGraw-Hill, New York, 1959.

4. Girkmann, K.
   FLAECHENTRAGWERKE, Sixth Edition, Springer, Vienna, 1963.

5. Przemieniecki, J. S.
   THEORY OF MATRIX STRUCTURAL ANALYSIS, McGraw-Hill, New York, 1968.

6. Zienkiewicz, O. C. and Cheung, Y. K.
   THE FINITE ELEMENT METHOD IN STRUCTURAL AND CONTINUUM MECHANICS, Second Edition, McGraw-Hill, New York, 1970.

7. Argyris, J. H.
   THE MATRIX ANALYSIS OF STRUCTURES WITH CUT-OUTS AND MODIFICATIONS, Proc. Ninth Intern. Congr. Appl. Mech., Section II, Mech. Solids, Sept., 1956.

8. Turner, M. J., Clough, R. W., Martin, H. C. and Topp, L. J.
   STIFFNESS AND DEFLECTION ANALYSIS OF COMPLEX STRUCTURES, Journal of Aeronautical Sciences, 23, No. 9, 1956.

9. Argyris, J. H.
   ON THE ANALYSIS OF COMPLEX ELASTIC STRUCTURES, Appl. Mech. Rev., 11, 1958.

10. Becker, M.
THE PRINCIPLES AND APPLICATIONS OF VARIATIONAL METHODS, Research Monograph No. 27, The M.I.T. Press, Cambridge, Massachusetts, 1964.

11. Oliveira, E. R.
THEORETICAL FOUNDATIONS OF THE FINITE ELEMENT METHOD, International Journal of Solids and Structures, V. 4, No. 10, Oct., 1968.

12. Melosh, R. J.
BASIS FOR DERIVATION OF MATRICES FOR THE DIRECT STIFFNESS APPROACH, AIAA Journal, V. 1, pp. 1631-1637, July 1963.

13. Fraijs de Veubeke, B.
DISPLACEMENT AND EQUILIBRIUM MODELS IN THE FINITE ELEMENT METHOD, Stress Analysis (Zienkiewicz and Hollister, Ed.), J. Wiley Book Co. Ltd., London, 1965.

14. Bogner, F. K., Fox, R. L. and Schmit, L. A.
THE GENERATION OF INTERELEMENT, COMPATIBLE STIFFNESS AND MASS MATRICES BY THE USE OF INTERPOLATION FORMULAS, Proc. First Conference on Matrix Methods in Structural Mechanics, Wright-Patterson AFB, Ohio, Nov., 1965.

15. Birkhoff, G. and Garabedian, H.
SMOOTH SURFACE INTERPOLATION, Journal Math. Phys., V. 39, pp. 353-368, 1960.

16. Deak, A. and Pian, T.
APPLICATION OF SMOOTH-SURFACE INTERPOLATION TO THE FINITE ELEMENT ANALYSIS, AIAA Journal, V. 5, No. 1, Jan., 1969.

17. Ergatoudis, J. G.
ISO-PARAMETRIC FINITE ELEMENTS IN TWO- AND THREE-DIMENSIONAL ANALYSIS, Ph.D. Dissertation, University of Wales, Swansea, 1968.

18. Irons, B. M. and Zienkiewicz, O. C.
THE ISO-PARAMETRIC ELEMENT SYSTEM - A NEW CONCEPT IN FINITE ELEMENT ANALYSIS, Conf. - Recent Advances in Stress Analysis, Royal Aero Soc., London, March, 1968.

19. Washizu, K.
VARIATIONAL METHODS IN ELASTICITY AND PLASTICITY, Pergamon Press, Oxford, 1960.

20. Fraijs de Veubeke, B.
UPPER AND LOWER BOUNDS IN MATRIX STRUCTURAL ANALYSIS, Pergamon Press, Oxford, 1964.

21. Pian, T. H. and Tong, P.
BASIS OF FINITE ELEMENT METHODS FOR SOLID CONTINUA, International Journal for Numerical Methods in Engineering, V. 1, No. 1, Jan., 1969.

22. Bell, K.
A REFINED TRIANGULAR PLATE BENDING FINITE ELEMENT, International Journal of Numerical Methods in Engineering, V. 1, No. 1, Jan., 1969.

23. Gallagher, R. H.
ANALYSIS OF PLATE AND SHELL STRUCTURES, Proc. on Application of Finite Element Methods in Civil Engineering, Vanderbilt University, Nov., 1969.

24. Clough, R. and Tocher, J.
FINITE ELEMENT STIFFNESS MATRICES FOR THE ANALYSIS OF PLATE BENDING, First Conf. on Matrix Methods in Structural Mechanics, Wright-Patterson AFB, Ohio, Nov., 1965.

25. Pappenfuss, S. W.
LATERAL PLATE DEFLECTION BY STIFFNESS MATRIX METHODS WITH APPLICATION TO A MARQEE, M.S. Thesis, Dept. of Civil Engineering, University of Washington, Seattle, 1959.

26. Melosh, R. J.
A STIFFNESS MATRIX FOR THE ANALYSIS OF THIN PLATES IN BENDING, Journal of Aeronautical Sciences, Vol. 28, 34, 1961.

27. Fraijs de Veubeke, B.
A CONFORMING FINITE ELEMENT FOR PLATE BENDING, International Journal of Solids and Structures, V. 4, No. 1, 1968.

28. Clough, R. and Felippa, C.
A REFINED QUADRILATERAL ELEMENT FOR ANALYSIS OF PLATE BENDING, Proc. Second Conf. on Matrix Methods in Structural Mechanics, Wright-Patterson AFB, Ohio, Oct., 1968.

29. Pian, T. H.
ELEMENT STIFFNESS MATRICES FOR BOUNDARY COMPATIBILITY AND FOR PRESCRIBED BOUNDARY STRESSES, First Conf. on Matrix Methods in Structural Mechanics, Wright-Patterson AFB, Ohio, Oct., 1968.

30. Allwood, R. and Cornes, G.
A POLYGONAL FINITE ELEMENT FOR PLATE BENDING PROBLEMS USING ASSUMED STRESS APPROACH, Int. Journal for Numerical Methods in Engineering, V. 1, No. 2, 1969.

31. Clough, R. W.
THE FINITE ELEMENT METHOD IN STRUCTURAL MECHANICS, Chapter 7 of Stress Analysis, edited by O. C. Zienkiewicz and G. S. Hollister, John Wiley and Sons, 1965.

32. Whetstone, W. D.
COMPUTER ANALYSIS OF LARGE LINEAR FRAMES, Journal of Structural Division, ASCE, Vol. 95, No. ST11, Nov., 1969.

33. Melosh, R. J. and Bamford, R. M.
EFFICIENT SOLUTION OF LOAD-DEFLECTION EQUATIONS, Journal of Structural Division, ASCE, Vol. 95, No. ST4, April, 1969.

34. Adini, A. and Clough, R. W.
ANALYSIS OF PLATE BENDING BY THE FINITE ELEMENT METHOD, Report submitted to the National Science Foundation, 1960.

35. VanHorn, D. A.
STRUCTURAL BEHAVIOR CHARACTERISTICS OF PRESTRESSED CONCRETE BOX-BEAM BRIDGES, Fritz Engineering Laboratory Report No. 315.8, June, 1969.

36. Kerfoot, R. P. and Ostapenko, A.
GRILLAGES UNDER NORMAL AND AXIAL LOADS - PRESENT STATUS, Fritz Engineering Laboratory Report No. 323.1, June, 1967.

37. Lightfoot, E. and Sawko, F.
GRID FRAMEWORKS RESOLVED BY GENERALIZED SLOPE-DEFLECTION, Engineering, London, Vol. 187, 1959, pp. 18-20.

38. Hendry, A. W. and Jaeger, L. G.
THE ANALYSIS OF GRID FRAMEWORKS AND RELATED STRUCTURES, Chatto and Windus, London, 1958.

39. Clarkson, J.
THE ELASTIC ANALYSIS OF FLAT GRILLAGES, Cambridge University Press, 1965.

40. Vitols, V., Clifton, R. and Au, T.
ANALYSIS OF COMPOSITE BEAM BRIDGES BY ORTHOTROPIC PLATE THEORY, ASCE Proc., Vol. 89, No. ST4, Pt.1, Paper 3581, August, 1963.

41. Bares, R. and Massonnet, C.
LE CALCUL DES GRILLAGES DE POUTRES ET DALLES ORTHOTROPES Selon La Methode Guyon - Massonnet - Bares, Dunod, Paris, 1966.

42. Hrennikoff, A.
SOLUTIONS OF PROBLEMS OF ELASTICITY BY THE FRAMEWORK METHOD, Trans. ASME, Journal of Appl. Mech., Vol. 8, No. 4, Dec., 1941.

43. Newmark, N. M.
NUMERICAL METHODS OF ANALYSIS OF BARS, PLATES AND ELASTIC BODIES, Edited by L. E. Grinter, MacMillan Co., New York, 1949.

44. Lopez, L. A. and Ang, A. H. S.
FLEXURAL ANALYSIS OF ELASTIC-PLASTIC RECTANGULAR PLATES, Civil Engineering Studies, Structural Research Series No. 305, University of Illinois, Urbana, Illinois, May, 1966.

45. Gustafson, W. C. and Wright, R. N.
ANALYSIS OF SKEWED COMPOSITE GIRDER BRIDGES, ASCE Proc., Vol. 94, No. ST4, April, 1968.

46. Timoshenko, S. P. and Gere, J. M.
THEORY OF ELASTIC STABILITY, Second Edition, McGraw-Hill, New York, 1961.

47. Galambos, T. V.
STRUCTURAL MEMBERS AND FRAMES, Prentice-Hall, Inc., New Jersey, 1968.

48. Sokolnikoff, I. S.
MATHEMATICAL THEORY OF ELASTICITY, McGraw-Hill, New York, 1956.

49. Prandtl, L.
ZUR TORSION VON PRISMATISCHEN STAEBEN, Physik. Z., 4, 1903, pp. 758-759.

50. Kollbrunner, C. F. and Basler, K.
TORSION IN STRUCTURES, Springer, New York, 1963.

51. Chen, C. and VanHorn, D. A.
STATIC AND DYNAMIC FLEXURAL BEHAVIOR OF A PRESTRESSED CONCRETE I-BEAM BRIDGE - BARTONSVILLE BRIDGE, Fritz Engineering Laboratory Report No. 349.2, Jan., 1971.

52. Wegmuller, A. and VanHorn, D. A.
SLAB BEHAVIOR OF A PRESTRESSED CONCRETE I-BEAM BRIDGE - BARTONSVILLE BRIDGE, Fritz Engineering Laboratory Report No. 349.3, May, 1971.

53. Motarjemi, D. and VanHorn, D. A.
THEORETICAL ANALYSIS OF LOAD DISTRIBUTION IN PRESTRESSED CONCRETE BOX-BEAM BRIDGES, Fritz Engineering Laboratory Report No. 315.9, Oct., 1969.

54. American Association of State Highway Officials,
STANDARD SPECIFICATIONS FOR HIGHWAY BRIDGES,
Tenth Edition, Washington, D.C., 1969.

55. Beedle, L. S.
PLASTIC DESIGN OF STEEL FRAMES,
John Wiley & Sons, New York, 1958.

56. Hodge, P. G.
PLASTIC ANALYSIS OF STRUCTURES,
McGraw-Hill, New York, 1959.

57. Neal, B. G.
THE PLASTIC METHODS OF STRUCTURAL ANALYSIS,
John Wiley & Sons, New York, 1956.

58. Bach, C.
ELASTIZITAT UND FESTIGKEIT, Third Edition,
Julius Springer, Berlin, 1898.

59. Johansen, K. W.
THE ULTIMATE STRENGTH OF REINFORCED CONCRETE SLABS,
Final Report, Third Congr., IVBH, Liege, Belgium, 1948.

60. Drucker, D. C., Greenberg, H. J. and Prager, W.
THE SAFETY FACTOR FOR AN ELASTIC-PLASTIC BODY IN PLANE STRAIN, Journal of Applied Mechanics, 18, 1951.

61. Wood, R. H.
ELASTIC AND PLASTIC DESIGN OF SLABS AND PLATES, Thames and Hudson, London, 1961.

62. Sawzuk, A. and Jaeger T.
GRENZTRAGFAEHIGKEITS - THEORIE DER PLATTEN, Springer, Berlin, 1963.

63. Shull, H. E. and Hu, L. W.
LOAD CARRYING CAPACITIES OF SIMPLY SUPPORTED RECTANGULAR PLATES, Journal of Applied Mechanics, ASME, Dec., 1963.

64. Koopman, D. C. and Lance, R. H.
ON LINEAR PROGRAMMING AND PLASTIC LIMIT ANALYSIS, Journal of the Mechanics and Physics of Solids, London, Vol. 12, 1964.

65. Wolfensberger, R.
TRAGLAST UND OPTIMALE BEMESSUNG VON PLATTEN, Doctoral Dissertation, ETH Zurich, 1964.

66. Bhaumik, A. K. and Hanley, J. T.
ELASTO-PLASTIC PLATE ANALYSIS BY FINITE DIFFERENCES, Journal of the Structural Division, ASCE, Vol. 93, ST5, Oct., 1967.

67. Armen, H., Pifko, A. B., Levine, H. S., and Isakson, G.
PLASTICITY, Chapter 8 of the Conference on Finite Element Techniques, University of Southampton, April, 1970.

68. Pope, G. G.
THE APPLICATION OF THE MATRIX DISPLACEMENT METHOD IN PLANE ELASTO-PLASTIC PROBLEMS, Proc. of Conference on Matrix Methods in Structural Mechanics, Wright-Patterson AFB, Ohio, Oct., 1965.

69. Anand, S. C., Lee, S. L., and Rossow, E. C.
FINITE ELEMENT ANALYSIS OF ELASTIC-PLASTIC PLANE STRESS PROBLEMS BASED UPON TRESCA YIELD CONDITION, Ingenieur-Archiv, 39. Band, Zweites Heft, 1970.

70. Armen, H., Pifko, A. B., and Levine, H. S.
FINITE ELEMENT ANALYSIS OF STRUCTURES IN THE PLASTIC RANGE, NASA Report CR1649, Washington, D.C., Feb., 1971.

71. Popov, E. P., Khojasteh-Bakht, M. and Yaghmai, S.
ANALYSIS OF ELASTIC-PLASTIC CIRCULAR PLATES, Journal of the Engineering Mechanics Division, ASCE, Vol. 93, No. EM6, Dec., 1967.

72. Whang, B.
ELASTO-PLASTIC ORTHOTROPIC PLATES AND SHELLS, Proc. of the Symposium on Application of Finite Element Methods in Civil Engineering, Vanderbilt University, Nashville, Tennessee, Nov., 1969.

73. Oden, T. J.
FINITE ELEMENT APPLICATIONS IN NONLINEAR STRUCTURAL ANALYSIS, Proc. of the Symposium on Application of Finite Element Methods in Civil Engineering, Vanderbilt University, Nashville, Tennessee, Nov., 1969.

74. Mendelson, A.
PLASTICITY: THEORY AND APPLICATION, The MacMillan Co., New York, 1968.

75. Ziegler, H.
A MODIFICATION OF PRAGER'S HARDENING RULE, Quarterly of Applied Mathematics, Vol. 17, No. 1, 1959.

76. Drucker, D. C.
A MORE FUNDAMENTAL APPROACH TO PLASTIC STRESS-STRAIN RELATIONS, Proc., First U. S. National Congr. of Applied Mechanics, New York, 1952.

77. Felippa, C. A.
REFINED FINITE ELEMENT ANALYSIS OF LINEAR AND NONLINEAR TWO-DIMENSIONAL STRUCTURES, Report No. SESM 66-22, University of California, Oct., 1966.

78. Hodge, P. G. and Belytscho, T.
NUMERICAL METHODS FOR THE LIMIT ANALYSIS OF PLATES, Journal of Applied Mechanics, Vol. 35, Dec., 1968.

79. Ranaweera, M. P. and Leckie, F. A.
BOUND METHODS IN LIMIT ANALYSIS, Chapter 9 of the Conference on Finite Element Techniques, University of Southampton, April, 1970.

80. Prager, W.
THE GENERAL THEORY OF LIMIT DESIGN, Proc., Eighth International Congr. on Theory and Applied Mechanics, Istanbul, Vol. 2, 1952.

81. Severn, R. and Taylor, P.
THE FINITE ELEMENT METHOD FOR FLEXURE OF SLABS WHEN STRESS DISTRIBUTIONS ARE ASSUMED, Proc. Inst. of Civil Engineers, 34, p. 153, 1966.

82. Lee, S. L. and Ballesteros, P.
UNIFORMLY LOADED RECTANGULAR PLATE SUPPORTED AT THE CORNERS, International Journal of Mechanical Science, Vol. 2, No. 3, 1960.

12. VITA

The author, born on April 10, 1938 as the seventh child of the late Emma and Johann Wegmuller-Muller, is a native of Selzach, Switzerland.

After attending the Technical College of the State of Bern, in Biel, Switzerland, where he received his first academic degree in mechanical engineering, in April 1960, he served in the Swiss Army for five months. In December 1960, he joined Bell Inc., in Kriens, Switzerland, where he was engaged in the design of steel structures.

In September 1961, he entered the Swiss Federal Institute of Technology, in Zurich, and received the Diploma in Civil Engineering, in November 1965. After graduation, he was employed as a research assistant at the Swiss Federal Institute of Technology.

The author came to the United States in September 1967 and was appointed research assistant at the Fritz Engineering Laboratory. He has been associated with the research projects on lateral distribution of loads in I-beam and box-beam bridges.

The author is an associate member of ASCE and of the Society of Sigma Xi.